

**THE EFFECT OF APPLIED FIELDS ON
CRYSTALLISATION**

A Thesis submitted for the degree of Doctor of Philosophy

by

Marina Maria Miller

CER,
Brunel University

May 2000

This thesis, which is submitted for consideration of an award of Doctor of Philosophy, is a record of research work carried out under the supervision of Dr Sue Grimes in the Centre for Environmental Research, Brunel University, except where due reference is made, has been presented for no other degree.

To Innes,

my motivation

ACKNOWLEDGEMENTS

I would like to thank my academic supervisor Dr Sue Grimes for all the encouragement, support and guidance at those crucial times throughout the duration of my PhD and Professor John Donaldson for his invaluable input into interpretation of the results. I would also like to thank Steve Beckett, my industrial supervisor, for all his enthusiasm and Nestle, my industrial sponsors, for not only their financial support, but also for their technical expertise and use of their resources, to you I owe my very good results.

I must thank my two brilliant project students Lois Douglas and Shaheda Jeraj for all their hard work carried out on this project and for the two excellent reports they produced.

To my two most special friends, Kirsty and Madhuri, thank you for being different from the crowd, for getting me through my weekly personal traumas and for teaching me how to fall over in the road after a few vodkas.

I would like to thank Bijita and Michele for all of our 'Academy' gossip sessions and Phil for his absolutely spot-on, dry sense of humour that made my final year bearable. Sorry for trying to force you all to drink alcoholic beverages at unsuitably early hours in the day, however being a bad influence was important to me.

I feel to complete my thesis has been a personal triumph over all the world could throw at me to try to drive me from the straightest path, I could not have achieved this without the support of my family, my Mum, Dad and sisters Nik and Dawn. Thank you.

Finally I would like to thank the two most special men in my life, my boyfriend Paul and my son Innes for their encouragement, patience and understanding and for just knowing that I would never give up.

ABSTRACT

The thesis provides a background on crystallisation, the effects of applied fields and summarises the techniques used for characterisation and analysis. The study of applied magnetic fields was carried out on three crystallising systems (a) sucrose, (b) lactose and (c) cocoa butter. Both sucrose and lactose were crystallised from aqueous solutions in incubators at 50°C in applied magnetic fields and the resulting crystals compared to the those obtained under zero field conditions. The results for the sucrose study where the magnetic treatment was carried out under static, dynamic pumped and dynamic syphoned conditions demonstrated that changes in phase, crystallinity, morphology and microcrystallinity were a result of the applied magnetic fields and additional strongly bound water was found to be present within the sucrose crystals most likely to be sucrose hydrates. The resulting sucrose crystals were dependant on the type of field applied, the purity of the sucrose solution and the residence time within the applied field. The lactose study under static conditions provided similar results concluding that applied fields resulted in a more controlled crystallisation resulting in increased crystal size, increased crystallinity and changes in morphology. Crystallisation of cocoa butter from the melt, under normal production conditions in applied fields, resulted in changes in morphology and the time taken to reach optimum tempering which were dependant on the type of applied field and the residence time in the applied field.

THE EFFECT OF APPLIED FIELDS ON CRYSTALLISATION

Statement	i
Dedication	ii
Acknowledgements	iii
Abstract	iv
Contents	vi

CONTENTS

CHAPTER ONE	INTRODUCTION	1
CHAPTER TWO	THE EFFECT OF APPLIED FIELDS ON THE CRYSTALLISATION OF SUCROSE	59
CHAPTER THREE	THE EFFECT OF APPLIED FIELDS ON THE CRYSTALLISATION OF LACTOSE	203
CHAPTER FOUR	THE EFFECT OF APPLIED FIELDS ON THE CRYSTALLISATION OF COCOA BUTTER	265
CHAPTER FIVE	CONCLUSIONS	313

CONTENTS

CHAPTER 1 INTRODUCTION

1.0	SUMMARY	1
1.1	CRYSTALLISATION	2
1.1.1	THE CRYSTALLINE STATE	2
	(a) Crystal symmetry	2
	(b) Crystal systems	3
	(c) Isomorphs, polymorphs, enantiomers and racemates	3
	(d) Crystal habit and common forms	5
1.1.2	SOLUTIONS AND SOLUBILITY	7
	(a) Solutions and melts	7
	(b) Preparation of a solution	7
	(c) Choosing a solvent	7
	(d) Supersolubility	9
1.1.3	NUCLEATION	11
	(a) Primary homogeneous nucleation	11
	(b) Primary heterogeneous nucleation	12
	(c) Secondary nucleation	13
1.1.4	CRYSTAL GROWTH	13
	(a) Surface energy theories	14
	(b) Adsorption layer theories	14
	(c) Diffusion-reaction theories	15
	(d) Combination of effects	16
	(e) Crystallisation from melts	16
1.2	MAGNETISM AND BACKGROUND OF APPLIED FIELD EFFECTS	17
1.2.1	CLASSIFICATION OF MAGNETIC MATERIALS	17
	(a) Diamagnetic	17
	(b) Paramagnetic	17
	(c) Ferromagnetic	18
	(d) Antiferromagnetic	18
	(e) Ferrimagnetic	19
1.2.2	PERMANENT MAGNETS	19
	(a) Classification of Permanent-Magnet materials	19
1.2.3	ELECTROMAGNETIC FIELDS	20
1.2.4	PULSED MAGNETIC FIELDS	21
1.2.5	BACKGROUND ON THE EFFECTS OF APPLIED FIELDS	22
	(a) The origins of magnetic treatment	22
	(b) Other examples of application of applied fields	22
	(c) Evidence of the effect of applied fields	25
	(d) Proposed mechanisms	27
	(e) Conclusions	32
1.3	TECHNIQUES USED FOR ANALYSIS	33

1.3.1	POWDER X-RAY DIFFRACTION (XRD)	33
	(a) Interpretation	35
1.3.2	THERMAL ANALYSIS	36
	(a) Thermogravimetry (TG)	36
	(b) Derivative Thermogravimetry (DTG)	37
	(c) Differential Thermal Analysis (DTA)	37
	(d) Simultaneous Thermal Analysis	38
	(e) Differential Scanning Calorimetry (DSC)	39
1.3.3	SCANNING ELECTRON MICROSCOPY (SEM)	39
	(a) Resolution	40
	(b) Components of the SEM	40
	(c) The Electron Gun	41
	(d) The Electron Lens	42
	(e) Specimen Stage	43
	(f) Construction and Image Formation	43
1.3.4	POLARISING LIGHT MICROSCOPY (PLM)	43
	(a) Properties of light	44
	(b) Interaction of light with matter	45
	(c) Interference	46
	(d) Polarisation colours	47
1.3.5	NUCLEAR MAGNETIC RESONANCE	48
1.3.6	KARL FISCHER TITRATIONS	51
1.4	REFERENCES	52

CHAPTER 2	THE EFFECT OF APPLIED FIELDS ON THE CRYSTALLISATION OF SUCROSE	59
2.0	SUMMARY	59
2.1	INTRODUCTION	60
2.1.1	HISTORY	60
2.1.2	STRUCTURE OF SUCROSE	60
2.1.3	CRYSTALLISATION MECHANISM	63
2.1.4	THE SOLUBILITY OF SUCROSE	66
2.1.5	ADDITIONAL CRYSTALLINE FORMS OF SUCROSE	68
	(a) Sucrose thin films	68
	(b) Sucrose hydrates	70
2.2	METHODOLOGY AND EXPERIMENTAL TECHNIQUES	71
2.2.1	AIMS	71
2.2.2	METHODOLOGY	71
2.2.3	PRELIMINARY STATIC CRYSTALLISATION STUDIES	72
	(a) Experiment 1 - Control	72
	(b) Experiment 2 - Weakest permanent field, at sides in parallel	72
	(c) Experiment 3 - 2nd Weakest permanent field, at sides in parallel	73

	(d) Experiment 4 - 2nd Strongest permanent field, at sides in parallel	73
	(e) Experiment 5 - Strongest permanent field, at sides in parallel	73
	(f) Experiment 6 - Permanent magnets in square	73
	(g) Experiment 7 - Permanent field, in parallel above and below	74
	(h) Experiment 8 - Pulsed field	74
	(i) Experiment 9 - Weakest DC electromagnetic field	75
	(j) Experiment 10 - 2nd weakest DC electromagnetic field	75
	(k) Experiment 11 - 2nd strongest DC electromagnetic field	75
	(l) Experiment 12 - Strongest DC electromagnetic field	75
2.2.4	CONTROLLED CONDITIONS, STATIC CRYSTALLISATION INVESTIGATION Experiments 13 - 24	77
2.2.5	MAGNETIC TREATMENT OF SUCROSE WHERE THE SOLUTION IS PUMPED	78
	(a) Normal grade sucrose, Experiments 25 - 37	79
	(b) Analytical grade sucrose, Experiments 38 - 50	81
2.2.6	MAGNETIC TREATMENT OF SUCROSE WHERE THE SOLUTION IS SYPHONED	82
	(a) Normal grade sucrose, Experiments 51 - 55	82
	(b) Analytical grade sucrose, Experiments 56 - 60	84
2.3	RESULTS AND DISCUSSION	85
2.3.1	RESULTS	85
	(a) Preliminary studies on static sucrose crystal growth	85
	(b) Controlled conditions, static crystallisation of sucrose	87
	(c) Magnetic treatment of sucrose where the solution is pumped	106
	(i) NORMAL GRADE SUCROSE	106
	(1) Visual observations	106
	(2) Scanning Electron Microscopy	116
	(3) Differential Scanning Calorimetry	123
	(ii) ANALYTICAL GRADE SUCROSE	128
	(1) Visual observations	128
	(2) Scanning Electron Microscopy	137
	(3) Differential Scanning Calorimetry data	143
	(d) Magnetic treatment of sucrose where the solution is syphoned	148
	(i) NORMAL GRADE SUCROSE	148
	(1) Visual observations	148
	(2) Scanning Electron Microscopy	152
	(3) Differential Scanning Calorimetry data	155
	(ii) ANALYTICAL GRADE SUCROSE	156
	(1) Visual observations	156
	(2) Scanning Electron Microscopy	160

	(3) Differential Scanning Calorimetry	163
2.3.2	DISCUSSION	165
	(a) Preliminary studies on static sucrose crystal growth	165
	(1) Discussion of preliminary applied field studies	165
	(2) Conclusion	167
	(b) Controlled conditions, static crystallisation of sucrose	168
	(1) Visual observations	169
	(2) Scanning Electron Microscopy	170
	(3) Polarising Light Microscopy	171
	(4) Differential Scanning Calorimetry	171
	(5) Investigation of the additional features revealed by DSC	173
	(6) Powder X-ray Diffraction	179
	(7) Conclusions	181
	(c) Magnetic treatment of sucrose where the solution is pumped	182
	(i) NORMAL GRADE SUCROSE	183
	(1) Visual observations	183
	(2) Scanning Electron Microscopy	184
	(3) Differential Scanning Calorimetry	186
	(4) Conclusions for magnetic treatment studies on normal grade sucrose	186
	(ii) ANALYTICAL GRADE SUCROSE	187
	(1) Visual observations	187
	(2) Scanning Electron Microscopy	188
	(3) Differential Scanning Calorimetry data	192
	(4) Conclusions for magnetic treatments studies on analytical grade sucrose	193
	(d) Magnetic treatment of sucrose where the solution is syphoned	194
	(i) NORMAL GRADE SUCROSE	194
	(1) Visual observations	194
	(2) Scanning Electron Microscopy	195
	(3) Differential Scanning Calorimetry data	195
	(4) Conclusion	195
	(ii) ANALYTICAL GRADE SUCROSE	196
	(1) Visual observations	196
	(2) Scanning Electron Microscopy	196
	(3) Differential Scanning Calorimetry	197
	(4) Conclusion	197
2.4	CONCLUSIONS	197
2.5	REFERENCES	200

CHAPTER 3	THE EFFECT OF APPLIED FIELDS ON	
	CRYSTALLISATION OF LACTOSE	203
3.0	SUMMARY	203

	(i) Conclusion	250
	(b) Scanning Electron Microscopy	250
	(i) Solution/glass interface	250
	(ii) Solution/air interface	251
	(iii) Crystals in lactose solution	251
	(iv) Conclusion	252
	(c) Differential Scanning Calorimetry	252
	(i) Conclusion	253
	(d) Powder X-ray Diffraction	253
	(i) Controls	254
	(ii) Permanent field studies (in parallel at sides)	255
	(iii) Permanent field studies (parallel above and below)	256
	(iv) Pulsed field study	257
	(v) DC electromagnetic field studies	257
	(vi) Conclusion	257
	(e) Karl Fischer data	258
	(i) Conclusion	258
	(f) Related thermal analysis data	258
	(i) Conclusion	260
3.4	CONCLUSION	260
3.5	REFERENCES	262

CHAPTER 4 THE EFFECT OF APPLIED FIELDS ON CRYSTALLISATION OF COCOA BUTTER

	BUTTER	265
4.0	SUMMARY	265
4.1	INTRODUCTION	266
	4.1.1 HISTORY	266
	4.1.2 COCOA BUTTER	267
	(a) Structure and composition	267
	(b) General triacylglycerol crystallisation	270
	(c) Polymorphism and cocoa butter	272
	(d) Analysis of polymorphs in cocoa butter	275
	(i) X-ray diffraction (XRD)	275
	(ii) Differential scanning calorimetry (DSC)	277
	4.1.3 CRYSTALLISATION OF COCOA BUTTER	279
	(a) Tempering and organoleptics	279
	(b) Cocoa butter seed crystals	281
	(c) Measurement of tempering	282
	4.1.4 COCOA BUTTER IN CHOCOLATE	284
4.2	METHODOLOGY AND EXPERIMENTAL TECHNIQUES	285
	4.2.1 MEASUREMENT OF INCUBATOR COOLING RATES	288
	(a) Experiment 1 - Cooling rate of incubators containing hot cocoa butter	288
	(b) Experiment 2 - Cooling rates of empty incubators	288

(c) Experiment 3	-Cooling rates of incubators containing AC or DC electromagnets and cocoa butter	287
4.2.2	CRYSTALLISATION OF COCOA BUTTER IN APPLIED MAGNETIC FIELDS	288
(a) Experiment 4	- Control	288
(b) Experiment 5	- Permanent magnetic field	289
(c) Experiment 6	- DC electromagnetic field	289
(d) Experiment 7	- AC electromagnetic field	290
(e) Experiment 8	- Pulsed magnetic field	290
4.2.3	CRYSTALLISATION OF COCOA BUTTER FOLLOWING MAGNETIC TREATMENT	291
(a) Experiment 9	- Permanent magnetic field	291
(b) Experiment 10	- DC electromagnetic field	291
(c) Experiment 11	- AC electromagnetic field	292
(d) Experiment 12	- Pulsed field	292
4.3	RESULTS AND DISCUSSION	293
4.3.1	RESULTS	293
(a) Incubator studies		293
(b) Crystallisation of cocoa butter in applied magnetic fields		297
(c) Crystallisation of cocoa butter following magnetic treatment		298
4.3.4	DISCUSSION	299
(a) Incubator studies		299
(b) Conclusion		301
(c) Crystallisation of cocoa butter in applied magnetic fields		301
(d) Conclusion		306
4.4	CONCLUSIONS	307
4.5	REFERENCES	310
CHAPTER 5	CONCLUSIONS	313
5.1	SUMMARY OF OBSERVATIONS	313
5.1.1	SUCROSE STUDY	313
5.1.2	LACTOSE STUDY	315
5.1.3	COCOA BUTTER STUDY	315
5.2	THE NATURE OF CRYSTALLISATION	317
5.2.1	MAGNETIC FIELD-CHARGED SPECIES INTERACTIONS	317
5.2.2	CRYSTALLISATION AND MAGNETIC FIELD EFFECTS	318
5.3	INTERPRETATION OF AVAILABLE DATA	319

1.0 SUMMARY

This chapter serves to introduce the concepts of crystallisation and magnetic fields.

The chapter is divided into the following categories:

Crystallisation: *The crystalline state, solutions and solubility, phase - nucleation and crystal growth are reviewed.*

Magnetism and background of applied field effects: *Basic magnetic properties, classification of magnetic materials and types of magnetic fields are discussed in addition to a small review on the effects of applied fields and a survey of the proposed mechanisms for these effects.*

Techniques used for analysis: *The theoretical principles and practical aspects behind the techniques used to analyse and characterise the materials prepared in this work are described. The analytical techniques described include:*

- *X-ray diffraction techniques*
- *Thermal analysis*
- *Scanning electron microscopy*
- *Polarising light microscopy*
- *Solid state nmr techniques*
- *Karl Fischer Titrations*

1.1 CRYSTALLISATION

The three general states of matter, gaseous, liquid and solid, represent different degrees of atomic or molecular mobility. In the gaseous state, the molecules are in constant, vigorous and random motion. This is considerably more restricted and less vigorous in the liquid state. In contrast, the molecular motion in the solid state is confined to an oscillation about a fixed position within a rigid system.

1.1.1 The crystalline state

The solid crystal is made up of molecules, atoms or ions held in a rigid lattice structure and their locations within the internal structure are characteristic of the material. The regular arrangement within the crystal results in crystals having shape and smooth surfaces or faces. Crystal growth results in planes of these faces parallel to atomic planes in the lattice.

Each different substance has its own unique exterior crystal shape, however, this shape may also be a direct result of the environment in which it is grown. The same substance therefore may appear to have several crystal shapes, with reference to size and development of faces (crystal habit), however the angles between corresponding faces remain constant, and are characteristic of the substance. This does not apply to polymorphs which are different structural arrangements.

1.1.1(a) Crystal symmetry

Many of the geometrical shapes that appear in the crystalline state possess some degree of symmetry that can be used as a means of classification. The three simple elements of symmetry are:

- (1) symmetry about a point (a centre of symmetry),
- (2) symmetry about a line (an axis of symmetry), and
- (3) symmetry about a plane (a plane of symmetry).

Crystals can possess no symmetry elements, a single symmetry element or in most cases a combination of several axes and planes of symmetry.

1.1.1(b) Crystal systems

The symmetry elements mentioned above result in 32 possible combinations which are called point groups or classes. These 32 classes may be applied to the six crystal classes:

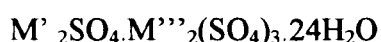
- (1) Cubic,
- (2) Tetragonal,
- (3) Orthorhombic,
- (4) Monoclinic,
- (5) Triclinic, and
- (6) Hexagonal/Rhombohedral.

These systems are grouped with reference to a, b and c cell edges and in terms of angles α , β and γ .

The *unit cell* is generally defined as the smallest symmetrical cell which on repetition in space will completely describe the lattice. Every crystal class must have a primitive cell associated with it but multiple unit cells are also possible. The four possible types of cell, primitive (P), body centred (I), face-centred (F) and face-centred on one face (or end-centred: A, B or C depending upon the face which is centred). Primitive cells contain only one lattice point within their boundaries; the body- and face-centred (one face) cells contain two lattice points and the face-centred (all faces) cell contains four lattice points. Given the four possible cell types, Bravais postulated in 1948 that there were only 14 possible basic types of lattice that could be used to identify the environment. Consideration of the 32 crystal point groups, 6 crystal classes and 14 Bravais lattices and allowing for translation symmetry, there are 230 possible space groups

1.1.1(c) Isomorphs, polymorphs, enantiomers and racemates

Two or more substances that crystallise in almost identical forms are said to be *isomorphous*. The crystals themselves differ only in small changes in interfacial angles and in general show very close similarity. An example of this is the class of 'Alums' which has the general formula:



where M' is univalent e.g. K or NH_4

M'' is trivalent e.g. Al, Cr or Fe.

Many phosphates, arsenates, sulphates and selenates are also isomorphous.

A substance capable of crystallising into different, but chemically identical crystalline forms is said to exhibit *polymorphism*. One of the most common polymorphs known is carbon which has polymorphs diamond (regular) and graphite (hexagonal). The term allotropy is applied to polymorphism of an element.

Variation in crystallising temperatures and changes in solvent used may result in different crystalline forms. For example, sulphur crystallises in the orthorhombic form (α -sulphur) from a carbon disulphide solution and the monoclinic form (β -sulphur) from the melt. β -sulphur cooled below $95.5^\circ C$ changes to α -sulphur. This process of polymorphic transition occurring at a definite temperature is called enantiotropy, and is usually accompanied by a change in volume. When polymorphs are not interconvertible, the crystal forms are said to be monotropic e.g. diamond and graphite are monotropic forms of carbon.

Two crystals of the same substance which are mirror images of each other are said to be *enantiomorphous*. These crystals do not possess any symmetry elements other than identity, and most are capable of rotating plane polarised light: this is termed optical activity. One enantiomer will rotate plane polarised light to the left (L-form) and the other to the right (D-form). Molecules which possess optical activity can also be termed chiral.

All known optically active substances are capable of being crystallised into enantiomorphous forms. Where the optical activity persists in the solution form, the molecules themselves are enantiomorphous. Where melting or dissolution removes optical activity, enantiomorphism is confined to the crystal structure only.

In organic compounds optical activity is often favoured by the presence of an asymmetric carbon atom. Certain sugars are well known examples of optically active

substances, one example is tartaric acid which has three possible forms shown in Fig. 1.1.1. The (a) form and the (b) form are mirror images, each has two chiral carbon atoms and both are optically active. In contrast, the *meso*- form of tartaric acid shown in (c) is optically inactive although it contains two chiral carbons. The potential optical activity of one half of the molecule is cancelled out by the opposite potential optical activity of the other half.

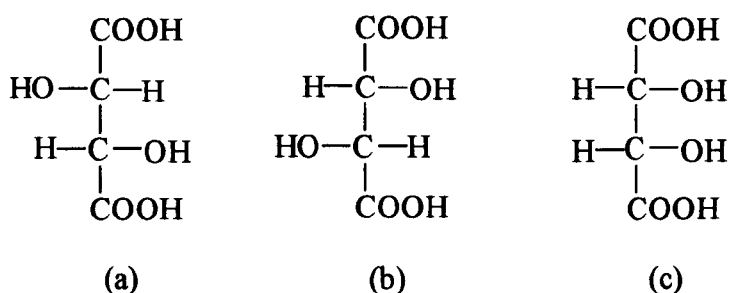


Fig 1.1.1 The tartaric acid enantiomers, (a) and (b) are optically active, (c) the *meso* form is optically inactive.

A mixture of definite proportions of D- and L-tartaric acids dissolved in water can produce an optically inactive solution. This property is known as *racemism*. Crystallisation of the racemic solution will result in a crystal form that is different from the D- and L- forms. The difference of the racemic crystal from the *meso*- form is that although both demonstrate optical inactivity, the racemic crystal may be redissolved and separated into D- and L- forms.

1.1.1(d) Crystal habit and common forms

Although the internal structure of a crystal may be classified according to one of the seven symmetry systems, there can be large variations in external crystal appearance because different faces can grow at different rates, depending on the conditions. The external form of the crystal is referred to as the *crystal habit*. Thus elongated growth of the prismatic habit gives a needle-like (acicular habit) and a stunted growth gives a flat-like crystal (tabular, platy or flakey habit).

There are a number of factors that can control the relative growth rates of the faces on a crystal. Examples of these include rapid crystallisation caused by sudden cooling; seeding of a supersaturated solution; impurities in the crystallising solution;

crystallisation from different solvents; degree of supersaturation; agitation etc. All are known to have an effect, sometimes dramatic, on the resulting crystal habit.

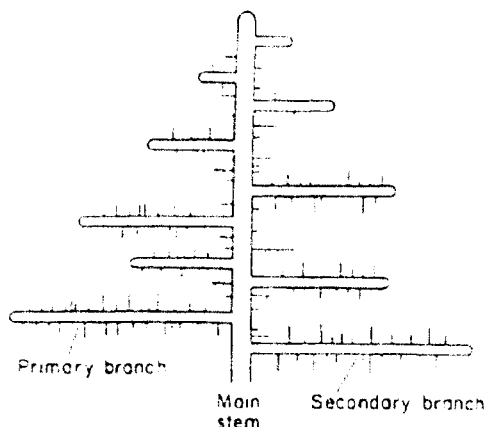


Fig. 1.1.2 Dendritic growth.

Tree-like formations called *dendrites* (shown in Fig. 1.1.2) are frequently produced under conditions of rapid crystallisation from supercooled melts, supersaturated solutions and vapours. The main crystal stem grows rapidly in a supercooled system, then primary branches grow at a slower rate out of the stem and in some cases, small secondary branches may grow slowly from the primaries. Branching continues until the pattern or surface becomes filled with crystalline material. The patterns that a snowflake produces are good examples of dendritic growth. Dendrites are most commonly formed at the early stages of crystal growth and are followed by more normal uniform growth. They are also common in thin liquid layers where the evaporation rate is fairly high, however agitation tends to suppress this type of growth.

Crystal aggregation or intergrowth is common in most crystalline natural minerals and many crystals produced industrially, and is one of the main problems in large-scale crystallisation. The free-flowing nature and the appearance of the product may be ruined by the presence of aggregates, and generally increased impurities in the crystal from the mother liquor are not easily removed by washing.

Composite crystals can occur in random clusters or in simple symmetrical forms. *Parallel growth* is one of the simplest forms of aggregation, where individual forms of the same substance grow on top of one another and crystal twinning is another

common composite crystal form and is made up of two intergrown individual crystals joined symmetrically about an axis (a twin axis) or a plane (a twin plane).

1.1.2 Solutions and solubility

1.1.2(a) Solutions and melts

A homogeneous mixture of two or more substances, whether they are in solid, liquid or gaseous state is termed a *solution*. It is normally convenient to refer to the constituents of liquid solutions as ‘solvents’ and ‘solutes’ when referring to the bulk liquid and the dissolved substance respectively. There are however many examples where these terms are inappropriate. Although there is no precise definition of a melt, it is generally assumed to be a liquid close to its freezing point. It can however also be a homogeneous liquid mixture of two or more substances which individually would solidify on cooling. There are no rigid rules to these definitions. *Solubility*, refers to a wide field and takes into account all degrees of solubility. Taking water as the solvent, solubility can range from materials that will dissolve in their own water of crystallisation at certain temperatures, down through the limited solubilities of materials like KClO_4 and CaSO_4 , to almost insoluble materials like BaSO_4 and HgO .

1.1.2(b) Preparation of a solution

Preparation of a solution normally involves mixing of solid and liquid components. A finer powder will dissolve more rapidly than a coarse one. Likewise, stirring or vigorous shaking will speed up dissolution by the action of rapid mixing, but will have no effect on the amount of solid material that a given solvent can take in, which varies according to temperature. However a definite point will be reached at a given temperature where no more solid material will dissolve. This is called the *saturation point* and normally increases with temperature. For every given solvent, a succession of saturation points at different temperatures can be plotted resulting in a solubility curve.

1.1.2(c) Choosing a solvent

When deciding on a solvent for use in crystallisation several factors need to be considered: The solute must be soluble in the solvent, the desired crystalline form must

be easily obtainable following cooling and/or evaporation etc., and the general rule is 'like dissolves like' when referring to polarity of the solvent and bonding interactions of the solid. The intermolecular bonding interactions of solvents can be used as a basis for classification as follows:

1. Polar protic, e.g. water, methanol, acetic acid etc.,
2. Dipolar aprotic, e.g. nitrobenzene, acetonitrile, chloroform etc., and
3. Non-polar aprotic, e.g. hexane, benzene, ethyl ether etc.

Polar protic solvents interact by forming strong hydrogen bonds. In order to dissolve, the solute, these bonds must be broken and replaced by bonds of similar strength. Therefore the solute must be capable of forming hydrogen bonds i.e. be sufficiently basic to accept a donated hydrogen atom or be hydrogen bonded itself. It follows that an aprotic non-basic solute cannot form strong bonds with the solvent molecules and therefore will have a very low solubility.

Dipolar aprotic solvents are classified by their high dielectric constants and interact via dipole-dipole interactions. Where the solute is dipolar and aprotic, solvation will occur via similar dipole-dipole interactions with the solute. Non-polar solutes are considered insoluble in such solvents because no dipole-dipole interaction with the solute is possible.

Protic solutes are soluble in basic dipolar aprotic solvents but have low solubility in non-basic dipolar aprotic solvents. This is because in basic dipolar aprotic solvents, strong hydrogen bonds are formed with the protic solutes, however, in the case of the non basic solvents, the hydrogen bonding within the solid state of the solute can only be replaced with very weak dipole-dipole interactions within the solution.

Non-polar aprotic solvents have low dielectric constants and the molecules interact by weak van der Waals forces. Therefore non-polar solutes are readily replaced by solutes with similar interactions. Dipolar and polar protic solutes are generally found to have very low solubilities in these solvents except in cases where non-polar complexes are formed.

The 'power' of a solvent is usually expressed as the mass of solute that can be dissolved in a given mass of pure solvent at one specified temperature. For example, water is a more powerful solvent than *n*-propanol for sodium chloride at 20°C (75 and 16g/100g solvent respectively) and, for benzoic acid *n*-propanol is more powerful than water at the same temperature (42.5 and 0.29g/100g solvent respectively).

The temperature coefficient must be considered carefully when deciding on a solvent. For example when considering potassium sulphate and potassium chlorate in water at 20°C their solubilities are 11g and 7g/100g water respectively. However, at 80°C, potassium chlorate is more soluble than potassium sulphate (39g and 21g/100g water respectively). Therefore, on cooling from 80° to 20°C, 80% of the dissolved potassium chlorate would be deposited compared with around 50% for the potassium sulphate.

Both solvent power and the temperature coefficient must be considered when choosing a solvent, for a cooling crystallisation process. Solvent power influences the volume of the crystalliser required and temperature coefficient influences the yield. In addition, when choosing a suitable solvent, it should be as clean and pure as possible. It should be stable under operating conditions and should neither decompose nor oxidise. Likewise, the solute and solvent must not react together. Where anhydrous forms are required, additional drying is required and may be difficult to obtain.

1.1.2(d) Supersolubility

It is often possible to cool a hot concentrated solution slowly without agitation, to prepare solutions containing more dissolved solids than expected from the saturation values. These solutions are said to be supersaturated. Supersaturation is a requirement for all crystallisation operations. The terms 'labile' and 'metastable' were introduced in 1897 to classify supersaturated solutions that spontaneously nucleate or not.^[5] A relationship between supersaturation and spontaneous crystallisation was developed in 1906, and in 1907 a diagrammatic representation of the metastable zone on a solubility-supersolubility curve was proposed^[6,7] (see Fig. 1.1.3) in which there are three regions, one well-defined and the other two are variable:

1. The stable (unsaturated) region, where crystallisation is impossible,

2. The metastable (supersaturated) region, between the solubility and supersolubility curves, where spontaneous crystallisation is improbable unless a seed crystal is added,
3. The unstable or labile (supersaturated) region, where spontaneous crystallisation is more probable.

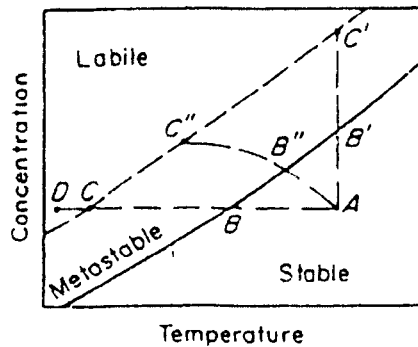


Fig. 1.1.3 The solubility -supersolubility diagram.

A solution of solubility and concentration A can be brought to the equilibrium saturation condition by lowering the temperature to reach point B on the solubility curve. Evaporating the solvent off at constant temperature results in increasing the concentration to reach point B' on the solubility curve. In practice, a combination of both cooling and evaporation takes place; this is illustrated on the solubility curve as point A to B''. At points B, B' or B'' a crystal could remain indefinitely in solution without growth or dissolution taking place. Theoretically, any further cooling or solvent removal above these points on the solubility line should result in crystallisation, however this does not take place, although crystal growth will take place on crystals already formed.

Spontaneous crystallisation will not occur after point B until the solution cools to point C where seeding or the slightest shock or disturbance will bring about immediate crystallisation. Further cooling may be required to some point D before crystallisation can be induced especially with very soluble substances. Similarly, removal of solvent from point B' will bring about spontaneous crystallisation at point C'. Penetration does not normally occur into the labile region because the evaporation takes place at the surface and it is unlikely that the entire surface reaches the solubility indicated at point C' at the same time. It is more likely that some areas reach point C' and form seed crystals while the rest of the solution is at some point in between B' and C'. The seed

crystals in the metastable region will then grow so that the bulk solution never in fact reaches concentration C^* . A combination of both cooling and solvent evaporation are used more frequently in practise and are represented on the graph by points B'' to C''.

1.1.3 Nucleation

Nucleation is the process of development of minute solid bodies, embryos, nuclei or seeds in a solution that must occur to act as centres of crystallisation, before crystal growth can proceed. Nucleation may occur spontaneously or it may be artificially induced^[8] by e.g. mechanical shock, friction, agitation extreme pressures etc.

Generally, there is no standard terminology to describe types of nucleation, therefore in order to avoid confusion the terminology referred to here needs to be clearly defined. The term 'primary' refers to cases where nucleation occurs in systems that do not contain crystalline material. Secondary nucleation, however, refers to the case in which nuclei are generated in the vicinity of crystals present in the supersaturated system. This is illustrated below in Fig. 1.1.4.

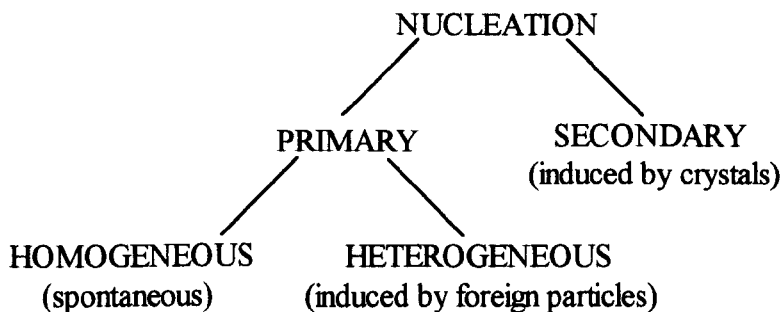
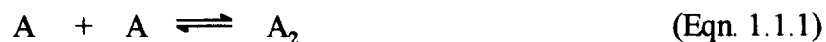


Fig. 1.1.4 Scheme introducing nucleation nomenclature.

1.1.3(a) Primary homogeneous nucleation

In the process of formation of a stable crystal nucleus within a homogeneous fluid, it is assumed that a number of constituent molecules must coagulate and become orientated in a fixed lattice. For example, sucrose is thought to require 6 sucrose molecules to form a stable nucleus. It is proposed that the process of nuclei formation is likely to be via the bimolecular addition scheme shown below in Equations 1.1.1 to 1.1.3.



Each molecular addition to the critical cluster results in nucleation and crystal growth which can only occur in regions of very high supersaturation. Short lived clusters can form, but many fail to achieve maturity because of instability. However, if a nucleus grows beyond a certain critical size, it becomes stable in the bulk of the fluid.

Excessive supercooling does not aid nucleation and in many cases may decrease the tendency to nucleate. Although nucleation can theoretically occur at any temperature, in practice there is an optimum range over which nucleation will occur. If the solution system sets to a glassy, highly viscous state, the temperature must be increased to the optimum region before nucleation may take place, decreasing the temperature further will not affect nucleation.

It has also been suggested that there is an induction period i.e. a time interval between the mixing of two reacting solutions and the appearance of crystals, which may range from microseconds to days depending on the level of supersaturation.^[9] The interval is thought to represent the time needed for assembly of a critical nucleus although this may be oversimplified.

There are difficulties in investigating true homogeneous nucleation since impurity-free solutions are virtually impossible to prepare.

1.1.3(b) Primary heterogeneous nucleation

Trace impurities in a system (solution or melt) can have a dramatic effect on the rate of nucleation resulting in inhibited or accelerated rates. There are however no general rules to be applied and each case must be investigated separately.

The addition of small particles to a supersaturated solution, known as *seeding*, is the best method of inducing crystallisation, and is frequently used in industrial scale crystallisers to control product size and size distribution. The seed crystals do not always have to be the same as the material being crystallised. An example where isomorphous substances will induce nucleation is the use of AgI, used as an artificial rainmaker, suitable because it is very similar to the ice crystal. Seeding can also prevent

crystallisation of thermodynamically unstable phases, for example, hydrates or polymorphs, that may appear during other conditions of crystallisation.

Nucleation occurs in local regions of high supersolubility which are normally found near or on the cooling surface. However, crystallisation centres can also be observed to grow from a point on the vessel wall, or on the stirrer. This phenomenon can be explained either by the presence of small cracks or crevices on the surfaces that retain minute seed crystals from previous crystallisations, or the surface may act as a catalyst for nucleation i.e. a surface that may induce nucleation at lower degrees of supercooling than required for spontaneous nucleation.

1.1.3(c) Secondary nucleation

Secondary nucleation is distinguished from primary nucleation simply by the definition of whether there are crystals of the solute initially present in a supersaturated solution or not respectively. Where crystals are present, secondary nucleation will take place at a lower supersolubility than primary nucleation.^[10-14]

Investigations have also found that there are several examples where seed crystal size may influence secondary nucleation rates. Large seeds have been found to generate more secondary nuclei in agitated systems than do small seeds because of greater contact potentials and collision energies, as would be expected. However, the number of seeds added may not have an effect on secondary nucleation rate unless the number of seeds of the optimum size is increased.

Although there have been a great many theories proposed to explain secondary nucleation (and nucleation in general) no single theory can offer a suitable explanation for all the phenomena observed.

1.1.4 Crystal growth

Following the formation of stable nuclei from a supersaturated or a supercooled system, crystal growth takes place, resulting in crystals of variable size. There are many proposed mechanisms of crystal growth which can be separated into several

groups from surface energies (which have been abandoned in recent years) to diffusion theories, and more recently adsorption layer theories which are more generally accepted in modified forms .

1.1.4(a) Surface energy theories

One of the first theories of crystal growth put forward which gained serious consideration from crystallographers was that by Curie.^[15] He suggested that there was a connection between the crystalline form and the surface energy of the solid, which was the total sum of the surface energies from all the faces. Later work suggested that the crystal faces would grow at rates proportional to the respective surface energies i.e. the equilibrium shape is related to the surface energies.^[16]

The surface energy should however be inversely proportional to the lattice density of the plane such that faces having low lattice densities would be expected to grow more rapidly. The velocity of growth of a face on a crystal is defined as the outward movement of a face in a direction perpendicular to the direction of growth. To maintain constant interfacial angles in the crystal during growth or dissolution, each layer would have to be parallel to the preceding or previous layer respectively.

1.1.4(b) Adsorption layer theories

The original concept of crystal growth via adsorption of solute molecules onto a crystal face was suggested by Volmer in 1939.^[17] It is based on the fact that when a crystallising particle arrives at a crystal surface it only loses a portion of its latent heat. This process results in the particle remaining bound to the surface but is free to migrate over the crystal face. This is effectively the same as losing one degree of freedom.

The adsorption layer becomes like a 'third phase' and is a loosely adsorbed layer of integrating units at the interface which is in dynamic equilibrium with the bulk solution. This layer is assumed to play an important role in crystal growth and secondary nucleation. Kossel suggested a model which was made up of monolayers growing across a crystal surface containing one or more *kinks*.^[18] In addition, he suggests there are vacancies on the surface and loosely adsorbed growth units (atoms, molecules or

ions). Incorporation of the growth units would occur most easily at the kinks and growth would continue along the step until the face was eventually complete. Surface nucleation commonly occurs at the corners and creates a fresh step for growth. The Kossel theory, however does not explain rapid face growth at low supersaturation, lower than normally required for surface nucleation.

A solution was given by Frank, who postulated that crystal growth never occurred in the ideal layer-by-layer fashion but had many imperfections.^[19] The most significant is the screw dislocation that perpetuates growth while not requiring further nucleation. Surface diffusion of adsorbed layers obviously plays a major role in this growth mechanism, however very little is known about the process. In addition, ion dehydration in or near these layers must complicate factors. Further reviews on surface and bulk diffuse models of crystal growth have been published.^{[20] - [23]}

1.1.4(c) Diffusion-reaction theories

Diffusion theories of crystallisation date back as early as 1897,^[24] where the rate of deposition of solid on the face of a growing crystal was considered to be a diffusional process. This theory assumes that crystallisation is the opposite of dissolution, and that there is a thin stagnant film of liquid adjacent to the growing crystal face. For crystallisation to proceed, diffusion of the solute molecules through the stagnant film must occur.

The degree of agitation would have a significant effect on the thickness of the stagnant film. Therefore it would be possible that an infinite range of rates of crystal growth could be obtained which would be dependent on the agitation of the crystallising system. Diffusion, however was not the only factor requiring consideration in the mechanism of crystal growth.

Dissolution rates were generally found to be faster than crystallisation rates, under the same conditions of temperature and concentration, suggesting that crystallisation and diffusion processes were not, in actual fact, the reverse of each other. In addition to

this, measurement of refractive indices near a crystal surface indicated that the solution was not saturated, but supersaturated.^[25]

These facts led to modifications of the diffusion theory and consequently a two-stage process was suggested.^[26,27] The first step was the diffusion process, where the solute molecules are transported from the bulk solution to the solid crystal surface. The second, a first-order 'reaction' where the solute molecules arrange themselves into the crystal lattice.

1.1.4(d) Combinations of effects

The crystal growth mechanisms considered for the purpose of this thesis have been described simply and there are several other complicated factors that may be considered. In reality, crystallisation is a complex process and the application of one theory to determine crystal growth is not usually possible. In any complete analysis of the growth process the combined effects of diffusion, surface integration and size-solubility may have to be considered together.

1.1.4(e) Crystallisation from melts

The process of crystallisation from melts must be mentioned, however, details will be limited to basic theory. The rate of crystallisation from a melt is dependent upon the rate of heat transfer from the crystal surface to the bulk liquid. Since the change of liquid phase to solid phase involves the evolution of heat of crystallisation, the surface of the crystal will generally have a slightly higher temperature than the supercooled melt. Like diffusion theories discussed in Section 1.1.4(c), there is a similar relationship with agitation and film thickness i.e. agitation will reduce film thickness, increase the heat transfer to the surface and lead to an increase in temperature of the surface crystal to close to its melting point.

1.2 MAGNETISM AND BACKGROUND OF APPLIED FIELD EFFECTS

The purpose of this section is essentially to provide the background theory to consideration to the effects of applied fields.

1.2.1 Classification of magnetic materials

In general, the more 'molecular magnets' are aligned inside a magnetic material, the stronger is its magnetic effect. A material reaches magnetic saturation once all its molecular magnets are aligned and no further increase of its resultant magnetic effect is possible. A material may be classified as a hard or soft magnetic material. The former describes materials which retain their magnetism fairly well after being magnetised, with only a small number of molecular magnets reverting to the random orientations once the magnetising force has been removed. The latter term describes materials which lose most of their magnetism once the magnetising force has been removed. The majority of the molecular magnets, which are easily aligned by the applied magnetising force, readily assume their disorientated and random state. All substances are affected by magnetic fields and are classified as being diamagnetic, paramagnetic, ferromagnetic, antiferromagnetic or ferrimagnetic.

1.2.1(a) Diamagnetic

Diamagnetic substances have a negative susceptibility. Apply an external magnetic field to a diamagnetic material and the external field is slightly reduced because of an interaction of the atomic electron orbits produced by the field.^[28] All substances have a basic diamagnetic term which is nearly always a constant value independent of temperature. Diamagnetism is due to the effect of applied fields on the movement of the inner electrons. There is no spontaneous magnetisation and atoms have no permanent dipole moments.^[29] Examples of diamagnetic materials are inert gases, copper and mercury, silicon and sulphur, ions such as Na^+ , N_2 and water and most organic compounds.

1.2.1(b) Paramagnetic

Paramagnetic materials have positive magnetic susceptibilities. Apply an external magnetic field to paramagnetic materials and the external field is slightly increased by

the alignment of electron orbits, but much more weakly than ferromagnetic materials. Above the Curie temperature ferromagnets become paramagnets. The magnitude of this effect is stronger than diamagnetism however, there is no spontaneous magnetisation and atoms have permanent dipole moments. Examples of paramagnetic materials are some metals including chromium and manganese, some diatomic gases such as O₂ and NO, ions of transition metals and their salts and rare earth oxides.

1.2.1(c) Ferromagnetic

Ferromagnetic materials have a very large positive magnetic susceptibility. Ferromagnetic materials have a critical temperature, known as the Curie temperature. If the temperature is raised above this temperature these ferromagnetic materials revert to paramagnetic condition. The Curie temperature can be defined as the temperature at which spontaneous magnetisation becomes zero. The magnitude of the effect is large below the Curie temperature since atoms have permanent dipole moments and interaction produces ↑↑ alignment. The only elements which are ferromagnetic are iron, nickel, cobalt, gadolinium and dysprosium.^[30] Ferromagnetism also occurs in many alloys containing these elements and in other alloys made up entirely of non-ferromagnetic elements such as MnBi and Cu₂MnAl.

1.2.1(d) Antiferromagnetic

Antiferromagnetic materials resemble paramagnetic materials in that they have small, positive susceptibilities at all temperatures. However, their susceptibilities do not increase steadily as the temperature decreases all the way down to absolute zero. The materials are characterised by a relationship between susceptibility and temperature which has a sharp discontinuity at a critical temperature, in this case called the Neel temperature. Below this temperature the material is ordered and antiferromagnetic, while at higher temperatures it is disordered and behaves as a paramagnetic substance. Atoms have permanent dipole moments and interaction produces ↑↓ alignment. Many compounds of transition metals behave in this way such as MnO, CoO, NiO and Cr₂O₃.

1.2.1(e) Ferrimagnetic

The ferrimagnetic material group may be considered as a special case of antiferromagnetism. The atoms have permanent dipole moments and interaction produces $\uparrow\downarrow$ alignment, but the moments are unequal. Examples of ferrimagnetic materials are magnetite (Fe_3O_4), maghemite ($\gamma\text{-Fe}_2\text{O}_3$) and mixed oxides of iron and other elements.

1.2.2 Permanent magnets

Permanent magnets are possible because magnetism exhibits the phenomenon of hysteresis: when the magnetising force applied to a body is changed and then restored to its original value, the resulting magnetisation of the body does not return to its original condition. If H (the magnetising force) is changed cyclically between values of $+H_c$ and $-H_c$ the value of B (the induced magnetic field) follows a closed symmetrical loop. When dealing with permanent-magnet properties, however, interest rarely centres on the complete hysteresis loop because permanent magnets operate in the second quadrant where B is positive and H is negative.

1.2.2(a) Classification of Permanent-Magnet materials

Classification of permanent-magnet materials is divided into (i) Alnico (Fe-Co-Ni-Al) series, (ii) Ferrites, (iii) Steels, (iv) Precipitation-hardening alloys, (v) Cobalt-rare earth alloys and (vi) Miscellaneous alloys. Permanent magnets may be used in any branch of technology and the design of the magnet system is important. The range of different permanent-magnetic alloys in each of the above categories makes good provision for an adequate selection of material for a particular application. For the work undertaken in this thesis the permanent-magnet materials were ferrites in the form of flat plates. The ferrite used was a barium hexaferrite with the general formula $\text{Ba}_x\text{Sr}_{1-x}\text{Fe}_2\text{O}_3$, where x can have any value between 0 and 1.

Design of magnetic components in systems must ensure that materials chosen remain stable in the specific working environment or that any changes be predictable. The main cause of magnetic instability are temperature changes, exposure to stray magnetic fields and mechanical shock or vibration, although in each case the same underlying

mechanism is possible. When a magnet is fully magnetised it is thermodynamically unstable with the least stable domain trying to return to a state of lower energy by domain boundary movement or reversals. If the magnet is subjected to stray magnetic fields or if thermal agitation is increased by a rise in temperature, then these unstable domains are the first to revert to their equilibrium state, leading to a loss of magnetisation in the magnet. Deliberate flux reduction can be affected by the application of a small alternating field which affects the unstable domains and since these have already relaxed a subsequent increase in temperature will have a reduced effect. Thus, stabilisation by alternating flux reduction is a good general insurance against further loss, but for the highest stability requirements this should be followed by repeatedly passing it through a temperature range slightly wider than that which the magnet will be exposed to.

Magnetic materials differ greatly in their structural stability. The ferrites are structurally quite stable until temperatures well above the Curie point (approximately 450°) are reached. In the work in this thesis, temperatures used were too low (<50°C) to present any possible losses in flux density. Additionally, efforts were made to ensure that magnetic components were isolated from one another to prevent loss from stray fields and that vibrations and shocks were kept to a minimum.

1.2.3 Electromagnetic fields

The magnetic fields of the individual turns of wire in a solenoid add up to give the overall magnetic field of the solenoid. Inside the solenoid the lines of magnetic flux are closely packed and straight. They are all equidistant. Outside the solenoid the lines of magnetic flux open out and then close in a long loop. The magnetic flux density inside the solenoid is thus much greater than on the outside. Furthermore, the internal magnetic field is evenly distributed *i.e.* it is uniform. The end of the solenoid from which the lines of magnetic flux emanate is called the north pole (as in the case of a bar magnet) and the end where they re-enter, is termed the south pole. The north and south poles can be readily determined by the clock rule:

If the current flows through the solenoid in a clockwise direction, one sees it as the south pole.

If the current flows in a counter-clockwise direction, one sees it as the north pole.

A current-carrying solenoid produces magnetic flux in the same way as a permanent magnet. The magnetic flux of a solenoid can be considerably increased by insertion of a ferromagnetic core, without having to increase the number of turns in the solenoid or the current. The reason for this increased magnetic flux is the alignment of the molecular magnets of the core material due to the magnetic field of the solenoid. The molecular magnets assist the solenoid magnetic field and by the correct choices of a suitable core material it is possible to increase the magnetic flux many times over.

1.2.4 Pulsed magnetic fields

Transducers produce complex pulsed electromagnetic waveforms which are fed to a ferrite core. It was designed specifically to be placed around a pipeline and the signal is propagated in both an upstream and downstream direction. The version of this unit type (Supplied by Hydropath^[31]) used in the present studies was a Hydroflow HS38 pulsed magnet and uses a 5V supply. The sample must be placed in the centre of the magnet to allow propagation of the generated signal into the fluid medium. The frequency of oscillation is between 100 to 160 kHz and a typical waveform is shown in Fig. 1.2.1. There is speculation as to how this device actually induces a field into the flowing fluid as the manufacturers claim that it is due to the 'skin-effect'.

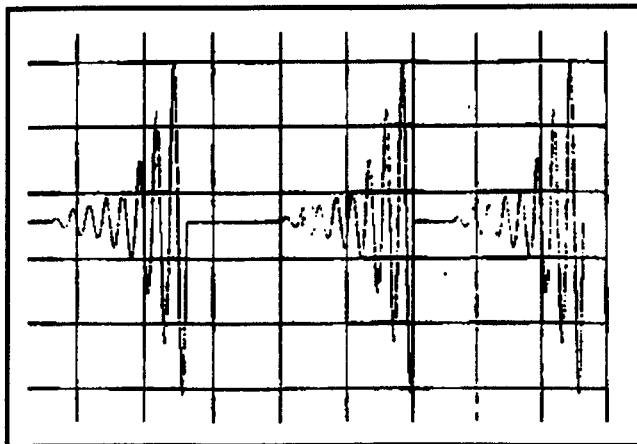


Fig. 1.2.1 Typical waveform of the Hydroflow HS38 pulsed magnet.

1.2.5 Background of the Effect of Applied Fields

The literature contains much evidence that magnetic field phenomena arise as a result of the application of an applied magnetic field. The concept of the interaction of applied fields with charged species is not new and neither is the controversy which surrounds it. The lack of a suitable theory and explanation to cover all the reported effects on the application of magnetic fields has fuelled the argument over explanations of observed effects. In addition, most experiments quoted are rather qualitative and the results are not necessarily reproducible.

1.2.5(a) The origins of magnetic treatment

The effect of applied fields was observed and recorded as early as 1847 on the diamagnetic conditions of flame and gases,^[32] however, the magnetic treatment of water for scale prevention and removal of accumulated scale is probably the most common application of magnetic treatment. This was patented in 1945 by Vermeiren who is recognised as discovering the effects of magnetic fields on water.^[33]

More recent literature has been published by Eastern European countries for the magnetic treatment of water describing the effect on water-formed scale deposits. The data presented in the Eastern literature appear in many cases to be in conflict and adequate information concerning reproducibility and precise conditions in the working solutions was lacking.^[34-39]

1.2.5(b) Other examples of the application of applied fields

The literature includes many examples where magnetic treatment has been used for purposes other than descaling or scale prevention.

Construction of a pulsed magnetic field treatment apparatus used for the study of the effects of magnetic fields on the pulp in a flotation cell is documented.^[40] Strong effects of the pulsed magnetic field on flotation were observed from a large number of experiments.

Magnetic treatment of water used in concrete manufacture improves its quality, including strength, density and frost resistance.^[41] The concrete porosity and water absorption were lower, causing a shorter hardening period. Magnetic treatment of hard water was concluded to result in increases in both tensile and compressive strengths of Portland cement, sulphate resisting Portland cement and oilwell cement.^[42]

It was reported that the quality of aviation fuels and oils is improved through magnetic treatment.^[43]

Treatment of colloid systems $\text{Al}(\text{OH})_3$ and $\text{Fe}(\text{OH})_3$ with magnetic treatment resulted in a 12-14% decrease in the ζ (zeta) potential (charge associated with particle surface).^[44] The claimed mechanism was that the magnetic field caused dehydration of the counterions which stabilise the colloidal system, and hence diminishing the ζ potential. It was also observed that the total surface area of the particles decreased, and an increase was found in the electrical conductivity of the CaCO_3 slurry. According to the results of statistical analyses, the changes in the above properties were significant.

In the case of organic molecules, it was found that when benzophenone was crystallised in a high magnetic field, the direction of the long axis of the needles formed tended to align perpendicular to the direction of the magnetic field.^[45] With a more complex organic molecule, a considerable degree of alignment was found when fibrin was allowed to polymerise in a magnetic field and a possible effect on blood clotting *in vivo* was suggested.^[46]

A recent report has also suggested that application of a magnetic field can influence the selectivity ratios in the nickel catalysed hydrogenation of fats such as sesame oil and soybean oil.^[47]

A single crystal of silicon can be manufactured from melt using an applied magnetic field resulting in longer single crystals having a larger diameter,^[48] which is of obvious benefit to the electronics industry.

Studies have been carried out on the effects of magnetic fields on the evaporation rate of sugar solutions.^[49] Results showed that viscosity, surface tension and boiling point of a solution decrease and the evaporation rate increases when a solution is treated with a suitable magnetic field. The magnetic field not only affects the solvent (water) but also on the solute (sugar) and the whole solution system.

Applied fields were shown to dramatically increase the reaction rate of anionic polymerisation of acrylonitrile and by acting upon the ion pair catalyst species, propan-2-oxide and potassium hydroxide. In addition to this several examples are demonstrated where applied magnetic fields interact with charged species in solution.^[50]

A number of different systems were studied in detail, on the effects of externally applied magnetic fields on charged species in solution.^[51] The effects of applied magnetic fields on plant growth of french dwarf beans (*P. Vulgaris*) demonstrated differential plant growth that was attributed to the direct field-charged species interactions with charged surfaces of the root membranes. Accelerated settling characteristics of aluminium hydroxide flocculations under applied permanent magnetic field conditions of study were interpreted in terms of direct field-charge interactions at the solid-liquid interface and of the charge interactions involved in the dehydration of aluminium hydroxide hydrates.

Changes in rates of electrodeposition of metal species from dilute aqueous solution were observed under applied magnetic fields and were demonstrated to be dependant on a number of factors; (1) direct field-charge interactions affecting the Lorentz energy, (2) the relative motion of the charged species, and (3) cluster formation in relation to the diffusion layer thickness and the effects of these on electrodeposition rates.

Magnetic fields were also reported to result in hypochromic and hyperchromic shifts in absorption intensities of Lanaset Red 2B and Methylene blue dyes under static conditions in the presence of applied magnetic fields.

1.2.5(c) Evidence of the effect of applied fields

The effect of applied fields has been studied using measurements of different physical parameters under different conditions. Some of these are mentioned below including the observed changes as a result of the applied fields.

- ***Effects on crystallinity/morphology*** - of the three calcium carbonate polymorphs (calcite, aragonite and vaterite) calcite is the most thermodynamically stable form at standard temperatures and pressures.^[52] However, the surface temperatures commonly encountered in systems such as heat exchangers and boilers, aragonite is normally the first phase to be precipitated out of solution. Magnetic treatment has been found to cause differences in the crystal habit of the precipitate.^[53,54] A study of DL-valine resulted in alteration of the crystal form from flat plates to small discrete crystals under applied magnetic field conditions, and a similar study of anthranilic acid resulted in the formation of microcrystalites within applied fields.^[55] On the other hand, promotion of calcite has been reported when supersaturation is achieved.^[56]
- ***Changes in nucleation and growth*** - both acceleration^[54,57-59] and suppression^[53,56,60] have been noted in the literature.
- ***Effects on coagulation*** - many researchers claim that the principal action of magnetic treatment devices is through formation of hydrophilic crystallites following interaction with a magnetic field with modified surface charge instead of attached scales.^[54,56,61] This implies that colloidal stability is influenced by the application of a magnetic field. Growth on existing scale is thermodynamically favourable^[62] and for a magnetic treatment device to prevent scale or produce descaling it could act so as to alter the size and surface charge of growing crystallites, thereby increasing their tendency to remain entrained within the bulk of the solution. Prevention of scaling thus takes place by avoiding precipitation on to solid surfaces. However, this phenomenon is difficult to confirm for particles as small as crystallisation nuclei.

It was found that treatment of the colloidal solutions alone produced a more marked effect than similar treatment of the electrolytic solutions (though treatment of both solutions proved the most effective). Good correlation between magnetically-increased colloidal stabilisation and decreasing particle size was recorded.^[63]

- ***Effects on corrosion (of metals)*** - magnetic treatment has often been reported as having an effect on corrosion, although the published data is once again contradictory in this respect. The corrosion rate of iron and steel has generally been observed to increase as a result of magnetic treatment,^[64,65] although a reduction in corrosion has been reported.^[66] Reduction in corrosion has been reported for aluminium^[65,67] and zinc^[65] whereas increased corrosion of active state titanium has been reported.^[68]

The corrosion rates of steel were found^[69] to increase with in increasing field strength and corrosion solution, however slower flow rates have been shown to promote stifling of the metal surfaces and decrease the overall corrosion rate (stifling is described as a build up of insoluble corrosion products very close to the reaction site, protecting it from further attack, i.e. competing corrosion effects are taking place.

- ***Influence on ionic strength*** - according to the literature, the magnitude of the magnetic effect was dependent upon electrolytic concentration.^[57,70-73]
- ***Effect on viscosity*** - small changes in viscosity, an increase of the order of 10^{-3} was reported for water^[74,75] using magnetic fields of up to 1200G. In some cases claims are made that a permanent change in the properties of water was observed after exposure to a magnetic field.

Although the literature contains examples where applied magnetic fields have effects that can be measured or studied, there is also a large amount of sceptical literature^[64,76-89] that has been unable to report any differences between 'unmagnetised'

and 'magnetised' samples. The scepticism with magnetic treatment has focused on either the reproducibility of the observed phenomena, or the absence of a generally accepted mechanism. The three main factors responsible for poor reproducibility of experiments are summarised below:

- (1) Variation in water composition,
- (2) The impact of external effects which are not taken into account (including geomagnetic field fluctuations, and
- (3) differences in the conditions of treatment and measurement.

1.2.5(d) Proposed mechanisms

Water can be affected by magnetic treatment, the fact is unquestionable, but there are still many inconsistencies in the theories that have been proposed to explain it. Postulations that the effects of the magnetic field might be connected with some changes in the structure of the water include: ion displacement, the deformation of their hydrated sheaths and the formation of aqueous calcium complexes in addition to the formation of pre-nuclear clusters. In addition, more substantial effects are known to occur in heterogeneous systems.^[90]

Several water quality parameters were monitored such as total dissolved solids, alkalinity etc. in order to develop a model for predicting calcite nucleation, and the results indicated that the nucleation of calcite crystals was enhanced by application of magnetic and electrostatic fields.^[91] It was suggested that the electrostatic or magnetic fields induced velocities which may contribute to molecular collisions, which if successful contribute to nuclei formation.

A study that subjected triple distilled water to permanent magnetic fields resulted in permanent measurements of increased pH, decreased surface tension and increased dielectric constant.^[92] They inferred that the decrease in concentration of H_3O^+ ions probably resulted from a change in the ionisation constant of water under the influence of the magnetic field, however no mechanisms were suggested for these changes and no statistical results were quoted.

A mechanism was postulated to interpret the nature of the observed coagulation in colloid systems.^[93] When a CaCO₃ suspension coagulates following magnetic treatment, the resulting surface area decreases which causes some of the ions which have been adsorbed by the particles to re-enter the liquid phase. The result of this is a decrease in the thickness of the diffuse layer and thus a decrease in ζ potential and also changes in the concentration of the ions in solution.

A mechanism whereby CaCO₃ scale formation is prevented by magnetic treatment has also been suggested on the principle of ‘magnetohydrodynamics’.^[94] The magnetic field is said to add energy to charged particles within water such as ions and small solid particles with electrostatic charges. The energy is thought to arise from the momentum of the particles and remains with these particles as surface energy.

The principle of magnetohydrodynamics has been represented by Equation 1.2.1:

$$\mathbf{E}_T = \mathbf{E}_S + \mathbf{E}_{ind} = \mathbf{E}_S + (\mathbf{V} \times \mathbf{B}) \quad (\text{Eqn. 1.2.1})$$

where \mathbf{E}_T = total electric field vector (NC⁻¹),
 \mathbf{E}_S = static electric field vector in the absence of fluid flow (NC⁻¹),
 \mathbf{E}_{ind} = electric field vector induced by the fluid flow,
 \mathbf{V} = flow velocity vector, (ms⁻¹), and
 \mathbf{B} = magnetic field vector (T).

From this equation a hypothesis using variables which can be experimentally determined was proposed and is given by Equation 1.2.2:

$$\begin{aligned} e_T &= e_s + (e_{ind} \cdot L) && (\text{Eqn. 1.2.2}) \\ &= e_s + [(\mathbf{V} \times \mathbf{B}) \cdot \mathbf{L}] \end{aligned}$$

where e_T = measured voltage (V),
 e_s = static voltage (V), and
 L = distance between two electrodes placed in the magnetic field to measure voltage (m)

A commercial magnetic device was modified to induce potential differences and currents when conducting solutions, which consisted of distilled water and up to 0.16M NaCl, flowed through the magnetic fields.^[95] The magnitude of the induced voltage was found to increase linearly as the flow velocity of the solution increased. Alternatively, a higher voltage was induced with higher magnetic field strength at constant flow. The slopes of the voltage versus velocity plots were independent of

solution conductivity. A result which verified the hypothesis was to obtain B from the slope versus velocity plot (since L was fixed) which was in agreement with the measured field strength. Current increasing exponentially with increase in flow velocity and increase in pH with increasing time, suggests that electrolytic reactions might exist during the operation.

Other workers have suggested that magnetic fields change the behaviour of water on solid surfaces.^[96] Changes in water adsorption due to magnetic fields were determined from pressure changes to the water-solid systems which were in equilibrium. The amount of adsorbed water changed, just after application of the magnetic field, and reached a constant value within a few minutes and returned to the initial value on its removal. Magnetic fields of below 7600 Gauss were reported to depress adsorption while fields above 9600 Gauss were said to promote adsorption. There was therefore thought to be an adsorption-to-desorption transition in the range 8000 to 9000 Gauss.

The phenomenon of descaling by magnetic treatment was also explained in terms of modification of crystal nucleation, i.e. the charged particles of nuclei would be subjected to considerable forces when passing through a magnetic field. It is suggested that modification of the nature of the charges at the surface and consequently modification of the growth of the crystals in general on specific planes is affected.^[97] The influence of the magnetic field on crystal growth is thought to be due to effects on the crystal surface and on the diffusion layer between the solution and the faces of the growing crystal. Furthermore, the 'Lorentz Effect', which is defined as the combined effects of an applied magnetic field, the charged species and the flow rate of the fluid, could result in the production of energy that could be used to remove or prevent scale formation. The Lorentz Effect has been formulated as shown in Equation 1.2.3:

$$\mathbf{F}_L = q [\mathbf{V}_o \times \mathbf{B}] \quad (\text{Eqn 1.2.3})$$

where \mathbf{F}_L = Lorentz Force (N),
 q = charge of the particle, and
 \mathbf{V}_o = moving velocity of the charged particle (ms^{-1}).

This is essentially the same as Equation 1.2.1, but without the effect of the static electric field vector.^[98]

Many workers have proposed that the principal effect of the magnetic field is the creation of crystallisation nuclei.^[58,99-101] Others demonstrated (from thermodynamic principles) that on the basis of current crystallisation theory, magnetic treatment could produce no effect on nucleation and growth of crystals.^[102]

Assessment of the many proposed mechanisms for magnetic water treatment is made difficult by the varied and often contradictory nature of the experimental results presented. The integrity of reported results and their interpretation are compromised by a number of factors:

1. irreproducibility by subsequent research,
2. inadequate or unspecified control of solution chemistry, in particular the solution pH and the level of contamination by scale-adjusting ions, and
3. unspecified physical conditions, for example the magnetic field orientation and treatment time.

The proposed mechanisms can be broadly divided into four basic categories:

1. Inter-atomic effects (e.g. changes in electron configuration),^[56,85,94,103,104]
2. Contamination effects (due to magnetically enhanced dissolution),^[105-110]
3. Inter-molecular/ionic effects (e.g. changes in co-ordination of water with ions),^[108,111-113] and
4. Interfacial effects (e.g. distortion of the double layer).^[60,61,63,70,96,109,114-118]

In many cases mechanisms put forward involve Lorentz forces acting on moving charged particles in the magnetic field, which increases linearly with particle charge, particle velocity and orthogonal vector component of the magnetic field.

In relation to magnetic treatment of water applied to flowing systems it is worth noting that the number of passes through a field may play an important role in the magnitude of the observed effects. Single pass systems can be associated with the large number of sceptical published data^[64,79,83-85] with the very few exceptions.^[104] The reported negative results for single pass systems is in contrast to the many apparently positive results reported in both the scientific and trade literature for recirculatory or other

systems where magnetic exposure is prolonged.^[49] In particular, the number of passes through a magnetic field has been shown to increase with surface tension and viscosity depression of a sucrose solution, up to a maximum of 5 to 6 passes, but as the number of passes through the magnetic field goes beyond this (up to 8 passes), the magnetic effects on the solution reduce.

Some literature exists on a phenomenon known as the thermodielectric effect first documented in 1950.^[119] Costa Ribeiro discovered that electric charges are always produced at an interface between a solid and a liquid and may be observed when a phase change is occurring. In addition, charge transfer is produced in other changes of physical state when one phase is a solid.

Charge separation and migration is known to occur in a solution of camphor in CCl_4 .^[120] In the presence of a non-uniform electric field the charges are forced to the surface of the solution. External electric fields must influence a liquid at an interface where the permittivity ϵ undergoes an abrupt change and therefore $\Delta\epsilon$ is not zero, as in the bulk solution. As the field is increased, a force is exerted on the surface of the liquid. If the field is strong enough, surface disruption takes place and spikes appear and a nucleation centre is formed. As the field is further increased the spike grows into a plate-like crystal. Similarly, ice nucleation is known to be influenced by non-uniform electric fields. This is the inverse of the thermodielectric effect.

Similar effects occur using magnetic fields since the magnetic and electric properties of molecules are analogous. Molecules subjected to applied electric or magnetic fields will experience induced dipole moments or magnetic moments respectively. Phase changes produced by inhomogeneous electric and magnetic fields are known as the Evans effects, and Group theoretical statistical mechanics were carried out^[121] providing the following indications:

1. The electric and magnetic Evans effects depend on the different symmetries on the liquid and crystalline sides of the interface. If there is no symmetry difference, there is no effect.

2. The interface between environments of different point group symmetry is in general forced into that of a lesser symmetry. Thus, a crystal grows into a liquid, a crystal into a gas etc.
3. The relevant consideration is the point group of the ENVIRONMENT either side of the interface, NOT the point group of the molecules themselves. In consequence, electric and magnetic Evans effects are expected in molecular solutions, suspensions, colloids, aggregates etc. where the environmental point groups are different either side of the interface.
4. The mechanism proposed accounts for the fact that the field gradients produce linear force through interaction with the appropriate molecular multipole moment.
5. The point group analysis can be extended straightforwardly to interactions of electromagnetic fields with environments either side of the interface.

Because of the relevance to the work contained in this thesis it is worth noting the results of a study published on sodium nitrate crystals grown in magnetic fields from aqueous media.^[113] It is proposed that the resulting crystals contain a small amount of geolitic water which was identified using NMR. A peak at 5.53ppm was found in the spectra which was observed to be a broad curve in the controlled crystal sample. It is postulated that the water insertion into the crystal occurs while solute clusters are crystallised as a result of aggregating in the solution. These findings mean that a small amount of water exist in crystallised solute clusters and that the rotation and/or vibration of the controlled water molecules are more restricted than those of exposed ones.

1.2.5(e) Conclusions

Most of the antiscaling reports support the Lorentz forces mechanism and can be used to explain the possible action of the magnetic effect on the electrochemical double layer^[83] which envisages isotropic distortion of the diffuse layer. A change in the charge distribution within the double layer caused by displacement of co- and counterions by Lorentz forces is thought to result in a semipermanent change in the charge and potential at the boundary of the Stern Layer. This mechanism could explain both coagulation and crystallisation behaviour whilst offering a quantifiable

performance parameter in the form of the ζ potential changes, however it does not explain coagulation effects recorded under quiescent conditions, downfield effects or on solutions containing no suspended matter. However, the Evans effects seem to provide a mechanism which is capable of explaining these phenomenon.

1.3 TECHNIQUES USED FOR ANALYSIS

For the purpose of this thesis, it is necessary to describe the theoretical principles and practical aspects behind the techniques used to analyse and characterise the crystalline materials prepared in this work.

1.3.1 Powder X-ray Diffraction

X-ray powder diffraction is a physical technique used in the characterisation of solids. It has been in use since the early part of this century for the identification of crystalline materials and for the determination of crystal structures.

X-rays are electromagnetic radiation of wavelength approximately 1\AA , that lie between gamma-rays and ultra-violet rays in the electromagnetic spectrum. They are produced by high energy collisions of charged particles with matter. Usually a beam of accelerated electrons is allowed to strike a metal target, such as copper, and this has sufficient energy to ionise some of the copper 1s electrons. An electron from an outer orbital (2p or 3p) immediately drops down to occupy the vacant 1s level and the energy released in the transition appears as X-radiation. The transition energies have fixed values, therefore a characteristic spectrum of X-rays results. For copper, the 2p \rightarrow 1s transition called $K\alpha$, has wavelength 1.5418\AA , and the 3p \rightarrow 1s transition, $K\beta$, 1.3992\AA . The $K\alpha$ transition is usually used in diffraction because it occurs more frequently and is more intense. In order to obtain a monochromatic X-ray beam, all other wavelengths can be filtered out.

A finely powdered sample, which ideally consists of randomly orientated crystals, has the power of scattering an X-ray beam incident on it because the separation of the atoms in a crystal sample is of the same order of magnitude as the wavelength of

X-rays. In such a sample, the various lattice planes are also randomly orientated and will diffract the radiation in an analogous way to the refraction of light by an optical grating. Every crystalline substance scatters the X-rays in its own unique diffraction pattern producing a “fingerprint” of its atomic and molecular structure.

When crystals, which are regarded as being built of layers of planes, are struck by a monochromatic X-ray beam, some of the X-rays are reflected such that the angle of incidence equals the angle of reflection as shown in Fig. 1.3.1. The rest are transmitted to be subsequently reflected by succeeding planes.

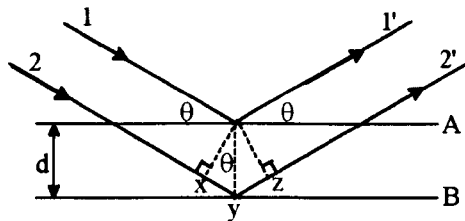


Fig. 1.3.1 Derivation of Bragg's law for X-ray diffraction.

Two X-ray beams, 1 and 2, are reflected from adjacent planes, A and B, within the crystal. For the beams to be in phase, beam 22' has to travel the extra distance xyz compared to beam 11'. Therefore, for beams 11' and 22' to be in phase, the distance xyz must be equal to a whole number of wavelengths. The *d-spacing*, *d* (the perpendicular distance between pairs of adjacent planes) and the angle of incidence, or *Bragg angle*, θ , are related to the distance *xy* by:

$$xy = yz = d \sin \theta$$

and

$$xyz = 2d \sin \theta$$

and to be in phase

$$xyz = n\lambda, \quad (\text{where } n \text{ is an integer})$$

Therefore

$$2d \sin \theta = n\lambda \quad \text{Bragg's Law} \quad (\text{Eqn. 1.3.1})$$

It is only when Bragg's law is satisfied that the reflected beams are in phase and interfere constructively. At angles of incidence other than Bragg angle, the reflected beams are out of phase and destructive interference occurs, therefore Bragg's law imposes stringent conditions on the angles at which reflection may occur. Diffracted beams are referred to as reflections and the angle between incident and diffracted beam is denoted by 2θ and not simply θ .

The basic information required in crystal structure determination may be obtained from the intensity of each reflection. Each atom has a different number of electrons and the relative scattering will vary according to this. As a result, two identical crystal lattices differing only in atoms, will have different positions and intensities of refracted beams, and each crystal species will diffract X-rays in a characteristically different way.^[122]

Since a sample of powder contains many small crystallites that are randomly orientated, any one reflection at particular Bragg angle will result in cones of reflection.^[123] These are observed as lines or peaks on the detector rather than the single points seen with single crystals. A simplistic diagram of a Powder X-Ray Diffractometer is shown in Fig. 1.3.2.

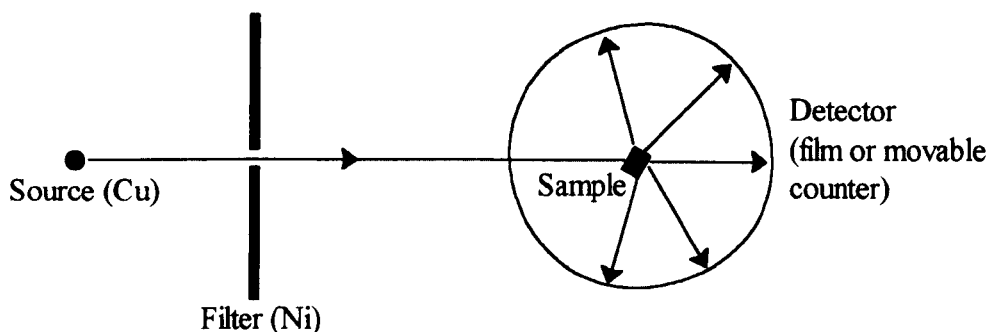


Fig. 1.3.2 A simplified Diffractometer arrangement.

1.3.1(a) Interpretation

The d-spacings and their intensities are the most important features of a powder pattern. The d-spacings (positions) of the lines in a powder pattern are governed by the values of the unit cell parameters (a , b , c , α , β , γ). The intensities provide information on the types of atoms present in the sample. Intensities are recorded relative to the intensity of the strongest line of the pattern which is arbitrarily assigned 100. For a particular substance, the line positions are essentially fixed and are characteristic of that substance. Intensities may vary somewhat from sample to sample, depending on the method of sample preparation and instrument conditions.

The substance can be identified from its powder pattern either by the indirect method, visual comparison of the pattern of the unknown sample with those of likely substances, or

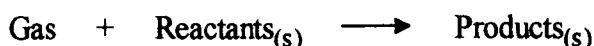
by the direct method, where the key spacings are measured and examined against indices of known compounds. The powder method can also be used for the qualitative analysis of crystalline phases.

1.3.2 Thermal Analysis

Thermal analysis refers to the group of methods in which some physical property of the sample is continuously measured as a function of temperature, whilst the sample is subjected to a controlled temperature change. Data obtained as continuously recorded curves may be considered as thermal spectra. The most widely used techniques are Thermogravimetry (TG) which involves measuring changes in weight, Differential Thermal Analysis (DTA) and Differential Scanning Calorimetry (DSC) which monitor changes in energy, and Differential Thermogravimetry (DTG) which is a method of expressing the results of TG by giving the first derivative curve as a function of temperature or time.^[124,125]

1.3.2 (a) Thermogravimetry (TG)

Dynamic thermogravimetry (TG) measures the weight of a sample as a function of temperature, during controlled heating or cooling.^[124] Static gravimetry on the other hand measures weight changes whilst the temperature is kept constant. This technique provides quantitative information on weight changes and enables the stoichiometry of a reaction to be followed directly. In practice two types of process can be followed using TG:



TG data of a sample is usually given in the form of weight loss against temperature, although weight loss as a percentage of the original weight can be used instead of absolute weight loss and a time axis can be used instead of a temperature axis.

Two temperatures are used in characterising a single stage weight loss process: the initial temperature T_i (the lowest temperature at which the onset of a weight change can be

measured under the conditions of the experiment) and T_f , the final temperature (the temperature at which the decomposition process appears to be complete). At a linear heating rate, T_f is higher than T_i and the difference, $T_f - T_i$ is known as the reaction interval. The extent of the reaction is not influenced by the instrumentation, but the rate of reaction and T_i and T_f are dependent on the experimental conditions. For example, in an endothermic process T_i and T_f both increase with an increase in heating rate. While TG has a relatively low precision, it provides useful analytical confirmation and a fairly simple and rapid method for the determination of water.

A number of physical and chemical process such as crystalline transition, melting, decomposition etc may be followed using TG. The technique provides a useful confirmation of a formula, and may aid suggestion of reaction schemes to account for degradation of pure compounds.

1.3.2 (b) Derivative Thermogravimetry (DTG)

In a derivative thermogravimetry, the first derivative of the weight loss, dw/dt . Is measured as a function of temperature or time. The DTG curve is therefore a plot of rate of change of weight and the area under the curve is proportional to the total weight change. The points of inflection are dependent on experimental conditions, especially heating rate, however T_i and T_f are usually much easier to identify than in simple TG plots. In complex processes, e.g. decomposition processes, where overlapping reactions occur, it is often easier to identify the reaction stages from the DTG curve than the TG curve. Normally these techniques are most powerful when used simultaneously. DTG curves often provide a better means of comparison with DTA and DSC than the corresponding TG data.

1.3.2 (c) Differential Thermal Analysis (DTA)

Differential thermal analysis measures the temperature difference between the sample and an inert reference material as a function of temperature or time, whilst both the sample and reference material are subjected to identical conditions of heating or cooling. Any physical

or chemical change occurring in the sample will be associated with a change in temperature (Δt) relative to the reference material. For an endothermic process, the temperature of the sample will be lower than that of the reference. For an exothermic process, the temperature of the sample will be higher than the reference.

A differential temperature usually develops between the sample and reference even when no physical or chemical change is occurring. Provided error due to sample mass and packing density are negligible, this differential temperature will be due to differences in the heat capacities and thermal conductivities of the two materials and usually manifests itself as a baseline drift.

The area under a DTA curve, obtained by integration, represents the total heat change in the reaction. DTA can therefore be used to study second order transitions in which no heat change is involved e.g. some solid-solid phase changes, for example, glass transition temperature. The baseline of the DTA trace will become irregular at the transition temperature leading to changes in slopes above and below this temperature. However, if a DTA peak appears at a temperature where TG shows no change in the sample weight, then either a chemical reaction or phase transition has occurred.

1.3.2 (d) Simultaneous Thermal Analysis

The TG curve can assist in providing information on the thermal stability and change in composition of the sample. The DTA curve indicates changes of state which are not necessarily accompanied by mass changes, and DTG curve represents rate of change of weight loss of sample. All three techniques run simultaneously can be used to identify physical reactions (e.g. melting point) from reactions involving no weight change. A typical Thermal Analyser is shown schematically in Fig. 1.3.3.

The system has 4 major components:

1. **Sample holder-measuring system** - which is made up of sample containers and thermocouples,

2. **Furnace-heat source** - which has a large uniform temperature zone,
3. **Temperature programme module** - which supplies energy to the furnace in such a manner as to ensure a reproducible (and preferably linear) rate of change of temperature,
4. **Recording system** - method of indicating and/or recording the emf (suitably amplified) from the differential- and temperature- measuring thermocouples.

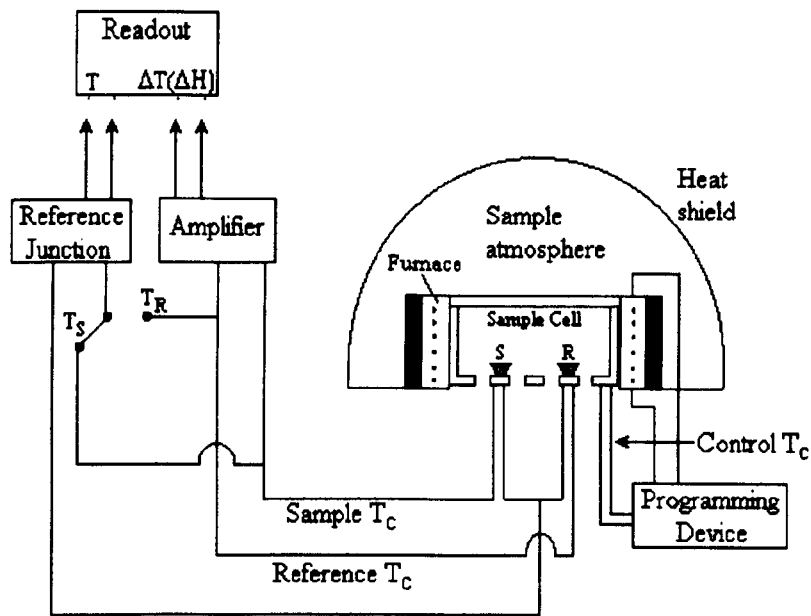


Fig. 1.3.3 Schematic diagram of a Differential Thermal Analyser System.

1.3.2 (e) Differential Scanning Calorimetry (DSC)

The Differential Scanning Calorimetry technique is very similar to DTA, however there is one fundamental difference. DTA is a dynamic technique that measures the temperature difference between a reference and sample. Calorimetry on the other hand, keeps the reference and sample temperatures the same and measures the changes in energy required to do this. The close similarities in DSC and DTA techniques means that the data obtained from either technique is usually very similar.

1.3.3 Scanning Electron Microscopy (SEM)

The Scanning Electron Microscope, initially constructed by Knoll and Ruska, is an extremely versatile tool and is particularly useful for examining surfaces of materials.

There are three types of scanning electron microscope in use today, the Transmission Electron Microscope (TEM), the Scanning Electron Microscope (SEM) and the Scanning Transmission Electron Microscope (STEM), but for the purposes of this work, only SEM will be discussed.

1.3.3 (a) Resolution

Resolution is the most important consideration as it is the increase in resolution gained by the use of electrons that is the whole basis of electron microscopy. The resolution is inversely proportional to the electron wavelength (λ) used. The 'limit of resolution' is defined as the minimum distance between two points that allows for their discrimination as two separate entities.

The resolution of a system is defined by Equation 1.3.2 below.

$$r = \frac{0.61\lambda}{n \sin \alpha} \quad (\text{Eqn. 1.3.2})$$

where r = resolution,
 0.61 = a constant,
 λ = wavelength of the medium used (nm),
 $\sin \alpha$ = sine of the semiangular aperture of the lens, and
 n = the refractive index of the medium in which the sample lies.

De Broglie showed in 1924 that an accelerated electron beam has an effective wavelength given by Equation 1.3.3 below.

$$\lambda = 0.1 \sqrt{\frac{150}{V}} \quad (\text{Eqn. 1.3.3})$$

where V = accelerating voltage.

For example, an 100kV accelerating voltage will result in electrons having a wavelength of 0.0039nm, five orders of magnitude shorter than visible light. In the electron microscope, electron beams have wavelengths $\lambda \sim 0.005\text{nm}$ (60keV).

1.3.3 (b) Components of the SEM^[126]

An SEM consists of an evacuated column containing an electron gun, electromagnetic lenses, apertures, electron detector, specimen stage and possibly other detectors such as

X-ray spectrometers. Modern SEM's are electronically controlled with the exception of the aperture. The control console houses all of the electronics and camera record tubes and viewing displays, both of which are cathode ray tubes (CRT). A simple diagram, illustrating the components of modern scanning electron microscopes, is shown in Fig. 1.3.4.

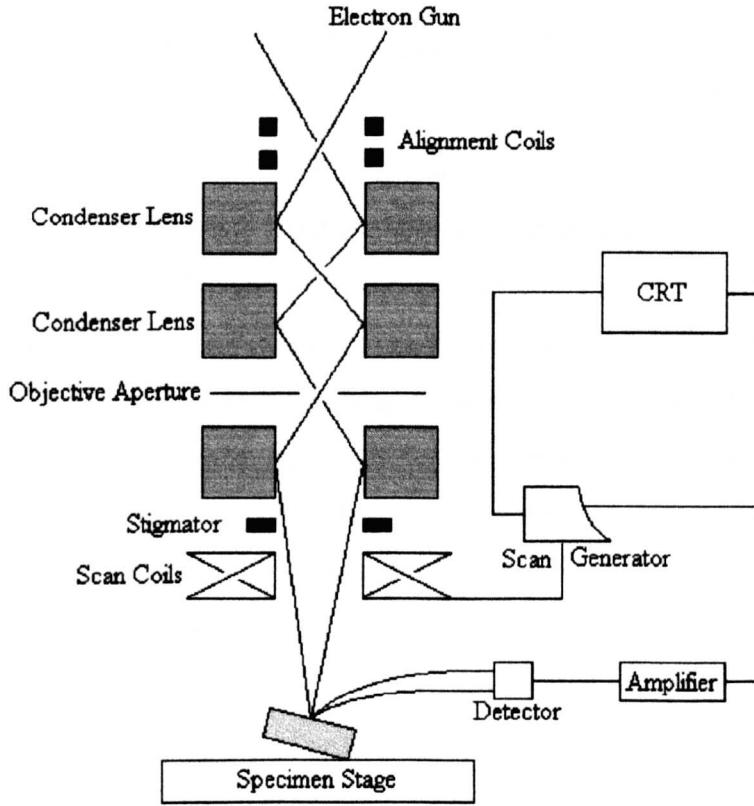


Fig. 1.3.4 A simple illustration of the components of a Scanning Electron Microscope.

1.3.3 (c) The electron gun

The SEM's produce a coherent beam of virtually monochromatic electrons which are focused by electromagnetic lenses onto the sample. The most commonly used electron source is the tungsten filament thermionic emission gun (see Fig. 1.3.5), which consists of a bent tungsten filament cathode with V-shaped tip and a radius of about $100\mu\text{m}$ (the area is $100 \times 150\mu\text{m}$). This is surrounded by a metal shield with a central hole called a Wehnelt Cylinder or cathode shield.

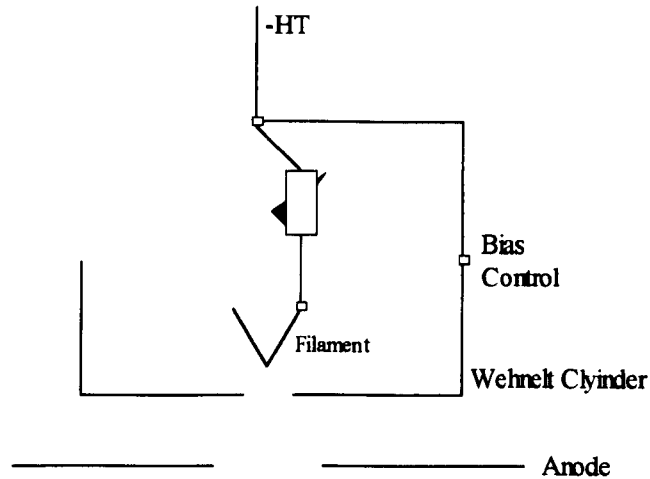


Fig. 1.3.5 An illustration of an electron gun.

The anode, situated below the cathode, is at ground potential. If the filament is heated to above 2700K, electrons are emitted from the filament tip and are accelerated away from the gun by applying a high negative voltage between the cathode and anode. The kinetic energy of the electrons is proportional to the voltage applied to the gun. The electrons can be focused to a point below the cathode shield by applying a bias voltage of between 0-500V between the cathode and cathode shield. The sample chamber is kept under a vacuum of 1×10^{-5} torr, which helps to reduce interference of the weakly penetrating electron beam by gaseous particles and reduces oxidation of the tungsten filament, therefore prolonging the gun's working life.

1.3.3 (d) The electron lens

Electron microscopes use electron lenses which are designed to provide a magnetic field almost parallel to the direction of travel of the electrons. The strength of the magnetic field is proportional to the number of windings of the lens multiplied by the current through the windings. Conversely, the effect of the lens on the electrons is inversely proportional to the accelerating voltage applied to the gun. The function of the electron lens is to bring to focus the beam of electrons produced by the gun. The focal length of a lens is the distance between the lens and the focal point and is inversely proportional to the strength of the magnetic field. Electron microscopes also contain small electromagnetic coils that are used

to correct astigmatism, deflect the beam for alignment and to scan the beam into its characteristic raster.

1.3.3 (e) Specimen stage

The samples for examination by SEM are mounted onto a specimen stage which is within the vacuum system, therefore the samples have to be dry and able to withstand vacuum. To enable examination of the sample, the stage has x, y and z translation, tilt and rotate facilities. The stage is electronically grounded to the microscope to provide a conducting pathway for the electrons.

1.3.3.(f) Construction and image formation

The electron beam generated by a tungsten filament thermionic emission electron gun and accelerated by an accelerating voltage enters the condenser lens system where it is demagnified, and then focused onto a sample by the objective lens. Between the objective lens and the sample are a set of scan coils which deflect the beam in a rectangular set of straight lines called a raster.

A fine probe of electrons interacts with the specimen to produce a variety of different signals: high-energy backscattered electrons, low energy secondary electrons, absorbed electrons, X-rays and cathodoluminescence. All the interaction products can be collected and amplified to produce a signal which can be used to control the brightness of the cathode ray tube. The nature of the interaction of the electron beam with the specimen will be affected by topography, composition, magnetic and electric character of the specimen.

1.3.4 Polarising Light Microscopy (PLM)⁽¹²⁷⁾

In order to explain the principles of Polarising Light Microscopy a brief background on light is required. Light is the term used to describe a radiation which forms part of a wide electromagnetic spectrum which also includes radio waves and X-rays. Visible light usually refers to the limited part of the spectrum to which our eyes are sensitive i.e. approximately 400 to 700nm wavelength.

1.3.4(a) Properties of light

Light has a dual nature in that electromagnetic radiation is propagated as waves but quantum theory is necessary to explain absorption, emission and photoelectric effects. There is no easily constructed analogy which adequately illustrates or describes the behaviour of light and its interaction with matter. Thus, light may for some purposes be shown graphically as a 2-dimensional sine wave and can be described in terms of its amplitude (A) and wavelength (λ). For light waves, the wavelength determines the colour: around 700nm corresponds to red light and around 400nm blue light. The 'intensity' of the rate of energy flow or the 'brightness' is proportional to the amplitude. Most sources of light are thermal sources and the light radiation is emitted by the behaviour of atoms in a heated wire or gas. An individual atom emits radiation in short bursts producing short trains of waves with no relationship between the instantaneous strength at the end of one and the start of the next. Under these conditions, there is a change of phase between successive wave trains.

When the phase difference ($\Delta\phi$) between two waves remains constant, the two waves are coherent. If $\Delta\phi$ was variable, the waves would be incoherent. The path difference can be obtained from measurement of $\Delta\phi$ since λ is usually known. If light contains only one wavelength, it is said to be monochromatic. In practice, a monochromatic source contains a narrow band of wavelengths that is obtained using filters. The spectrum of the light emitted from a monochromatic source has a number of narrow wavelength bands containing most of the energy being emitted which are called spectral lines. These consist of a narrow range of wavelengths defining a bandwidth, $\Delta\lambda$.

In free space (and air approximately), light waves travel with constant speed, c of just under $3 \times 10^8 \text{msec}^{-1}$. If light waves travel through a material in which the speed is dependent on the wavelength, the material is said to be dispersive. Refractive index, n , is as measure of the speed of light waves through a material and is defined so that $n > 1$ given by Equation 1.3.4 below.

$$\text{Refractive index, } n = \frac{c}{c'} \quad (\text{Equation 1.3.4})$$

where c = speed of light in free space, and
 c' = speed of light through material.

1.3.4(b) Interaction of light with matter

On encountering matter, light will be reflected, transmitted or absorbed. If the matter is inhomogeneous, scattering or diffraction may also occur. The law of reflection of light at a plane surface is well known and states that the angle of incidence of a plane wave on such a surface is equal to the angle of reflection. Any incident wave \bar{E} can be split into 2 components, \bar{e}_{\parallel} and \bar{e}_{\perp} , parallel and perpendicular to the plane of the reflecting surface. If the reflected intensities of a wave is plotted as a function of the angle of incidence, two curves are obtained \bar{e}_{\parallel} and \bar{e}_{\perp} . The reflectivity is different for each and \bar{e}_{\parallel} falls to zero at a certain angle which is dependent on the refractive index of the material and is known as the Brewsters angle. This angle corresponds to the angle at which the reflected and refracted waves are at right angles.

Reflecting material can be used to polarise light, since unpolarised light falling on a material at Brewsters angle will produce reflected light that contains only the \bar{e}_{\perp} component and so Brewsters angle is given by $\tan^{-1}n$.

Light is refracted as it passes from one medium to another, i.e. the wave will encounter a change in both velocity and direction. At a boundary, the angle of refraction r is related to the angle of incidence i by Equation 1.3.5 given as illustrated in Fig. 1.3.6.

$$n_1 \sin i = n_2 \sin r \quad (\text{Equation 1.3.5})$$

where n_1 = refractive index of the material of incidence,
 n_2 = refractive index of the material of refraction,
 $\sin i$ = sine of the angle of incidence, and
 $\sin r$ = sine of the angle of reflection.

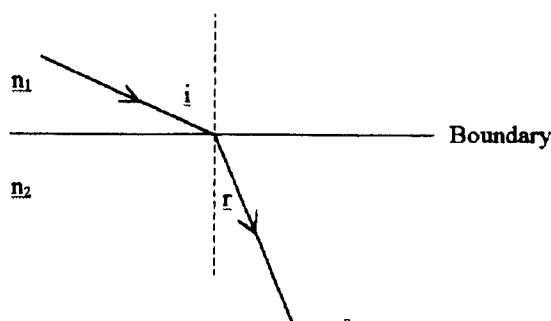


Fig. 1.3.6 Illustrating refraction of a wave passing from one medium to another.

If $n_1 > n_2$ and $r = 90^\circ$, then $\sin r = 1$, and

$$i \text{ max} = \sin^{-1} \frac{n_2}{n_1} \quad (\text{Equation 1.3.6})$$

where $i \text{ max}$ = the 'critical angle' of the material.

Where i is greater than $i \text{ max}$, no light can enter the material of refractive index n_2 .

A light wave passing through a material loses energy by absorption. The amount of light absorbed is an exponential function of the thickness of the material. Thus a beam of light of intensity I_0 is reduced in intensity to I on passing through a thickness of material.

1.3.4(c) Interference

Addition of two plane polarised waves E_1 and E_2 travelling in the same direction polarised in the same plane is simply the sum of the separate waves, E_R , and results in fluctuations in intensity. When considering coherent waves, if E_1 and E_2 have an angular phase difference of π , destructive interference results i.e. E_R is zero amplitude. Where the angular phase difference is $n\pi$ (where n is even), constructive interference results and E_R has twice the amplitude of either E_1 or E_2 and is in phase with both. Where both E_1 and E_2 differ in angular phase by $n\pi/2$ (where n is odd) E_R has an amplitude intermediate between E_1 and E_2 and also differs in phase from both. In general, both maximum and minimum intensities of light will be observed.

The use of white light instead of monochromatic will give rise to a series of colours with increasing phase difference between the waves. The action of the polariser and analyser is to produce a phase change so that the central or 'zero-fringe' is dark, not white. In

general, two plane polarised beams with orthogonal directions will not interfere; they must be in the same plane and from the same source to satisfy the conditions of interference.

1.3.4(d) Polarisation colours

Crossed polars are two polarising filters mounted 'in series' with the specimen between them. Polarisation colours can be observed under a microscope with one 'polaroid' sheet below the sample and one above. Normally they are orientated N-S and E-W and are at minimum intensity conditions in this orientation.

To produce polarisation colours, a beam splitter must be used to split the incident light which undergoes a phase change. The components are recombined in the same plane and result in amplitude and intensity variations. Transparent media behave in one or two ways to transmitted light:

- (a) *single refracting* or *isotropic* materials have only one speed of travel of light no matter what its direction of travel and place no restriction on the vibration direction of light, and
- (b) *doubly refracting* or *anisotropic* media, in general split a wave entering them into two components which travel at different speeds (or have different refractive indices) in different directions and vibrate at 90° to each other. This property is characteristic of the material and is controlled by its atomic structure.

The amount of path difference, Δ of the faster component over the slower one through the medium depends on the thickness of the medium, t , and the difference of the two components ($n_1 - n_2$) is given in Equation 1.3.7 below. This is termed birefringence.

$$\Delta = t(n_1 - n_2) \quad \text{(Equation 1.3.7)}$$

To satisfy interference conditions, parts of the two component waves produced by birefringent materials must be brought into the same vibrational direction. The second polarising filter performs this task, and when set at 90° to the first, shows any single refracting background as black.

If white light is used, a sequence of colours - Newton's scale of polarisation colours - is produced, which may be regarded as white light minus those colours or wavelengths which are interfering destructively. This technique is useful in distinguishing orientations of crystals since the slow and fast vibration directions will produce different polarisation colours. The function of the microscope is to magnify the specimens and view in more detail the crystal surfaces.

1.3.5 Nuclear Magnetic Resonance^[128]

Nuclei that have an odd number of protons or neutrons (or both) i.e. $I = \pm\frac{1}{2}$, have quantized spin. An external magnetic field will cause a 'split' in the nuclear energy levels and in the simplest examples (such as ^1H , ^{13}C , ^{19}F , ^{29}Si and ^{31}P) two spin energies will result. The energy difference observed is proportional to the strength of the applied magnetic field, but the energy gaps are much smaller. The wavelength of the incident (microwave) radiation is generally kept constant while the strength of the magnetic field is systematically varied. Absorption occurs when the nuclei are boosted from the more populous 'lower spin energy level' to the 'higher' level.

The frequency, ν , of the field required to induce a transition between adjacent levels is given below in Eqn. 1.3.8

$$\nu = \frac{E}{h} = \frac{\gamma H_0}{2\pi} \quad \text{(Equation 1.3.8)}$$

where E = is the energy of the nucleus,
 h = is Planck's constant,
 γ = is a constant for a nuclear species known as the magnetogyric ratio, and
 H_0 = is the applied external magnetic field.

The Boltzmann distribution may be used to calculate the ratios of the number of nuclei in the energy levels between which transitions occur. At room temperature it is found that the lower energy level is slightly more populated, thus a net absorption will occur. This absorption of energy is detected electronically and reproduced graphically giving the observed peaks in the NMR spectrum.

It can be seen that resonance for a particular nucleus will occur at a certain combination of ν and H_0 . This resonance condition may be reached by either varying ν and keeping H_0 constant or vice versa. It is usual to keep ν constant and the magnetic field is swept until resonance occurs. Nuclei of the same type would be expected to resonate at the same field values, but this is not observed. Electrons surrounding nuclei in a molecule modify the magnetic field experienced depending on its position within the molecule. The nuclei are magnetically screened and the magnitude (and sign) of the screening depends on the local electron density and neighbouring groups. Nuclei in different chemical environments will be shielded to different field values which will be characteristic of that chemical environment.

It is usual to measure the resonance position of a nucleus from a zero point reference position which is the resonance of a suitable compound. In proton NMR spectroscopy, tetramethyl-silane is frequently chosen as the reference compound due to the single resonance from the methyl protons which occur at a higher field than the majority of other proton resonances.

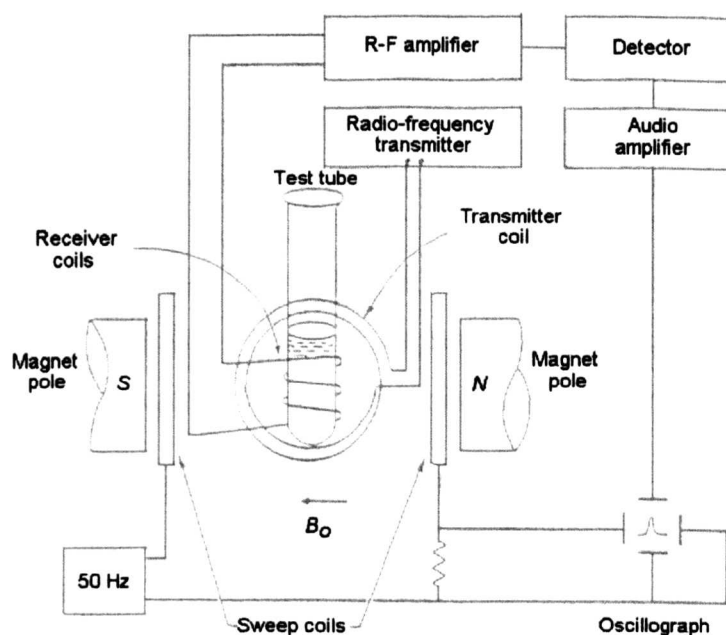


Fig. 1.3.7 Schematic diagram of an NMR Spectrometer.

Figure 1.3.7 below is a schematic diagram of an NMR spectrometer. The sample is placed in a small glass tube whose cross section is kept small (normally a few mm). The tube is

then placed in a non-magnetic sample holder which is spun at a rate of several hundred revolutions per minute to increase the homogeneity of the magnetic field throughout the sample. The sample holder is then placed between the poles of the magnet (B_0) which may be either an electromagnet or a permanent magnet. For high resolution spectra the field homogeneity between the pole pieces must very high.

The straightforward methods of NMR detection for powdered and amorphous solids is fairly limited because spectral details will not generally be observed. Since many interactions have an angular dependence, chemical shift resolved spectra are obtained by rapid rotation of the sample around an axis inclining at the ‘magic’ angle of $54^\circ 44'$ against B_0 as shown in Fig. 1.3.8.

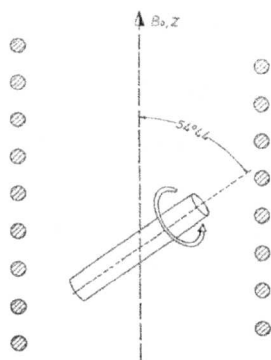


Fig. 1.3.8 ‘Magic Angle Spinning’ of a specimen in a field of a solenoid under the magic angle of $54^\circ 44'$.

Normally in order to obtain information from a powdered sample, a combination of decoupling and magic angle spinning is required (in combination with multiple pulse sequences) in order to improve the signal to noise ratio of the spectra as demonstrated in Figures 1.3.9 to 1.3.12.

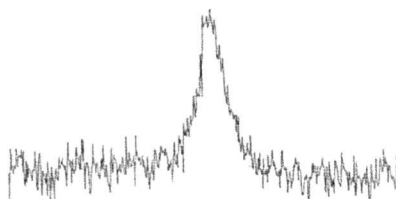


Fig. 1.3.9 ^{13}C spectrum without decoupling and rotation.



Fig. 1.3.10 ^{13}C spectrum without rotation, but decoupling with 48 kHz B_0 field.

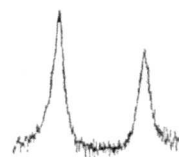


Fig. 1.3.11 MAS only, no proton decoupling. Note the low Signal to Noise ratio

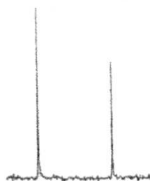


Fig 1.3.12 MAS and decoupling. The linewidth is narrowed as is the Signal to Noise ratio.

1.3.5 Karl Fischer Titrations

Karl Fischer titration equipment is essentially an extremely sensitive technique used to measure moisture content within solids. The technique is based on the following reactions:



The sulphur dioxide reacts with the alcohol to form an ester which is neutralised by the base. The anion of the alkyl sulphurous acid is the reactive component and is already present in Karl Fischer reagent. The titration of water constitutes the oxidation of the alkyl sulfite anion to alkyl sulphate by the iodine. This reaction consumes water.

Modern Karl Fischer titration equipment is generally completely automated. The Karl Fischer reagent and iodine are in a mixing vessel to which one third of your sample (which contains a percentage of water) for analysis is added. The equipment carries out the titration following rigorous mixing using a blender type instrument to thoroughly mix the sample with the reagent liquid. The equipment will then repeat this process and perform limited statistics on the measurements resulting in a mean moisture content with standard deviations.

1.4 REFERENCES

- [1] Mullin, J. W., *Crystallisation*, 3rd Edition, Butterworth-Heinemann Ltd, Oxford, 1993
- [2] Buckley, H. E., *Crystal Growth*, Chapman and Hall Ltd., London, 1951
- [3] West A. R., *Basic Solid State Chemistry*, John Wiley and Sons, New York, 1991
- [4] Donaldson, J.D. and Ross, S.D., *Symmetry and Stereochemistry*, Intertext books, London, 1972
- [5] Ostwald, W., *Zeitschrift für Physikalische Chemie*, 1897, **22**, 289-330
- [6] Miers, H.A. and Isaac, F., *J. Chem. Soc.*, 1906, **89**, 413-454
- [7] Miers, H.A. and Isaac, F., *Proc. Royal Soc.*, 1907, **A79**, 322-351
- [8] Young, S. W., *J. Am. Chem. Soc.*, 1911, **33**, 148-162
- [9] Nielsen, D., *Akad. Nauk Gruz. SSR, Inst. Inorg. Khim. Electrokhim.*, 1964, **20**, 95
- [10] Gyulai, Z., *Zeitschrift für Physik*, 1948, **125**, 1-17
- [11] Sung, C.Y., Estrin, J. and Youngquist, G.R., *AIChEJ*, 1973, **19**, 957-962
- [12] Strickland-Constable, R.F., *J. Chem. Soc. Far. Trans. I*, 1979, **75**, 921-924
- [13] Nienow, A.W., Bujac, P.D.B. and Mullin, J.W., *J. Cryst. Growth*, 1972, **13-14**, 488
- [14] Sarig, S. and Mullin, J.W., *Ind. Eng. Chem. Proc. Design and Development*, 1980, **19**, 490-494
- [15] Curie, P., *Bull. Soc. Franç. minéral.*, 1885, **8**, 145-150
- [16] Wulff, G., *Z. Krist.*, 1901, **34**, 449-530
- [17] Volmer, M., *Kinetik der Phasenbildung*, Steinkopff, Leipzig, 1939
- [18] Kossel, W., *Annalen der Physik*, 1934, **21**, 457-480
- [19] Frank, F.C., *Disc. Faraday Soc.*, 1949, **5**, 48-54
- [20] Bennema, P., *J. Cryst. Growth*, 1986, **3/4**, 331-334
- [21] Bennema, P., *J. Cryst. Growth*, 1969, **5**, 29-43
- [22] Chernov, A.A., *Modern Crystallography III: Crystal Growth*, Springer Verlag, Berlin, 1980
- [23] Chernov, A.A., *Cont. Phys.*, 1989, **30**, 251-276
- [24] Noyes, A.A. and Whitney, W.R., *J. Am. Chem. Soc.*, 1897, **19**, 930-934

- [25] Miers, H.A., *Phil. Trans.*, 1904, **A202**, 492
- [26] Berthoud, A., *J. Chim. Phys.*, 1912, **10**, 624
- [27] Valetton, J.J.P., *Zeitschrift für Kristallographie*, 1924, **59**, 483
- [28] *CRC Handbook of Chemistry and Physics*, 55th Edition, CRC Press Inc., 1974-1975
- [29] Jakubovics, J.P., *Magnetism and Magnetic Materials*, The Institute of Materials, London, 1994
- [30] Muncaster, R., *A Level Physics*, 2nd Edition, Stanley Thornes Ltd., England, 1985
- [31] Hydropath Ltd., Product Information Sheet, 1993
- [32] Faraday, M., *Phil. Mag. S.3.*, 1849, **31**, (12), No. 210, 401
- [33] Vermeiren, T., Belg. Pat. 460560, 1945
- [34] Klassen, V.I., Zhilenko, G.V., Berger, G.S., Larutukhin, I.V., Rryg, G.D. and Klynchnikov, N.G., *Dokl. Akad. Nauk SSSR*, 1968, **183**, 1123
- [35] Novozhilov, Y.L. and Batalin, B.S., *Izv. Vyshikh Uchebn. Zavedenii Stroit. Arkhitekt.*, 1968, **11**, 54
- [36] Klassen, V.I., Orel, M.A., Surukhanov, M.A., Kagarlitskaya, I.V., Rozenfeld, S.Sh., Lapatukhin, I.V. and Voloshina, L.B., *Dokl. Acad. Nauk SSSR*, 1971, **197**, 1104
- [37] Mirumyants, S.T., Vandynkov, E.A. and Tukhavatullin, R.S., *Russian J. Phys. Chem.*, 1972, **46**, 124
- [38] Dadunashvili, M.T., Pruidze, V.P., Kachibaya, E.I., Dzhaparidze, Sh.S., Smykova, S.M. and Tikhonova, N.F., *Akad. Nauk Gruz. SSR, Inst. Inorg. Khim. Elektrokhim.*, 1976, 33
- [39] Usatenko, S.T., Mordozov, V.I. and Klassen, V.I., *Kolloid Zh.*, 1977, **39**, 1018
- [40] Koumoundouros, G.C. and Frangiskos, A.Z., *Min. Wlth.*, 1991, **71**, 31
- [41] Lazarenko, L.N. and Zhuravlev, P.D., *Sov. Surf. Engng. Appl. Electrochem.* (English translation of *Elektronnaya Obrabotka Materialov*), 1985, **1**, 101
- [42] Ekaireb, S., Ph.D. Thesis, The City University, London, 1990

- [43] Tret'yakov, I.G., Rybak, M.A. and Stepanenko, E.Y., *Sov. Surf. Engng. Appl. Electrochem.*, (English translation of Elektronnaya Obrabotka Materialov), 1985, **6**, 80
- [44] Krylov, O.T., Vikulova, I.K., Eletsii, V.K., Rozno, N.A. and Klassen, V.I., *Coll. J. USSR*, (English translation of Kolloidnyi Zhurnal), 1985, **47**, 820
- [45] Katsuki, A., Tokunaga, R., Watanabe, S. and Tanimoto, Y., *Chem. Lett.*, 1996, 607
- [46] Yamagishi, A., Takeuchi, T., Higashi, T. and Date, M., *J. Phys. Soc. Jpn.*, 1989, **58**, 2280
- [47] Jart, A., *J. Am. Oil Chem. Soc.*, 1997, **74**, (5), 615
- [48] Susumu, S., Toshirou, H., Atsushi, I. and Tomohiko, O., *Fur. Pat. Appl.* EP 87,838, 6/8/97
- [49] Bisheng, Z., Siynan, G., Lin, L. and Miaoyan, C., *Int. Sugar J.*, 1996, **98**, (1166), 73
- [50] Thomas, A., Ph.D. Thesis, The City University, London, **1986**
- [51] Hardcastle, A., Ph.D. Thesis, Brunel University, London, 1996
- [52] Deer, W.A., Howie, R.A. and Zussman, J., *An Introduction to the Rock forming Minerals*, 13th Edition, Longman, London, 1982
- [53] Donaldson, J.D., *Tube Int.*, 1988, (10), 39
- [54] Deren, E., *L'Eau, L'Industrie, Les Nuisances*, 1985, **91**, 49
- [55] Prosser, J., personal communication
- [56] Ellingsen, F.T. and Vik, E.A., *Proc. 14th World Congr. Int. Wat. Suppl. Assoc. Zurich SS8*, 1982, 12
- [57] Koubikova, H., *Centre Belge d'Etude doc. Eaux.*, 1969, **132**, 564
- [58] Kronenberg, K.J., *IEEE Trans. Magn.*, 1985, **Mag-21**, 2059
- [59] Grimes, S.M., *Tube Int.*, 1988, (3), 111
- [60] Higashitani, K., Kage, A., Katamura, S., Imai, K. and Hatade, S., *J. Coll. Int. Sci.*, 1993, **156**, 90
- [61] Crolet, J.L. and Ledion, J., *Techn. Sci. Meth. L'Eau*, 1988, **83**, 435
- [62] Nielsen, A.E., *Kinetics of Precipitation*, Pergamon Press, Oxford, 1964

- [63] Higashitani, K., Okuhara, K. and Hatade, S., *Langmuir*, 1992, **5**, 861
- [64] Duffy, E.A., Ph.D. Thesis at Clemson University, Clemson, S.C, 1977
- [65] Grigorev, V.P., Ekilik, V.V., Ekilik, G.N. and Gontmakher, N.M., *Chem. Abs.*, 1973, **78**, 66086
- [66] Das, C.R. and Misra, H.P., *J. Inst. Engng. India*, 1982, **63**, 30
- [67] Chiba, A., Kawazu, K., Nakano, O., Tamura, T., Yoshihara, S. and Sato, E., *Corr. Sci.*, 1994, **36**, 539
- [68] Kelly, E.J., *J. Electrochem. Soc.*, 1977, **124**, 987
- [69] Gray, M., Ph.D. Thesis, The City University, London, 1993
- [70] Grutsch, J.F. and McClintock, J.W., *Corrosion 84, National Assoc. Corr. Eng.*, New Orleans, 1984, Paper No. 330
- [71] Szostak, R.J. and Toy, D.A., *Chem. Proc. Chicago*, 1985, **48**, 44
- [72] Donaldson, J.D. and Grimes, S., *New Scient.*, 1988, **117**, 43
- [73] Chou, S.F. and Lin, S.C., *Heat Transf. Equip. Fundament. Design Appl. Op. Prob.*, 1989, **108**, 239
- [74] Lielmezs, J., Aleman, H. and Fish, L., *Z. Phys. Chem. Neue Folge*, 1976, **99**, 117
- [75] Lielmezs, J. and Aleman, H., *Thermochim. Acta*, 1977, **21**, 225
- [76] Welder, B.Q. and Partridge, E.P., *Ind. Engng. Chem.*, 1954, **46**, 954
- [77] Mirumyants, S.O., Vandyukov, E.A. and Tukhvatullin, R.S., *Russ. J. Phys. Chem.*, 1972, **46**, 124
- [78] Wilkes, J.F. and Baum, R., *Int. Water Conf.:40th Annual Meeting*, 1979, Paper No. IWC-79-20
- [79] Hasson, D. and Bramson, D., *Ind. Engng. Chem. Proc.Des. Dev.*, 1985, **24**, 588
- [80] Dalas, E. and Koutsoukos, P.G., *J. Cryst. Growth*, 1989, **96**, 802
- [81] Levich, V.G., *Uspekhi Fizicheskikh Nauk*, 1966, **88**, 787
- [82] Evdokimov, V.B., *Zhurnal Fizicheskoi Khimii*, 1969, **43**, 2703
- [83] Limpert, G.J.C. and Raber, J.L., *Mater. Perform.*, 1985, **24**, 40
- [84] Gruber, C.E. and Carda, D.D., *WSA Research Report:Final Report*, Water Quality Assoc., 1981

- [85] Eliassen, D., Skrinde, R.T. and Davis, W.B., *J. Am. Wat. Works Assoc.*, 1958, **50**, 1371
- [86] Hasson, D. and Bramson, D., *Proc. Prog. Prevention of Fouling of Industrial Plant*, Nottingham, U.K., 1981, 217
- [87] Gonet, B., *Bioelectromagnetics*, 1985, **6**, 169
- [88] Kubat, J. and Söderlund, G., *Z. Phys. Chem. Neue Folge*, 1968, **62**, 180
- [89] Evdokimov, V.B., *Russian J. Phys. Chem.*, 1969, **43**, 1521
- [90] Klassen, V.I., *Developments in Mineral Processing, Part B, Mineral Processing*, 1981, 1077
- [91] Saam, R.D., *California: Civil Engineering*, Port Hueneme
- [92] Joshi, K.M. and Kamat, P.V., *J. Ind. Chem. Soc.*, 1966, **43**, 620
- [93] Krylov, O.T., Vikulova, I.K., Eletsii, V.I., Rozno, N.A. and Klassen, V.I., *Coll. J. USSR*, (English translation of *Kolloidnyi Z.*), 1985, **47**, 820
- [94] Raisen, E., *Corrosion 84*, NACE, Houston, 1984, Paper No. 117
- [95] Busch, K.W., Busch, M.A., Parker, D.H., Darling, R.E. and McAtree, J.L. Jr., *Corrosion 85*, NACE, Houston, 1985, Paper No. 251
- [96] Ozeki, S., Wakai, C. and Ono, S., *J. Phys. Chem.*, 1991, **95**, 10557
- [97] Donaldson, J.D., *Finishing*, 1988, **12**, 22
- [98] Bruk, O.B., Klassen, V.I. and Krylov, O.T., *Sov. Surf. Engng. Appl. Electrochim.*, (English translation of *Elektronnaya Obrabotka Materialov*), 1987, **6**, 45
- [99] Kochmarskii, V.Z., Kul'skii, L.A. and Krivtsov, V.V., *Sov J Wat. Chem. Technol.*, 1982, **4**, 32
- [100] Krivtsov, V.V., Kochmarskii, V.Z. and Kul'skii, L.A., *Sov. J. Wat. Chem. Technol.*, 1982, **4**, 25
- [101] Sinezuk, B.D., Fedoruk, T.Ya and Mal'ko, S.V., *Sov. J. Wat. Chem. Technol.*, 1987, **9**, 407
- [102] Söhnle, O. and Mullin, J., *Chem. Indus.*, 1988, **11**, 356
- [103] Ellingsen, F.T. and Kristiansen, H., *Vatten*, 1979, **35**, 309
- [104] Mitterand, P.G., *Sep. Processes Sugar Ind. Proc. S.P.R.I. Workshop*, 1996, 228

- [105] Busch, K.W., Busch, M.A., McAtree, J.L., Darling, R.E. and Parker, D.H., *Report by the American Petrol Institute*, Washington DC, 1985, Report No. 960
- [106] Busch, K.W., Busch, M.A., Parker, D.H., Darling, R.E. and McAtree, J.L., *Corrosion*, 1986, **42**, 211
- [107] Belova, V., *Societ Sci. Rev. Scient. Devel. USSR*, 1972, **3**, 150
- [108] Srebrenik, S., Nadiv, S. and Lin, I.J., *Magn. Electric. Sep.*, 1993, **5**, 71
- [109] Gamayunov, N.I., *J. Appl. Chem. USSR*, 1983, **56**, 975
- [110] Cole, F. and Clark, M.A., *Int. Sug. J.*, 1996, **98**, (1166), 71
- [111] Pandolfo, L., Colalé, R. and Paiaro, G., *La Chimica E L'Industria*, 1987, **69**, (11), 88
- [112] Higashitani, K., Oshitani, J. and Ohmura, N., *Colloid Surfaces A:Physiochem. Eng. Aspects*, 1996, **109**, 167
- [113] Ohgaki, K., Makihara, Y. and Sangawa, H., *Chem. Eng. Sci.*, 1994, **49**, (6), 911
- [114] Gehr, R., Zhai, Z.A., Finch, J.A. and Rao, R., *Wat. Res.*, 1995, **29**, 933
- [115] Ledion, J., Leroy, P., Labbe, J.P., Durand, G. and Le Duigou, A., *Mater. Techn.*, 1980, **8**, 139
- [116] Donaldson, J.D., *Brewers Guardian*, 1990, (7), 20
- [117] Donaldson, J.D., *Eurocorr 94/UK Corrosion 94*, Bournemouth, U.K., 1994
- [118] Barret, R.A. and Parsons, S.A., *Wat. Res.*, 1998, **32**, (3), 609
- [119] Costa Ribeiro, J., *Acad. Bras. Sci. An.*, 1950, **22**, 325
- [120] Evans, G.J., *J. Chem. Soc. Faraday Trans. I*, 1984, **80**, 2343
- [121] Evans, M.W., *Mat. Res. Bull.*, 1989, **24**, 1557
- [122] Woolfson, M.M., *An introduction to X-Ray Crystallography*, Cambridge University Press, 1970
- [123] Ebsworth, E.A., Rankin, D.W.H and Cradock, S., *Structural Methods in Inorganic Chemistry*, 2nd Ed., Blackwell Scientific Publications, 1991
- [124] Dodd, J.W. and Tong, K.H., *Thermal Methods*, John Wiley and Sons, 1987
- [125] Pope, M.I. and Judd, M.D., *Differential Thermal Analysis*, Heydon & Sons Ltd, 1977
- [126] Experimental Techniques Centre, Brunel University, SEM Preparation and Basic

Operation manual, 1996

[127] Royal Microscopical Society, Polarised Light Microscopy Course Notes, 1981

[128] Williams, D. H. and Fleming, I., *Spectroscopic Methods of Organic Chemistry*, 4th Ed., McGraw-Hill, London, 1989

2.0 SUCROSE STUDY SUMMARY

This chapter introduces the background of sucrose, its structure, standard crystalline forms, the concept of crystallisation mechanism, solubility, and other crystalline forms.

A full account of the experimental conditions for each experiment is given.

The chapter is divided into four sections:

Preliminary studies on static sucrose crystal growth: *The initial investigation of sucrose forms obtained under the static conditions of study evaluated and techniques for examination of the sucrose crystals were explored.*

Controlled conditions, static crystallisation of sucrose: *The conditions of static sucrose crystal growth were optimised and sucrose crystals were grown in a range of magnetic fields and strengths. The crystals were analysed using several analytical techniques. Sucrose crystals grown in the presence of an applied magnetic field were shown to contain additional water within the crystal lattice that was most likely to be sucrose hydrate rather than trapped syrup. In addition improved regular crystalline forms and enhanced nucleation and growth at lower supersaturations were observed.*

Magnetic treatment of sucrose where the solution is pumped: *A set of dynamic magnetic treatment of sucrose solutions were carried out. The sucrose solutions were passed through an applied magnetic field and then crystallised. Similar improvements in crystalline forms, and enhancement of nucleation and growth were observed however the interaction of the solution with an electromagnetic field associated with the pump was assumed since the 'Control' experiment gave evidence of magnetic treatment. Two grades of sucrose were used in this study, normal and analytical grades. The difference in the effects observed indicated that the observed magnetic treatment effects were not a result of action of the magnetic field on impurity ions.*

Magnetic treatment of sucrose where the solution is syphoned: *The dynamic magnetic treatment of sucrose solutions was repeated without the pump via syphoning on both grades of sucrose. The results reinforced the presence of the associated electromagnetic field from the pump since no effects were observed in the 'Control' study. The strongest applied field effects were observed on normal grade sucrose crystals.*

2.1 INTRODUCTION

Sucrose (along with salt) is in the unique position of being not only a very important foodstuff, but also a mass-produced chemical in industry. A very high degree of purity can be obtained through use of its crystallisation properties that have been studied for generations.

2.1.1 History

Sugar refining is thought^[1] to have been performed as early as 500A.D. in Persia where the term *kandi-sefid*, meaning white sugar, was used and the implication being that white sugar can only be obtained from refined crystallised sugar. In addition, the Indians used the term *shekar* or *shakey* as an early form of the word sugar that probably refers to evaporated juice known as *gur*. It is assumed since then, that the separation of crystals from mother liquor has been studied using drainage under gravity.

The early years of the nineteenth century saw further advances in sugar refinement following the development of the vacuum pan, the centrifuge and decolorisation techniques. Their use allowed growth of fairly regular crystals rapidly and without serious decomposition and colour formation. Well formed uniform crystals were still sought, as this would aid separation from the syrup under normal gravity or under centrifugal drainage.

Today, many additional techniques are used to give improved and accelerated refining processes.^[2-6] The work presented in this chapter is more concerned with the technology of the crystallisation of sucrose therefore a brief background to the theory of factors relevant to sucrose crystallisation are given.

2.1.2 Structure of sucrose

Sucrose has the molecular formula $C_{12}H_{22}O_{11}$ (see Figure 2.1.1) and forms crystals belonging to the monoclinic system, characterised by three unequal axes of which the b

and c axes are mutually perpendicular whilst the a axes makes an angle of $103^{\circ}30'$ with the c axis. [7-10]

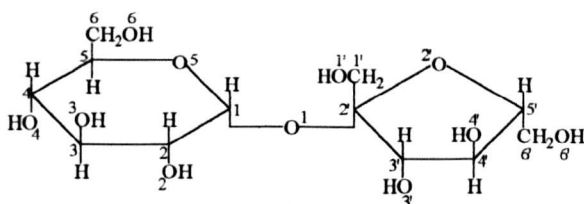


Fig. 2.1.1 Structure of sucrose.

A typical sucrose crystal grown from a pure aqueous-sucrose solution is shown in Figure 2.1.2.

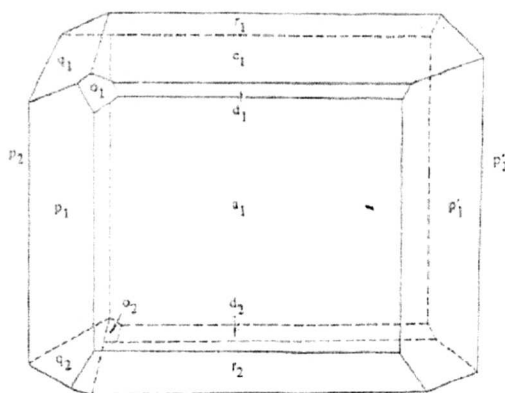


Fig. 2.1.2. A typical sucrose crystal.

Although the crystal has an axis of symmetry which coincides with the b-axis, it shows marked hemi-morphic properties in crystallography as chemically and physically one end of the crystal is different from the other along the b-axis. This difference not only becomes apparent in the variety of the observed simple forms and in the size and quality of the faces, but it also shows up in solution rates, growth rates, the shape of etching figures, the piezo- and thermo-electric behaviour, etc.

Figure 2.1.2 shows only 8 face pairs as these are the most important and frequent forms but there are altogether 15 simple face pairs or forms that have been identified. A great variety of shapes have been recorded arising from the very large number of probable combinations of forms which depend on specific growth environment. Much work was undertaken by Kukhareno^[11] whose detailed study provided the basis of sucrose crystallisation.

Cross-sectional representations of the crystal normal to the c axis and b axis are given below in Figures 2.1.3(a) and (b).

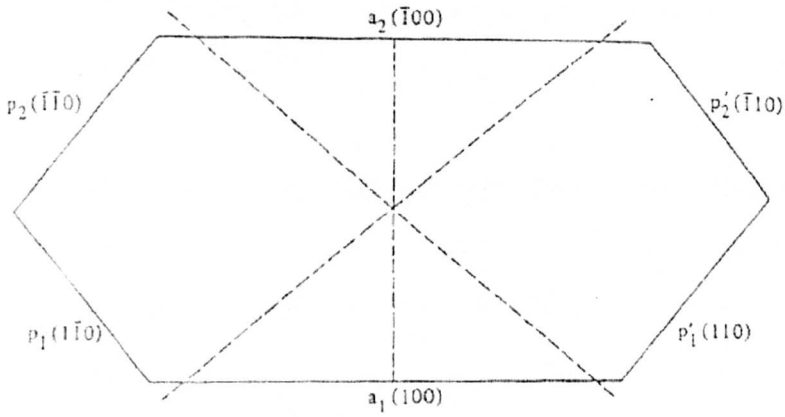


Fig. 2.1.3(a). Cross-section of a Kukharenko crystal normal to the c-axis.

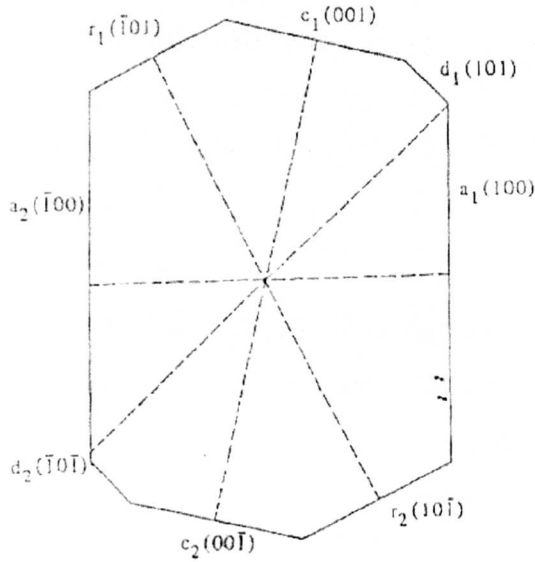


Fig. 2.1.3(b). Cross-section of a Kukharenko crystal normal to the b-axis.

Kukharenko also provided a substantial amount of data on the influence of impurities on over all growth rates. However this was not complemented with the corresponding morphological information and therefore could not be related to the influence of impurities on the growth rate of individual faces. Other authors^[12-15] have published a great deal of information on specific impurity effects.

Kukharenko recorded his kinetic information in terms of the relationship between surface area and weight, however a sphericity concept^[16] is more generally used in connection

with sugar morphology studies. This is defined as the ratio of the surface area of a sphere of the same volume as the crystal to the actual surface area of the crystal. By this definition, the shape factor for the Kukharenko crystals corresponds to 0.87, slightly more spherical than a cube which has sphericity.

Kukharenko devised a nomenclature system for the faces of the sucrose crystals (shown in Figures 2.1.3) but the more generally accepted are those adopted by Vavrinecz^[12] and Seager.^[15] In addition, Miller indices for the faces are used for general ease of recognition.

2.1.3 Crystallisation mechanism

The sucrose crystal growth is thought occur via a polar mechanism, rather than simple hydrogen bonding, resulting in the consideration that weak covalent bonds are formed. The hydroxyls are considered to be polarised into anionic and cationic sites at the oxygen and hydrogen atoms respectively. It is believed that the active sites for crystal growth are the anionic sites exposed on the sucrose molecule.

Kinetic studies^[17] have shown that crystal growth is controlled by the rate at which a single sucrose molecule fits itself into the crystal structure. However, there will be competition between sucrose and water molecules to become attached to the active anionic sites. In the event that a water molecule becomes attached, the anionic site of the water molecule has three possibilities, (a) it can be neutralised by a neighbour on the same sucrose molecule, (b) it can add to itself another water molecule, or (c) it can add to another sucrose molecule that is ready to crystallise. Therefore if the activity of sucrose and water is considered to be similar, there is a one in three chance of the crystal growing sucrose or adding a further water molecule.

In all sugar solutions, the concentration of water molecules is far greater than sucrose molecules e.g. a saturated solution at 9-10°C has a ratio of 10:1 for water:sucrose molecules. However, there are eight possible polar sites on a sucrose molecule compared

to just one for a water molecule, i.e. a sucrose solution of 10% oversaturation at 30°C would give sucrose more advantage in crystallisation.

If a sucrose surface in contact with water is considered, the water molecule has two alternative mechanisms to hydrogen bond to the sucrose molecule. The classical route is where one of the hydrogen atoms of the water molecule is bonded to an oxygen atom of a hydroxyl group of the sucrose, and hydrogen bonding is propagated through water molecules that are attached to the surface of the sucrose crystal (see Figure 2.1.4(a)).

The other mechanism is to consider the hydrogen bonding through the association of the oxygen of the first water molecule with the hydrogen of a neighbouring sucrose hydroxyl. In this mechanism, the first molecule becomes a link in perpetuating a sheath of water molecules or can become a water inclusion (see Figure 2.1.4(b)).

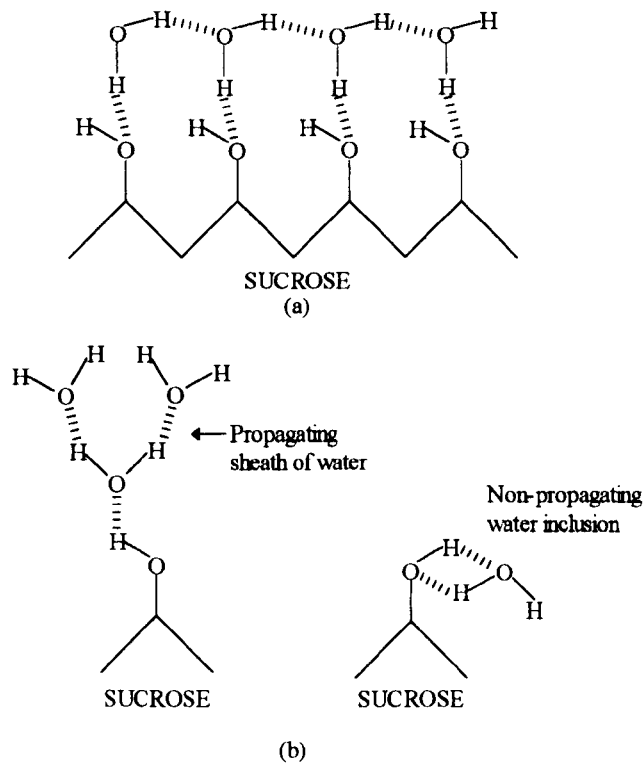


Fig. 2.1.4 Mechanisms of sucrose crystal surface equilibration with water.

Within sucrose crystal growth, a large amount of kinetic crystal data is available for larger crystals. However, nucleation and the initial stages of growth are difficult to model and have in fact been derived from extrapolation of data from larger crystals.

A crystal nucleus is considered to be a hexameric unit i.e. made up of 6 sucrose molecules. This is the minimum number needed to satisfy crystallographic molecular structure and morphology requirements which are important prerequisites of crystal development.

Examination of the hexameric unit from comparison with a fully grown crystal shows that there are only 26 actual exposed bonding sites (not the theoretical 42) available for crystal growth exposed by the common face pairs. There is a difference of 16 active bonding sites that will obviously be propagated in the growth process.

The sucrose molecule is considered to utilise $7\frac{1}{2}$ hydroxyls for crystalline bonding resulting in 15 ($7\frac{1}{2} \times 2$) active sites. The hexamer nucleus would therefore have 90 active sites (15×6) and have 26 active sites for crystal growth and utilize the other 64 for the internal crystalline bonding.

Comparison of hydroxyl bond distances within crystalline sucrose to other similar hydroxyl bonded crystals e.g. phenols, alcohols, tartaric acid $(\text{CHOHCOOH})_2$ ^[18] shows that they are much longer than found in many known organic crystals. The relatively weak bonding is also reflected in its high solubility in water.

The dissolution of one sucrose molecule from a crystal at 26°C has been calculated to require only 9 water molecules to form a sufficiently strong hydroxyl bond to detach it from its crystal which is a surprisingly small number.^[19]

Kukharenko^[11] has reported on the measurement of dissolution rates of sucrose crystals immersed in undersaturated solutions however, there has been surprisingly little work reported in the literature since then as the focus has been on crystal growth. It is more generally known that dissolution results in rounding of crystal edges and the formation of etch pits on crystal surfaces.

It is straightforward to express growth and dissolution rates in dimensions of area, time and concentration, however it is the definition of surface area which is uncertain resulting in measurement uncertainties. Surface roughness must also be taken into consideration.

2.1.4 The solubility of sucrose

It has been established for many years that sugar will readily form supersaturated solutions and the existence of at least three zones has been postulated (see Fig. 2.1.5).^[20,21]

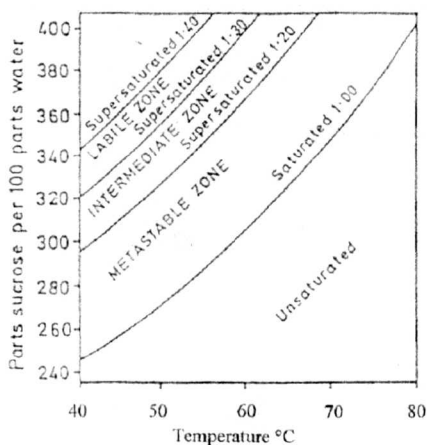


Fig. 2.1.5 Supersaturation curves for sucrose.

The three zones beyond the saturated solution are firstly a region called the metastable zone, where a sugar will crystallise on to existing crystals (growth) but will not spontaneously crystallise (nucleate). Above this region is an intermediate zone where existing crystals will continue to grow, but also new crystals will form in the presence of existing crystals (nucleation). Finally there is a labile zone where crystals will form spontaneously. Thus, spontaneous nucleation would appear to be related to the presence of hydrogen bonding sites which are unoccupied by water and therefore available to form sucrose/sucrose bonds.^[22,23]

There are in general two main reasons for interest in solubility of sucrose; (1) to know how much sucrose there is in a particular solution i.e. concentration, and (2) to be able to specify the degree of oversaturation or undersaturation for the purpose of studying crystallisation. The most satisfactory relationship for establishing the latter is to know the molal concentration (or its equivalent in g sucrose/g water) of the actual solution under

study and the ratio of this concentration to the corresponding concentration of the saturated solution at the same temperature.

$$\text{Degree of over saturation} = \frac{\text{Concentration of solution}}{\text{Concentration of saturated solution}}$$

Generally, equilibration between water and sucrose must be achieved before solubility measurements can be carried out at a specific temperature. There are two documented methods to determine this equilibrium point. The first involves the angle of reflection of a beam of light from the surface of a crystal in the solution as the temperature is changed. A clearly defined change in the angle of reflection is associated with the saturation temperature.^[24,25] The second method involves microscopic observations at the edge of a chip of a sucrose crystal around the saturation temperature. As the temperature of the solution is raised, the temperature at which the edge of the chip starts to dissolve is recorded as the saturation temperature.^[19]

Both of these methods require the concentration of a specific solution to be known to a high degree of precision that in practice has been particularly difficult to achieve. Several authors have endeavoured to satisfy this criterion using various methods of measurement, however large differences have been recorded.^[19,24,26,27,28-36] The saturation of sucrose is thought to be merely a point in the solubility system and the complexity and irregularities of the system are accepted as being an effect of the smaller, more mobile water molecules rather than the sucrose molecules.

It is assumed that in a dilute sucrose solution the molecules are mostly in a monomeric condition, but as the concentration increases approaching saturation the probability of polymer formation could be expected to increase until finally the hexamers appear. It is thought that a sucrose crystal cannot form until hexamers are present, i.e. hexamers are present in over-saturate the solutions but not in under-saturated solutions. It is also thought that there may be sucrose dimers and trimers present in solution as sucrose crystallisation develops but there is no evidence to support this theory.

Kukhareenko's studies^[11] mentioned 'crystallones' which he considered to be made available during the process of solution at high concentrations but did not occur when solutions were at low concentrations. This is considered to be early observations of the formation of hexamers.

2.1.5 Additional crystalline forms of sucrose

2.1.5 (a) Sucrose thin films^[37]

When considering crystallisation of sucrose in thin films, the degree of supersaturation is a crucial factor that must be considered. Sugar technologists rarely refer to supersaturation levels above 1.3 when considering vacuum pan crystallisations. Solutions that are exposed to extreme drying conditions produce supersaturations of 2 to possibly above 10 at the interface and result in an amorphous glass being formed on the surface of the solution. At these higher levels of supersaturation the rate of crystallisation is progressively retarded and exhibits a very low vapour pressure that may take days, weeks or months to crystallise by dehydration.^[38]

A sucrose crystal, dried far too rapidly to keep pace with concentration, may achieve a very low Equilibrium Relative Humidity^[39] and may include an appreciable amount of water of solution. Crystallisation will take place extremely slowly, the surface layer will exhibit a rising E. R. H. and an increasing amount of the solution water will be able to send water molecules into the surrounding air space. This reaction would proceed more rapidly at higher E. R. H. levels, thus producing the unexpected phenomenon that sugar submitted to too extreme drying conditions may take longer to equilibrate than that dried under milder conditions.

The quantity of water concerned is small, around 0.02 to 0.06% and in some cases the water can remain in the form of inclusions within the crystal structure.^[40,41]

Thin films of syrup exposed to an atmosphere of controlled humidity resulting in molecular evaporation may produce very high degrees of supersaturation (SS) where

nucleation may be slow (in the absence of mechanical nucleation). When nucleation does occur the nuclei produced at about 1.5 to 2.0 SS are predominantly euhydral with euhydral growth and can show some signs of internal disorder (see Fig. 2.1.6). At 2.0 to 3.0 SS multicrystals known to crystallographers as spherulites are observed (see Fig. 2.1.7). By 4.0 SS all nuclei appear to be spherulitic. In the case of spherulites, the component crystals appear to radiate from a common origin, and each ray is a single crystal with recognition of the usual interfacial angles possible. Under suitable conditions these growths are dendritic (branched) and rhythmic, the pattern being repeated again and again.



Fig. 2.1.6 Euhydral nucleation and growth has become well established before syrup has attained the degree of SS which lead to spherulitic nucleation.

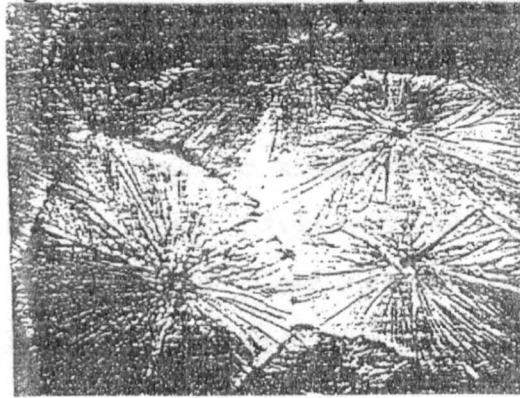


Fig 2.1.7 Well-spaced spherulitic nucleation resulting in radialitic growth.

Experimental thin film crystallisation may be classified under three headings according to the nature of the bounding media:

- (A) Glass or plastic (relatively inert) - thus, **glass/syrup/glass**
- (B) Atmosphere with controlled humidity (this facilitates migration of the molecules to or

from the film) - thus, **glass/syrup/atmosphere**

(C) sucrose cleavage faces (offering or receiving sucrose molecules to or from the film) - thus, **sucrose crystal/syrup/atmosphere**.

The research in this thesis is concerned only with thin films crystallisation of type (B) which is by far the most variable. A thin film of syrup will be able to freely interchange water molecules with the surrounding atmosphere and the initial formation of nuclei only takes place when a suitable number of sugar molecules have by chance come together: hence the first appearance of nuclei will be approximately proportional to the amount of syrup.

Thin films of this type can be grown from very high SS (1 to 10) and the vapour pressure can be controlled by various means, for example, by using moistened salts, or sulphuric acid or glycerine etc. Nucleation and growth appear to be maximal at about 3SS; at 1.5SS the rate is slower whilst at 10SS nucleation will be unlikely to occur.

2.1.8 (b) Sucrose hydrates

It is generally accepted that sucrose forms exclusively anhydrous crystals, however during the study of the sucrose-water phase diagram at temperatures of 0° to -34°C, this was found to be not to be the case and that there were some circumstances that resulted in the formation of sucrose hydrates.^[42] A sucrose hemipentahydrate - $C_{12}H_{22}O_{11} \cdot 5/2 H_2O$ and a sucrose hemiheptahydrate - $C_{12}H_{22}O_{11} \cdot 7/2 H_2O$ were isolated and characterised. Both hydrates demonstrated specific powder X-ray diffraction patterns distinct from the anhydrous phase and melting points of 45.7° and 27.8°C respectively. Progressively decreasing the temperature was shown to result in increasing complexity of the metastability characteristics of the system, especially on approach of the ice eutectic where no less than eight solid phases seemed to be possible in addition to the anhydrous phase. Unfortunately, these additional phases were not positively identified.

2.2 METHODOLOGY AND EXPERIMENTAL TECHNIQUES

The Differential Scanning Calorimetry (DSC) was carried out using a Perkin Elmer DCS7. The powder X-Ray Diffraction was carried out using a Philips PW 1710 diffractometer with Cu K_α radiation. The Scanning Electron Microscopy was carried out using a Cambridge 5250 stereoscan. The Karl Fischer was carried out using an Orion Research Inc. Turbo 2 Titrator. The incubators used in the studies were SANYO MIR 152 and operated at a range of $\pm 0.5^{\circ}\text{C}$ to the set temperature. The peristaltic pump used was used at a flow speed of 11.42mlmin^{-1} . Thermogravimetry (TG), Differential Thermogravimetry (DTG), and Differential Thermal Analysis (DTA) were measured on a Stanton Redcroft STA 780 Simultaneous Thermal Analyser. All crystals prepared in this work were crystallised under the conditions listed.

2.2.1 Aims

The aim of this study was to demonstrate that the crystallisation of sucrose could be affected by applied magnetic fields. The study was concerned with the changes in crystal form of the resulting sucrose crystals rather than changes in the rate of crystallisation.

2.2.2 Methodology

At the outset of the study, it was important to become familiar with sucrose solutions, solubility and crystal forms, in addition to establishing the optimum conditions for study. The preliminary studies were carried out to determine the optimum conditions for the incubator temperature, concentration and volume of the crystallising sucrose solution in order to obtain a standard, reproducible sucrose crystal form suitable for comparison with sucrose crystals grown under applied magnetic fields conditions.

Following the preliminary study, a full static crystallisation of sucrose in applied magnetic fields study was carried out under suitably controlled conditions. Characterisation of the resulting sucrose crystals was carried out using Differential Scanning Calorimetry (DSC), Powder X-ray Diffraction (Powder XRD), Scanning Electron Microscopy (SEM),

Polarising Light Microscopy (PLM), simultaneous Thermogravimetry (TG), Differential Thermogravimetry (DTG) and Differential Thermal Analysis (DTA), Solid State Nuclear Magnetic Resonance (NMR) techniques in addition to recording visual observations.

2.2.3 Preliminary static crystallisation studies

Solutions of sucrose were prepared in 5cm petri dishes on a hot plate at 50°C by addition of sucrose to a minimum volume of de-ionised water until no more sucrose could be dissolved during a 10 min period. In the cases of over-addition of sucrose, more water was added to take the sucrose into solution. The sucrose solutions contained in the petri-dishes, were placed in incubators at 50°C where they were left to evaporate and crystallise under different magnetic fields listed below. The sucrose used was from Fisher Scientific and was Normal grade purity (impurities <0.132%).

2.2.3(a) Experiment 1 - Control

No magnetic field around the petri-dish containing the crystallising sucrose solution.

2.2.3(b) Experiment 2 - Weakest permanent field, at sides in parallel

Permanent magnets were placed in parallel as shown in Fig. 2.2.1. The 5cm diameter petri dish containing the crystallising sucrose solution was placed in the centre between the magnets on a raised platform. The field strengths were measured using a Gaussmeter and found to be ~300G at the edges of the petri dish and ~265G at the centre.

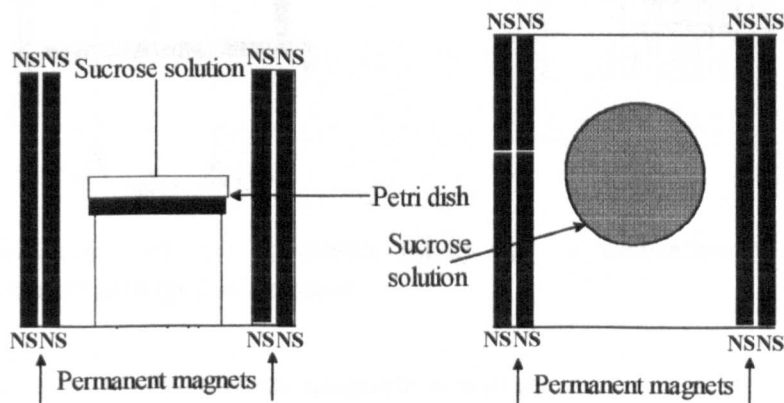


Fig. 2.2.1 Illustration of the apparatus set-up for crystallisation under a permanent field, parallel at sides of sample.

2.2.3(c) Experiment 3 - 2nd weakest permanent field, at sides in parallel

Permanent magnets were placed in parallel as shown in Fig. 2.2.1. The 5cm diameter petri dish containing the crystallising sucrose solution was placed in the centre between the magnets on a raised platform. The field strengths were measured using a Gaussmeter and found to be $\sim 400\text{G}$ at the edges of the petri dish and $\sim 350\text{G}$ at the centre.

2.2.3(d) Experiment 4 - 2nd strongest permanent field, at sides in parallel

Permanent magnets were placed in parallel as shown in Fig. 2.2.1. The 5cm diameter petri dish containing the crystallising sucrose solution was placed in the centre between the magnets on a raised platform. The field strengths were measured using a Gaussmeter and found to be $\sim 640\text{G}$ at the edges of the petri dish and $\sim 540\text{G}$ at the centre.

2.2.3(e) Experiment 5 - Strongest permanent field, at sides in parallel

Permanent magnets were placed in parallel as shown in Fig. 2.2.1. The 5cm diameter petri dish containing the crystallising sucrose solution was placed in the centre between the magnets on a raised platform. The field strengths were measured using a Gaussmeter and found to be $\sim 760\text{G}$ at the edges of the petri dish and $\sim 630\text{G}$ at the centre.

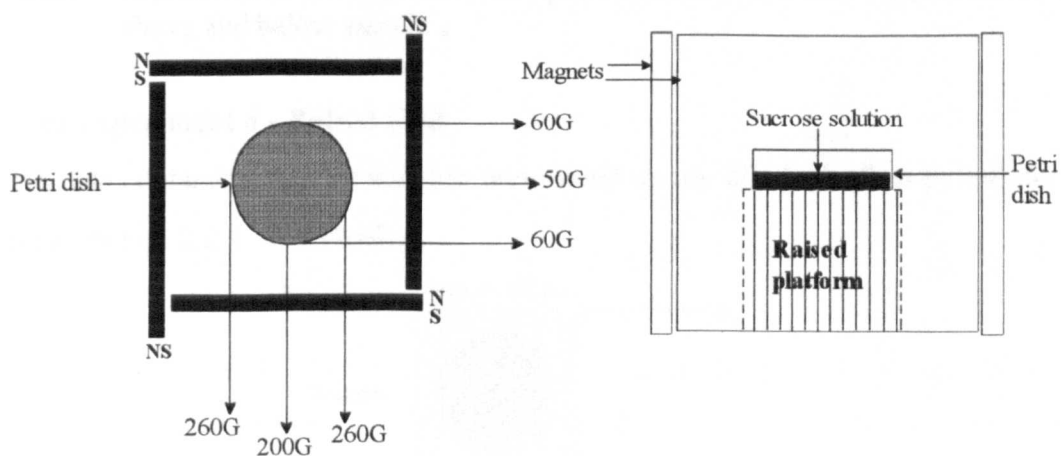


Fig. 2.2.2 Illustration of the apparatus set-up for crystallisation under permanent magnets arranged in a square

2.2.3(f) Experiment 6 - Permanent magnets in square

Permanent magnets were placed in a square as shown in Fig. 2.2.2. The 5cm diameter petri dish containing the crystallising sucrose solution was placed at the centre of the

magnets on a raised platform. The field strengths, measured using a Gaussmeter, are illustrated.

2.2.3(g) Experiment 7 - Permanent field, in parallel above and below

Permanent magnets were placed in parallel as shown in Fig. 2.2.3. The 5cm diameter petri dish containing the crystallising sucrose solution was placed in the centre between the magnets on a raised platform. The field strengths were measured using a Gaussmeter and found to be ~60G at the edges of the petri dish and ~60G at the centre.

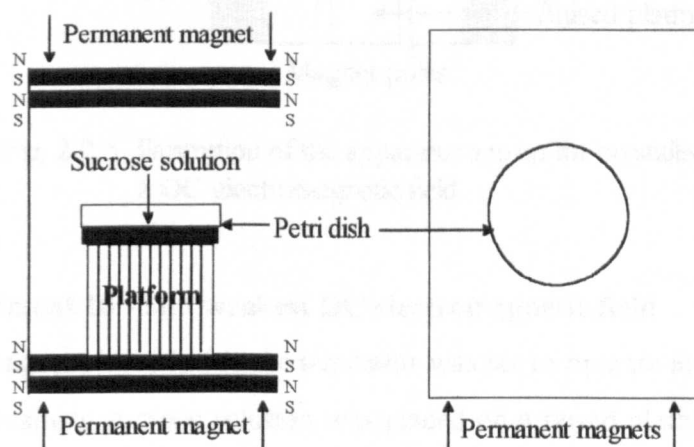


Fig. 2.2.3 Illustration of the apparatus set-up for crystallisation under a permanent field, above and below sample.

2.2.3(h) Experiment 8 - Pulsed field

A petri dish containing sucrose solution was placed on top of a hydroflow pulsed magnet, as shown in Fig. 2.2.4, to crystallise.

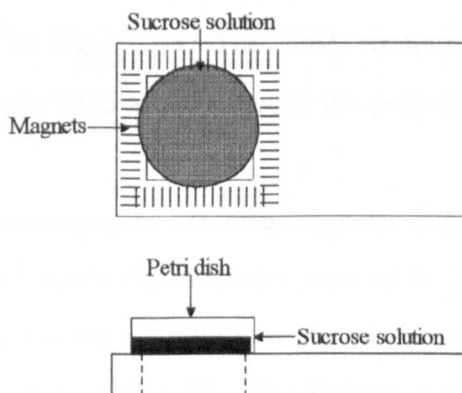


Fig. 2.2.4 Illustration of the apparatus set-up for crystallisation under a pulsed magnetic field.

2.2.3(i) Experiment 9 - Weakest DC electromagnetic field

A DC electromagnet placed inside the incubator was set to operate at 2.0V (2.93mA), and a petri dish containing sucrose solution was placed on a raised platform between the two magnet poles as shown in Fig. 2.2.5. The field strengths were measured using a Gaussmeter and found to be ~100G at the edges of the petri dish and ~50G at the centre.

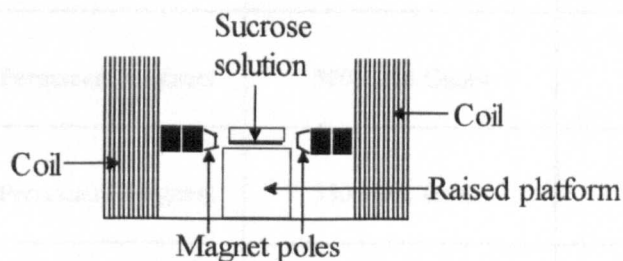


Fig. 2.2.5 Illustration of the apparatus set-up for crystallisation under a DC electromagnetic field.

2.2.3(j) Experiment 10 - 2nd weakest DC electromagnetic field

A DC electromagnet placed inside the incubator was set to operate at 5.0V (2.93mA), and a petri dish containing sucrose solution was placed on a raised platform between the two magnet poles as shown in Fig. 2.2.5. The field strengths were measured using a Gaussmeter and found to be ~320G at the edges of the petri dish and ~140G at the centre.

2.2.3(k) Experiment 11 - 2nd strongest DC electromagnetic field

A DC electromagnet placed inside the incubator was set to operate at 8.0V (2.93mA), and a petri dish containing sucrose solution was placed on a raised platform between the two magnet poles as shown in Fig. 2.2.5. The field strengths were measured using a Gaussmeter and found to be ~500G at the edges of the petri dish and ~195G at the centre.

2.2.3(l) Experiment 12 - Strongest DC electromagnetic field

A DC electromagnet placed inside the incubator was set to operate at 10.0V (2.93mA), and a petri dish containing sucrose solution was placed on a raised platform between the two magnet poles as shown in Fig. 2.2.5. The field strengths were measured using a Gaussmeter and found to be ~600G at the edges of the petri dish and ~220G at the centre.

Visual observations of the resulting crystals in each case were recorded. The magnets used in each experiment are summarised in Table 2.2.1.

Experiment No.	Field Type	Frequency/Strength	Geometry
1	Control	N/A	N/A
2	Permanent magnets	300 - 265 Gauss	N-S, NH Parallel at sides
3	Permanent Magnets	350 - 400 Gauss	N-S, NH Parallel at sides
4	Permanent magnets	540 - 640 Gauss	N-S, NH Parallel at sides
5	Permanent magnets	630 - 760 Gauss	N-S, NH Parallel at sides
6	Permanent magnets	50 - 260 Gauss	N-S, NH Square
7	Permanent magnets	60 Gauss	N-S, H Above and below
8	Pulsed	100-160 kHz	N-S, NH Below
9	DC Electromagnet	50 - 100 Gauss	N-S, NH Parallel at sides
10	DC Electromagnet	140 - 320 Gauss	N-S, NH Parallel at sides
11	DC Electromagnet	195-500 Gauss	N-S, NH Parallel at sides
12	DC Electromagnet	220 - 600 Gauss	N-S, NH Parallel at sides

Table 2.2.1 Applied field configurations used in preliminary static crystallisation sucrose studies, where N-S=North-South geometry, NH=Non homogeneous, and H=Homogeneous.

2.2.4 Controlled conditions, static crystallisation investigation

Experiments were performed using the procedures described in 2.2.3 with the following exceptions. A known weight of sucrose (4.69g) was added to de-ionised water (10ml) to prepare a 0.8S saturated solution and the solutions contained in the petri dishes were heated on a hot-plate at 50°C for two hours until fully dissolved. Samples were prepared free of dust or foreign material by covering the petri dishes during the sucrose dissolution. The petri dishes were placed uncovered in the incubator and the incubator door remained closed during the crystallisation process.

Each experiment was repeated 3 times (Experiments 13 to 24) resulting in samples 13A, 13B, 13C to 24A, 24B and 24C. The magnets used in each experiment are summarised in Table 2.2.2. Visual observations of the resulting crystals were noted in addition with analysis of the resulting crystals using Powder X-ray Diffraction (Powder XRD), Scanning Electron Microscopy (SEM), Differential Scanning Calorimetry (DSC), Polarising Light Microscopy (PLM) and Karl Fischer moisture content equipment.

Experiment No.	Field Type	Frequency/Strength	Geometry
13	Control	N/A	N/A
14	Permanent magnets	300 - 265 Gauss	N-S, NH Parallel at sides
15	Permanent Magnets	350 - 400 Gauss	N-S, NH Parallel at sides
16	Permanent magnets	540 - 640 Gauss	N-S, NH Parallel at sides
17	Permanent magnets	630 - 760 Gauss	N-S, NH Parallel at sides
18	Permanent magnets	50 - 260 Gauss	N-S, NH Square
19	Permanent magnets	60 Gauss	N-S, H Above and below

20	Pulsed	100-160 kHz	N-S, NH Below
21	DC Electromagnet	50 - 100 Gauss	N-S, NH Parallel at sides
22	DC Electromagnet	140 - 320 Gauss	N-S, NH Parallel at sides
23	DC Electromagnet	195-500 Gauss	N-S, NH Parallel at sides
24	DC Electromagnet	220 - 600 Gauss	N-S, NH Parallel at sides

Table 2.2.2 Applied field configurations used in controlled conditions sucrose studies using normal grade sucrose, where N-S=North-South geometry, NH=Non homogeneous, and H=Homogeneous.

2.2.5 Magnetic treatment of sucrose where the solution is pumped

The literature documents^[49] that effects of applied fields are maximised around 5 or 6 passes through a magnetic field, so the dynamic study involved the recirculation of the solution, up to 8 times through the magnetic field with an aliquot of sample being removed following each pass and then allowed to crystallise. In this study therefore, the number of passes through the field and the resulting effect on the sucrose crystals could be studied in order to establish whether or not it was an important factor worth consideration.

The literature on applied magnetic field effects describes several theories^[105-110] behind the phenomenon observed (Section 1.2.5(d)) including the supposition that ‘contamination effects’ lead to magnetically enhanced dissolution. In the ‘dynamic’ application of magnetic fields therefore, two grades of sucrose were used, (1) normal grade sucrose, which has impurities <0.132%, and (2) analytical grade sucrose, which has impurities <0.013%. Any changes in the crystals grown under the same conditions will determine whether impurity effects are important or relevant or not in this study of applied field phenomena of crystallising sucrose solutions.

A peristaltic pump was used in this study since the effects of vibration from the pump would be minimised, since a motorised pump would have associated agitation effects.

2.2.5(a) Normal grade sucrose

An 0.8S saturated stock solution (4.66g per 10ml at 50°C) of normal grade sucrose (impurities <0.132%) was prepared and stored at 50°C in an incubator.

Experiment 25 - Control

Sucrose solution (200ml) in a storage bottle, within the incubator at 50°C, was passed through the silicon tubing (1m of 4mm diameter) via a peristaltic pump into a second storage bottle and 10ml were removed using a pipette, placed in a petri dish with the lid on and labelled Sample 1. The positions of the delivery and receiving bottles was reversed and the procedure repeated to give Sample 2. This was carried out a total of 8 times and after each pass 10ml aliquots of sucrose solution was removed and placed in a petri dish. The time taken to perform the procedure was 60 mins. The samples were then transferred to a second incubator set at 50.0°C containing 1kg of blue silica gel on a shelf at the bottom, the lids were removed and the solutions were allowed to crystallise. This procedure was repeated resulting in samples 25(1) to 25(8) each in duplicate.

The procedure described for Experiment 25 was repeated for the field studies with silicon tubing passing through the centre of the magnetic fields indicated in Table 2.2.3 below and is illustrated in Fig. 2.2.6.

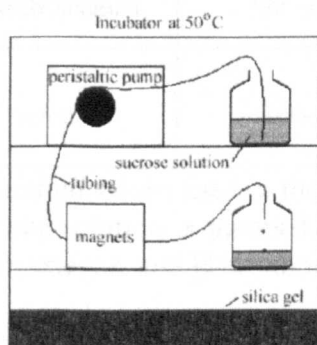


Fig. 2.2.6 Illustration of the apparatus used in Experiments 25 to 50.

Experiment No.	Field Type	Frequency/Strength	Geometry
26	Permanent magnets	265 - 300 Gauss	N-S, NH Parallel at sides
27	Permanent Magnets	350 - 400 Gauss	N-S, NH Parallel at sides
28	Permanent magnets	540 - 620 Gauss	N-S, NH Parallel at sides
29	Permanent magnets	630 - 760 Gauss	N-S, NH Parallel at sides
30	AC electromagnet	240MHz	N-S, NH Parallel at sides
31	DC Electromagnet	50 - 100 Gauss	N-S, NH Parallel at sides
32	DC Electromagnet	100 - 220 Gauss	N-S, NH Parallel at sides
33	DC Electromagnet	150 - 340 Gauss	N-S, NH Parallel at sides
34	DC Electromagnet	190 - 500 Gauss	N-S, NH Parallel at sides
35	DC Electromagnet	220 - 600 Gauss	N-S, NH Parallel at sides
36	DC Electromagnet	300 - 680 Gauss	N-S, NH Parallel at sides
37	Pulsed	100-160 kHz	N-S, NH Below

Table 2.2.3 Applied field configurations used in the magnetic treatment of normal grade sucrose where the solution is pumped, where N-S=North-South geometry, NH=Non homogeneous, and H=Homogeneous.

Visual observations of the resulting crystals were recorded for all Experiments 25 to 37 inclusive. Differential Scanning Calorimetry was carried out only on samples from

Experiments 25, 26, 27, 29, 30, 31, 33, 36 and 37. Scanning Electron Microscopy (SEM) was carried out on a selection of samples from these experiments.

2.2.5(b) Analytical grade sucrose

Experiments 38 to 50 were performed under the same format as the normal grade sucrose studies but using analytical grade sucrose from Fisher Scientific (impurities <0.0113%), resulting in samples 38(1) to 38(8) to 50(1) to 50(8) each in duplicate. The magnets used in each experiment are summarised in Table 2.2.4. Visual observations of the resulting crystals were recorded for all Experiments 38 to 50 inclusive. Differential Scanning Calorimetry (DSC) was carried out only on samples from Experiments 38, 39, 40, 42, 43, 44, 46, 49 and 50. Scanning Electron Microscopy was carried out on a selection of samples from these experiments.

Experiment No.	Field Type	Frequency/Strength	Geometry
38	Control	N/A	N/A
39	Permanent magnets	265 - 300 Gauss	N-S, NH Parallel at sides
40	Permanent Magnets	350 - 400 Gauss	N-S, NH Parallel at sides
41	Permanent magnets	540 - 620 Gauss	N-S, NH Parallel at sides
42	Permanent magnets	630 - 760 Gauss	N-S, NH Parallel at sides
43	AC electromagnet	240MHz	N-S, NH Parallel at sides
44	DC Electromagnet	50 - 100 Gauss	N-S, NH Parallel at sides
45	DC Electromagnet	100 - 220 Gauss	N-S, NH Parallel at sides

46	DC Electromagnet	150 - 340 Gauss	N-S, NH Parallel at sides
47	DC Electromagnet	190 - 500 Gauss	N-S, NH Parallel at sides
48	DC Electromagnet	220 - 600 Gauss	N-S, NH Parallel at sides
49	DC Electromagnet	300 - 680 Gauss	N-S, NH Parallel at sides
50	Pulsed	100-160 kHz	N-S, NH Below

Table 2.2.4 Applied field configurations used in the magnetic treatment of analytical grade sucrose where the solution is pumped, where N-S=North-South geometry, NH=Non homogeneous, and H=Homogeneous.

2.2.6 Magnetic treatment of sucrose where the solution is syphoned

2.2.6(a) Normal grade sucrose

An 0.8S saturated stock solution (4.66g per 10ml at 50°C) of normal grade sucrose (impurities <0.132%) was prepared and stored at 50°C in an incubator.

Experiment 51 - Control

Sucrose solution (200ml) in a storage bottle, within the incubator at 50°C, was passed through the silicon tubing via syphoning through silicon tubing (im of 4mm diameter), into a second storage bottle and 10ml were removed using a pipette, placed in a petri dish with the lid on and labelled Sample 1. The positions of the delivery and receiving bottles was reversed and the procedure repeated to give Sample 2. This was carried out a total of 8 times resulting in 8 petri dishes each containing 10ml aliquots of sucrose solution. The time taken to perform the procedure was 60 mins. The samples were then transferred to a second incubator set at 50.0°C, and allowed to crystallise. This procedure was repeated resulting in samples 51(1) to 51(8) each in duplicate.

The procedure described for Experiment 51 was repeated for the field studies with silicon tubing passing through the centre of the magnetic fields (indicated in Table 2.2.5) as illustrated in Fig. 2.2.7.

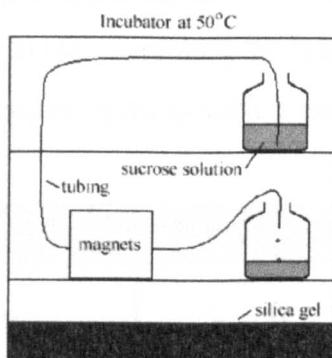


Fig. 2.2.7 Illustration of the apparatus used in Experiments 51 to 60.

Experiment No.	Field Type	Frequency/Strength	Geometry
52	Permanent magnets	630 - 760 Gauss	N-S, NH Parallel at sides
53	AC electromagnet	240MHz	N-S, NH Parallel at sides
54	DC Electromagnet	300 - 680 Gauss	N-S, NH Parallel at sides
55	Pulsed	100-160 kHz	N-S, NH Below

Table 2.2.5 Applied field configurations used in the magnetic treatment of normal grade sucrose where the solution is syphoned, where N-S=North-South geometry, NH=Non homogeneous, and H=Homogeneous.

Visual observations of the resulting crystals were recorded for all Experiments 51 to 60 inclusive. Scanning Electron Microscopy (SEM) was carried out on a selection of samples. Differential Scanning Calorimetry (DSC) was carried out only on one set of duplicated samples.

2.2.6(b) Analytical grade sucrose

Analytical grade sucrose was again used in the syphoning study to investigate 'contamination effect' of applied fields. Experiments 56 to 60 were performed under the same format as the normal grade sucrose studies but using analytical grade sucrose from Fisher Scientific (impurities <0.0113%), resulting in samples 56(1) to 56(8) to 60(1) to 60(8) each in duplicate. The magnets used in each experiment are summarised in Table 2.2.6.

Experiment No.	Field Type	Frequency/Strength	Geometry
56	Control	N/A	N/A
57	Permanent magnets	630 - 760 Gauss	N-S, NH Parallel at sides
58	AC electromagnet	240MHz	N-S, NH Parallel at sides
59	DC Electromagnet	300 - 680 Gauss	N-S, NH Parallel at sides
60	Pulsed	100-160 kHz	N-S, NH Below

Table 2.2.6 Applied field configurations used in the magnetic treatment of analytical grade sucrose where the solution is syphoned, where N-S=North-South geometry, NH=Non homogeneous, and H=Homogeneous.

Visual observations of the resulting crystals were recorded for all Experiments 56 to 60 inclusive. Scanning Electron Microscopy (SEM) was carried out on a selection of samples. Differential Scanning Calorimetry (DSC) was carried out only on one set of duplicated samples.

2.3 RESULTS AND DISCUSSION

The information obtained in the static study, although relevant, is of no practical use to Industry since there is no situation in production where a solution of sucrose would be allowed to crystallise statically. Standard production usually involves some form of stirring or mixing of the sucrose solutions in addition to pumping it along a length of pipe. With this in mind therefore, the study would be of far greater use and importance, if the magnetic fields were applied to a 'dynamic' situation. Since the stirring involves consideration of shear forces to the crystallising solution and can mechanically induce nucleation, a simpler arrangement would be to flow the sucrose solution through a magnetic field followed by static crystallisation. Analysis carried out on the resulting sucrose crystals could therefore be compared to the previous static crystallisation results.

2.3.1 Results

The results and data collected for each study are presented in the following sections (2.3.1 (a) to (d)) and are discussed at length in Section 2.3.2.

2.3.1(a) Preliminary studies on static crystal growth of sucrose solutions

The four thin film crystal forms obtained for sucrose under different conditions are illustrated below in Figures 2.3.1(a) to (d) and represent 'wedge' growth, 'dendritic' growth, 'euhydral' growth and 'glassy' forms respectively obtained in the preliminary study.

In all cases where the concentration of sucrose solution was greater than about 6g in 10ml water at 50°C (greater than 0.83S, S = saturated concentration which is 7.21g sucrose in 10ml water at 50°C) the glassy form of sucrose was obtained following 3 or 4 hours within the incubator. Catastrophic solidification (Fig. 2.3.1(d)) occurred on the surface of a very viscous sucrose solution and very little crystal form was observed other than the semi-hexagonal shapes illustrated.

The incubator was initially set at 50°C and the crystallisation time for a 10ml sucrose solution of 0.65S concentration (4.69g sucrose in 10ml water at 50°C) was around 24

hours. 50°C is the maximum operating temperature of the incubator and this was considered to be the most suitable for all experiments.

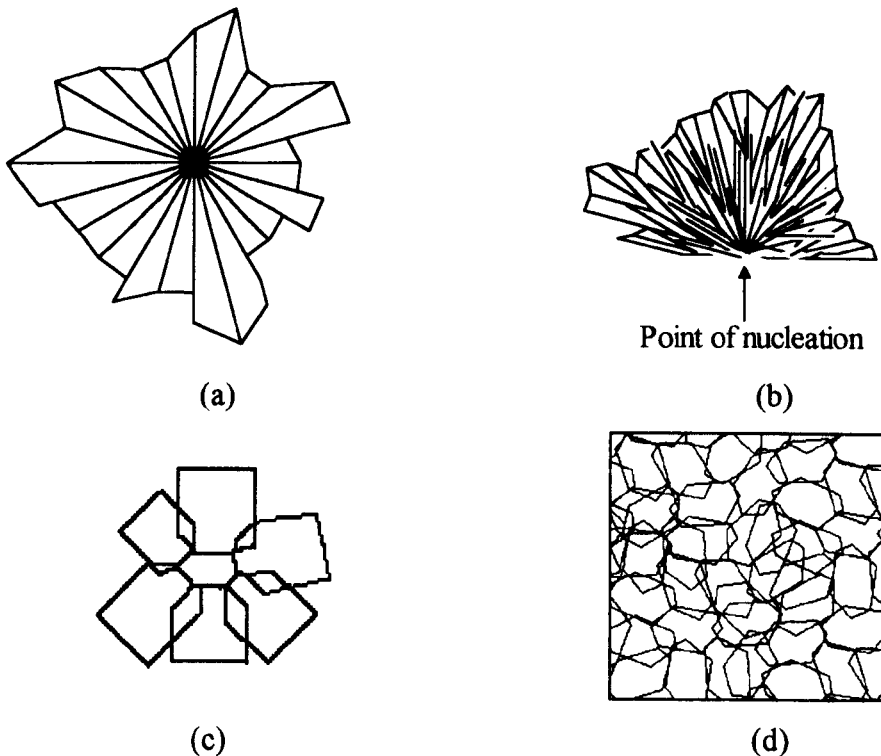


Fig. 2.3.1 Illustrations of the four thin film forms of sucrose obtained in the Preliminary investigation where (a) is wedge growth, (b) is dendritic growth, (c) is euhydral growth, and (d) is the glassy form.

10ml of sucrose solution within a 5cm diameter petri dish under the evaporation conditions within the incubator resulted in a thin film across the surface of the solution around 1-2mm thick with solution remaining trapped beneath the surface. Where the volume of solution was less than 10ml, the sucrose crystals would not form a complete layer across the surface and evaporation to dryness would occur resulting in areas of shapeless sucrose crystals. Where the volume of the solution was greater than 10ml the danger of spillage of solution over the sides of the petri dish made it impractical.

Therefore, the optimum conditions of growth were as follows: 10ml of sucrose solution at 0.65S concentration (4.69g per 10ml water), in a 5cm diameter petri dish, evaporated in a sealed incubator set at 50°C.

These conditions were applied to all cases of study in Experiments 1 to 12. The visual observations are recorded in Table 2.3.1 below.

Exp. No.	No. primary nucleations	No. secondary nucleations	Total no. nucleation centres	Crystal form		Time taken to crystallise
1	3	2	5	wedge	irregular and chunky	24 hours
2	3 or 4	3 or 4	6 to 8	wedge	fine	24 hours
3	4	1	5	wedge	fine needles	24 hours
4	4	0	4	wedge	regular	24 hours
5	1 or 2	1 or 2	2 to 4	wedge (dendritic)	large prim. wedges (small sec.)	24 hours
6	2	3 or 4	5 to 6	dendritic	fine needles	24 hours
7	3	0	3	wedge (dendritic)	large & regular (small & fine)	24 hours
8	3 or 4	4 or 5	7 to 9	wedge & dendritic	regular & well formed	24 hours
9	3	3 or 4	6 to 7	wedge & dendritic	fine wedges & needles	24 hours
10	5	3 or 4	8 to 9	dendritic	needles	24 hours
11	3 or 4	3 or 4	6 to 8	euhydral	flat, square plates	48 hours
12	10/11	0	10 to 11	euhydral	flat, square plates	72 hours

Table 2.3.1 A summary of the visual observations recorded in the preliminary studies in addition to rough estimates of time taken to crystallise.

2.3.1(b) Controlled conditions, static crystallisation of sucrose

The visual observations for this study are recorded below in Table 2.3.2 and the corresponding SEM and PLM photographs are presented in Figures 2.3.2 to 2.3.25 and 2.3.26 to 2.3.47 respectively. DSC data are given in Tables 2.3.3 and XRD patterns are presented in Figures 2.3.48 to 2.3.85.

Exp. No.	No. primary nucleations	No. secondary nucleations	Total no. nucleation centres	Crystal form		Time taken to crystallise
13	4	0 or 3	4 or 5	wedge	irregular and chunky	24 hours
14	3	4	7	wedge	fine	24 hours
15	4	1	5	wedge and dendritic	fine needles	24 hours
16	3	0	3	wedge	regular	24 hours
17	1 or 2	2 to 3	3 to 5	wedge and dendritic	large prim. wedges & small fine sec.	24 hours
18	2	0 or 1	2 to 3	dendritic	fine needles	24 hours
19	5	1	6	wedge & dendritic	large & regular prim. small fine sec.	24 hours
20	4	4 to 6	8 to 10	wedge (some euhydrat)	regular & well formed	24 hours
21	5	2 to 3	7 to 8	wedge & dendritic	fine wedges & needles	24 hours
22	5	3 to 6	8 to 11	dendritic	needles	24 hours
23	6	2 to 4	8 to 10	euhydrat	flat, square plates	48 hours
24	15 to 27	0	15 to 27	euhydrat	flat, square plates	72 hours

Table 2.3.2 A summary of the visual observations recorded in the controlled static crystallisation of sucrose studies in addition to rough estimates of time taken to crystallise.

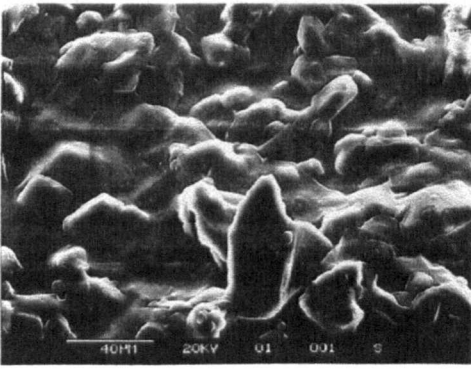


Fig. 2.3.2 SEM of sucrose Sample 13A.

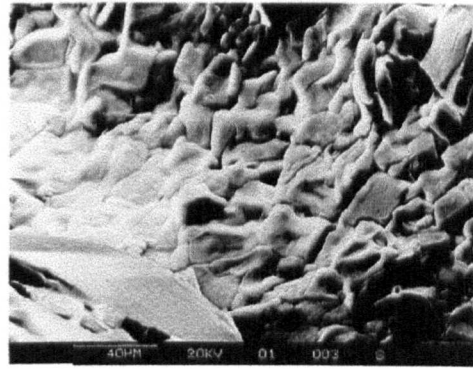


Fig. 2.3.3 SEM of sucrose Sample 13B.

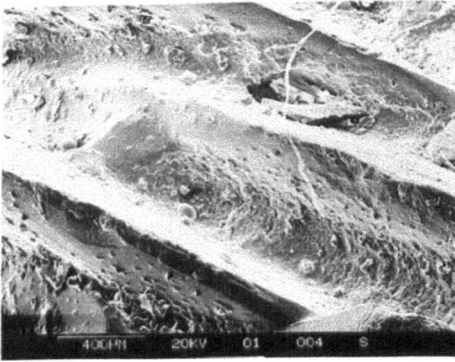


Fig. 2.3.4 SEM of sucrose Sample 13B.



Fig. 2.3.5 SEM of sucrose Sample 14B.

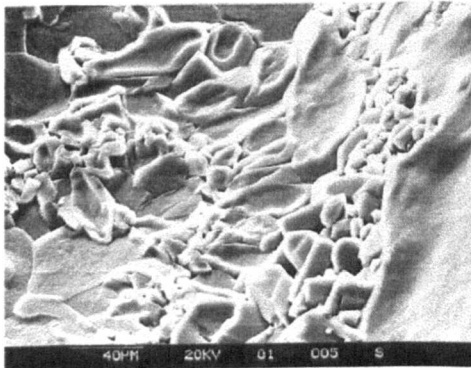


Fig. 2.3.6 SEM of sucrose Sample 14B.

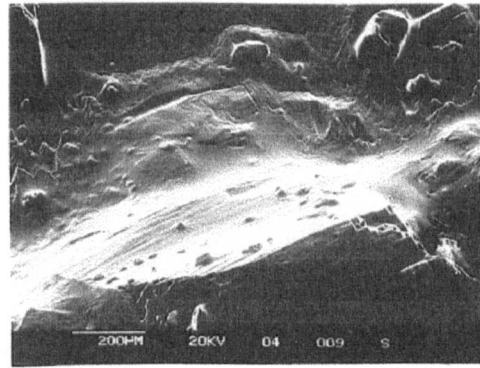


Fig. 2.3.7 SEM of sucrose Sample 15A.

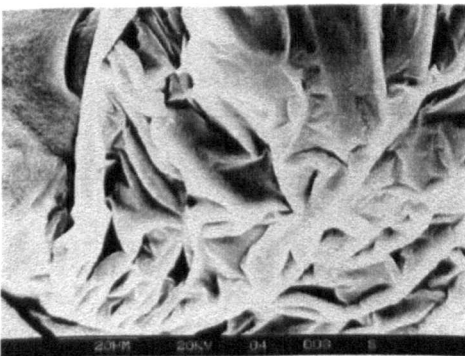


Fig. 2.3.8 SEM of sucrose Sample 15A.

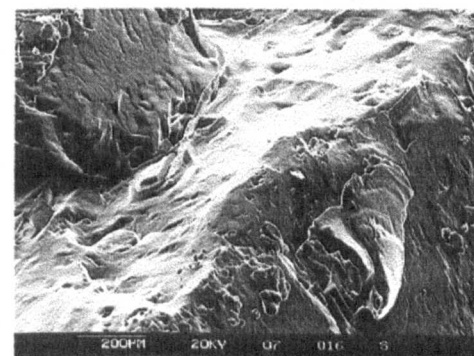


Fig. 2.3.9 SEM of sucrose Sample 16A.

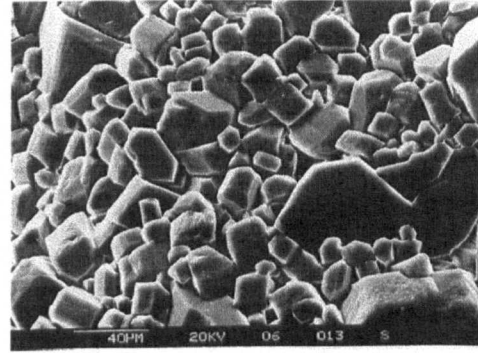
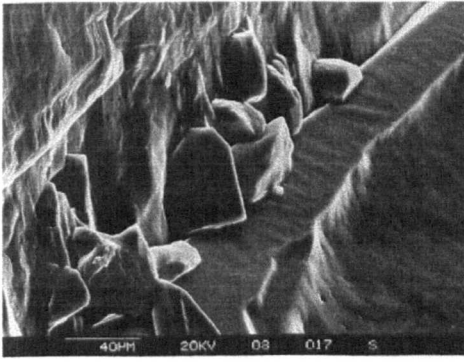


Fig. 2.3.10 SEM of sucrose Sample 16A. Fig. 2.3.11 SEM of sucrose Sample 17A.

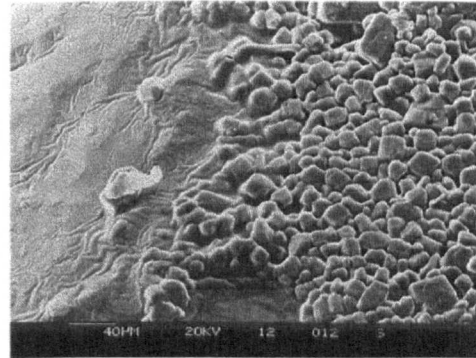
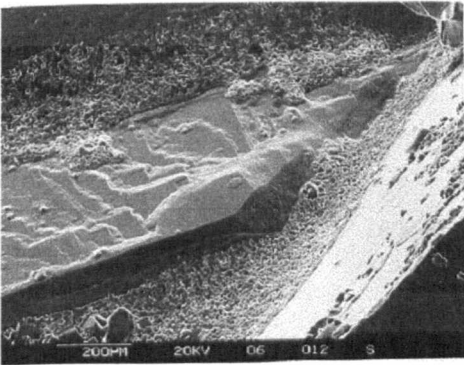


Fig. 2.3.12 SEM of sucrose Sample 17A. Fig. 2.3.13 SEM of sucrose Sample 18A.

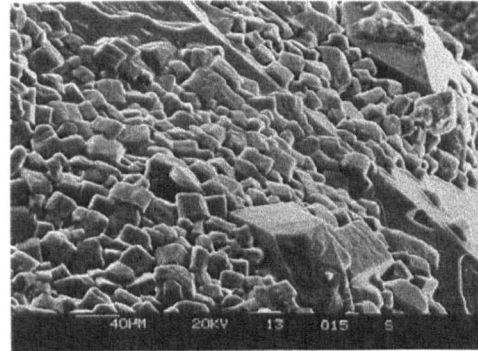
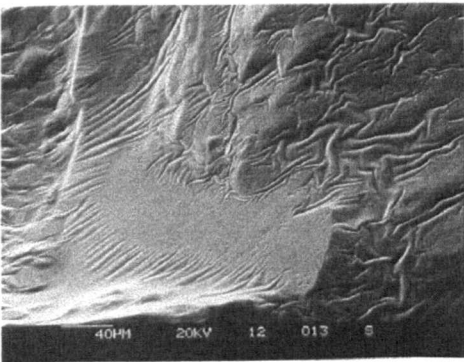


Fig. 2.3.14 SEM of sucrose Sample 18A. Fig. 2.3.15 SEM of sucrose Sample 19A.

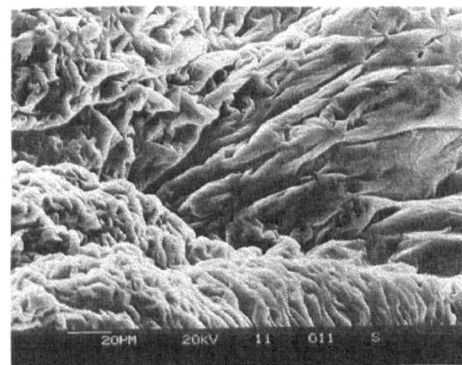
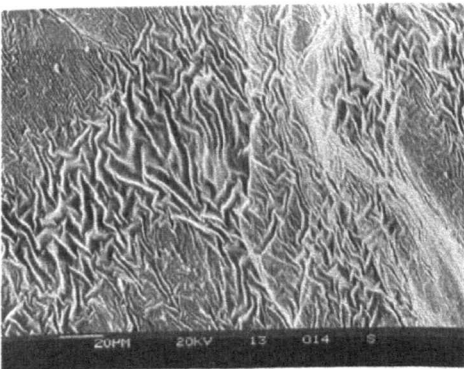


Fig. 2.3.16 SEM of sucrose Sample 19A. Fig. 2.3.17 SEM of sucrose Sample 20A.

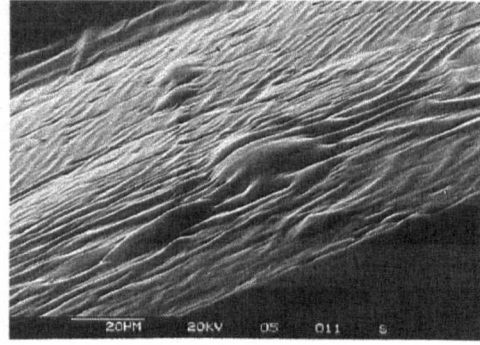
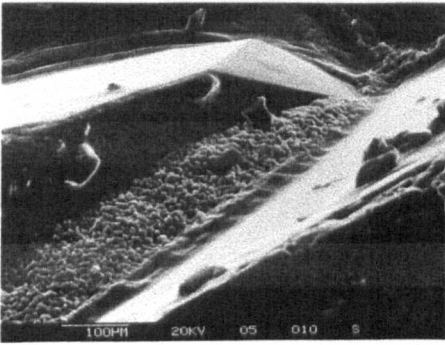


Fig. 2.3.18 SEM of sucrose Sample 21A. Fig. 2.3.19 SEM of sucrose Sample 21A.

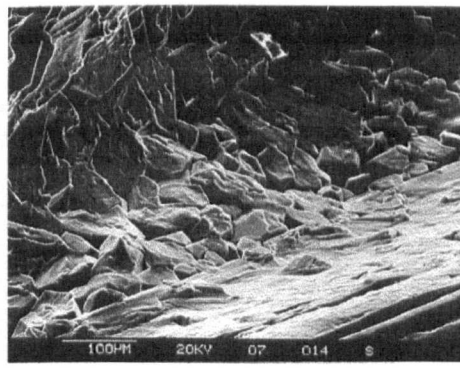
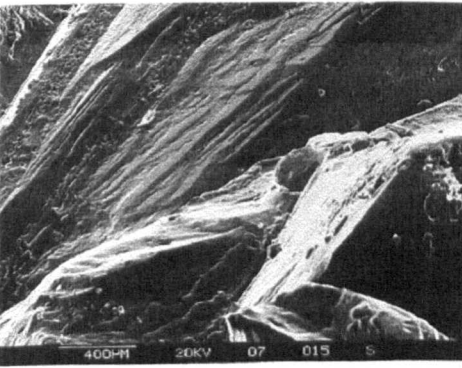


Fig. 2.3.20 SEM of sucrose Sample 22A. Fig. 2.3.21 SEM of sucrose Sample 22A.

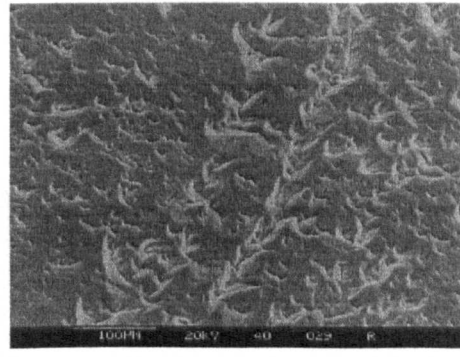
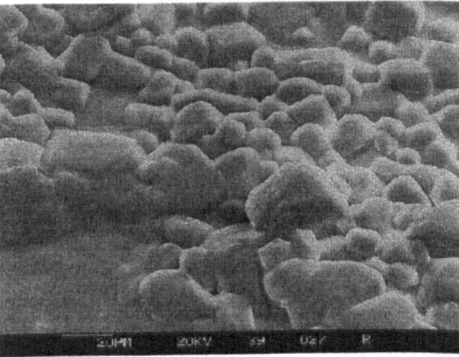


Fig. 2.3.22 SEM of sucrose Sample 23A. Fig. 2.3.23 SEM of sucrose Sample 23A.

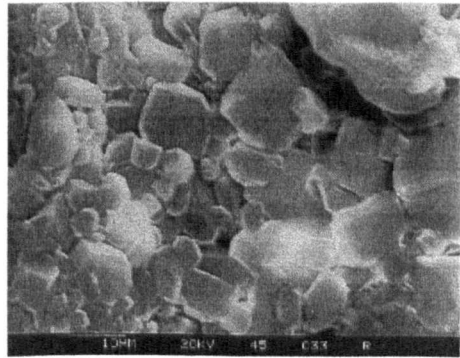
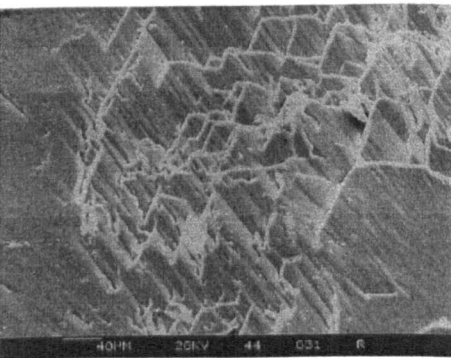


Fig. 2.3.24 SEM of sucrose Sample 24A. Fig. 2.3.25 SEM of sucrose Sample 24A.



Fig. 2.3.26 PLM of sucrose Sample 13D.

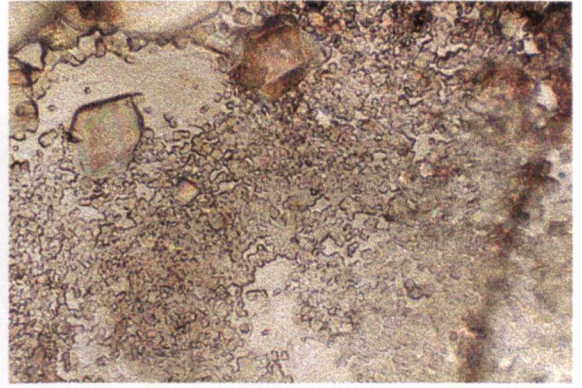


Fig. 2.3.27 PLM of sucrose Sample 14C.



Fig. 2.3.28 PLM of sucrose Sample 15C.

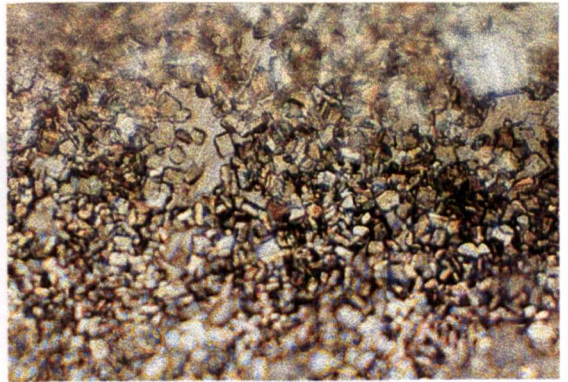


Fig. 2.3.29 PLM of sucrose Sample 16A.



Fig. 2.3.30 PLM of sucrose Sample 16B.

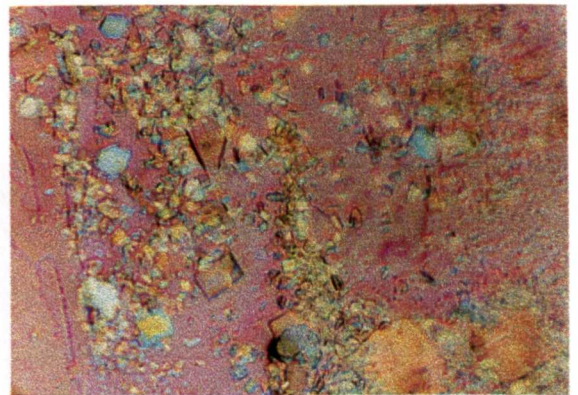


Fig. 2.3.31 PLM of sucrose Sample 17A.

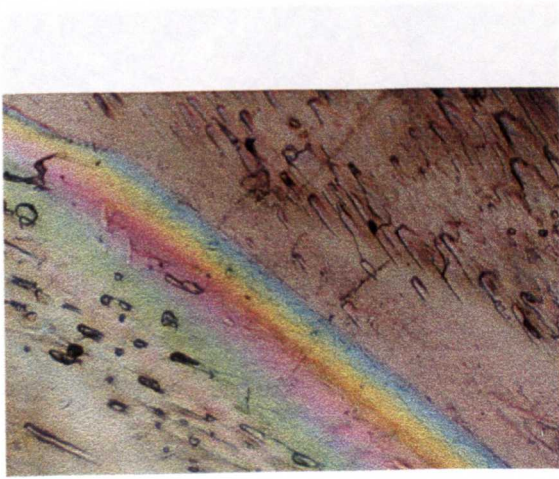


Fig. 2.3.32 PLM of sucrose Sample 17B.



Fig. 2.3.33 PLM of sucrose Sample 18A.

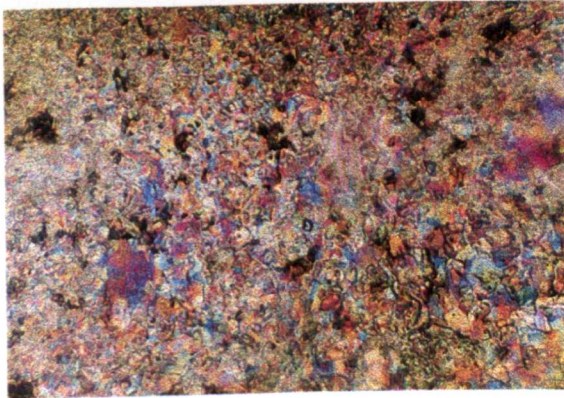


Fig. 2.3.34 PLM of sucrose Sample 18B.

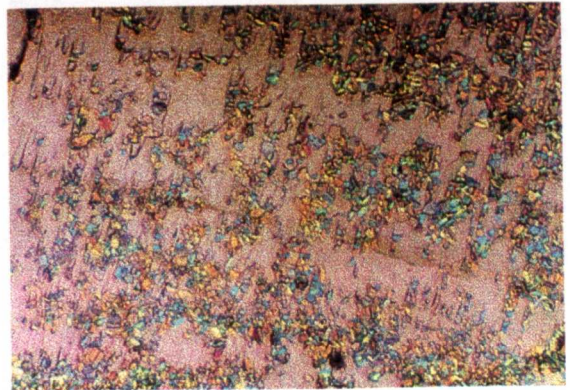


Fig. 2.3.35 PLM of sucrose Sample 18C.

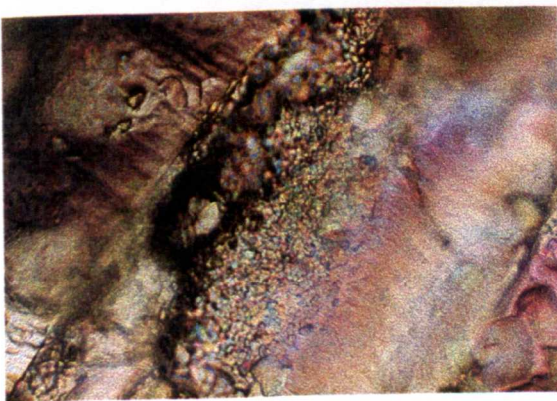


Fig. 2.3.36 PLM of sucrose Sample 19A.



Fig. 2.3.37 PLM of sucrose Sample 19B.

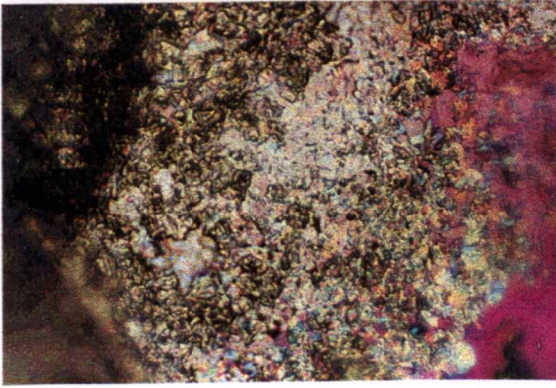


Fig. 2.3.38 PLM of sucrose Sample 20A.



Fig. 2.3.39 PLM of sucrose Sample 20B.



Fig. 2.3.40 PLM of sucrose Sample 21A.



Fig. 2.3.41 PLM of sucrose Sample 22A.

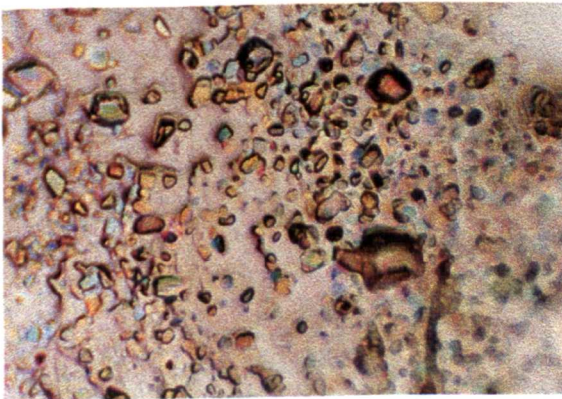


Fig. 2.3.42 PLM of sucrose Sample 22C.

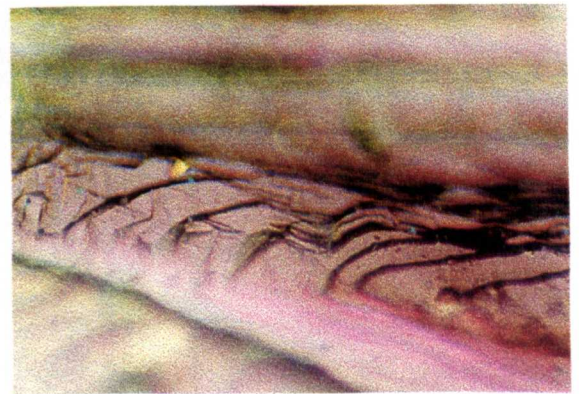


Fig. 2.3.43 PLM of sucrose Sample 23A.

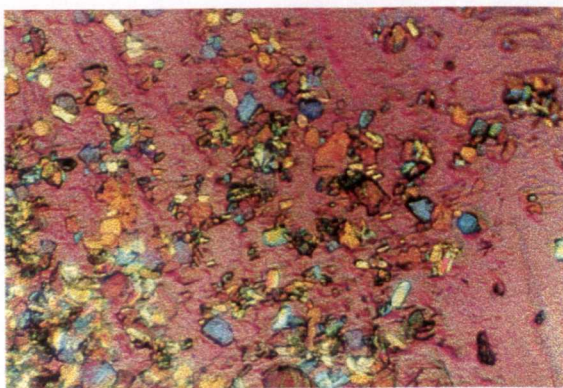


Fig. 2.3.44 PLM of sucrose Sample 23B.

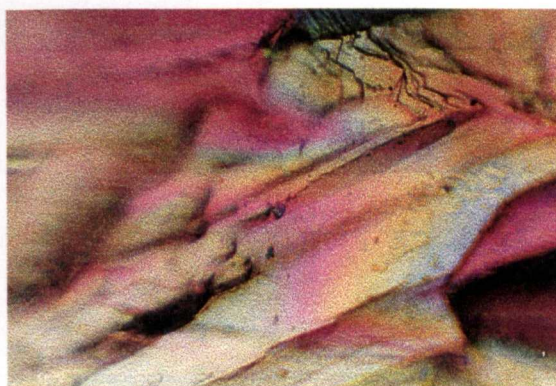


Fig. 2.3.45 PLM of sucrose Sample 23C.

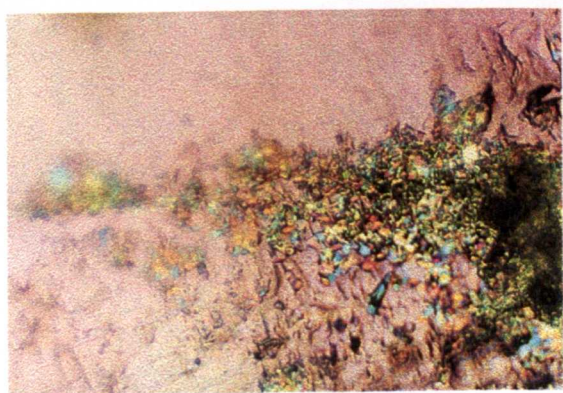


Fig. 2.3.46 PLM of sucrose Sample 24B.

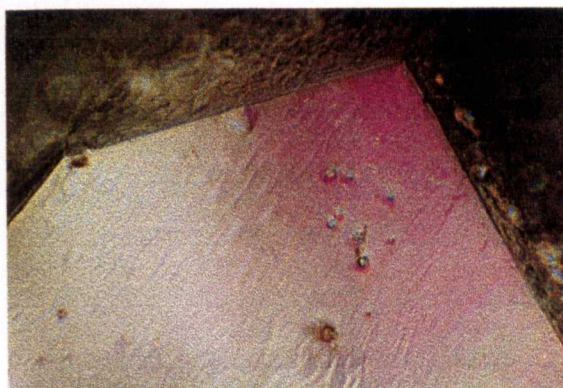


Fig. 2.3.47 PLM of sucrose Sample 24C.

Experiment	Sample A (°C)	Sample B (°C)	Sample C (°C)	Sample D (°C)	Sample E (°C)
13	182.346	182.373	186.334	180.006	184.547
14	180.803	179.067	185.226		
	152.80	152.80	153.80		
15	180.451	187.170	185.226		
		154.80	153.80		
16	182.724	176.912	180.043		
	160.00	147.95	155.40		
	153.90				
17	188.565	177.683	183.969		
	156.20	152.80	155.40		
18	177.896	186.414	178.968		
	153.80	155.40	153.80		
19	188.317	185.890	190.509		
	153.80	154.80			
20	179.389	186.501	185.063		
	153.80	153.80	153.80		

Experiment	Sample A (°C)	Sample B (°C)	Sample C (°C)
21	184.100	188.148	182.710
	153.80	153.80	154.80
22	178.933	180.304	176.948
	155.40	152.80	153.80
23	188.217	187.884	183.394
	152.80	157.40	157.40
24	180.266	177.453	182.822
	153.80	153.80	152.80

Table 2.3.3 DSC data for sucrose crystals grown in applied magnetic fields under static conditions.

2θ	d _i Å	I/I _o (I)
12.011	7.373	13
13.363	6.614	18
15.752	5.623	18
19.081	4.644	40
19.855	4.469	100
25.124	3.543	25
43.729	2.069	13

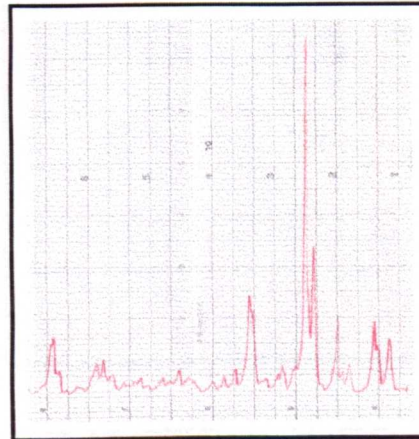


Fig 2.3.48 Powder XRD data for sucrose sample 13A.

2θ	d _i Å	I/I _o (I)
11.730	7.54	10
12.903	6.857	13
18.853	4.704	14
24.791	3.589	17
40.466	2.228	100

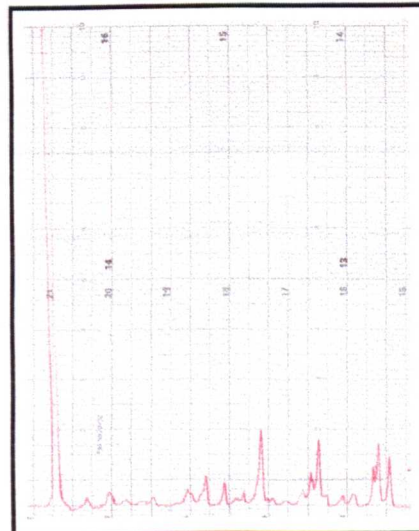
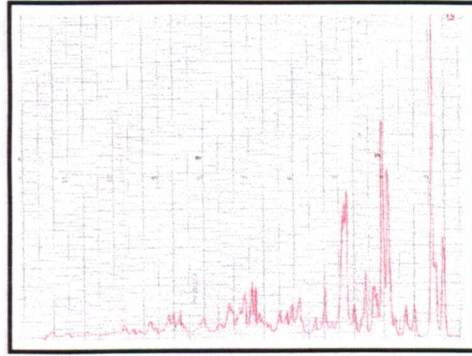


Fig. 2.3.49 Powder XRD data for sucrose sample 13B.

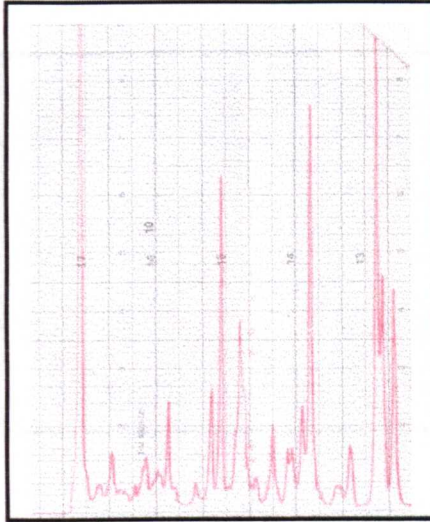
2θ	d_i Å	I/Io(I)
11.690	7.579	31
12.758	6.935	100
18.903	4.692	53
19.582	4.530	68
24.685	3.605	44
25.115	3.539	35

Fig. 2.3.50 Powder XRD data for sucrose sample 13C.



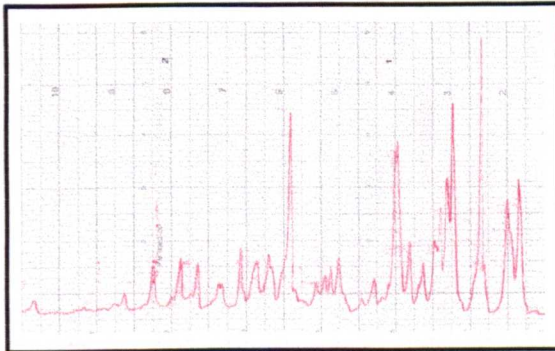
2θ	d_i Å	I/Io(I)
11.474	7.708	36
12.506	7.074	37
13.021	6.795	55
18.662	4.752	95
24.687	3.604	60
38.818	2.320	100

Fig. 2.3.51 Powder XRD data for sucrose sample 13D.



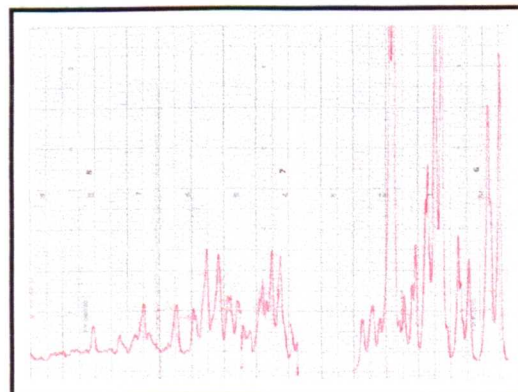
2θ	d_i Å	I/Io(I)
11.639	7.599	49
12.532	7.059	42
15.376	5.760	100
18.647	4.756	75
19.420	4.568	47
24.671	3.607	63
36.140	2.484	74

Fig. 2.3.52 Powder XRD data for sucrose sample 13E.



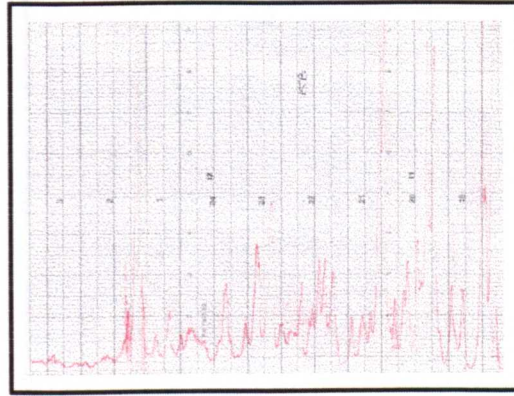
2θ	d_i Å	I/Io(I)
11.651	7.591	65
13.079	6.765	55
18.822	4.712	100
19.583	4.531	80
24.744	3.592	100
25.235	3.527	45

Fig. 2.3.53 Powder XRD data for sucrose sample 14A.



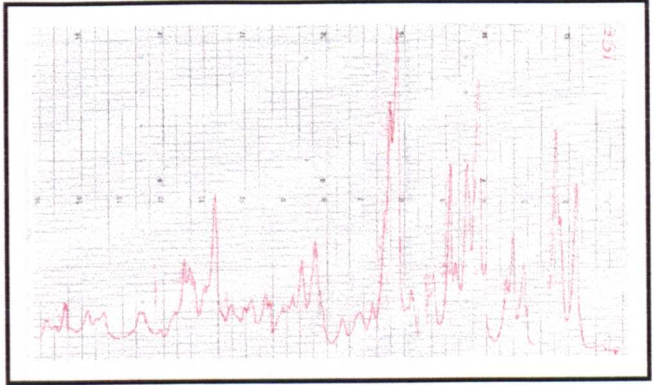
2θ	d_i Å	I/I ₀ (I)
11.679	7.573	65
13.140	6.734	55
18.831	4.710	100
19.579	4.532	80
24.795	3.589	100
25.266	3.523	45
43.679	2.072	100

Fig. 2.3.54 Powder XRD data for sucrose sample 14B.



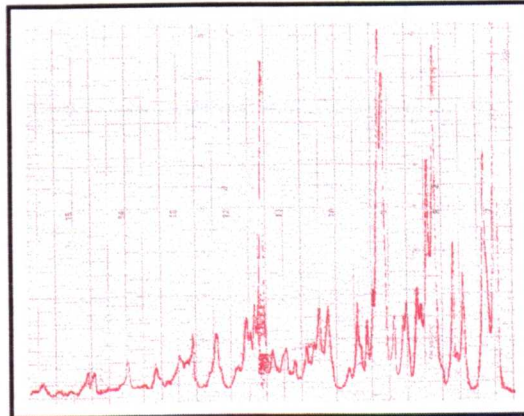
2θ	d_i Å	I/I ₀ (I)
11.611	7.617	50
13.187	6.710	68
18.873	4.699	81
19.617	4.523	56
20.807	4.269	56
24.804	3.588	100

Fig. 2.3.55 Powder XRD data for sucrose sample 14C.



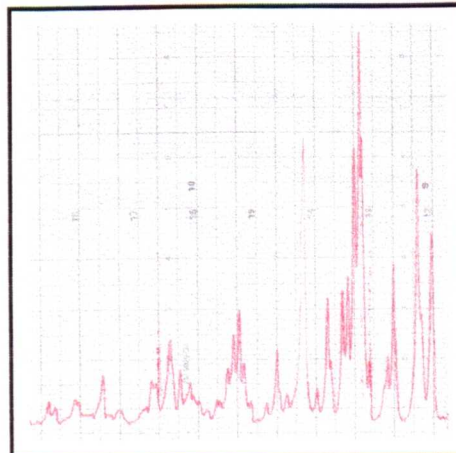
2θ	d_i Å	I/I ₀ (I)
11.984	7.381	100
13.442	6.584	55
19.195	4.621	75
19.911	4.452	50
24.959	3.568	70
25.066	3.551	80
38.737	2.323	74

Fig. 2.3.56 Powder XRD data for sucrose sample 15A.



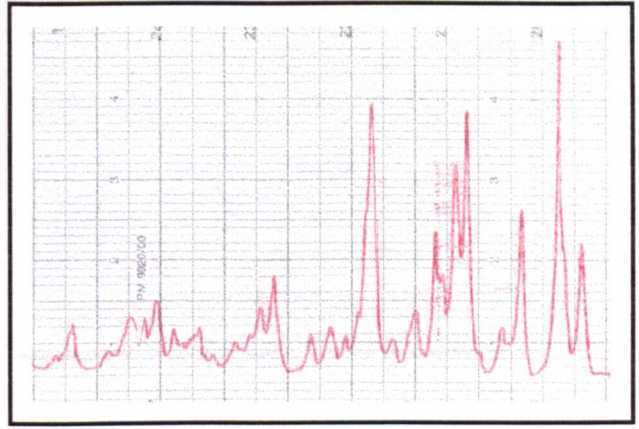
2θ	d_i Å	I/I ₀ (I)
11.369	7.779	48
12.838	6.892	65
15.301	5.788	41
18.777	4.723	100
19.280	4.601	70
24.432	3.641	73

Fig. 2.3.57 Powder XRD data for sucrose sample 15B.



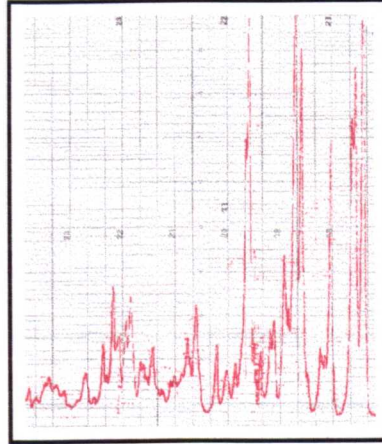
2θ	d_i Å	I/Io(I)
11.492	7.696	39
12.621	7.010	100
18.690	4.745	79
19.374	4.579	62
24.478	3.635	81

Fig. 2.3.58 Powder XRD data for sucrose sample 15C.



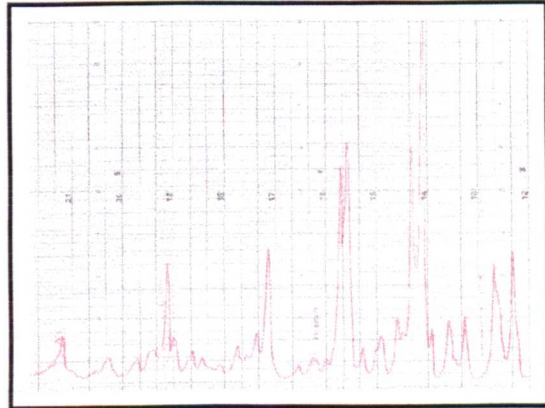
2θ	d_i Å	I/Io(I)
11.428	7.739	100
12.482	7.086	65
15.230	5.814	60
18.559	5.814	70
19.289	4.599	95
24.493	4.599	75

Fig. 2.3.59 Powder XRD data for sucrose sample 16A.



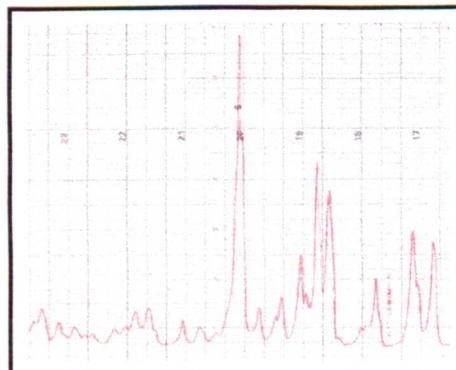
2θ	d_i Å	I/Io(I)
11.546	7.904	27
12.599	7.022	26
18.634	4.759	100
19.420	4.568	53
24.516	3.629	53
25.122	3.543	49
30.719	2.902	28
38.719	2.324	26

Fig. 2.3.60 Powder XRD data for sucrose sample 16B.



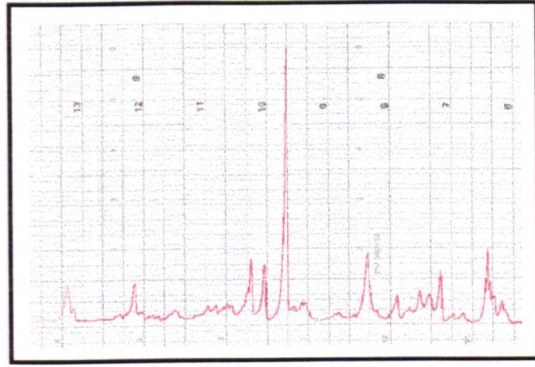
2θ	d_i Å	I/Io(I)
11.407	7.753	34
15.220	5.818	23
19.256	4.607	51
20.172	4.400	60
24.922	3.571	100

Fig. 2.3.61 Powder XRD data for sucrose sample 16C.



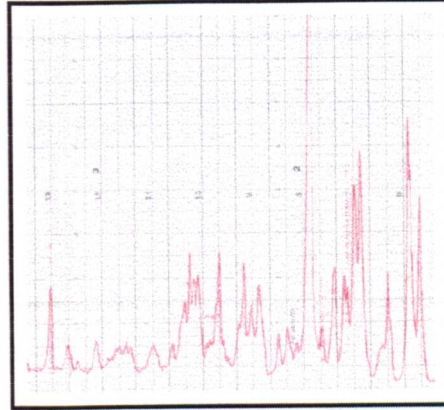
2θ	$d_i, \text{\AA}$	$I/I_0(I)$
13.285	6.661	28
15.843	5.591	20
19.089	4.647	27

Fig. 2.3.62 Powder XRD data for sucrose sample 17A.



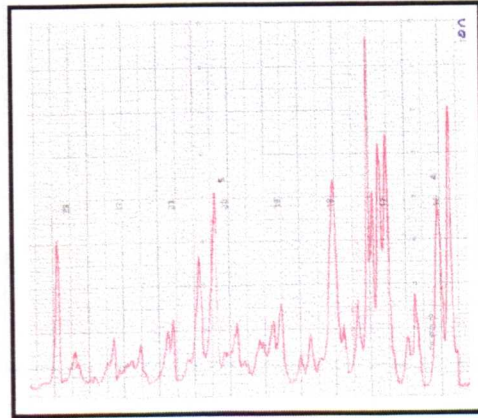
2θ	$d_i, \text{\AA}$	$I/I_0(I)$
11.626	7.607	37
13.087	6.761	52
18.685	4.746	45
19.498	4.550	38
24.555	3.623	100

Fig. 2.3.63 Powder XRD data for sucrose sample 17B.



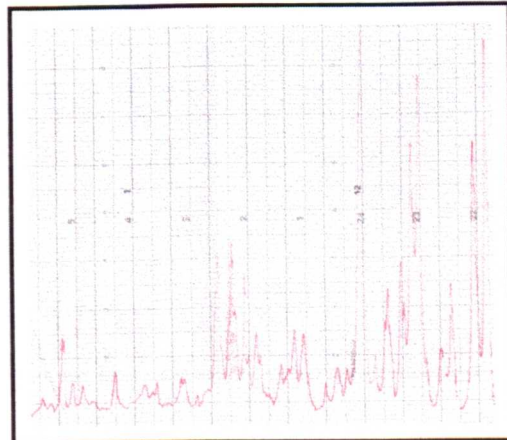
2θ	$d_i, \text{\AA}$	$I/I_0(I)$
11.626	7.607	80
13.087	6.761	54
15.399	5.751	25
18.685	4.746	73
19.498	4.550	69
20.357	4.360	55
20.860	4.256	100
24.555	3.623	58
38.211	2.354	55
39.808	2.263	37

Fig. 2.3.64 Powder XRD data for sucrose sample 17C.



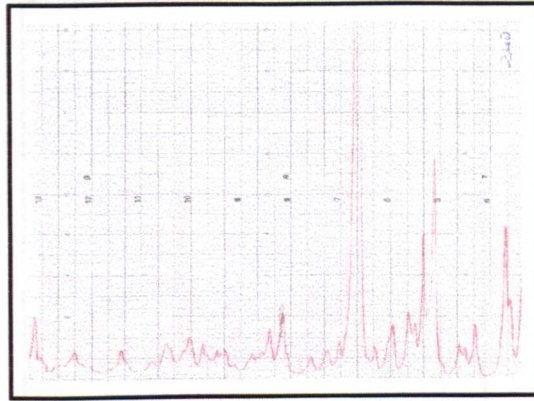
2θ	$d_i, \text{\AA}$	$I/I_0(I)$
11.435	7.734	84
12.784	6.921	62
15.200	5.826	30
18.562	4.778	75
19.302	4.596	60
24.993	3.563	100
40.136	2.247	34
40.686	2.218	41
41.801	2.111	39

Fig. 2.3.65 Powder XRD data for sucrose sample 18A.



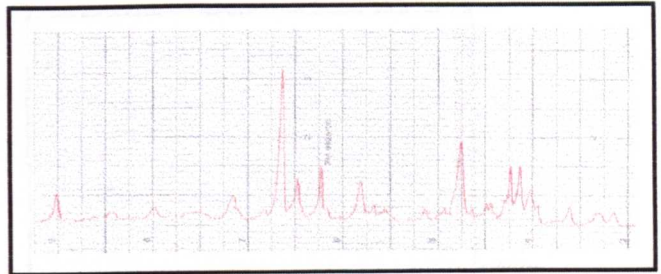
2θ	d_i Å	I/Io(I)
11.608	7.619	38
12.652	6.993	34
18.777	4.723	48
19.567	4.534	31
24.733	3.598	100

Fig. 2.3.66 Powder XRD data for sucrose sample 18B.



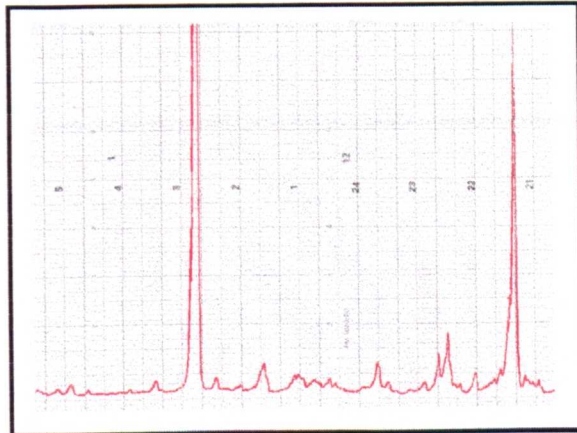
2θ	d_i Å	I/Io(I)
19.515	4.549	39
20.370	4.360	39
25.346	3.514	58
33.801	2.652	30
37.177	2.418	39
37.642	2.390	30
40.461	2.229	100

Fig. 2.3.67 Powder XRD data for sucrose sample 18C.



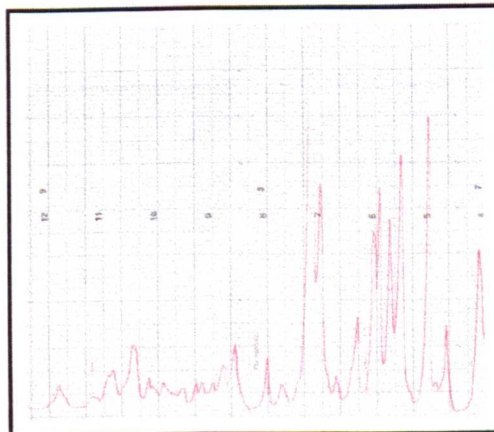
2θ	d_i Å	I/Io(I)
11.409	7.752	80
18.477	4.802	9
19.081	4.651	5
38.107	2.360	100

Fig. 2.3.68 Powder XRD data for sucrose sample 19A.



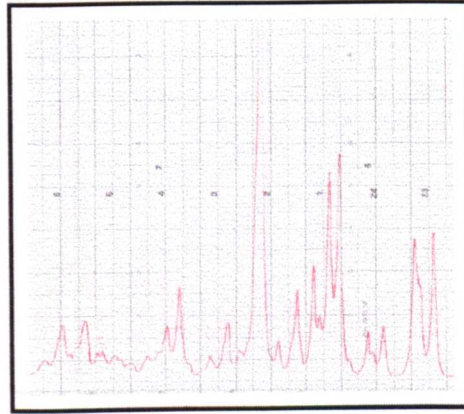
2θ	d_i Å	I/Io(I)
11.904	7.430	40
15.758	5.621	63
17.071	5.191	55
19.059	4.654	56
19.364	4.584	59
19.854	4.469	100
20.934	4.244	57
25.238	3.529	62
25.862	3.445	100

Fig. 2.3.69 Powder XRD data for sucrose sample 19B.



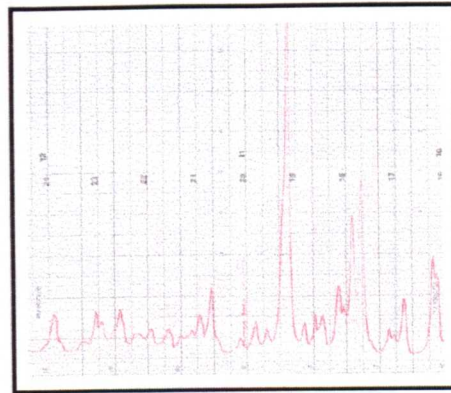
2θ	d_i , Å	I/Io(I)
11.735	7.537	34
13.177	6.715	33
18.904	4.692	50
19.679	4.509	46
25.263	3.523	100

Fig. 2.3.70 Powder XRD data for sucrose sample 19C.



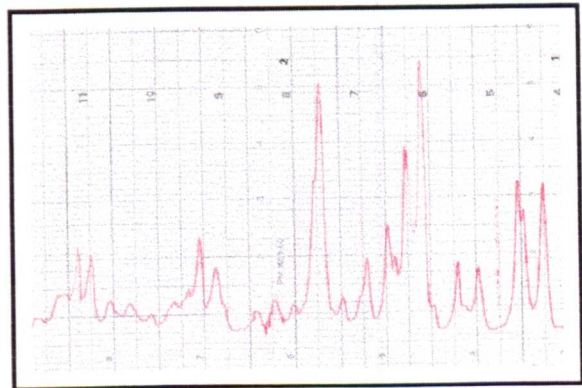
2θ	d_i , Å	I/Io(I)
12.733	6.948	27
18.734	4.734	46
19.171	4.627	36
24.580	3.620	100

Fig. 2.3.71 Powder XRD data for sucrose sample 20A.



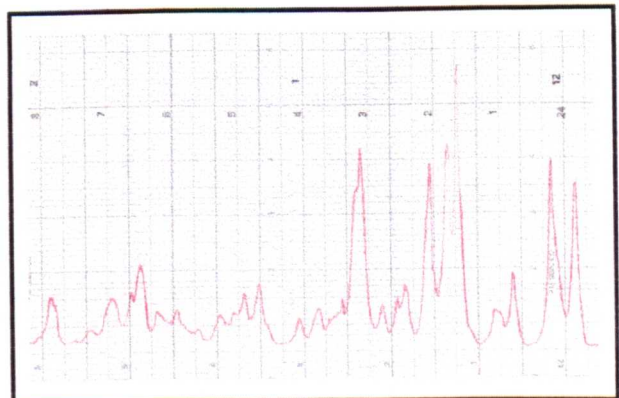
2θ	d_i , Å	I/Io(I)
11.572	7.643	49
13.070	6.770	50
15.410	5.747	22
16.629	5.328	24
18.684	4.747	100
19.492	4.552	67
21.216	4.188	34
22.434	3.963	25
25.110	3.545	87

Fig. 2.3.72 Powder XRD data for sucrose sample 20B.



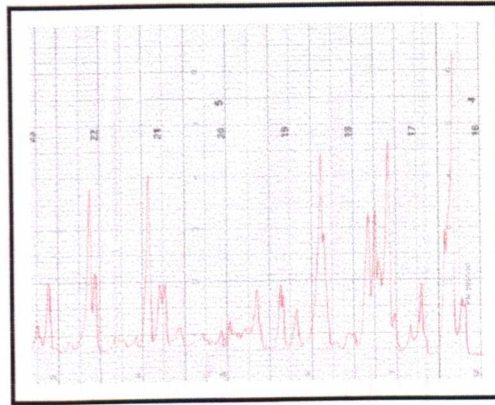
2θ	d_i , Å	I/Io(I)
11.627	7.607	57
13.122	6.743	68
15.461	5.728	26
19.472	4.556	100
20.451	4.340	74
21.969	4.044	67
24.685	3.605	74
25.097	3.546	56

Fig. 2.3.73 Powder XRD data for sucrose sample 20C.



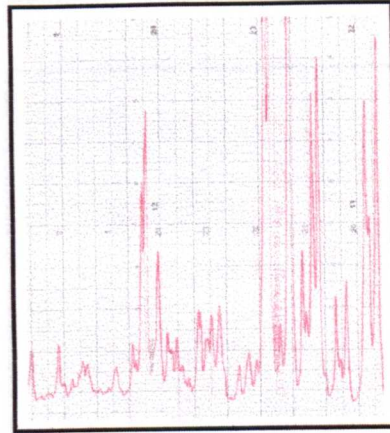
2θ	d_i Å	I/Io(I)
11.949	7.40	19
13.181	6.713	100
19.072	4.651	71
19.933	4.454	35
20.842	4.262	46
22.247	3.994	46
24.999	3.560	65
38.617	2.330	53
46.780	1.942	50

Fig. 2.3.74 Powder XRD data for sucrose sample 21A.



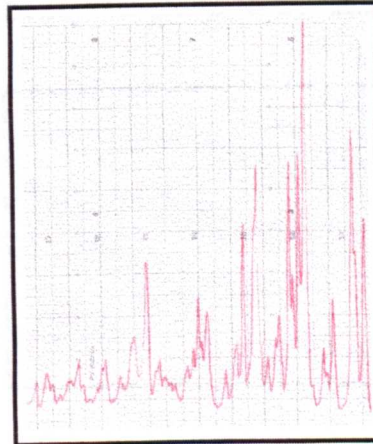
2θ	d_i Å	I/Io(I)
11.658	7.587	60
13.110	6.749	47
18.760	4.728	53
19.502	4.549	50
22.024	4.034	80
24.631	3.612	100
38.310	2.348	47

Fig. 2.3.75 Powder XRD data for sucrose sample 21B.



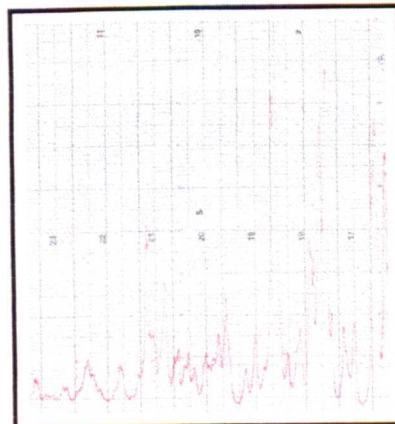
2θ	d_i Å	I/Io(I)
11.625	7.608	48
13.090	6.760	70
15.458	5.729	28
18.727	4.738	100
19.538	4.541	65
20.763	4.276	62
24.721	3.599	60
25.117	3.544	47
31.112	2.875	29
32.237	2.777	26
38.236	2.353	36

Fig. 2.3.76 Powder XRD data for sucrose sample 21C.



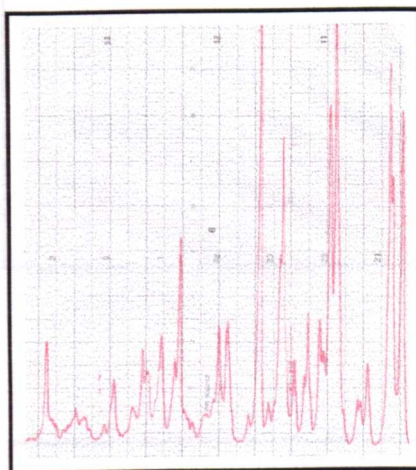
2θ	d_i Å	I/Io(I)
11.930	7.414	65
13.115	6.747	73
15.732	5.630	23
16.674	5.314	22
19.097	4.665	86
19.808	4.482	42
20.865	4.257	39
25.077	3.549	100
38.613	2.330	39
40.700	2.217	47

Fig. 2.3.77 Powder XRD data for sucrose sample 22A.



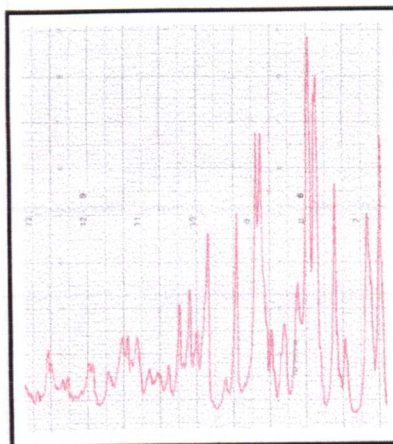
2θ	d_i Å	I/Io(I)
11.611	7.617	72
12.984	6.815	83
15.400	5.751	18
18.776	4.724	100
19.392	4.575	74
22.473	3.954	66
24.678	3.606	98
30.789	2.804	42

Fig. 2.3.78 Powder XRD data for sucrose sample 22B.



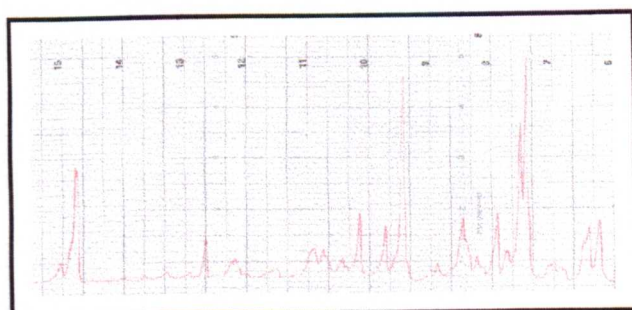
2θ	d_i Å	I/Io(I)
11.559	7.651	73
12.686	6.974	54
16.926	5.773	61
18.615	4.764	89
19.401	4.573	100
24.732	3.598	69
25.281	3.521	69
27.369	2.926	53
30.925	2.890	46

Fig. 2.3.79 Powder XRD data for sucrose sample 22C.



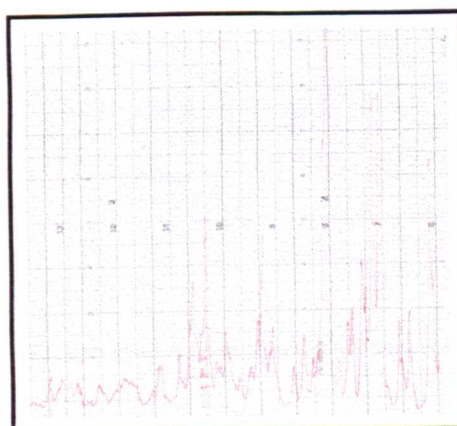
2θ	d_i Å	I/Io(I)
11.456	7.720	29
12.924	6.846	25
19.103	4.646	100
19.392	4.573	73
24.601	3.617	100
38.221	2.353	53

Fig. 2.3.80 Powder XRD data for sucrose sample 23A.



2θ	d_i Å	I/Io(I)
11.626	7.607	46
12.804	6.910	73
15.758	5.621	24
16.199	5.469	22
19.118	4.642	81
19.912	4.459	81
22.911	3.882	48
24.580	3.620	100
31.754	2.816	37
38.357	2.345	45
40.201	2.243	46

Fig. 2.3.81 Powder XRD data for sucrose sample 23B.



2θ	d_i Å	I/Io(I)
11.521	7.677	56
12.961	6.827	69
15.287	5.793	42
18.684	4.747	84
19.429	4.566	100
24.584	3.619	91
30.951	2.88	42
31.834	2.810	42
38.596	2.333	21
40.189	2.244	20
51.233	1.78	42

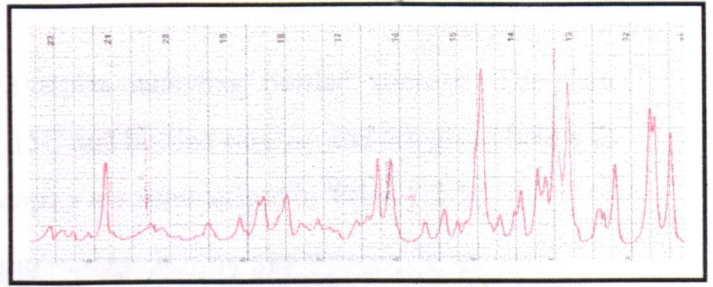


Fig. 2.3.82 Powder XRD data for sucrose sample 23C.

2θ	d_i Å	I/Io(I)
11.935	7.415	40
12.995	6.812	40
13.529	6.545	71
15.688	5.649	36
19.103	4.646	76
19.892	4.463	78
24.997	3.562	100

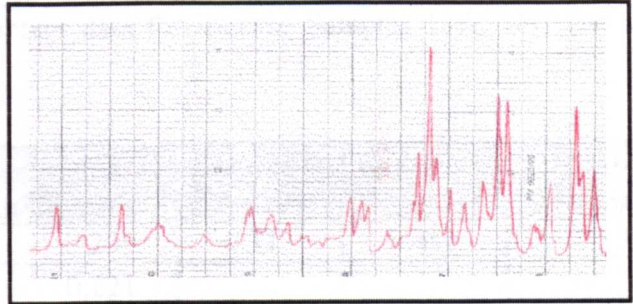


Fig. 2.3.83 Powder XRD data for sucrose sample 24A.

2θ	d_i Å	I/Io(I)
18.702	4.741	87
19.423	4.568	73
24.596	3.617	100
37.309	2.410	29
38.589	2.333	27

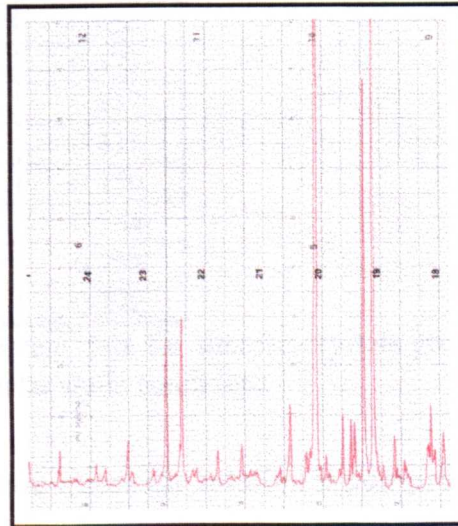


Fig. 2.3.84 Powder XRD data for sucrose sample 24B.

2θ	d_i Å	I/Io(I)
11.811	7.489	70
12.782	6.922	50
19.055	4.655	100
19.545	4.539	90
24.78	3.590	92
27.520	3.239	64

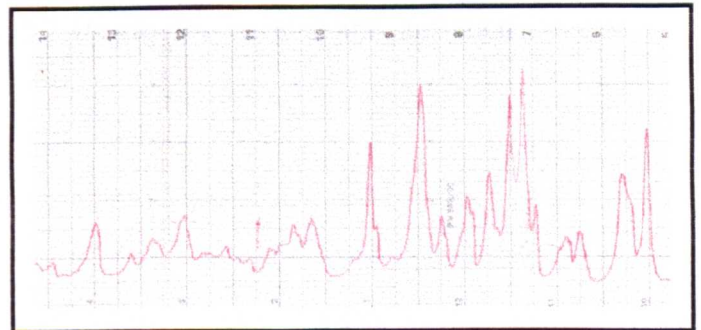


Table 2.3.85 Powder XRD data for sucrose sample 24C.

Karl Fisher data were collected for samples including bottled sucrose. The data (including error data) for samples 13A, 15C and bottled sucrose and are given below in Table 2.3.4 and the data for all other samples are summarised in Table 2.3.5.

Sample	1 % wt/wt	2 % wt/wt	3 % wt/wt	Mean % wt/wt	Std. Dev. %
13A	1.096	0.608	0.800	0.834	0.201
15C	0.000691	0.000509	-0.000263	0.000600	0.000091
Bottled sucrose	0.000224	-----	-----	0.000224	0.000

Table 2.3.4 Karl Fisher moisture content data for sucrose Samples 13A, 15C and bottled sucrose.

Experiment	Sample A % wt/wt	Sample B % wt/wt	Sample C % wt/wt	Sample D % wt/wt	Sample E % wt/wt	Mean % wt/wt
13	0.225	0.359	0.299	0.313	0.498	0.339
14	1.650	0.450	0.221			0.774
15	0.579	0.789	0.834			0.734
16	0.560	0.418	0.431			0.470
17	0.434	0.981	0.858			0.758
18	1.553	0.465	0.573			0.864
19	0.585	1.075	0.517			0.726
20	0.580	0.402	0.413			0.465
21	0.093	0.277	0.350			0.240
22	0.364	0.722	0.254			0.447
23	0.388	0.202	0.258			0.287
24	0.098	0.564	0.272			0.311

Table 2.3.5 Karl Fischer moisture content data for sucrose crystals grown in applied magnetic fields under static conditions.

2.3.1(c) Magnetic treatment of sucrose where the solution is pumped

This study was done in two parts: The first was carried out on normal grade sucrose and the second an identical repeat using analytical grade sucrose. The results are presented in Sections 2.3.1(c)(i) and 2.3.1(c)(ii) for normal and analytical grades respectively.

2.3.1(c)(i) NORMAL GRADE SUCROSE

2.3.1(c)(i)(1) Visual observations

The visual observations recorded for each sucrose sample within each experiment (there are 8 sucrose samples for each experiment) are given in Tables 2.3.6 to 2.3.18 and graphs 2.3.1 to 2.3.13. The morphology of each of the sucrose samples is

described as being either wedge, dendritic or euhedral or combinations of some or all of these forms, in addition with some notes describing the morphology. The graphs indicate the number of primary nucleation centres in red and the total number of nucleation centres is shown in blue. There are two sets of data for each experiment, since each was carried out in duplicate are referred to as A and B.

Experiment 25 - Control

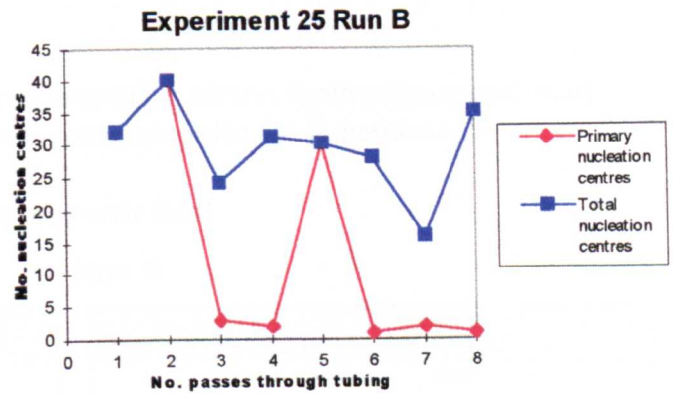
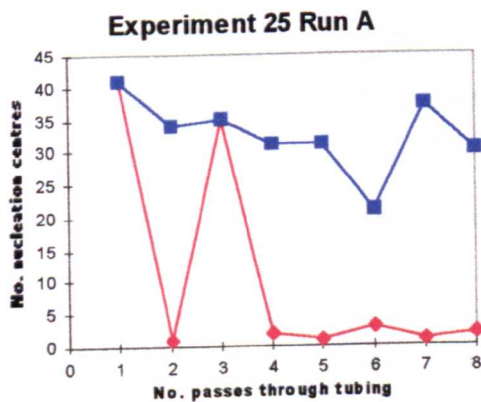
Run A

SAMPLE	MORPHOLOGY	NOTES
1	wedge and dendritic	fine, clear crystals
2	wedge	fine, clear crystals
3	wedge	fine sec. and chunkier prim. crystals
4	wedge	fine sec. and chunkier prim. crystals
5	wedge	fine sec. and chunkier prim. crystals
6	wedge and dendritic	fine sec. and chunkier prim. crystals
7	wedge	fine sec. and chunkier prim. crystals
8	wedge	fine sec. and chunky prim. crystals

Run B

SAMPLE	MORPHOLOGY	NOTES
1	wedge	fine, clear crystals
2	wedge	fine, clear crystals
3	wedge	chunky prim. and v. fine sec. crystals
4	wedge	chunky prim. and v. fine sec. crystals
5	wedge	fine, clear crystals
6	wedge (some euhedral)	fine sec. and chunkier prim. crystals
7	wedge (some euhedral)	fine sec. and chunkier prim. crystals
8	wedge (some euhedral)	fine sec. and chunkier prim. crystals

Tables 2.3.6 A and B Summary of the visual observations of sucrose crystal morphology recorded for Experiment 25.



Graphs 2.3.1 A and B Number of nucleation centres (both primary and total) versus No. passes recorded for Experiment 25.

Experiment 26 - 265-300G permanent magnetic field

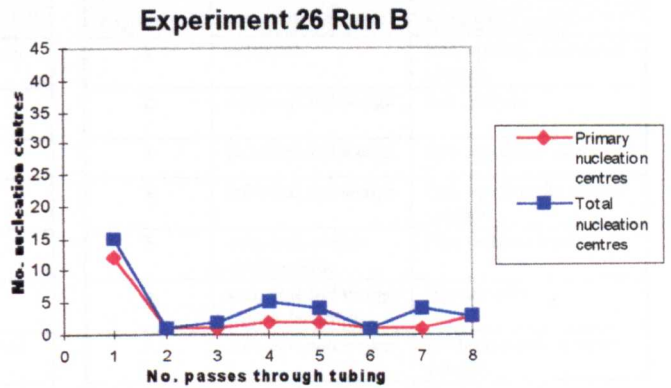
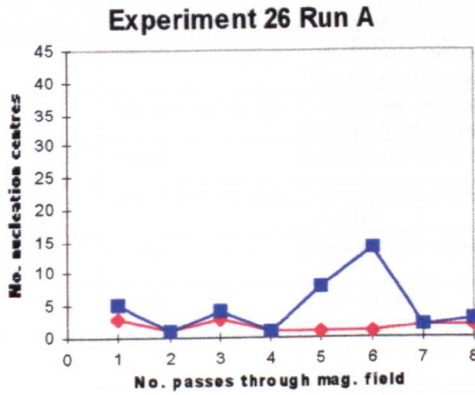
Run A

SAMPLE	MORPHOLOGY	NOTES
1	euhedral and wedge	fine, clear crystals
2	wedge and dendritic	chunky crystals
3	wedge (some dendritic)	fine, opaque v. ordered crystals
4	euhedral, wedge (some dendritic)	ordered crystals
5	dendritic and wedge	fine, wedge crystals
6	dendritic (some wedge)	fine sec. and chunkier prim. crystals
7	wedge and dendritic	fine opaque crystals
8	wedge and dendritic	fine opaque crystals

Run B

SAMPLE	MORPHOLOGY	NOTES
1	euhedral	fine, clear crystals
2	euhedral, wedge and dendritic	chunky, opaque crystals
3	wedge	chunky, opaque crystals
4	wedge (some dendritic)	chunky crystals
5	wedge (some dendritic)	fine, opaque crystals
6	wedge (some dendritic)	chunky, opaque crystals
7	wedge (some dendritic)	chunky crystals
8	wedge (some dendritic)	fine, disordered crystals

Tables 2.3.7 A and B Summary of the visual observations of sucrose crystal morphology recorded for Experiment 26.



Graphs 2.3.2 A and B Number of nucleation centres (both primary and total) versus No. passes recorded for Experiment 26.

Experiment 27 - 350-400G permanent magnetic field

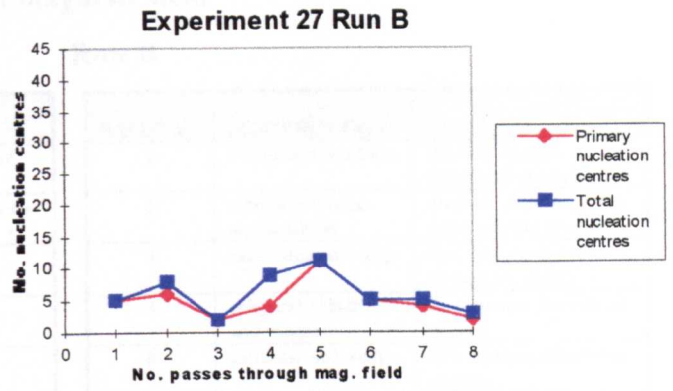
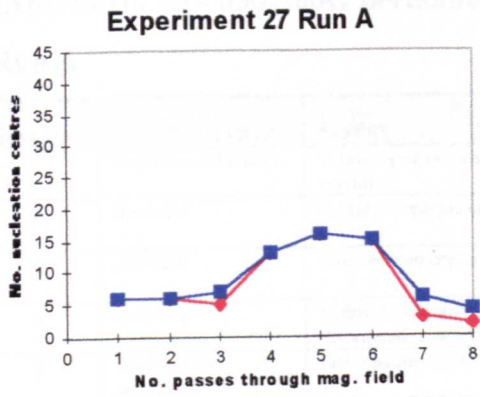
Run A

SAMPLE	MORPHOLOGY	NOTES
1	euhedral and wedge	chunky, opaque, disordered crystals
2	euhedral and dendritic	ordered, chunkier crystals
3	euhedral and dendritic	fine, opaque, disordered crystals
4	euhedral	clear, ordered crystals
5	euhedral (some wedge)	fine, clear, ordered crystals
6	euhedral	fine, v. clear crystals
7	wedge (some dendritic)	v. fine, opaque crystals
8	wedge (some dendritic)	v. fine, opaque crystals

Run B

SAMPLE	MORPHOLOGY	NOTES
1	euhedral and dendritic	chunky, opaque crystals
2	euhedral	chunky crystals
3	wedge and dendritic	fine, opaque, ordered crystals
4	euhedral (some wedge)	medium sized crystals
5	euhedral	medium, opaque crystals
6	wedge and dendritic	fine, opaque crystals
7	euhedral, wedge and dendritic	medium sized crystals
8	wedge and dendritic	fine, opaque, ordered crystals

Tables 2.3.8 A and B Summary of the visual observations of sucrose crystal morphology recorded for Experiment 27.



Graphs 2.3.3 A and B Number of nucleation centres (both primary and total) versus No. passes recorded for Experiment 27.

Experiment 28 - 540-620G permanent magnetic field

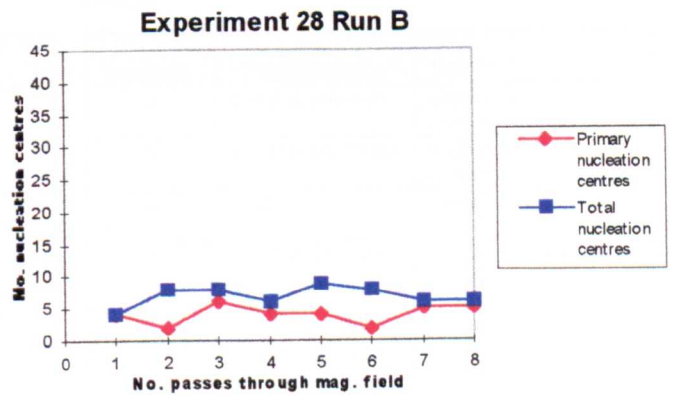
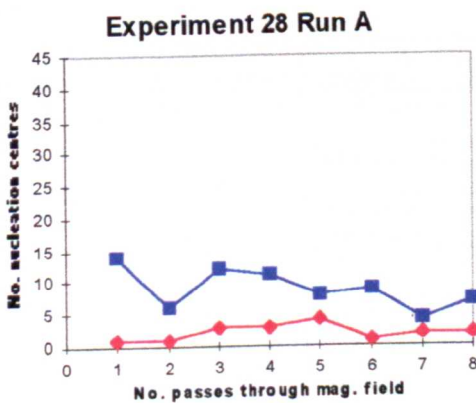
Run A

SAMPLE	MORPHOLOGY	NOTES
1	euhedral and wedge	chunky eu., and medium wedge sized crystals
2	euhedral and wedge	chunky eu., and fine wedge sized crystals
3	wedge	fine, ordered crystals
4	euhedral and wedge	fine, opaque, ordered crystals
5	wedge	fine, ordered crystals
6	wedge	fine crystals
7	euhedral	chunky, opaque, ordered crystals
8	euhedral and wedge (some dendritic)	v. chunky eu. and fine wedge, opaque crystals

Run B

SAMPLE	MORPHOLOGY	NOTES
1	euhedral	fine, opaque, disordered crystals
2	euhedral and wedge	fine crystals
3	euhedral and wedge	fine, opaque crystals
4	euhedral and wedge	fine, opaque, disordered crystals
5	euhedral, wedge and dendritic	fine, ordered crystals
6	euhedral and wedge (some dendritic)	fine crystals
7	euhedral and wedge	medium sized, opaque crystals
8	euhedral	fine, clear ordered crystals

Tables 2.3.9 A and B Summary of the visual observations of sucrose crystal morphology recorded for Experiment 28.



Graphs 2.3.4 A and B Number of nucleation centres (both primary and total) versus No. passes recorded for Experiment 28.

Experiment 29 - 630-760G permanent magnetic field

Run A

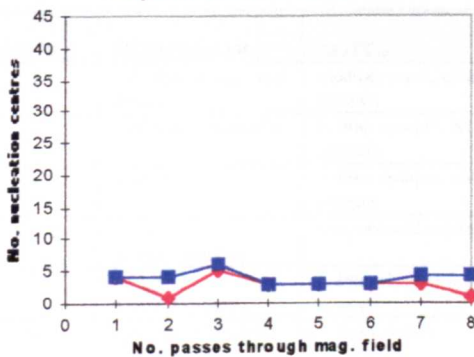
SAMPLE	MORPHOLOGY	NOTES
1	dendritic and wedge	v. fine, opaque, ordered crystals
2	dendritic	v. fine, v. opaque crystals
3	euhedral	fine, ordered crystals
4	dendritic	v. fine, v. opaque, disordered crystals
5	dendritic and euhedral	fine, opaque crystals
6	euhedral (some dendritic)	fine, opaque crystals
7	euhedral, wedge and dendritic	chunky eu., v. fine dend., ordered crystals
8	euhedral (some dendritic)	medium sized and clear, ordered crystals

Run B

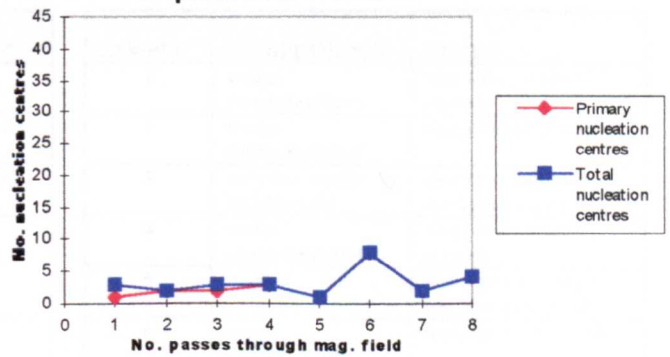
SAMPLE	MORPHOLOGY	NOTES
1	wedge and dendritic	chunky, opaque, disordered crystals
2	euhedral, wedge and dendritic	med. eu. and we., v. fine dend. opaque crystals
3	dendritic and wedge	fine, opaque crystals (wedge are clear)
4	euhedral, dendritic and wedge	fine, opaque, disordered crystals
5	dendritic and wedge	fine, opaque, disordered crystals
6	euhedral	clear crystals
7	dendritic and wedge	v. fine, v. opaque, disordered crystals
8	wedge and dendritic	opaque, ordered crystals

Tables 2.3.10 A and B Summary of the visual observations of sucrose crystal morphology recorded for Experiment 29.

Experiment 29 Run A



Experiment 29 Run B



Graphs 2.3.5 A and B Number of nucleation centres (both primary and total) versus No. passes recorded for Experiment 29.

Experiment 30 - AC electromagnetic field

Run A

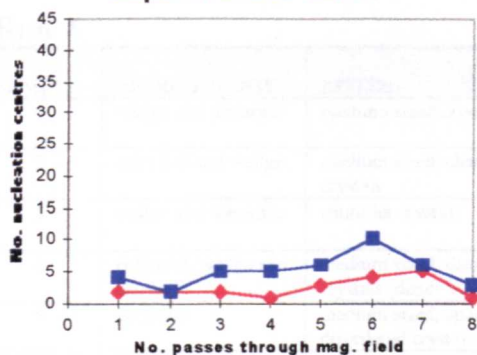
SAMPLE	MORPHOLOGY	NOTES
1	euhedral and wedge	chunky crystals
2	euhedral centered wedge and dendritic	ordered crystals
3	wedge (some dendritic)	finer dendritic, clear, ordered crystals
4	wedge (some dendritic)	clear crystals
5	euhedral	medium sized crystals
6	wedge	medium sized, clear, ordered crystals
7	euhedral and wedge	chunky, clear, ordered crystals
8	wedge (some dendritic)	medium sized and clear, ordered crystals

Run B

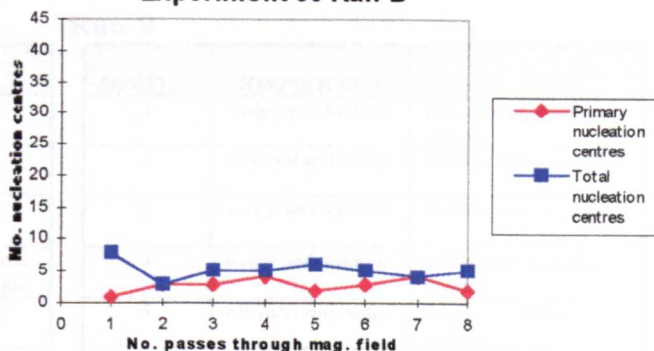
SAMPLE	MORPHOLOGY	NOTES
1	euhedral and wedge	chunky, opaque, ordered crystals
2	euhedral and wedge	v. chunky, ordered crystals
3	wedge	chunky, clear crystals
4	euhedral and wedge	chunky, opaque, disordered crystals
5	wedge (some dendritic)	fine, ordered crystals
6	euhedral and wedge	chunky wedge, medium sized euhedral crystals
7	euhedral and wedge	chunky, clear, ordered crystals
8	wedge and dendritic	fine, opaque, crystals

Tables 2.3.11 A and B Summary of the visual observations of sucrose crystal morphology recorded for Experiment 30.

Experiment 30 Run A



Experiment 30 Run B



Graphs 2.3.6 A and B Number of nucleation centres (both primary and total) versus No. passes recorded for Experiment 30.

Experiment 31 - 50-100G DC electromagnetic field

Run A

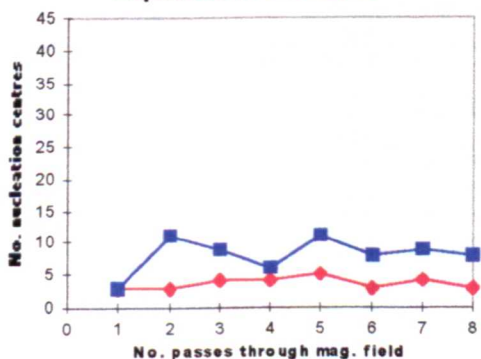
Run B

SAMPLE	MORPHOLOGY	NOTES
1	euhedral, wedge and dendritic	medium sized, clear crystals
2	wedge and dendritic	v. fine, opaque, ordered crystals
3	wedge	v. fine, opaque, ordered crystals
4	wedge (some euhedral)	fine, ordered crystals
5	wedge (some dendritic)	v. fine, clear, ordered crystals
6	wedge and dendritic	v. fine crystals
7	dendritic and wedge	fine, opaque, disordered crystals
8	wedge (some dendritic)	fine and clear, ordered crystals

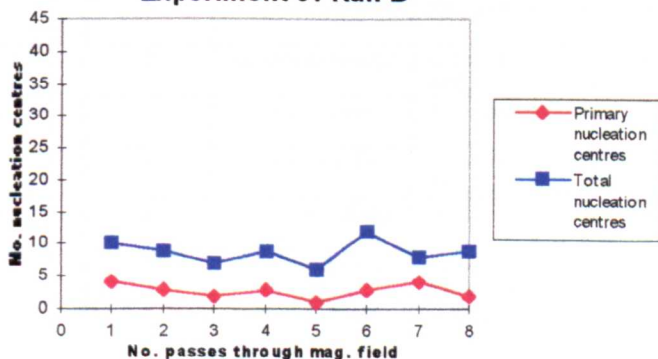
SAMPLE	MORPHOLOGY	NOTES
1	wedge (some dendritic)	fine, clear, ordered crystals
2	wedge (some dendritic)	fine, ordered crystals
3	euhedral, wedge and dendritic	chunky eu., fine we. & dend., opaque crystals
4	wedge (some dendritic)	fine, clear, ordered crystals
5	wedge	fine primary, chunky sec., opaque crystals
6	wedge (some dendritic)	medium sized crystals
7	euhedral, wedge and dendritic	chunky, opaque crystals
8	dendritic (some wedge)	medium sized crystals

Tables 2.3.12 A and B Summary of the visual observations of sucrose crystal morphology recorded for Experiment 31.

Experiment 31 Run A



Experiment 31 Run B



Graphs 2.3.7 A and B Number of nucleation centres (both primary and total) versus No. passes recorded for Experiment 31.

Experiment 32 - 100-220G DC electromagnetic field

Run A

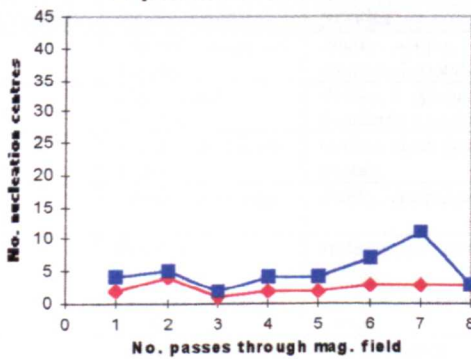
SAMPLE	MORPHOLOGY	NOTES
1	wedge and dendritic	medium sized crystals
2	euhedral and wedge	medium sized, clear crystals
3	wedge and dendritic	chunkier crystals
4	euhedral, wedge and dendritic	medium sized, disordered crystals (dend. V. opaque)
5	dendritic	medium sized, opaque, disordered crystals
6	dendritic	fine, opaque, disordered crystals
7	wedge and dendritic (some euhedral)	fine, clear, ordered crystals
8	wedge (some dendritic)	fine crystals

Run B

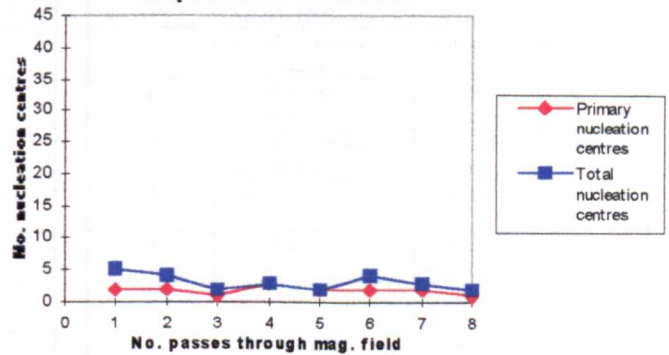
SAMPLE	MORPHOLOGY	NOTES
1	wedge and dendritic	fine, opaque, disordered crystals
2	euhedral and wedge	chunky, ordered crystals
3	wedge and dendritic	chunky, clear crystals
4	wedge and dendritic	medium sized, ordered crystals
5	euhedral and wedge	chunky, ordered crystals
6	wedge and dendritic	fine, opaque, disordered crystals
7	dendritic and wedge	chunky, opaque, disordered crystals
8	euhedral and wedge (some dendritic)	v. chunky euhedral and wedge crystals (dend. medium sized)

Tables 2.3.13 A and B Summary of the visual observations of sucrose crystal morphology recorded for Experiment 32.

Experiment 32 Run A



Experiment 32 Run B



Graphs 2.3.8 A and B Number of nucleation centres (both primary and total) versus No. passes recorded for Experiment 32.

Experiment 33 - 150-340G DC electromagnetic field

Run A

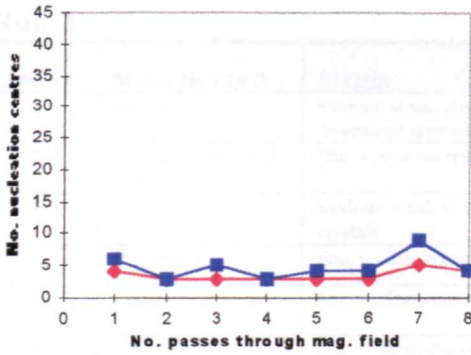
SAMPLE	MORPHOLOGY	NOTES
1	wedge	fine, clear, ordered crystals
2	euhedral, wedge and dendritic	fine crystals
3	wedge and dendritic (some euhedral)	medium sized, ordered crystals
4	wedge (some dendritic)	chunky wedge & fine dendritic, clear crystals
5	euhedral, wedge and dendritic	chunky wedge & v. fine dendritic, clear crystals
6	wedge	medium sized, ordered crystals
7	wedge and dendritic	fine, clear, disordered crystals
8	dendritic and wedge	fine crystals

Run B

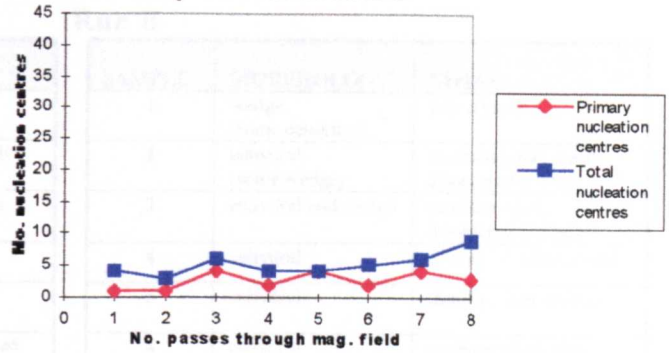
SAMPLE	MORPHOLOGY	NOTES
1	wedge and dendritic	fine, disordered crystals
2	euhedral and wedge	v. chunky wedge & fine dend., opaque, crystals
3	wedge and dendritic	fine, ordered crystals
4	wedge and dendritic	v. chunky wedge & fine dend., ordered crystals
5	euhedral and wedge	chunky wedge & fine dend., opaque, crystals
6	wedge and dendritic	chunky, clear, disordered crystals
7	dendritic and wedge	medium sized, clear, disordered crystals
8	euhedral and wedge (some dendritic)	v. chunky euhedral and wedge crystals (dend. medium sized)

Tables 2.3.14 A and B Summary of the visual observations of sucrose crystal morphology recorded for Experiment 33.

Experiment 33 Run A



Experiment 33 Run B



Graphs 2.3.9 A and B Number of nucleation centres (both primary and total) versus No. passes recorded for Experiment 33.

Experiment 34 - 190-500G DC electromagnetic field

Run A

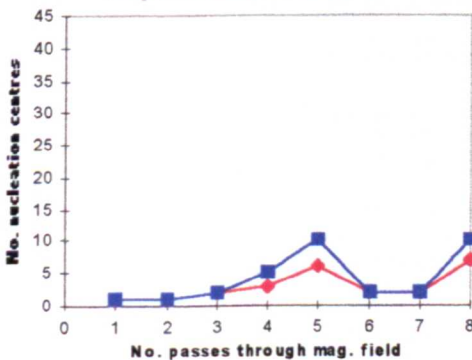
SAMPLE	MORPHOLOGY	NOTES
1	euhedral, wedge and dendritic	chunky, opaque, disordered crystals
2	euhedral and dendritic	chunky, v. opaque, disordered crystals
3	euhedral, wedge and dendritic	medium sized, opaque crystals
4	euhedral and wedge	chunky, opaque crystals
5	euhedral	medium sized, disordered crystals
6	euhedral, wedge and dendritic	fine, opaque, disordered crystals
7	euhedral and wedge	chunky crystals
8	euhedral and wedge	medium sized, clear ordered crystals

Run B

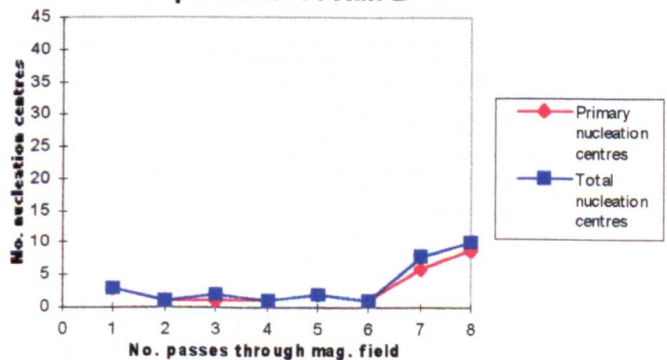
SAMPLE	MORPHOLOGY	NOTES
1	euhedral, wedge and dendritic	chunky, opaque, disordered crystals
2	euhedral and dendritic	chunky, v. opaque, disordered crystals
3	euhedral, wedge and dendritic	medium sized, opaque crystals
4	euhedral and wedge	chunky, opaque crystals
5	euhedral	medium sized, opaque, disordered crystals
6	euhedral, wedge and dendritic	chunky, opaque, disordered crystals
7	euhedral and wedge (some dendritic)	chunky crystals
8	euhedral and wedge	medium sized, clear, ordered crystals

Tables 2.3.15 A and B Summary of the visual observations of sucrose crystal morphology recorded for Experiment 34.

Experiment 34 Run A



Experiment 34 Run B



Graphs 2.3.10 A and B Number of nucleation centres (both primary and total) versus No. passes recorded for Experiment 34.

Experiment 35 - 220-600G DC electromagnetic field

Run A

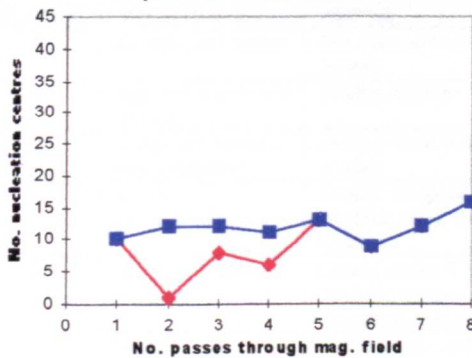
SAMPLE	MORPHOLOGY	NOTES
1	euhedral	medium sized, clear, disordered crystals
2	wedge-strange grey scales	fine, v. opaque crystals
3	euhedral	medium sized, v. clear crystals
4	euhedral	fine, v. clear crystals
5	euhedral	fine, v. clear crystals
6	euhedral	fine, v. clear, disordered crystals
7	euhedral	fine, v. clear crystals
8	wedge	fine, v. clear crystals

Run B

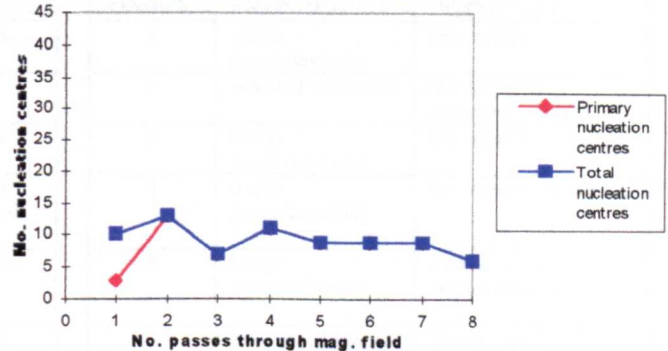
SAMPLE	MORPHOLOGY	NOTES
1	wedge (some dendritic)	fine crystals
2	euhedral (some wedge)	medium sized, clear, disordered crystals
3	euhedral and wedge	medium sized, disordered crystals
4	euhedral	chunky, v. clear crystals
5	euhedral	chunky, clear crystals
6	euhedral	medium sized, clear crystals
7	euhedral	fine, clear, ordered crystals
8	euhedral (some grey scaly areas)	medium sized, opaque, disordered crystals

Tables 2.3.16 A and B Summary of the visual observations of sucrose crystal morphology recorded for Experiment 35.

Experiment 35 Run A



Experiment 35 Run B



Graphs 2.3.11 A and B Number of nucleation centres (both primary and total) versus No. passes recorded for Experiment 35.

Experiment 36 - 300-680G DC electromagnetic field

Run A

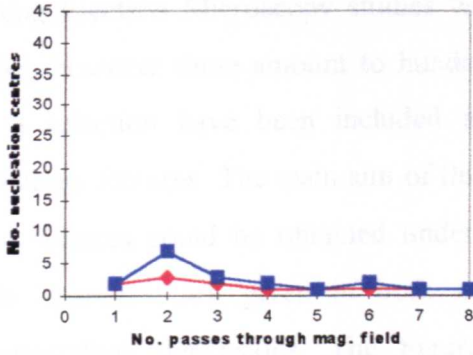
SAMPLE	MORPHOLOGY	NOTES
1	dendritic and wedge	fine, opaque crystals
2	dendritic and wedge	fine, v. opaque crystals
3	dendritic and wedge	medium sized, opaque, disordered crystals
4	wedge and dendritic	chunky, opaque, disordered crystals
5	wedge and dendritic	chunky, opaque, disordered crystals
6	wedge	fine, v. opaque crystals
7	wedge and dendritic	medium sized, opaque crystals
8	wedge and dendritic	chunky, ordered crystals

Run B

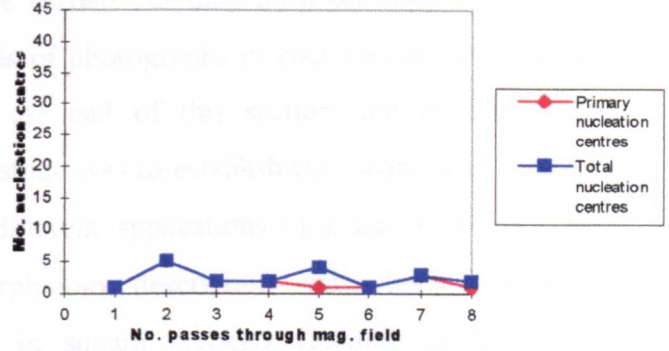
SAMPLE	MORPHOLOGY	NOTES
1	dendritic and wedge	fine, clear crystals
2	dendritic, wedge and euhedral (some grey scaly areas)	fine, opaque, disordered crystals
3	wedge, dendritic and euhedral	medium sized, opaque, disordered crystals
4	dendritic and wedge	medium sized, opaque disordered crystals
5	euhedral, wedge and dendritic	chunky, opaque crystals
6	wedge	medium sized, clear crystals
7	wedge and dendritic (some grey, scaly areas)	medium sized wedge & v. fine dendritic crystals
8	dendritic and wedge	v. fine, v. opaque crystals

Tables 2.3.17 A and B Summary of the visual observations of sucrose crystal morphology recorded for Experiment 36.

Experiment 36 Run A



Experiment 36 Run B



Graphs 2.3.12 A and B Number of nucleation centres (both primary and total) versus No. passes recorded for Experiment 36.

Experiment 37 - Pulsed field

Run A

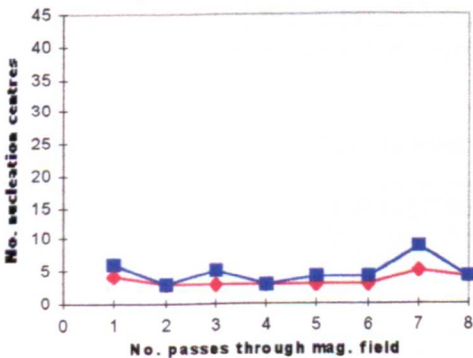
SAMPLE	MORPHOLOGY	NOTES
1	dendritic and wedge	fine, clear and ordered crystals
2	euhedral, wedge and dendritic	chunky, crystals
3	wedge and dendritic (some euhedral)	medium sized, ordered crystals
4	wedge (some dendritic)	chunky wedge & fine dendritic, clear, ordered crystals
5	euhedral, wedge and dendritic	chunky wedge & v. fine dendritic, opaque, disordered crystals
6	wedge	medium sized, ordered crystals
7	wedge and dendritic	fine, clear, disordered crystals
8	dendritic and wedge	fine crystals

Run B

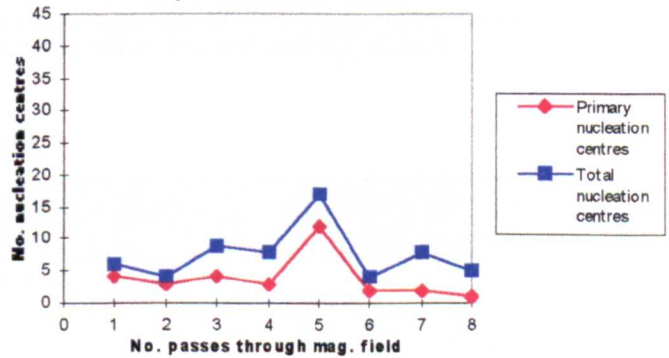
SAMPLE	MORPHOLOGY	NOTES
1	wedge (some dendritic)	fine crystals
2	euhedral and wedge	chunky, opaque, disordered crystals
3	wedge (some dendritic)	fine crystals
4	wedge (some dendritic)	fine, opaque crystals
5	wedge (some euhedral)	medium sized, clear, ordered crystals
6	euhedral and wedge	chunky, opaque crystals
7	euhedral and wedge	medium sized, opaque crystals
8	wedge	chunky, ordered crystals

Tables 2.3.18 A and B Summary of the visual observations of sucrose crystal morphology recorded for Experiment 37.

Experiment 37 Run A



Experiment 37 Run B



Graphs 2.3.13 A and B Number of nucleation centres (both primary and total) versus No. passes recorded for Experiment 37.

2.3.1(c)(i)(2) Scanning Electron Microscopy results

Scanning Electron Microscopy studies were carried out only on a selection of sucrose samples, however these amount to hundreds of photographs of sucrose crystal surfaces. Only a selection have been included at the end of this section and illustrate key morphology features. The main aim of this study was to establish that changes in sucrose crystal features could be obtained under different applications of magnetic fields. The results, therefore are given in both morphology description and where applicable, microcrystalline dimensions. The Figures in square brackets [2.3.86] to [2.3.114], correspond to the Figures given at the end of this section.

Experiment 25 - Control

Run A

Sample No.	Description of morphology	Microcrystalline dimensions
25(3)	Flat surfaces, angled edges and well formed microcrystals[2.3.86]	~30 μ m
25(4)	Rounded microcrystals	~40 μ m
25(7)	Layered[2.3.87], uneven surface, rounded microcrystals	~30 μ m

Table 2.3.19 SEM observations for sucrose Samples in Experiment 25, Run A.

Run B

Sample No.	Description of morphology	Microcrystalline dimensions
25(2)	Flat surfaces and angled edges[2.3.88], bubbled surface indicative of degassing sample[2.3.89], rounded microcrystals	~20-40 μ m
25(3)	Rounded microcrystals, bubbled rounded surface	~20-30 μ m
25(6)	Directional layers in regular straight lines across surface or possibly pitting, rounded microcrystals	~20-60 μ m
25(8)	Regular, stepped layers	

Table 2.3.20 SEM observations for sucrose Samples in Experiment 25, Run B.

Experiment 26 - 265-300G Permanent field

Sample No.	Description of morphology	Microcrystalline dimensions
26(2)	Extensively pitted surface[2.3.90], and layered growth	
26(4)	Rounded microcrystals[2.3.91]	~30-60 μ m
26(5)	Rounded microcrystals, flat surfaces	~10-30 μ m
26(6)	Rounded microcrystals, uneven cracked surface	~10-20 μ m

Table 2.3.21 SEM observations for sucrose Samples in Experiment 26.

Experiment 27 - 350-400G Permanent field

Sample No.	Description of morphology	Microcrystalline dimensions
27(2)	Rounded, uneven, pitted surface, no microcrystals	
27(6)	Extensively pitted surface, no microcrystals	

Table 2.3.22 SEM observations for sucrose Samples in Experiment 27.

Experiment 28 - 540-620G Permanent field

Sample No.	Description of morphology	Microcrystalline dimensions
28(2)	Flat surface with wave-like texture, no microcrystals	
28(8)	Flat surfaces, angled edges, rounded microcrystals[2.3.92]	~10-30 μm

Table 2.3.23 SEM observations for sucrose Samples in Experiment 28.

Experiment 29 - 630-760G Permanent field

Sample No.	Description of morphology	Microcrystalline dimensions
29(1)	Pitted layered surface surfaces	
29(4)	Directional layers on surface	
29(5)	Rounded microcrystals	~5-10 μm
29(8)	Scaly structure[2.3.93], well-formed microcrystals[2.3.94 & 96], very flat surfaces and angled edges[2.3.95]	~20-40 μm

Table 2.3.24 SEM observations for sucrose Samples in Experiment 29.

Experiment 30 - AC electromagnetic field

Sample No.	Description of morphology	Microcrystalline dimensions
30(2)	Microcrystals[2.3.97 & 98], directional extensively pitted surfaces[2.3.99].	~10 μm
30(7)	Layered, chunky stepped growth	
30(8)	Rounded, elongated crystals[2.3.100]	~10 $\mu\text{m}^2 \times \text{length}$

Table 2.3.25 SEM observations for sucrose Samples in Experiment 30.

Experiment 31 - 50-100G DC electromagnetic field

Sample No.	Description of morphology	Microcrystalline dimensions
31(3)	Microcrystals, on rounded surface	~5-20 μm
31(5)	Well formed microcrystals[2.3.101], rounded, pitted surface	~10-40 μm
31(8)	Flat surfaces and angled edges[2.3.102], layered growth[2.3.103], rounded microcrystals[2.3.104]	~20-60 μm

Table 2.3.26 SEM observations for sucrose Samples in Experiment 31.

Experiment 32 - 100-220G DC electromagnetic field

Sample No.	Description of morphology	Microcrystalline dimensions
32(2)	Rounded plate-like microcrystals and flat surfaces[2.3.105]	~50 μm
32(6)	Flat surfaces, rounded microcrystals[2.3.106]	~20-50 μm

Table 2.3.27 SEM observations for sucrose Samples in Experiment 32.

Experiment 33 - 150-340G DC electromagnetic field

Sample No.	Description of morphology	Microcrystalline dimensions
33(2)	Surface covered with well formed microcrystals and rounded surfaces	~20-60 μm
33(4)	Pitted surface and rounded microcrystals	~20-30 μm
33(5)	Rounded microcrystals, rounded surfaces	~60 μm
33(6)	Flat surfaces, rounded microcrystals	~20-50 μm
33(7)	Layered growth in straight lines, possibly pitting[2.3.107] elongated crystal growth[2.3.108]	~30 μm
33(8)	Rounded flat microcrystals, flat surfaces	~20-30 μm

Table 2.3.28 SEM observations for sucrose Samples in Experiment 33.

Experiment 34 - 190-500G DC electromagnetic field

Sample No.	Description of morphology	Microcrystalline dimensions
34(1)	Extensive surface coverage with microcrystals[2.3.109]	~20-40 μm
34(3)	Flat surfaces, pitted surfaces	~5-20 μm
34(6)	Well formed microcrystals[2.3.110], flat, layered surfaces	~50 μm

Table 2.3.29 SEM observations for sucrose Samples in Experiment 34.

Experiment 35 - 220-600G DC electromagnetic field

Sample No.	Description of morphology	Microcrystalline dimensions
35(3)	Microcrystals, elongated crystal morphology[2.3.111], rounded edges, pitted surfaces	~20-30 μm
35(5)	Microcrystals, elongated crystal morphology	~20-30 μm

Table 2.3.30 SEM observations for sucrose Samples in Experiment 35.

Experiment 37 - Pulsed field

Sample No.	Description of morphology	Microcrystalline dimensions
37(2)	Microcrystals, regular lined pitting[2.3.112], directional layered growth[2.3.113]	~20-30 μ m
37(4)	Layered pitted surface[2.3.114]	
37(5)	Rounded microcrystals, pitted surface	~30 μ m
37(7)	Rounded microcrystals	~20-40 μ m

Table 2.3.31 SEM observations for sucrose Samples in Experiment 37.

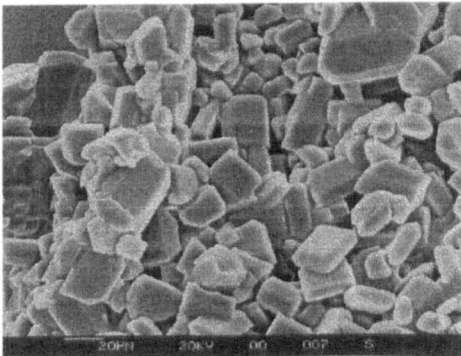


Fig. 2.3.86 Sucrose sample 25(3) Run A.

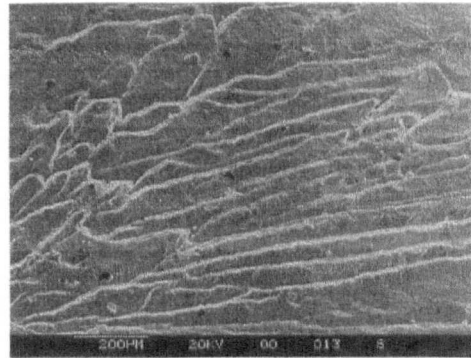


Fig.2.3.87 Sucrose sample 25(7) Run A.

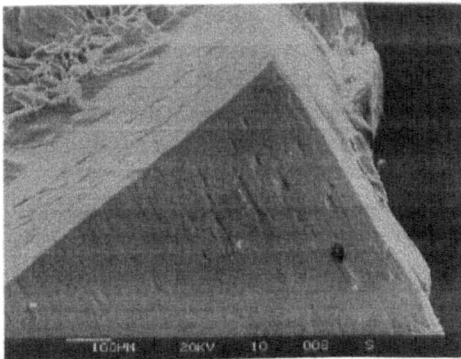


Fig. 2.3.88 Sucrose sample 25(2) Run B.

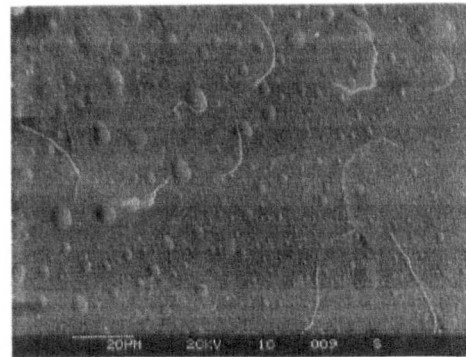


Fig. 2.3.89 Sucrose sample 25(2) Run B.

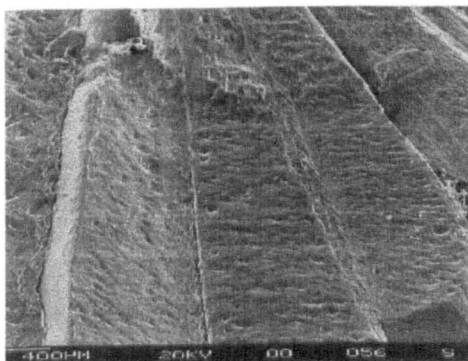


Fig. 2.3.90 Sucrose sample 26(2).

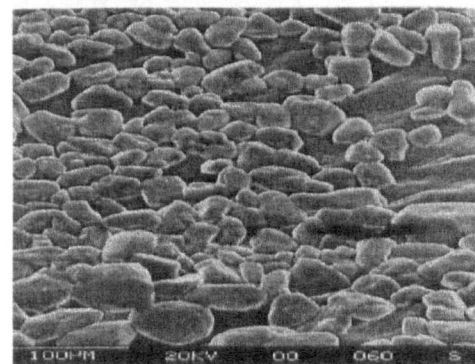


Fig. 2.3.91 Sucrose sample 26(4).



Fig. 2.3.92 Sucrose sample 28(8).

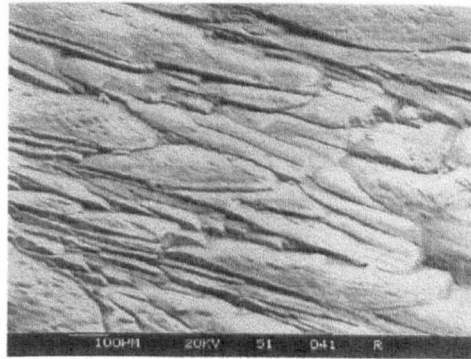


Fig. 2.3.93 Sucrose sample 29(8).

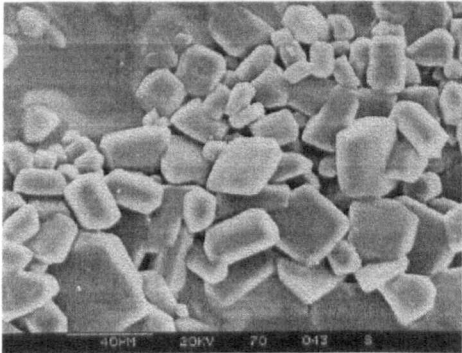


Fig. 2.3.94 Sucrose sample 29(8).



Fig. 2.3.95 Sucrose sample 29(8).

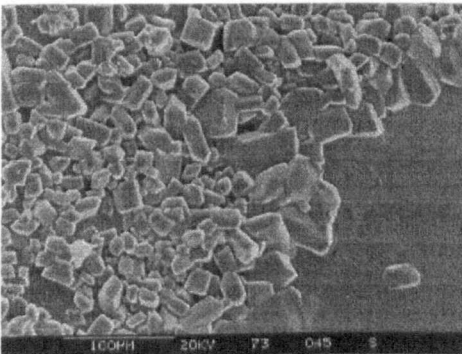


Fig. 2.3.96 Sucrose sample 29(8).

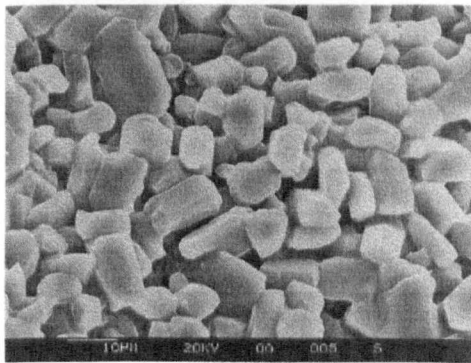


Fig. 2.3.97 Sucrose sample 30(2).

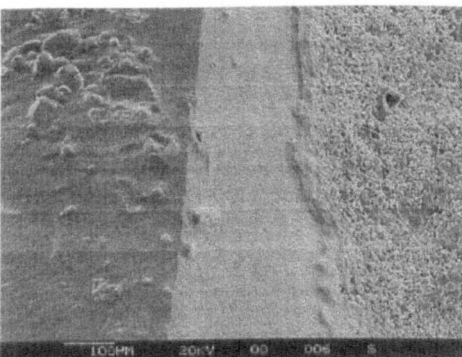


Fig. 2.3.98 Sucrose sample 30(2).

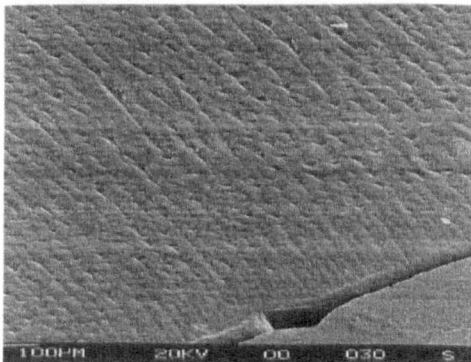


Fig. 2.3.99 Sucrose sample 30(2).

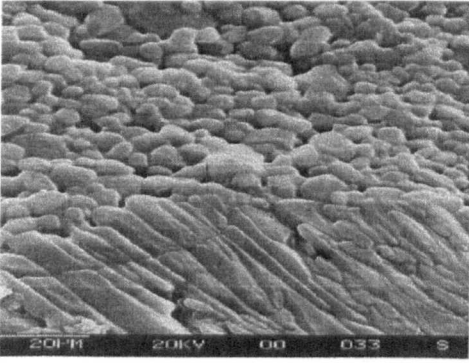


Fig. 2.3.100 Sucrose sample 30(8).

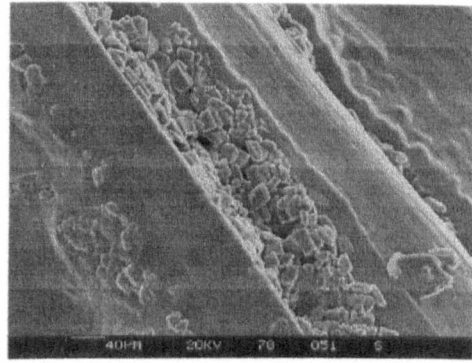


Fig. 2.3.102 Sucrose sample 31(5).

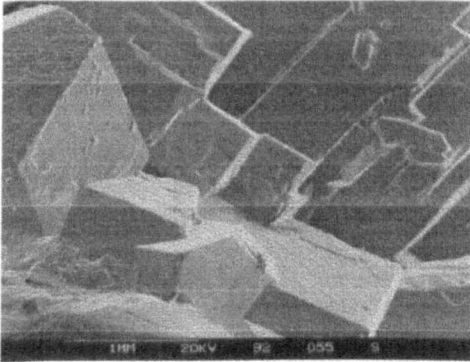


Fig. 2.3.103 Sucrose sample 31(8).

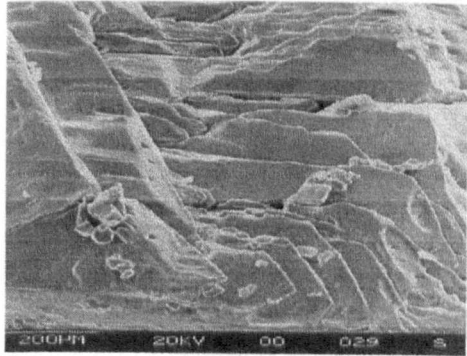


Fig. 2.3.104 Sucrose sample 31(8).

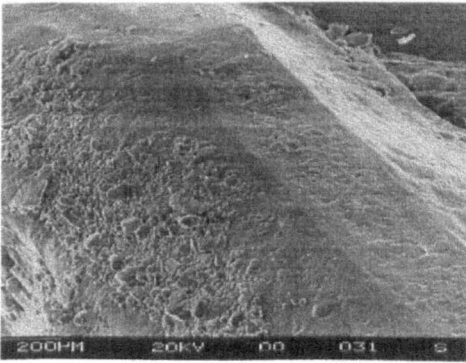


Fig. 2.3.104 Sucrose sample 31(8).

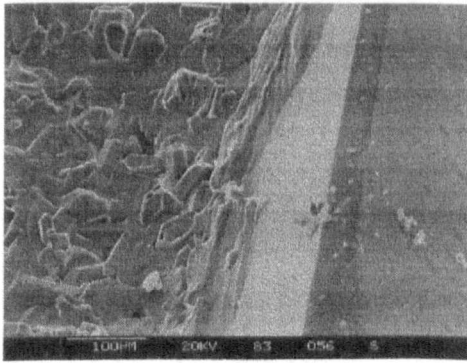


Fig. 2.3.105 Sucrose sample 32(2).

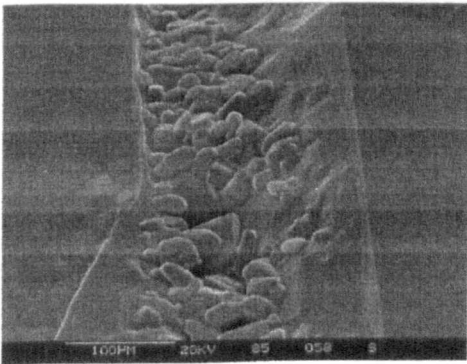


Fig. 2.3.106 Sucrose sample 32(6).

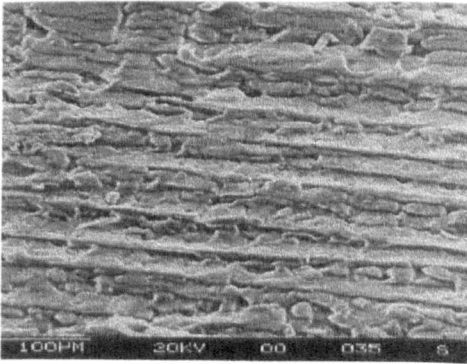


Fig. 2.3.107 Sucrose sample 33(7).

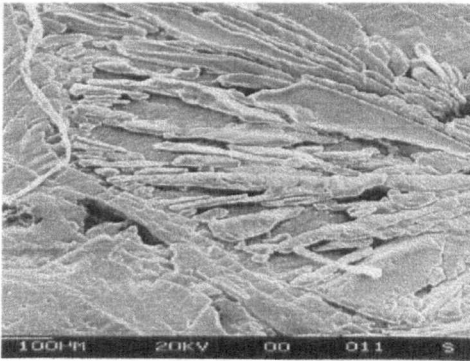


Fig. 2.3.108 Sucrose sample 33(7).

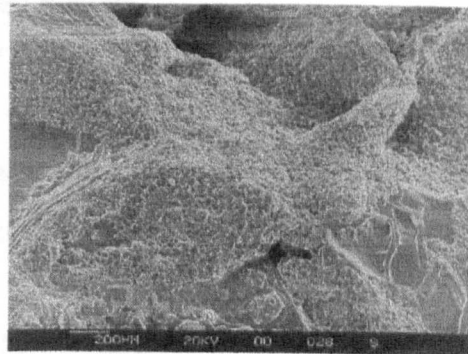


Fig. 2.3.109 Sucrose sample 34(1).

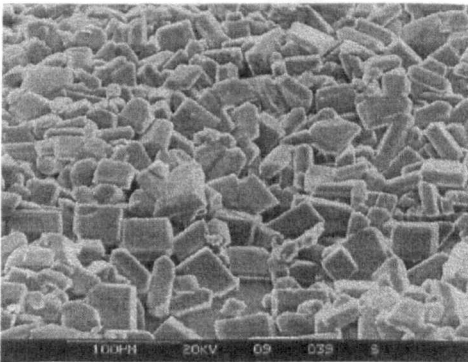


Fig. 2.3.110 Sucrose sample 34(6).

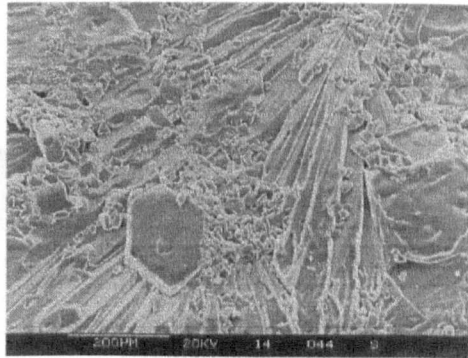


Fig. 2.3.111 Sucrose sample 35(7).

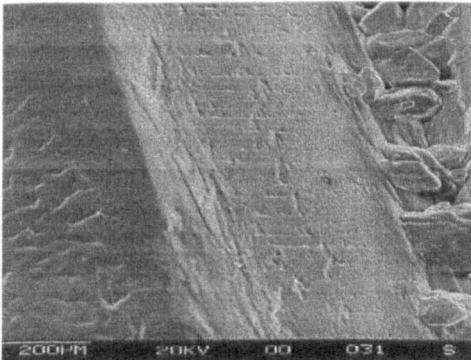


Fig. 2.3.112 Sucrose sample 37(2).

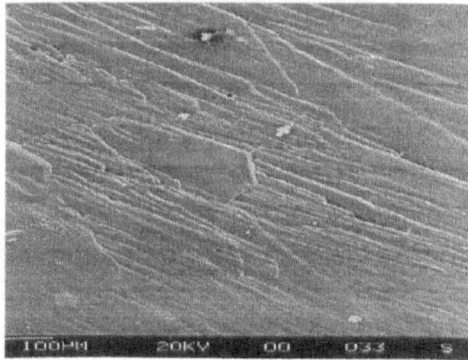


Fig. 2.3.113 Sucrose sample 37(2).

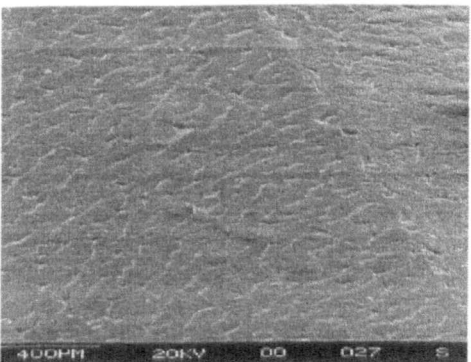


Fig. 2.3.114 Sucrose sample 37(4).

2.3.1(c)(i)(3) Differential Scanning Calorimetry Results

The DSC data are given in the form of tables of melting points (Tables 2.3.32 to 2.3.45). Where the table is blank no additional features were observed. The temperatures of the additional features, in addition to the main sucrose melting point, are given and the relative size of these features in comparison to the sucrose melting peak is indicated using the following abbreviations:

VVS = very, very small M = medium
 VS = very small L = large
 S = small VL = very large

Experiment 25 - Control

Run A

Sample	Feature 1 (°C)	Feature 2 (°C)	Melting Point (°C)
1	151.17 S		176.41
2	151.17 S		171.58
3	151.17 S		176.33
4	150.17 S		181.82
5	150.17 VS		182.58
6	152.17 VS		179.39
7	150.17 VS		177.48
8	153.83 VS		181.88

Table 2.3.32 DSC data on sucrose samples 1 to 8 from Experiment 25, Run A.

Run B

Sample	Feature 1 (°C)	Feature 2 (°C)	Melting Point (°C)
1	153.80 VS		181.00
2	152.80 S		180.90
3	153.80 S	157.40 S	183.60
4	152.80 VS		180.00
5	156.20 VVS		186.08
6			182.20
7	154.80 VS		183.95
8	153.80 VS		183.04

Table 2.3.33 DSC data on sucrose samples 1 to 8 from Experiment 25, Run B.

Experiment 26 - 265-300G Permanent field

Sample	Feature 1 (°C)	Feature 2 (°C)	Melting Point (°C)
1	153.83 VS		176.56
2	151.17 S		177.64
3	152.17 S		175.88
4	135.33 VS	152.17 M	178.08
5	152.17 S		179.25
6	152.83 S		180.23
7	152.83 S	157.50 S	178.17
8	152.83 S		178.30

Table 2.3.34 DSC data on sucrose samples 1 to 8 from Experiment 26.

Experiment 27 - 350-400G Permanent field

Sample	Feature 1 (°C)	Feature 2 (°C)	Melting Point (°C)
1	153.80 VS		181.64
2	153.80 S		182.51
3	153.80 S		177.83
4	152.80 S		182.31
5	153.80 S	158.80 S	181.99
6	155.40 VS		184.93
7	153.80 S		183.73
8	152.80 S		183.84

Table 2.3.35 DSC data on sucrose samples 1 to 8 from Experiment 27.

Experiment 28 - 540-620G Permanent field

Sample	Feature 1 (°C)	Feature 2 (°C)	Melting Point (°C)
1	153.80 VS		178.46
2	152.80 S		178.94
3	153.80 S		183.13
4	155.40 S		179.70
5			178.89
6			180.93
7	153.80 VS		183.06
8	155.40 VS		181.93

Table 2.3.36 DSC data on sucrose samples 1 to 8 from Experiment 28.

Experiment 29 - 630-760G Permanent field

Sample	Feature 1 (°C)	Feature 2 (°C)	Melting Point (°C)
1	153.40 VVS		182.94
2	153.40 VVS		175.06
3	153.40 VS		184.00
4	152.80 VS		180.95
5			186.33
6			185.85
7	154.20 VVS		185.69
8	154.80 VS		186.88

Table 2.3.37 DSC data on sucrose samples 1 to 8 from Experiment 29.

Experiment 30 - AC electromagnetic field

Sample	Feature 1 (°C)	Feature 2 (°C)	Melting Point (°C)
1	154.87 S		185.96
2	155.40 VS		184.20
3	153.80 S		185.37
4	153.80 S		185.21
5	152.80 S		185.41
6	153.80 VS		184.77
7	153.80 S		184.39
8	153.80 S		184.37

Table 2.3.38 DSC data on sucrose samples 1 to 8 from Experiment 30.

Experiment 31 - 50-100G DC electromagnetic field

Sample	Feature 1 (°C)	Feature 2 (°C)	Melting Point (°C)
1	153.83 S		176.77
2	152.83 S		183.11
3	152.83 S		180.43
4	152.83 S		179.92
5	152.83 S		182.71
6	152.83 S		180.63
7	152.83 VS		185.59
8	151.17 S		183.24

Table 2.3.39 DSC data on sucrose samples 1 to 8 from Experiment 31.

Experiment 32 - 100-220G DC electromagnetic field

Sample	Feature 1 (°C)	Feature 2 (°C)	Melting Point (°C)
1			182.42
2	153.80 VS		184.20
3	157.40 VS		177.60
4	155.40 VS		181.00
5	158.20 VVS		184.24
6	155.40 S		179.93
7	156.20 VS		180.44
8	154.80 VVS		183.27

Table 2.3.40 DSC data on sucrose samples 1 to 8 from Experiment 32.

Experiment 33 - 150-340G DC electromagnetic field

Sample	Feature 1 (°C)	Feature 2 (°C)	Melting Point (°C)
1	152.83 VS		179.94
2	152.83 S	168.67 S	180.38
3	155.50 VS		181.69
4	153.83 S		185.13
5	152.83 S		184.70
6	152.17 S		184.33
7	153.80 VS		170.19
8	153.83 VS	160.17 VS	184.14

Table 2.3.41 DSC data on sucrose samples 1 to 8 from Experiment 33.

Experiment 34 - 190-500G DC electromagnetic field

Sample	Feature 1 (°C)	Feature 2 (°C)	Melting Point (°C)
1	154.80 VVS		187.95
2	154.80 VVS		188.50
3	153.80 VS		185.79
4			188.34
5	152.80 VVS		188.27
6	157.40 VVS		190.25
7	153.80 VS		185.71
8	154.80 VVS		188.21

Table 2.3.42 DSC data on sucrose samples 1 to 8 from Experiment 34.

Experiment 35 - 220-600G DC electromagnetic field

Sample	Feature 1 (°C)	Feature 2 (°C)	Melting Point (°C)
1	153.40 VS		178.46
2	155.20 VVS		179.22
3			175.93
4	153.40 VVS		176.77
5			169.73
6			166.28
7			165.11
8			162.97

Table 2.3.43 DSC data on sucrose samples 1 to 8 from Experiment 35.

Experiment 36 - 300-680G DC electromagnetic field

Sample	Feature 1 (°C)	Feature 2 (°C)	Melting Point (°C)
1	152.83 S		176.03
2	152.17 VS		173.92
3	152.17 S		172.89
4	151.17 S		181.63
5	153.83 S		173.91
6	152.83 S		166.00
7	152.83 S		175.37
8	152.83 S		171.82

Table 2.3.44 DSC data on sucrose samples 1 to 8 from Experiment 36.

Experiment 37 - Pulsed field

Sample	Feature 1 (°C)	Feature 2 (°C)	Melting Point (°C)
1	152.83 S		181.48
2	151.50 S		176.79
3			180.59
4	152.83 VS		178.84
5	152.83 S		179.04
6	153.83 S		179.87
7	152.83 VVS		180.93
8	154.83 VS		188.97

Table 2.3.45 DSC data on sucrose samples 1 to 8 from Experiment 37.

2.3.1(c)(ii) ANALYTICAL GRADE SUCROSE

The results are presented for the second part of the pumped sucrose solution study carried out on analytical grade sucrose solutions.

2.3.1(c)(ii)(1) Visual observations

The visual observations recorded for each sucrose sample within each experiment 38 to 50 are given in Tables 2.3.46 to 2.3.58 and 2.3.14 to 2.3.26. The format in which the data is presented is the same as for the normal grade sucrose study.

Experiment 38 - Control

Run A

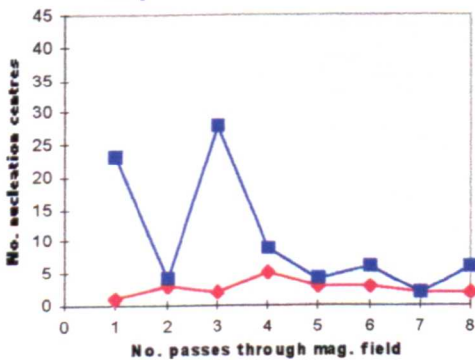
SAMPLE	MORPHOLOGY	NOTES
1	dendritic	fine, v. opaque, ordered crystals
2	wedge (some dendritic)	medium sized, v. ordered crystals
3	dendritic (some wedge)	fine, v. opaque, ordered crystals
4	wedge (some dendritic)	chunky, ordered crystals
5	wedge and dendritic	chunky, opaque, disordered crystals
6	wedge and dendritic	medium sized, opaque, disordered crystals
7	wedge (some dendritic)	v. fine, opaque, ordered crystals
8	wedge and dendritic	medium sized opaque, disordered crystals

Run B

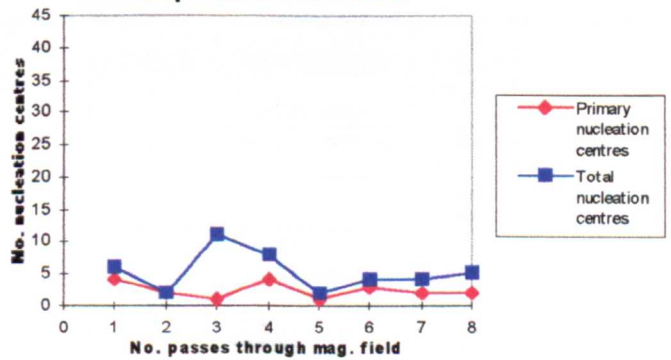
SAMPLE	MORPHOLOGY	NOTES
1	wedge (some dendritic)	v. fine, opaque, ordered crystals
2	wedge and dendritic	chunky (w) and fine (dend), v. opaque, crystals
3	wedge (some dendritic)	v chunky (w) and v. fine (dend), v, opaque, ordered crystals
4	wedge and dendritic	chunky, crystals
5	wedge (some dendritic)	chunky, opaque, ordered crystals
6	wedge and dendritic	v. chunky crystals
7	wedged and dendritic	v. chunky, v. opaque crystals
8	wedge	v. chunky (w) and v. fine (dend), opaque crystals

Tables 2.3.46 A and B Summary of the visual observations of sucrose crystal morphology recorded for Experiment 38.

Experiment 38 Run A



Experiment 38 Run B



Graphs 2.3.14 A and B Number of nucleation centres (both primary and total) versus No. passes recorded for Experiment 38.

Experiment 39 - 265-300G permanent field

Run A

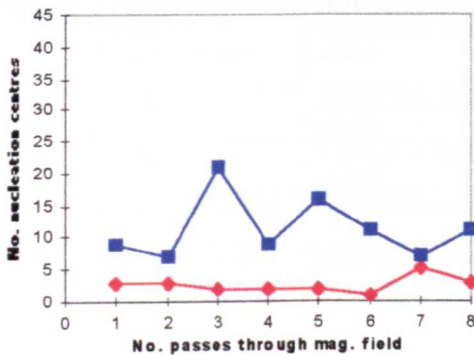
SAMPLE	MORPHOLOGY	NOTES
1	wedge	chunky, clear, ordered crystals
2	wedge	chunky, clear crystals
3	wedge and dendritic	v. fine, opaque, disordered crystals
4	wedge and dendritic	chunky, v. opaque, disordered crystals
5	wedge and dendritic	fine crystals
6	wedge	chunky, opaque, ordered crystals
7	wedge (some dendritic)	medium sized, ordered crystals
8	wedge and dendritic	medium sized opaque crystals

Run B

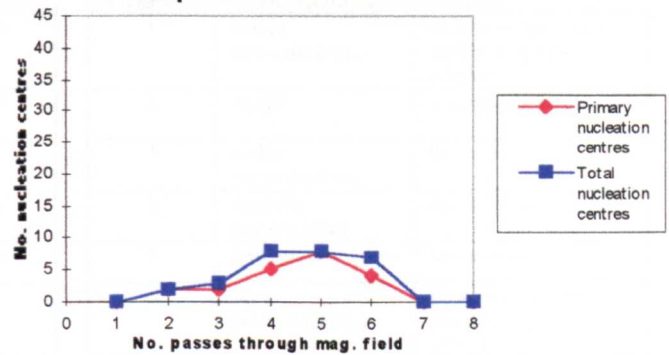
SAMPLE	MORPHOLOGY	NOTES
1	euhedral	chunky, v. clear crystals
2	euhedral, wedge and dendritic	medium sized, v. opaque, disordered crystals
3	euhedral, wedge and dendritic	chunky, v. opaque, disordered crystals
4	euhedral	chunky, disordered crystals
5	euhedral	medium sized, disordered crystals
6	euhedral	fine, clear crystals
7	euhedral	medium sized, clear crystals
8	euhedral	fine, v. clear crystals

Tables 2.3.47 A and B Summary of the visual observations of sucrose crystal morphology recorded for Experiment 39.

Experiment 39 Run A



Experiment 39 Run B



Graphs 2.3.15 A and B Number of nucleation centres (both primary and total) versus No. passes recorded for Experiment 39.

Experiment 40 - 350-400G permanent field

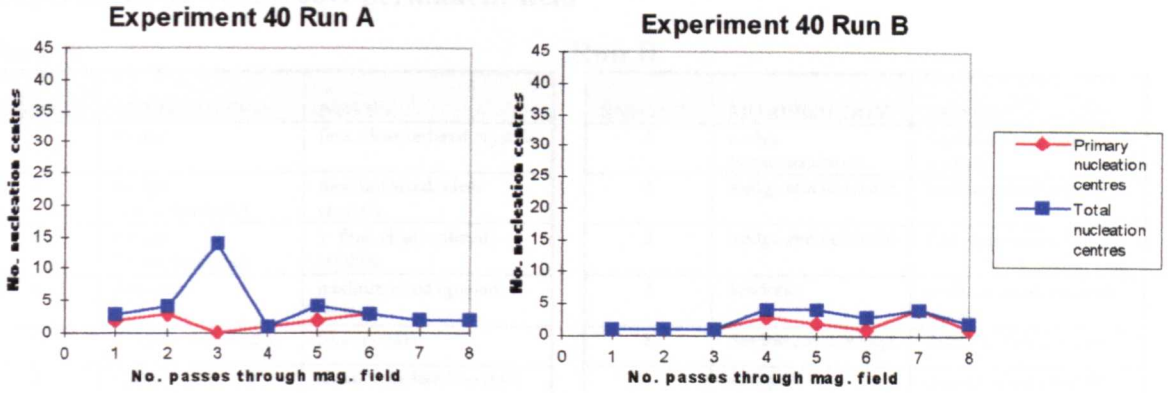
Run A

SAMPLE	MORPHOLOGY	NOTES
1	euhedral	chunky, opaque crystals
2	wedge and dendritic	chunky crystals
3	dendritic	fine, v. opaque crystals
4	dendritic	chunky, v. opaque crystals
5	wedge	chunky, ordered crystals
6	wedge (some dendritic)	chunky crystals
7	dendritic	medium sized, v. opaque crystals
8	euhedral and wedge	v. chunky, clear euhedral & chunky, v. opaque wedge crystals

Run B

SAMPLE	MORPHOLOGY	NOTES
1	wedge (some dendritic)	chunky, clear crystals
2	wedge and dendritic	chunky wedge & fine dend., v. opaque crystals
3	dendritic	v. fine, v. opaque crystals
4	dendritic (some wedge)	fine, v. opaque, disordered crystals
5	dendritic (some wedge)	fine, v. opaque, disordered crystals
6	wedge (some dendritic)	chunky, opaque crystals
7	wedge (some dendritic)	medium sized, opaque crystals
8	wedge	v. chunky, opaque crystals

Tables 2.3.48 A and B Summary of the visual observations of sucrose crystal morphology recorded for Experiment 40.



Graphs 2.3.16 A and B Number of nucleation centres (both primary and total) versus No. passes recorded for Experiment 40.

Experiment 41 - 540-620G permanent field

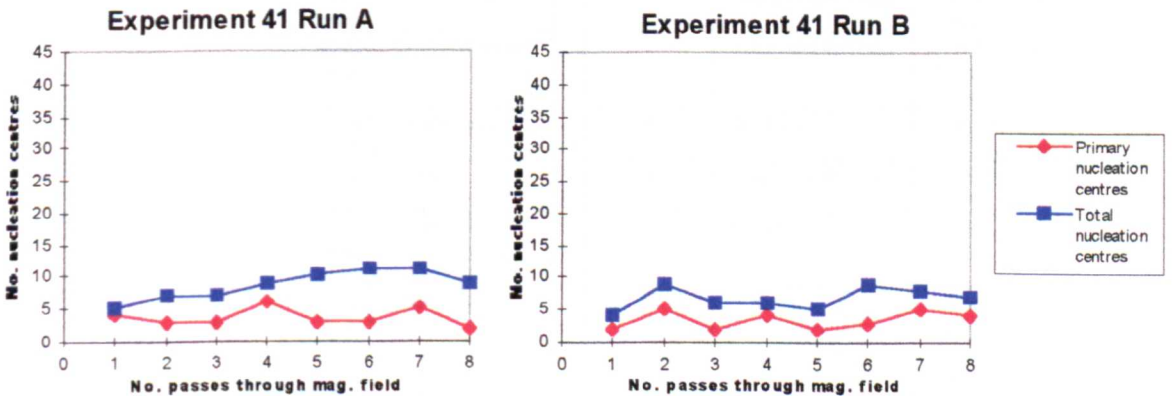
Run A

SAMPLE	MORPHOLOGY	NOTES
1	wedge (some dendritic)	chunky, clear, ordered crystals
2	wedge	chunky, clear, ordered crystals
3	wedge	v. chunky, ordered crystals
4	wedge and dendritic	medium sized crystals
5	wedge and dendritic	medium sized crystals
6	wedge and dendritic	medium sized crystals
7	wedge	fine, clear, ordered crystals
8	wedge (some dendritic)	chunky, ordered crystals

Run B

SAMPLE	MORPHOLOGY	NOTES
1	wedge (some dendritic)	chunky wedge & fine dendritic, opaque crystals
2	wedge	fine, opaque crystals
3	wedge (some dendritic)	fine crystals
4	dendritic (some wedge)	fine, v. opaque crystals
5	dendritic and wedge	fine crystals
6	wedge (some dendritic)	medium sized wedge & fine dend., opaque crystals
7	wedge	chunky, clear, ordered crystals
8	wedge (some dendritic)	chunky wedge & fine dendritic, opaque crystals

Tables 2.3.49 A and B Summary of the visual observations of sucrose crystal morphology recorded for Experiment 41.



Graphs 2.3.17 A and B Number of nucleation centres (both primary and total) versus No. passes recorded for Experiment 41.

Experiment 42 - 630-760G permanent field

Run A

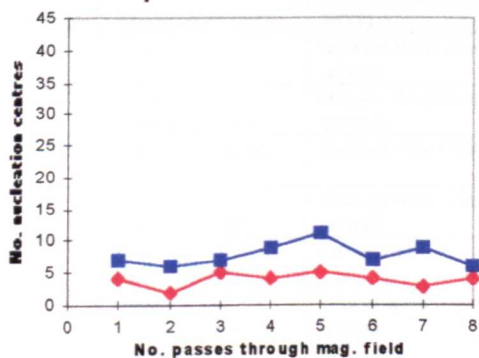
SAMPLE	MORPHOLOGY	NOTES
1	wedge	fine, clear ordered crystals
2	wedge (some dendritic)	medium sized, clear crystals
3	wedge (some dendritic)	v. fine, clear ordered crystals
4	dendritic	medium sized opaque crystals
5	dendritic and wedge	fine crystals
6	wedge (some dendritic)	chunky, ordered crystals
7	dendritic (some wedge)	v. chunky, opaque, disordered crystals
8	dendritic (some wedge)	fine crystals

Run B

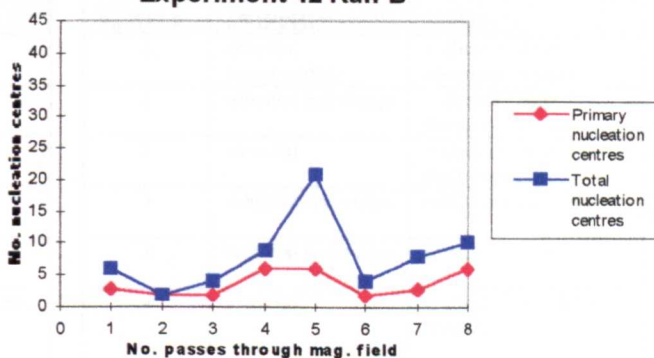
SAMPLE	MORPHOLOGY	NOTES
1	wedge (some dendritic)	medium sized, opaque crystals
2	wedge and dendritic	medium sized crystals
3	wedge and dendritic	fine, opaque crystals
4	dendritic	medium sized, ordered crystals
5	dendritic and wedge	chunky, clear crystals
6	wedge (some dendritic)	chunky, clear crystals
7	dendritic (some wedge)	chunky, clear crystals
8	dendritic	fine, opaque crystals

Tables 2.3.50 A and B Summary of the visual observations of sucrose crystal morphology recorded for Experiment 42.

Experiment 42 Run A



Experiment 42 Run B



Graphs 2.3.18 A and B Number of nucleation centres (both primary and total) versus No. passes recorded for Experiment 42.

Experiment 43 - AC electromagnetic field

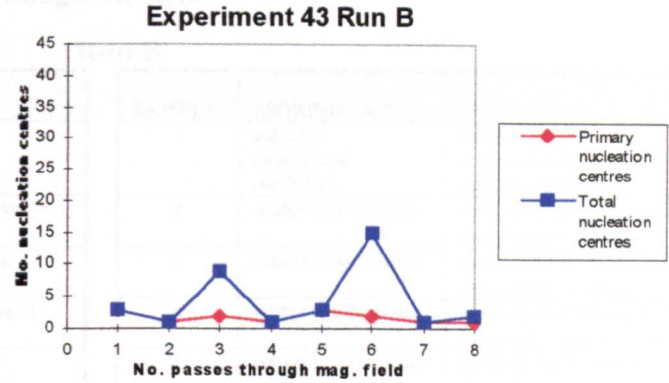
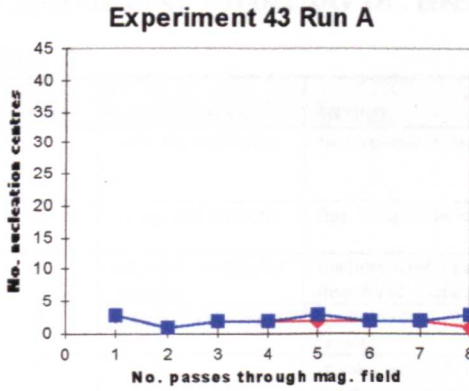
Run A

SAMPLE	MORPHOLOGY	NOTES
1	euhedral and wedge	chunky, clear, ordered crystals
2	wedge (some dendritic)	chunky, opaque, ordered crystals
3	wedge (some dendritic)	chunky, v. clear, ordered crystals
4	wedge and euhedral	v. chunky, clear, v. ordered crystals
5	wedge (some dendritic)	v. chunky wedge & medium sized euhedral, ordered crystals
6	wedge (some euhedral)	v. chunky, ordered crystals
7	wedge (some dendritic)	medium sized, clear crystals
8	wedge (some dendritic)	chunky, clear wedge & fine, opaque dend. crystals

Run B

SAMPLE	MORPHOLOGY	NOTES
1	euhedral and wedge	medium sized, clear crystals
2	wedge and dendritic	medium sized wedge & fine, v. opaque dendritic crystals
3	dendritic	v. fine, v. opaque, ordered crystals
4	wedge and dendritic	medium sized, opaque crystals
5	euhedral	chunky, opaque crystals
6	dendritic	v. fine, v. opaque, ordered crystals
7	wedge and dendritic (some euhedral)	chunky wedge & fine dendritic, clear crystals
8	euhedral and wedge (some dendritic)	chunky, clear, ordered crystals

Tables 2.3.51 A and B Summary of the visual observations of sucrose crystal morphology recorded for Experiment 43.



Graphs 2.3.19 A and B Number of nucleation centres (both primary and total) versus No. passes recorded for Experiment 43.

Experiment 44 - 50-100G DC electromagnetic field

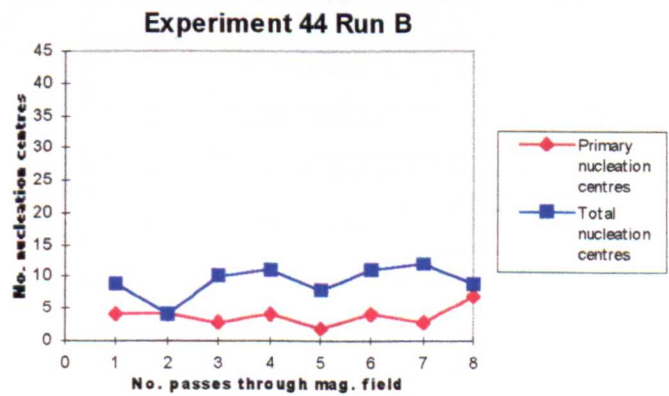
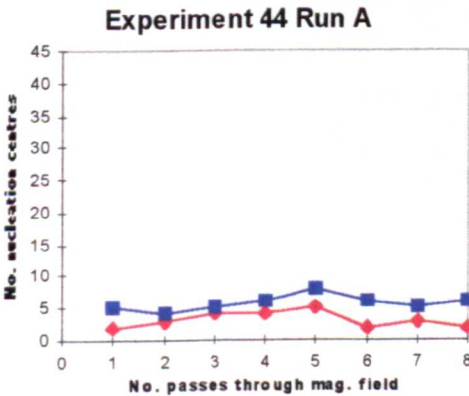
Run A

SAMPLE	MORPHOLOGY	NOTES
1	wedge	medium sized, clear crystals
2	wedge (some dendritic)	chunky, disordered crystals
3	wedge and dendritic	medium sized crystals
4	wedge (some euhydrat)	medium sized, clear crystals
5	wedge (some dendritic)	fine crystals
6	wedge (some dendritic and euhydrat)	v. fine, opaque, disordered crystals
7	euhydrat (some wedge)	chunky, opaque crystals
8	wedge and dendritic	chunky crystals

Run B

SAMPLE	MORPHOLOGY	NOTES
1	euhydrat (some wedge)	v. chunky, clear, disordered crystals
2	euhydrat and wedge	v. chunky, clear, disordered crystals
3	euhydrat	v. chunky, clear, disordered crystals
4	euhydrat and wedge	medium sized crystals
5	euhydrat and wedge	chunky, clear crystals
6	euhydrat	v. chunky, disordered crystals
7	euhydrat (some wedge)	v. chunky euhydrat & v. fine wedge, opaque, v. disordered crystals
8	euhydrat and wedge	chunky, clear, ordered crystals

Tables 2.3.52 A and B Summary of the visual observations of sucrose crystal morphology recorded for Experiment 44.



Graphs 2.3.20 A and B Number of nucleation centres (both primary and total) versus No. passes recorded for Experiment 44.

Experiment 45 - 100-220G DC electromagnetic field

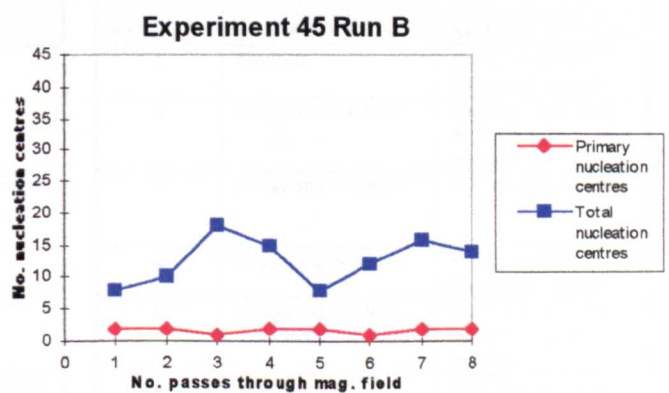
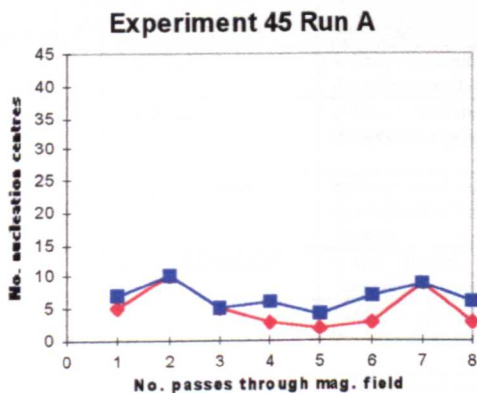
Run A

Run B

SAMPLE	MORPHOLOGY	NOTES
1	dendritic and wedge	fine, opaque crystals
2	wedge and dendritic	fine, clear, ordered crystals
3	euhedral, wedge and dendritic	medium sized, opaque, disordered crystals
4	euhedral and wedge	medium sized, disordered crystals
5	wedge (some dendritic)	chunky wedge & fine dendritic, clear crystals
6	wedge and dendritic	fine, clear, disordered crystals
7	wedge (some dendritic)	chunky, opaque, ordered crystals
8	euhedral, wedge (some dendritic)	chunky wedge & euhyd., v. fine dend., opaque crystals

SAMPLE	MORPHOLOGY	NOTES
1	euhedral (wedge and dendritic)	chunky euhyd. & fine wedge and dendritic, opaque crystals
2	wedge and dendritic	medium sized wedge & v. fine dendritic crystals
3	dendritic and wedge	medium sized wedge & v. fine, opaque crystals
4	wedge and dendritic	medium sized wedge & v. fine dend., opaque crystals
5	euhedral and wedge	medium sized, opaque crystals
6	wedge and dendritic (some euhedral)	v. chunky wedge & v. fine dend., opaque crystals
7	wedge	fine, opaque crystals
8	wedge (some dendritic)	v. fine, v. opaque crystals

Tables 2.3.53 A and B Summary of the visual observations of sucrose crystal morphology recorded for Experiment 45.



Graphs 2.3.21 A and B Number of nucleation centres (both primary and total) versus No. passes recorded for Experiment 45.

Experiment 46 - 150-340G DC electromagnetic field

Run A

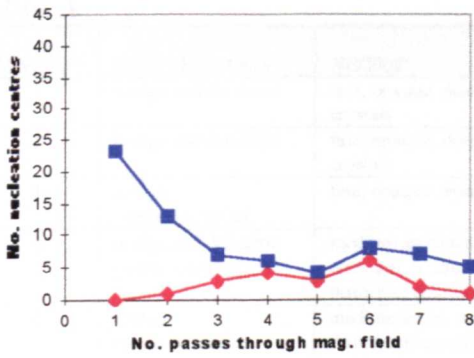
Run B

SAMPLE	MORPHOLOGY	NOTES
1	wedge (some dendritic)	v. chunky, opaque, disordered crystals
2	wedge (some dendritic)	medium sized, clear, ordered crystals
3	wedge and dendritic	fine, opaque crystals
4	euhedral	medium sized, clear, ordered crystals
5	euhedral and wedge	chunky wedge & fine dendritic, opaque crystals
6	wedge (some dendritic)	fine, ordered crystals
7	wedge	chunky wedge & fine dendritic, clear crystals
8	euhedral	v. chunky wedge & fine dendritic, clear crystals

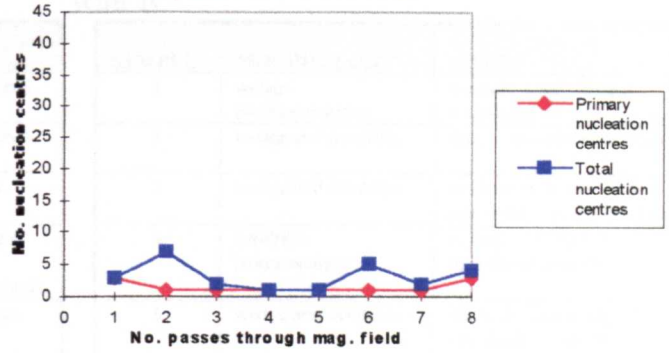
SAMPLE	MORPHOLOGY	NOTES
1	wedge and dendritic	chunky, disordered crystals
2	dendritic and wedge	chunky wedge & fine dend., opaque crystals
3	wedge and dendritic	medium sized, opaque crystals
4	wedge and dendritic	v. chunky wedge & med. sized dendritic, opaque crystals
5	wedge (some dendritic)	v. chunky, ordered crystals
6	dendritic	fine, opaque, v. disordered crystals
7	wedge and dendritic	v. chunky & v. fine dend., opaque crystals
8	wedge	chunky, clear crystals

Tables 2.3.54 A and B Summary of the visual observations of sucrose crystal morphology recorded for Experiment 46.

Experiment 46 Run A



Experiment 46 Run B



Graphs 2.3.22 A and B Number of nucleation centres (both primary and total) versus No. passes recorded for Experiment 46.

Experiment 47 - 190-500G DC electromagnetic field

Run A

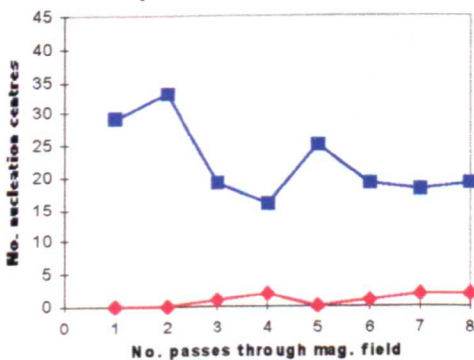
SAMPLE	MORPHOLOGY	NOTES
1	dendritic	v. fine, v. opaque, disordered crystals
2	dendritic	v. fine, v. opaque, disordered crystals
3	wedge and dendritic	medium sized wedge & v. fine dendritic, opaque crystals
4	wedge and dendritic	v. fine, opaque, disordered crystals
5	dendritic	v. fine, v. opaque, disordered crystals
6	euhedral and dendritic	medium sized euhedral & v. fine dendritic, opaque crystals
7	euhedral and dendritic	medium sized euhedral & v. fine dendritic, opaque crystals
8	wedge and dendritic	fine euhedral & v. fine wedge, opaque crystals

Run B

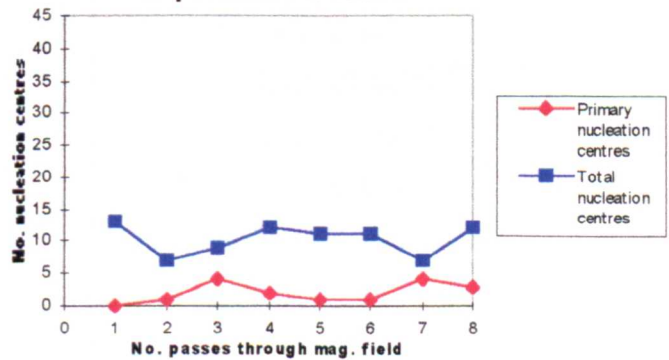
SAMPLE	MORPHOLOGY	NOTES
1	dendritic	v. fine, v. opaque, disordered crystals
2	wedge and dendritic	medium sized wedge & fine dendritic, clear crystals
3	wedge and dendritic	fine, opaque crystals
4	wedge and dendritic	v. fine, opaque, disordered crystals
5	wedge and dendritic	fine wedge & v. fine dendritic, opaque crystals
6	dendritic	fine, opaque crystals
7	wedge (some dendritic)	v. fine, ordered crystals
8	wedge (some dendritic)	fine, opaque crystals

Tables 2.3.55 A and B Summary of the visual observations of sucrose crystal morphology recorded for Experiment 47.

Experiment 47 Run A



Experiment 47 Run B



Graphs 2.3.23 A and B Number of nucleation centres (both primary and total) versus No. passes recorded for Experiment 47.

Experiment 48 - 220-600G DC electromagnetic field

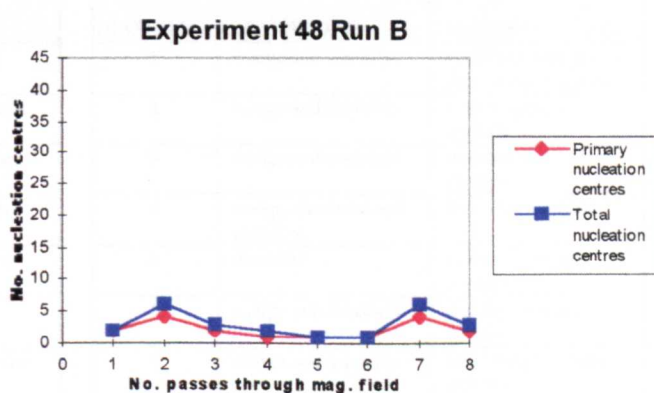
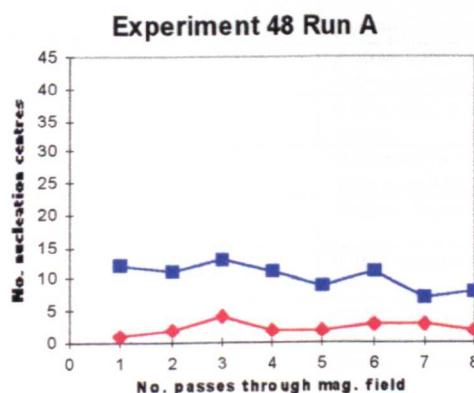
Run A

Run B

SAMPLE	MORPHOLOGY	NOTES
1	wedge and dendritic	fine, opaque, disordered crystals
2	wedge and dendritic	fine, opaque, disordered crystals
3	wedge (some dendritic)	fine, opaque crystals
4	wedge and dendritic (some euhedral)	medium sized wedge & euhedral, v. fine dendritic, opaque crystals
5	wedge (some dendritic)	medium sized, opaque, disordered crystals
6	wedge and dendritic	medium sized, opaque, disordered crystals
7	euhedral and wedge	chunky, ordered crystals
8	euhedral and wedge	v. chunky, ordered crystals

SAMPLE	MORPHOLOGY	NOTES
1	wedge (some dendritic)	medium sized, opaque, disordered crystals
2	wedge and dendritic	fine, v. disordered crystals
3	wedge and dendritic	medium sized wedge & v. fine dend., opaque crystals
4	dendritic (some wedge)	v. fine, v. opaque, v. disordered crystals
5	wedge and dendritic	medium sized wedge & v. fine dend., v. opaque, disord. crystals
6	wedge and dendritic	fine, v. opaque, disordered crystals
7	euhedral (some wedge)	chunky, opaque, disordered crystals
8	wedge and euhedral	medium sized crystals

Tables 2.3.56 A and B Summary of the visual observations of sucrose crystal morphology recorded for Experiment 48.



Graphs 2.3.24 A and B Number of nucleation centres (both primary and total) versus No. passes recorded for Experiment 48.

Experiment 49 - 300-680G DC electromagnetic field

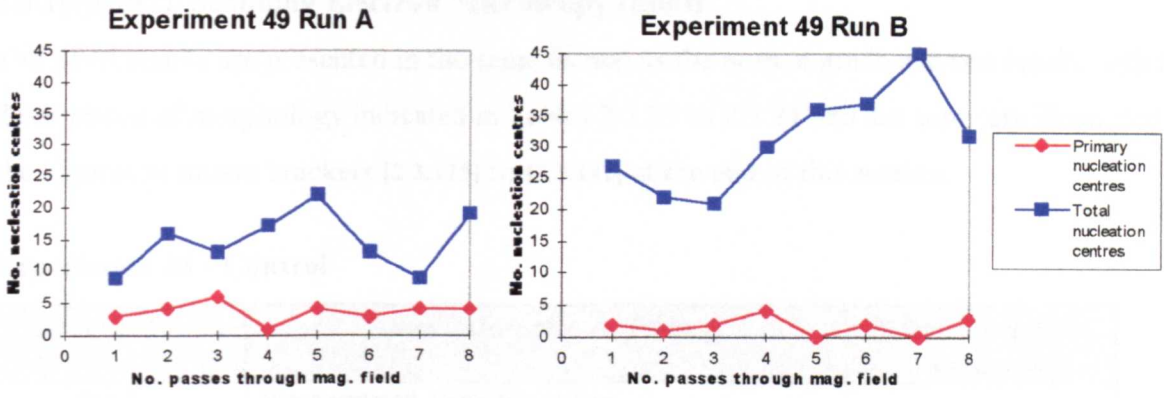
Run A

Run B

SAMPLE	MORPHOLOGY	NOTES
1	slightly euhedral	medium sized, clear crystals
2	wedge and dendritic	fine, opaque crystals
3	dendritic	fine, opaque, ordered crystals
4	euhedral and dendritic	chunky euhedral & v. fine dend., v. ord. crystals
5	wedge and dendritic	v. fine, clear, v. ordered crystals
6	euhedral and dendritic	fine, clear, v. ordered crystals
7	euhedral and dendritic	medium sized, clear crystals
8	wedge and dendritic	fine, clear crystals

SAMPLE	MORPHOLOGY	NOTES
1	dendritic	v. fine, clear, ordered crystals
2	wedge and dendritic	chunky wedge & v. fine dendritic crystals
3	wedge and dendritic	chunky wedge & v. fine dendritic crystals
4	wedge and dendritic	chunky, clear, ordered crystals
5	wedge and dendritic	v. fine, opaque, v. ordered crystals
6	wedge and dendritic	medium sized wedge & v. fine dend., clear, v. ordered crystals
7	wedge and dendritic	v. fine, opaque, v. ordered crystals
8	wedge and dendritic	fine, clear, ordered crystals

Tables 2.3.57 A and B Summary of the visual observations of sucrose crystal morphology recorded for Experiment 49.



Graphs 2.3.25 A and B Number of nucleation centres (both primary and total) versus No. passes recorded for Experiment 49.

Experiment 50 - Pulsed field

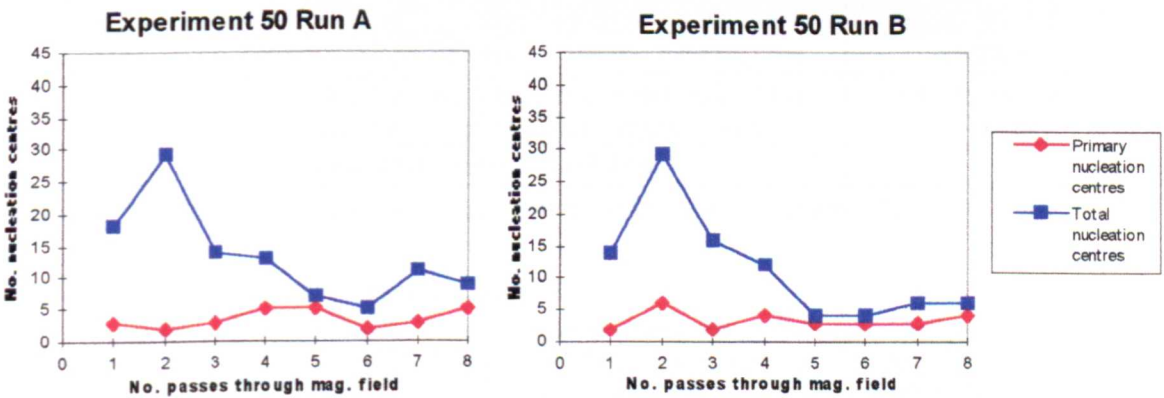
Run A

SAMPLE	MORPHOLOGY	NOTES
1	wedge	medium sized, clear, ordered crystals
2	wedge	v. fine, clear, v. ordered crystals
3	wedge	medium sized, v. clear, ordered crystals
4	wedge	chunky, clear crystals
5	wedge (some dendritic)	v. fine, opaque crystals
6	wedge (some euhydrated)	medium sized, clear, disordered crystals
7	wedge and dendritic	chunky, ordered crystals
8	wedge and dendritic	chunky, v. ordered crystals

Run B

SAMPLE	MORPHOLOGY	NOTES
1	wedge and dendritic	v. chunky wedge & v. fine, opaque crystals
2	wedge and dendritic	v. fine, opaque crystals
3	wedge and euhydrated	medium sized, clear crystals
4	wedge, dendritic and euhydrated	fine, clear crystals
5	dendritic	v. fine, v. opaque crystals
6	wedge and dendritic	chunky, opaque crystals
7	wedge and dendritic	fine, opaque, ordered crystals
8	wedge	v. chunky, ordered crystals

Tables 2.3.58 A and B Summary of the visual observations of sucrose crystal morphology recorded for Experiment 50.



Graphs 2.3.26 A and B Number of nucleation centres (both primary and total) versus No. passes recorded for Experiment 50.

2.3.1(c)(ii)(2) Scanning Electron Microscopy results

The SEM results are presented in the same format as the normal grade sucrose results with the descriptions of morphology indicated in Tables 2.3.59 to 2.3.71 and are some are illustrated in the Figures in square brackets [2.3.115] to [2.3.142] at the end of this section.

Experiment 38 - Control

Sample No.	Description of morphology	Microcrystalline dimensions
38(2)	Wave textured, fairly flat surface	
38(5)	Microcrystals and rough textured surface	~30-60µm
38(6)	Layered, stepped growth[2.3.115], some rounded microcrystals	~30-80µm

Table 2.3.59 SEM observations for sucrose Samples in Experiment 38.

Experiment 39 - 265-300G Permanent field

Sample No.	Description of morphology	Microcrystalline dimensions
39(2)	Large chunky stepped layers and amorphous material on surface in some areas, some strange shaped microcrystals[2.3.116]	~40µm
39(3)	Large chunky stepped growth[2.3.117] and some wave textured surfaces	
39(4)	Flat wave textured surfaces with areas of extensive pitting	
39(6)	Amorphous flaky material mixed with rounded, badly formed microcrystals on flat surface[2.3.118]	~30µm

Table 2.3.60 SEM observations for sucrose Samples in Experiment 39.

Experiment 40 - 350-400G Permanent field

Sample No.	Description of morphology	Microcrystalline dimensions
40(1)	Extensively pitted surfaces, rounded microcrystals	~15-20µm
40(5)	Flat plate-like, mal-formed microcrystals[2.3.119] alongside large crops of rounded microcrystals	~50-75µm [34] ~20-30µm
40(8)	Regularly pitted, flat surfaces[2.3.120]	

Table 2.3.61 SEM observations for sucrose Samples in Experiment 40.

Experiment 41 - 540-620G Permanent field

Sample No.	Description of morphology	Microcrystalline dimensions
41(2)	Rounded microcrystals	~30-40µm
41(6)	Large crops of rounded microcrystals[2.3.121]	~30-60µm

Table 2.3.62 SEM observations for sucrose Samples in Experiment 41.

Experiment 42 - 630-760G Permanent field

Sample No.	Description of morphology	Microcrystalline dimensions
42(1)	Extensively pitted surfaces[2.3.122]	
42(8)	Chunky microcrystals embedded with elongated, chunky stepped growth[2.3.123]	~10-20 μ m

Table 2.3.63 SEM observations for sucrose Samples in Experiment 42.

Experiment 43 - AC electromagnetic field

Sample No.	Description of morphology	Microcrystalline dimensions
43(1)	Well formed microcrystals embedded in pitted surface	~20-50 μ m
43(2)	Wave textured surface, well formed microcrystals	~30-80 μ m
43(3)	Wave textured surface, layered, stepped growth[2.3.124]	
43(6)	Extensively layered, pitted surface[2.3.125] and some well formed microcrystals	~15-60 μ m
43(7)	Directional pitted surface[2.3.126]	

Table 2.3.64 SEM observations for sucrose Samples in Experiment 43.

Experiment 44 - 50-100G DC electromagnetic field

Sample No.	Description of morphology	Microcrystalline dimensions
44(1)	Rounded microcrystals, some pitting on flat smooth surfaces	~15-30 μ m
44(3)	Well formed microcrystals embedded in surface, some pitting on flat surfaces and some layered growth	~15-20 μ m
44(6)	Large flat microcrystals on pitted surface[2.3.127]	~80-100 μ m
44(7)	Layered, step growth surface and microcrystalline material[2.3.128]	~10-20 μ m & ~50 μ m

Table 2.3.65 SEM observations for sucrose Samples in Experiment 44.

Experiment 45 - 100-220G DC electromagnetic field

Sample No.	Description of morphology	Microcrystalline dimensions
45(6)	Very flat surfaces with large amounts of microcrystals[2.3.129]	~15-30 μ m
45(7)	Odd-shaped microcrystals[2.3.130] with layered surfaces[2.3.131]	~20 μ m

Table 2.3.66 SEM observations for sucrose Samples in Experiment 45.

Experiment 46 - 150-340G DC electromagnetic field

Sample No.	Description of morphology	Microcrystalline dimensions
46(6)	Flat surfaces with extensive amounts of well formed microcrystals[2.3.232]	~20-40 μ m
46(7)	Rounded microcrystals and flat, wave textured and pitted surfaces	~20-30 μ m
46(8)	Unidirectional, layered surfaces with well formed microcrystals[2.3.233]	~20-40 μ m

Table 2.3.67 SEM observations for sucrose Samples in Experiment 46.

Experiment 47 - 190-500G DC electromagnetic field

Sample No.	Description of morphology	Microcrystalline dimensions
47(5)	Rounded microcrystals	~20-30 μ m
47(7)	Very straight lined, layered surface but bi-directional[2.3.234]	
47(8)	Rounded microcrystals covering wave textured crystal surface[2.3.235]	~20-40 μ m

Table 2.3.68 SEM observations for sucrose Samples in Experiment 47.

Experiment 48 - 220-600G DC electromagnetic field

Sample No.	Description of morphology	Microcrystalline dimensions
48(1)	Extensively pitted surfaces and some rounded microcrystals	~20-60 μ m
48(6)	Very flat surfaces and angled edges with some rounded microcrystalline material[2.3.236]	~30-80 μ m

Table 2.3.69 SEM observations for sucrose Samples in Experiment 48.

Experiment 49 - 300-680G DC electromagnetic field

Sample No.	Description of morphology	Microcrystalline dimensions
49(1)	Very small clumps of amorphous material on rough textured surface[2.3.237] and rounded microcrystals in other areas	~5-10 μ m
49(3)	Uneven, rough surface, some bubbles pushing through to surface	
49(4)	Rough textured surfaces, some angled edges	
49(7)	Rough, pitted surface, bubbles on surface, some rounded microcrystals[2.3.238]	~30-80 μ m

Table 2.3.70 SEM observations for sucrose Samples in Experiment 49.

Experiment 50 - Pulsed field

Sample No.	Description of morphology	Microcrystalline dimensions
50(3)	Chunky step growth with some pitting and well formed microcrystals[2.3.239]	~20-50 μ m
50(5)	Flat textured surfaces, well formed microcrystals with some strange angular shapes[2.3.240]	~20-70 μ m
50(6)	Well formed microcrystals and layered, pitted surfaces	~15-30 μ m
50(7)	Well formed microcrystals and uni-directional layered growth[2.3.241]	~20-40 μ m
50(8)	Very well formed microcrystals[2.3.242] on flat surface	~20-40 μ m

Table 2.3.71 SEM observations for sucrose Samples in Experiment 50.

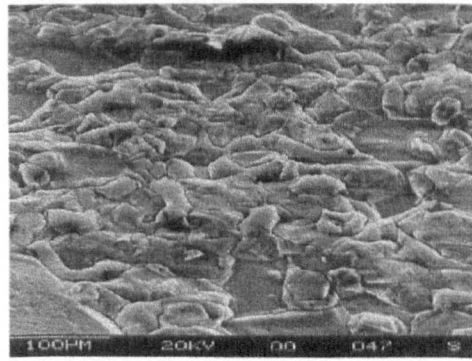
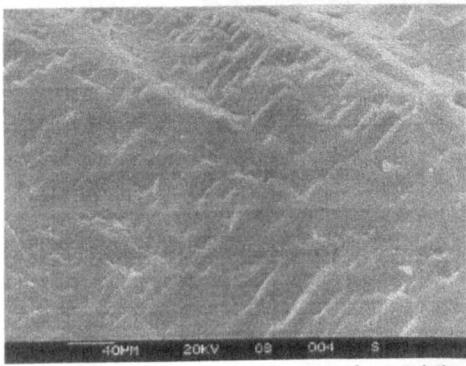


Fig. 2.3.115 Sucrose sample 38(6), Run A. Fig. 2.3.116 Sucrose sample 39(2), Run A.

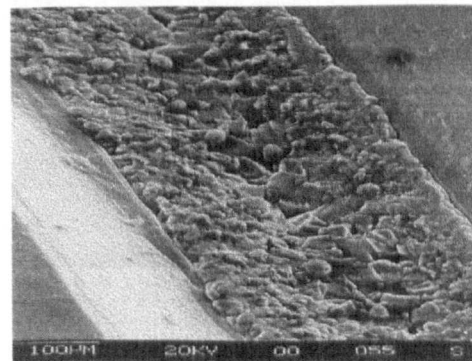
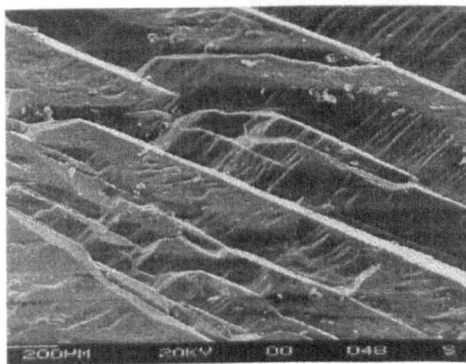


Fig. 2.3.117 Sucrose sample 39(3), Run A. Fig. 2.3.118 Sucrose sample 39(6), Run A.

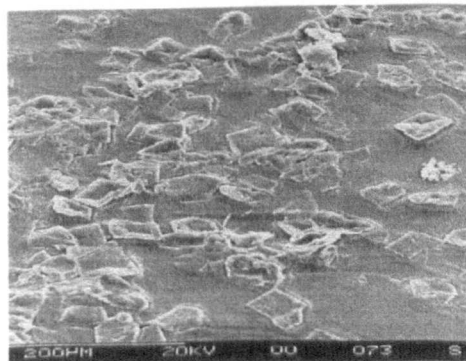


Fig. 2.3.119 Sucrose sample 40(5), Run A. Fig. 2.3.120 Sucrose sample 40(8), Run A.

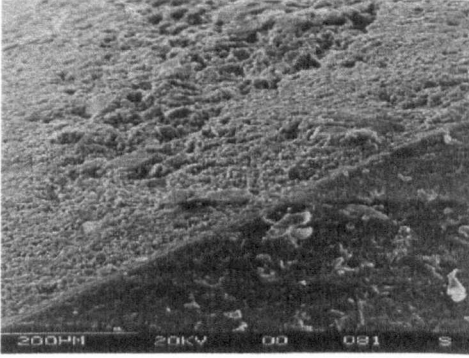


Fig. 2.3.121 Sucrose sample 41(6), Run A.

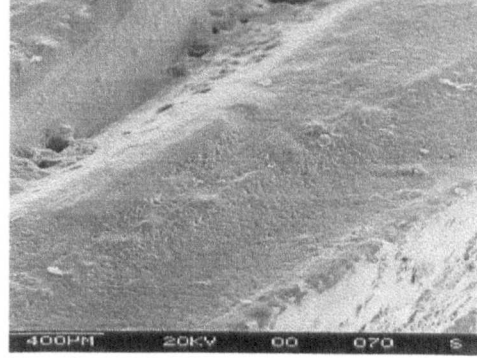


Fig. 2.3.122 Sucrose sample 42(1), Run A.

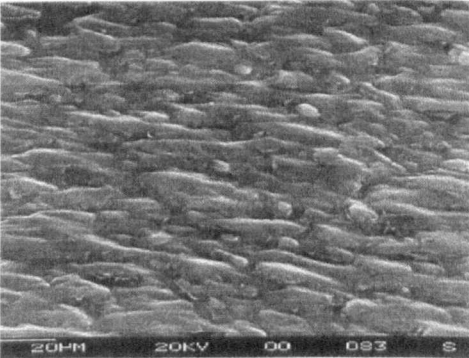


Fig. 2.3.123 Sucrose sample 42(8), Run B.

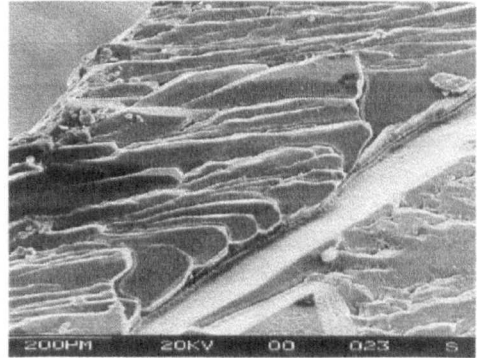


Fig. 2.3.124 Sucrose sample 43(3), Run A.

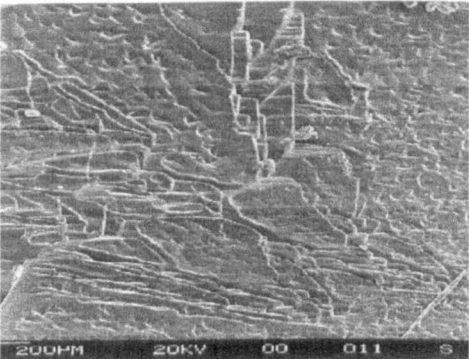


Fig. 2.3.125 Sucrose sample 43(6), Run A.

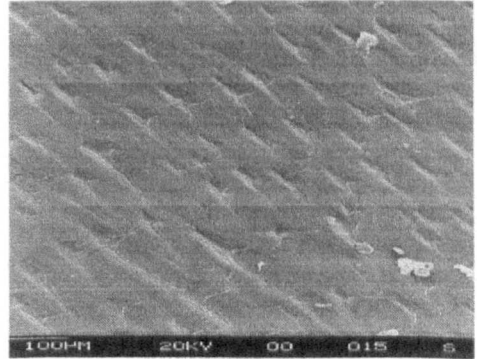


Fig. 2.3.126 Sucrose sample 43(7), Run A.

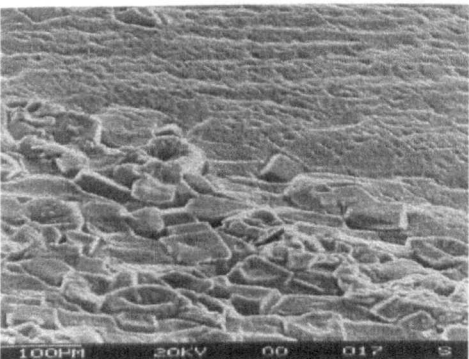


Fig. 2.3.127 Sucrose sample 44(6), Run A.

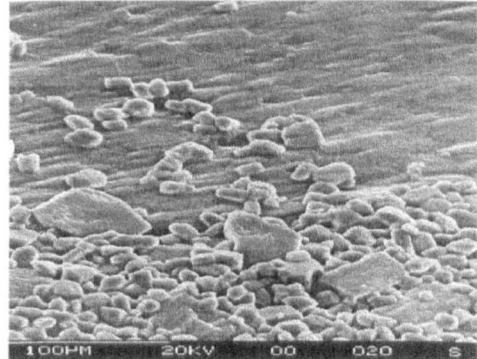


Fig. 2.3.128 Sucrose sample 44(7), Run B.

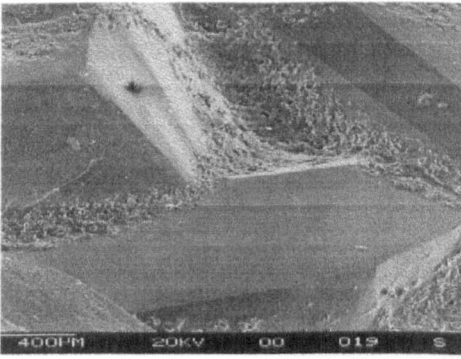


Fig. 2.3.129 Sucrose sample 45(6), Run B.

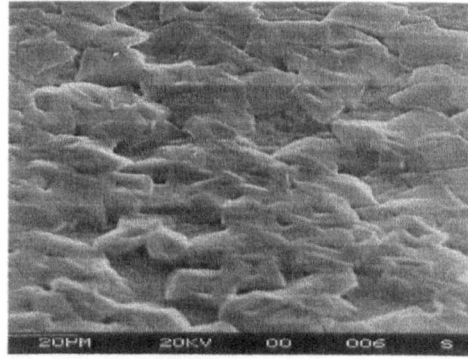


Fig. 2.3.130 Sucrose sample 45(7), Run A.

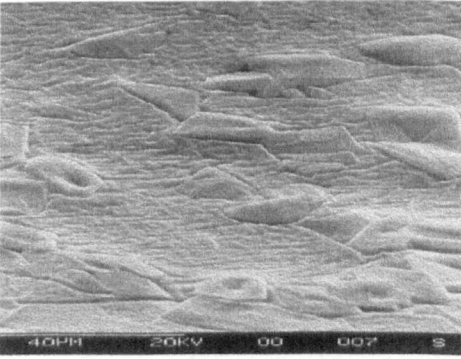


Fig. 2.3.131 Sucrose sample 45(7), Run A.

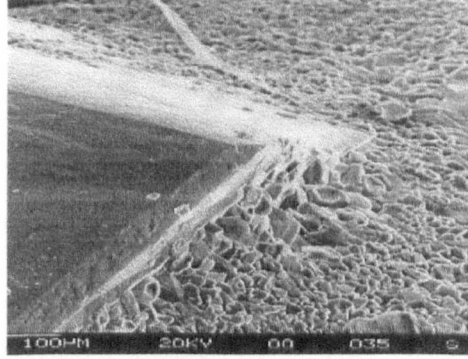


Fig. 2.3.132 Sucrose sample 46(6), Run A.

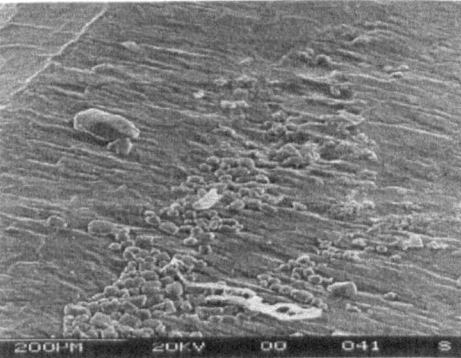


Fig. 2.3.133 Sucrose sample 46(8), Run A.

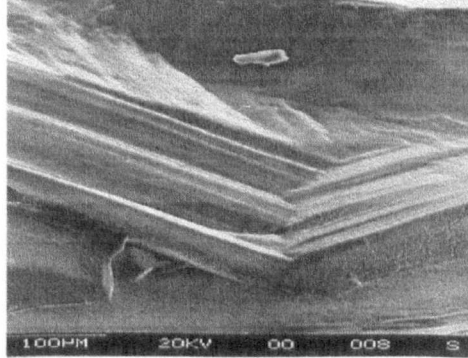


Fig. 2.3.134 Sucrose sample 47(7), Run A.



Fig. 2.3.135 Sucrose sample 47(8), Run A.

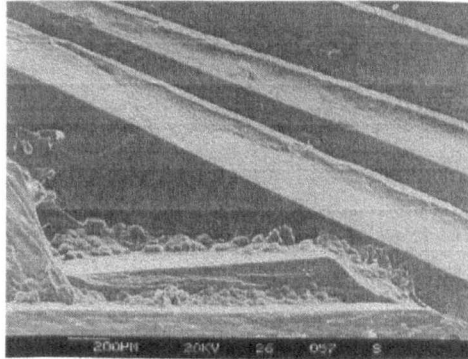


Fig. 2.3.136 Sucrose sample 48(6), Run A.

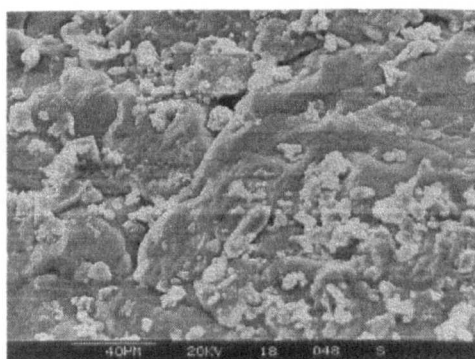


Fig. 2.3.137 Sucrose sample 49(1), Run A.



Fig. 2.3.138 Sucrose sample 49(7), Run A.

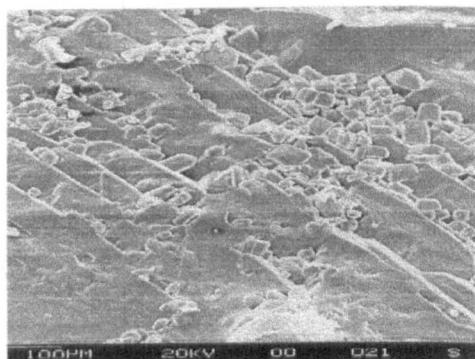


Fig. 2.3.139 Sucrose sample 50(3), Run A.

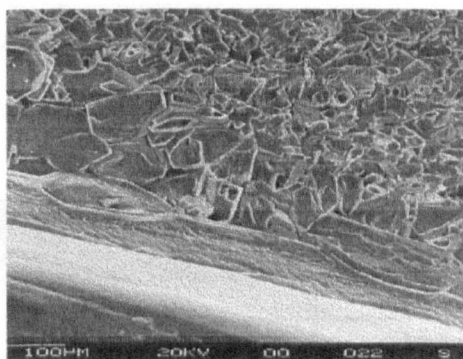


Fig. 2.3.140 Sucrose sample 50(5), Run A.

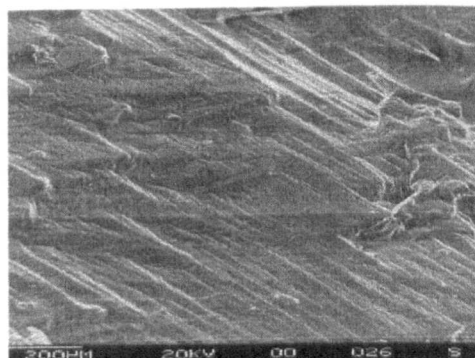


Fig. 2.3.141 Sucrose sample 50(7), Run A.

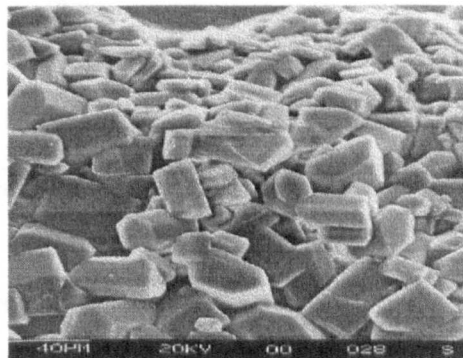


Fig. 2.3.142 Sucrose sample 50(8), Run A.

2.3.1(c)(ii)(3) Differential Scanning Calorimetry Results

The DSC melting point data are presented in tabular form (Tables 2.3.72 to 2.3.85) using the same classification as described in section 2.3.1(c)(i)(3) where:

VVS = very, very small	M = medium
VS = very small	L = large
S = small	VL = very large

Experiment 38 – Control

Run A

Sample	Feature 1 (°C)	Feature 2 (°C)	Feature 3 (°C)	Melting point (°C)
1	151.20 S	160.00 S		180.45
2	151.20 S			178.12
3	151.20 S			181.60
4	152.20 S			181.60
5	153.80 VS			187.32
6	152.20 S			183.27
7	151.20 S			182.99
8	152.80 S			181.60

Table 2.3.72 DSC results for sucrose samples from Experiment 38.

Run B

Sample	Feature 1 (°C)	Feature 2 (°C)	Feature 3 (°C)	Melting point (°C)
1	151.20 M			182.46
2	153.80 VVS			186.38
3	152.20 M			180.93
4	152.20 S			179.67
5	151.20 M			182.09
6	150.20 M			181.28
7	152.20 M	158.80 S		181.60
8	157.40 S			181.94

Table 2.3.73 DSC results for sucrose samples from Experiment 38.

Experiment 39 – 265-300G Permanent field

Sample	Feature 1 (°C)	Feature 2 (°C)	Feature 3 (°C)	Melting point (°C)
1	152.17 M			169.41
2	150.17 M			169.55
3	150.17 L	163.33 M		176.31
4	151.17 M			168.37
5	152.17 M			166.67
6	154.83 S			172.10
7	153.83 L	157.50 L		167.20
8	152.83 M	160.17 M		171.32

Table 2.3.74 DSC results for sucrose samples from Experiment 39.

Experiment 40 – 350-400G Permanent field

Sample	Feature 1 (°C)	Feature 2 (°C)	Feature 3 (°C)	Melting point (°C)
1	149.50 L	163.33 L		173.18
2	150.17 M			166.08
3	152.83 S			167.58
4	149.50 M			166.39
5	149.50 L			172.18
6	150.17 S			168.56
7	148.50 VL	162.83 L	166.67 L	172.92
8	147.83 L	163.33 M		174.60

Table 2.3.75 DSC results for sucrose samples from Experiment 40.

Experiment 41 – 540-620G Permanent field

Sample	Feature 1 (°C)	Feature 2 (°C)	Feature 3 (°C)	Melting point (°C)
1	151.17 S	157.50 S		174.25
2	157.50 S			180.04
3	151.17 M			170.36
4	151.17 L	166.67 L		176.78
5	151.17 L	155.50 M		172.39
6	151.17 S			176.23
7	151.17 M			173.49
8	150.17 VL	164.00 S		175.14

Table 2.3.76 DSC results for sucrose samples from Experiment 41.

Experiment 42 – 630-760G Permanent field

Sample	Feature 1 (°C)	Feature 2 (°C)	Feature 3 (°C)	Melting point (°C)
1	155.40 VVS			185.69
2	153.80 VVS			185.88
3	154.80 VS			187.20
4	153.80 VS			186.32
5	153.80 VVS			186.96
6	152.20 VS			185.01
7	153.80 VVS			187.18
8	152.80 S			184.39

Table 2.3.77 DSC results for sucrose samples from Experiment 42.

Experiment 43 – AC electromagnetic field

Sample	Feature 1 (°C)	Feature 2 (°C)	Feature 3 (°C)	Melting point (°C)
1	152.17 VS			175.80
2	160.17 M			180.34
3	150.17 L			165.49
4	152.83 M			174.37
5	153.83 M			178.10
6	149.50 VL			170.97
7	152.83 VS			184.47
8	155.50 M			179.00

Table 2.3.78 DSC results for sucrose samples from Experiment 43.

Experiment 44 – 50-100G DC electromagnetic field

Sample	Feature 1 (°C)	Feature 2 (°C)	Feature 3 (°C)	Melting point (°C)
1	154.83 S			182.10
2	152.17 L			170.68
3	152.83 M			174.86
4	158.17 L			167.37
5	151.17 VL	166.00 L	172.00 VL	176.95
6	152.83 VL			179.24
7	152.83 L			173.65
8	152.17 VL			171.57

Table 2.3.79 DSC results for sucrose samples from Experiment 44.

Experiment 45 – 100-220G DC electromagnetic field

Sample	Feature 1 (°C)	Feature 2 (°C)	Feature 3 (°C)	Melting point (°C)
1	153.83 S	167.67 M		175.91
2	151.17 M	158.83 M		169.98
3	151.17 L	158.83 L	166.11 VL	169.67
4	151.17 L	156.17 M		164.48
5	151.17 M			170.04
6	151.17 S	160.17 M		170.30
7	152.17 L	166.00 VL		168.72
8	151.17 VL			164.62

Table 2.3.80 DSC results for sucrose samples from Experiment 45.

Experiment 46 – 150-340G DC electromagnetic field

Sample	Feature 1 (°C)	Feature 2 (°C)	Feature 3 (°C)	Melting point (°C)
1	152.83 VL	167.67 L		177.18
2	150.17 VL	164.83 L		173.81
3	152.17 VL	164.00 VL		169.14
4	152.17 M	166.00 M		172.93
5	151.17 M	163.33 L		174.69
6	152.17 M			173.36
7	151.17 VL	165.00 VL		171.00
8	152.83 M			174.60

Table 2.3.81 DSC results for sucrose samples from Experiment 46.

Experiment 47 – 190-500G DC electromagnetic field

Sample	Feature 1 (°C)	Feature 2 (°C)	Feature 3 (°C)	Melting point (°C)
1	151.17 M	166.67 L		169.74
2	150.17 VL	162.83 L		172.81
3	153.83 M			175.32
4	152.83 M			172.54
5	150.17 VL	157.50 M	163.33 L	174.05
6	152.17 S			175.10
7	150.17 M	166.00 M		177.76
8	152.17 M	166.00 L		174.41

Table 2.3.82 DSC results for sucrose samples from Experiment 47.

Experiment 48 – 220-600G DC electromagnetic field

Sample	Feature 1 (°C)	Feature 2 (°C)	Feature 3 (°C)	Melting point (°C)
1	150.20 S	160.31 VS		180.59
2	150.20 S			179.06
3	150.20 S			183.92
4	150.20 M			182.14
5	150.20 S			181.43
6	150.20 VL			177.60
7	151.20 S			181.77
8	153.80 S			180.94

Table 2.3.83 DSC results for sucrose samples from Experiment 48.

Experiment 49 – 300-680G DC electromagnetic field

Sample	Feature 1 (°C)	Feature 2 (°C)	Feature 3 (°C)	Melting point (°C)
1	150.17 S			177.30
2	151.20 S			184.49
3	151.20 S			178.45
4	151.20 S	160.30 S		174.53
5	150.20 S			179.07
6	151.20 S			177.42
7	150.17 M	166.20 M		181.21
8	153.20 S	167.20 L		173.66

Table 2.3.84 DSC results for sucrose samples from Experiment 49.

Experiment 50 – Pulsed field

Sample	Feature 1 (°C)	Feature 2 (°C)	Feature 3 (°C)	Melting point (°C)
1	150.20 VVS			186.40
2	151.20 S			182.46
3	152.30 M			178.50
4	150.20 VVS			184.06
5	151.20 S			174.11
6	152.80 S			183.04
7	150.20 S			171.89
8	151.20 S			175.94

Table 2.3.85 DSC results for sucrose samples from Experiment 50.

2.3.1(d) Magnetic treatment of sucrose where the solution is syphoned

This study was also done in two parts: the first using normal grade sucrose and the second an identical repeat using analytical grade sucrose. The results presented in Sections 2.3.1(d)(i) and 2.3.1(d)(ii) for normal and analytical grades of sucrose respectively.

2.3.1(d)(i) NORMAL GRADE SUCROSE

2.3.1(d)(i)(1) Visual observations

The visual observations recorded for each sucrose sample, within each experiment, are given in Tables 2.3.86 to 2.3.90 and Graphs 2.3.27 to 2.3.31 in the same format as before.

Experiment 51 - Control

Run A

SAMPLE	MORPHOLOGY	NOTES
1	wedge	chunky, v. clear crystals
2	wedge	medium sized, clear crystals
3	wedge and dendritic	chunky crystals
4	wedge	chunky, disordered crystals
5	wedge and dendritic	medium sized crystals
6	wedge and dendritic	medium sized crystals
7	wedge and dendritic	medium sized crystals
8	wedge and dendritic	chunky crystals

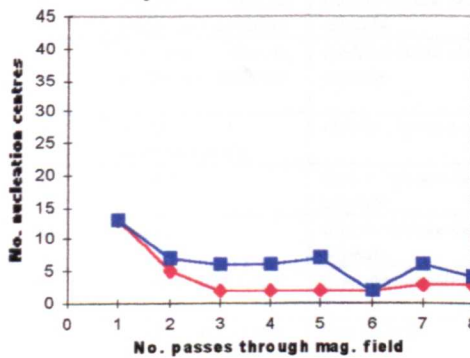
Run B

SAMPLE	MORPHOLOGY	NOTES
1	euhedral and wedge	chunky, v. clear, ordered crystals
2	wedge and dendritic	medium sized crystals
3	wedge and dendritic	medium sized, clear crystals
4	wedge and dendritic	medium sized crystals
5	wedge and dendritic	chunky wedge & medium sized dendritic, clear crystals
6	wedge and dendritic	medium sized, opaque crystals
7	wedge and dendritic	medium sized crystals
8	wedge	v. chunky primary & v. fine secondary crystals

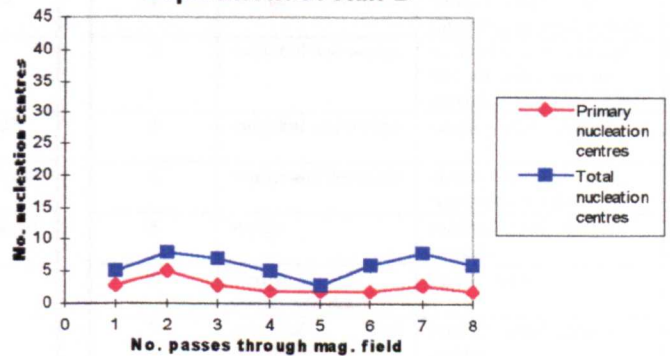
Tables 2.3.86 A and B

Summary of the visual observations of sucrose crystal morphology recorded for Experiment 51.

Experiment 51 Run A



Experiment 51 Run B



Graphs 2.3.27 A and B

Number of nucleation centres (both primary and total) versus No. passes recorded for Experiment 51.

Experiment 52 - 630-760G Permanent field

Run A

SAMPLE	MORPHOLOGY	NOTES
1	euhedral and wedge	fine, clear, ordered crystals
2	euhedral and wedge	chunky, opaque crystals
3	dendritic (some wedge)	chunky wedge & fine dendritic, opaque crystals
4	dendritic and wedge	med. sized, opaque crystals
5	euhedral and wedge (some dendritic)	v. chunky wedge & fine dendritic, opaque crystals
6	euhedral	medium sized crystals
7	euhedral and wedge (some wedge)	fine, opaque crystals
8	wedge and dendritic	v. chunky wedges & v. fine dend., v. opaque crystals

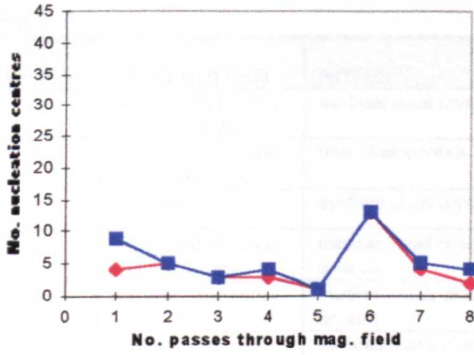
Run B

SAMPLE	MORPHOLOGY	NOTES
1	euhedral and wedge	chunky, opaque crystals
2	euhedral and wedge (some dendritic)	chunky, opaque crystals
3	euhedral and wedge	fine, opaque crystals
4	euhedral	chunky crystals
5	euhedral and wedge (some dendritic)	v. chunky wedge & fine euhedral and dendritic, opaque crystals
6	euhedral	chunky crystals
7	euhedral and wedge (some dendritic)	v. chunky wedge & euhedral, chunky dendritic, opaque crystals
8	euhedral and wedge	medium sized crystals

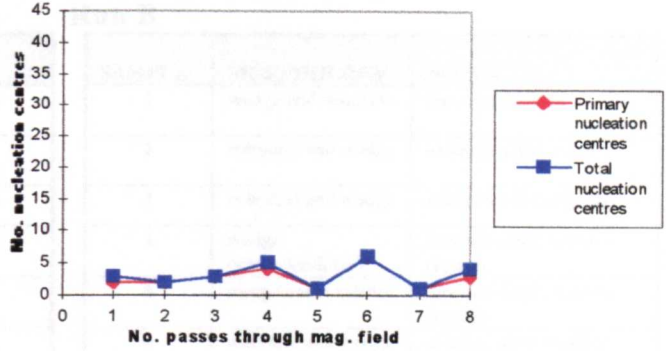
Tables 2.3.87 A and B

Summary of the visual observations of sucrose crystal morphology recorded for Experiment 52.

Experiment 52 Run A



Experiment 52 Run B



Graphs 2.3.28 A and B Number of nucleation centres (both primary and total) versus No. passes recorded for Experiment 52.

Experiment 53 - AC electromagnetic field

Run A

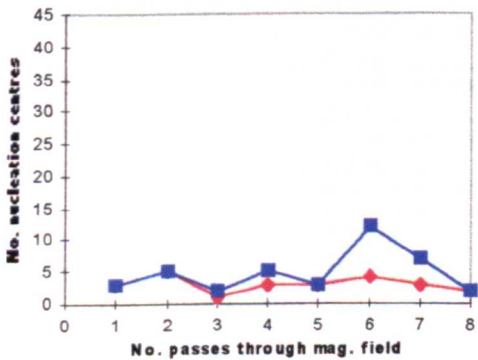
SAMPLE	MORPHOLOGY	NOTES
1	euhedral centres, wedge and dendritic	medium sized, ordered crystals
2	euhedral centres, wedge and dendritic	medium sized, clear crystals
3	wedge (some dendritic)	chunky, opaque crystals
4	dendritic	fine, v. opaque disordered crystals
5	dendritic	fine, v. opaque disordered crystals
6	euyhdral and wedge	fine, clear crystals
7	euyhdral and wedge	fine crystals
8	dendritic	fine, opaque crystals

Run B

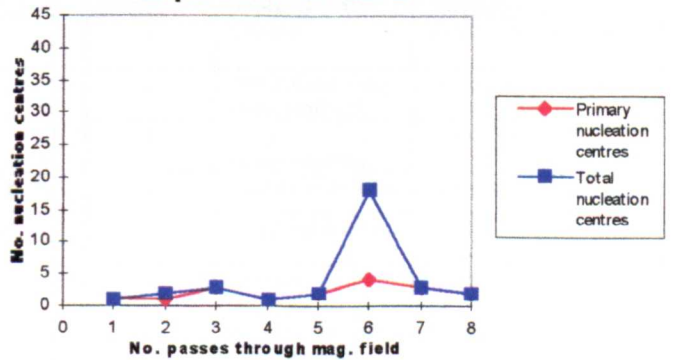
SAMPLE	MORPHOLOGY	NOTES
1	wedge and dendritic	chunky wedge & fine dendritic, opaque crystals
2	euhedral and wedge	v. chunky euhedral and fine dendritic, opaque crystals
3	euhedral and wedge	chunky, clear crystals
4	wedge and dendritic	chunky wedge & fine dendritic crystals
5	wedge	medium sized, opaque crystals
6	wedge (some euhedral)	fine crystals
7	euhedral and dendritic	medium sized, opaque crystals
8	wedge and dendritic	chunky wedge & fine dendritic, clear crystals

Tables 2.3.88 A and B Summary of the visual observations of sucrose crystal morphology recorded for Experiment 53.

Experiment 53 Run A



Experiment 53 Run B



Graphs 2.3.29 A and B Number of nucleation centres (both primary and total) versus No. passes recorded for Experiment 53.

Experiment 54 - 300-680G DC electromagnet field

Run A

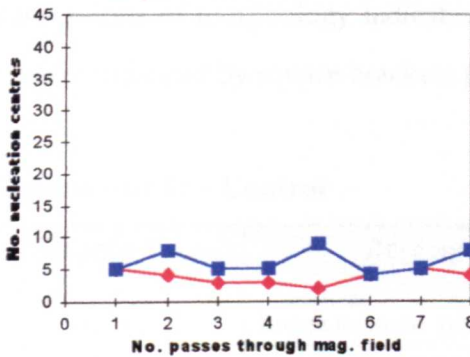
SAMPLE	MORPHOLOGY	NOTES
1	euhedral and wedge (some dendritic)	medium sized crystals
2	wedge and euhedral (some dendritic)	fine, clear crystals
3	euhedral	medium sized crystals
4	wedge and dendritic (some euhedral)	medium sized opaque crystals
5	euhedral and wedge	medium sized, clear crystals
6	wedge	medium sized, clear crystals
7	euhedral and wedge (some dendritic)	medium sized clear crystals
8	wedge (some euhedral)	fine, clear crystals

Run B

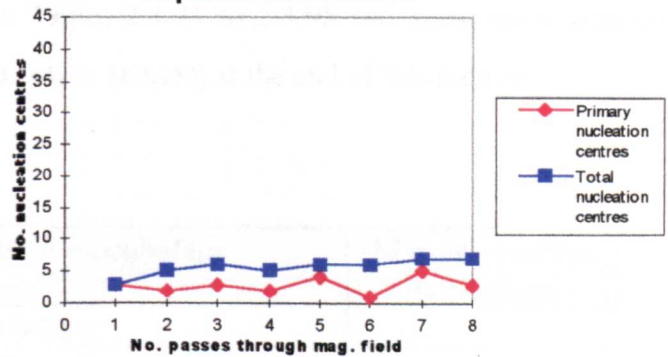
SAMPLE	MORPHOLOGY	NOTES
1	wedge and dendritic	fine crystals
2	euhedral and wedge	medium sized crystals
3	euhedral and wedge	medium sized crystals
4	wedge (some dendritic)	medium sized, opaque crystals
5	wedge and dendritic	medium sized, ordered crystals
6	euhedral and wedge	chunky, clear crystals
7	wedge and dendritic	fine crystals
8	wedge (some dendritic)	medium sized, clear crystals

Tables 2.3.89 A and B Summary of the visual observations of sucrose crystal morphology recorded for Experiment 54.

Experiment 54 Run A



Experiment 54 Run B



Graphs 2.3.30 A and B Number of nucleation centres (both primary and total) versus No. passes recorded for Experiment 54.

Experiment 55 - Pulsed field

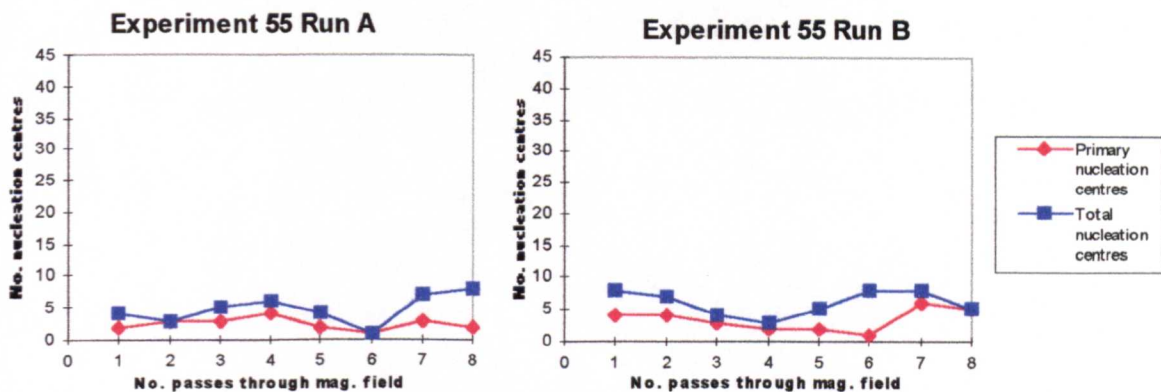
Run A

SAMPLE	MORPHOLOGY	NOTES
1	euhedral and wedge	v. chunky, opaque crystals
2	dendritic and wedge	v. chunky, v. opaque crystals
3	wedge and dendritic (some euhedral)	medium sized, opaque crystals
4	euhedral and wedge	chunky, opaque crystals
5	wedge (some dendritic)	chunky, opaque crystals
6	euhedral and wedge (some dendritic)	chunky, opaque crystals
7	euhedral and wedge	medium sized crystals
8	euhedral and wedge	v. chunky, opaque crystals

Run B

SAMPLE	MORPHOLOGY	NOTES
1	euhedral	chunky, opaque crystals
2	euhedral and wedge (some dendritic)	medium sized, opaque crystals
3	wedge (some euhedral)	chunky crystals
4	dendritic and wedge	fine, opaque crystals
5	wedge and dendritic	chunky primary & fine secondary crystals
6	euhedral	chunky, opaque crystals
7	euhedral and wedge (some dendritic)	medium sized crystals
8	euhedral (some wedge)	chunky, opaque crystals

Tables 2.3.90 A and B Summary of the visual observations of sucrose crystal morphology recorded for Experiment 55.



Graphs 2.3.31 A and B Number of nucleation centres (both primary and total) versus No. passes recorded for Experiment 55.

2.3.1(d)(i)(2) Scanning Electron Microscopy results

The SEM results are presented in the same format as the pumped sucrose study with the descriptions of morphology indicated in Tables 2.3.91 to 2.3.95 and some are illustrated in Figures indicated by square brackets [2.3.143] to [2.3.153] at the end of this section.

Experiment 51 - Control

Sample No.	Description of morphology	Microcrystalline dimensions
51(1)	Rough textured, pitted surfaces	
51(2)	Flat, rough textured pitted surfaces	
51(3)	Wave-like, step formations	
51(5)	Rough, surface blobs[2.3.143]	
51(6)	Rough surfaces, some chunky stepped morphology[2.3.144]	
51(8)	Irregularly formed material[2.3.145]	

Table 2.3.91 SEM observations for sucrose Samples in Experiment 51.

Experiment 52 - 630-760G Permanent magnets

Sample No.	Description of morphology	Microcrystalline dimensions
52(2)	Microcrystals[2.3.146] on flat smooth surfaces	~10-20µm
52(4)	Flat, angled surfaces and large microcrystals[2.3.147]	~80-100µm
52(7)	Flat, angled surfaces with plate-like microcrystals	~50-100µm

Table 2.3.92 SEM observations for sucrose Samples in Experiment 52.

Experiment 53 - AC electromagnets magnets

Sample No.	Description of morphology	Microcrystalline dimensions
53(3)	Leaf-type microcrystals on flat surfaces[2.3.148]	~30-80 μ m
53(4)	Flat, plate-like microcrystals on flat surfaces	~30-80 μ m
53(6)	Flat surfaces, with angled edges and large microcrystals[2.3.149]	~100-200 μ m

Table 2.3.93 SEM observations for sucrose Samples in Experiment 53.

Experiment 54 - 300-680G DC electromagnets magnets

Sample No.	Description of morphology	Microcrystalline dimensions
54(2)	Pitted surfaces, angled edges [2.3.150]	
54(4)	Microcrystals[2.3.151] on rough textured surfaces	~30-80 μ m
54(6)	Regular, layered, stepped growth[2.3.152] with very regular straight lines	

Table 2.3.94 SEM observations for sucrose Samples in Experiment 54.

Experiment 55 - Pulsed magnets

Sample No.	Description of morphology	Microcrystalline dimensions
55(2)	Microcrystals and flat surfaces	~30-60 μ m
55(6)	Layered, stepped growth and large microcrystals[2.3.152]	~75-300 μ m

Table 2.3.95 SEM observations for sucrose Samples in Experiment 55.

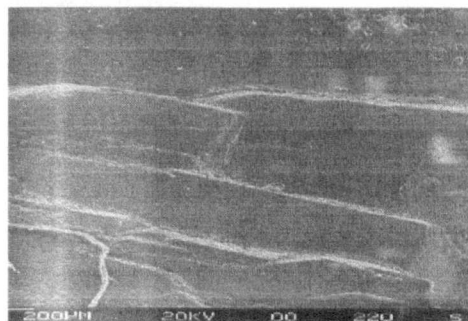
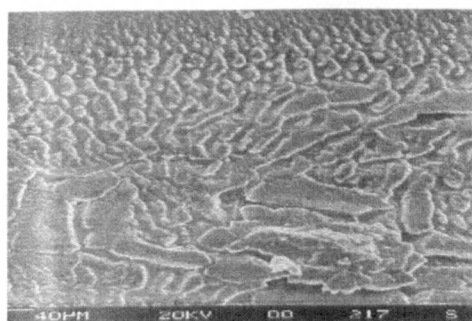


Fig. 2.3.143 Sucrose sample 51(5), Run A. Fig. 2.3.144 Sucrose sample 51(6), Run A.

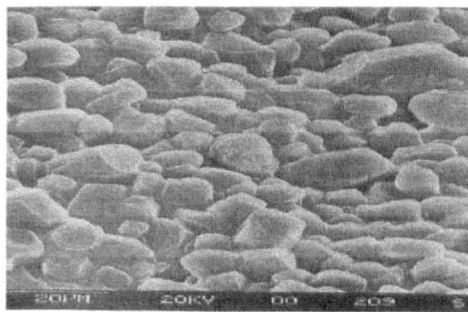
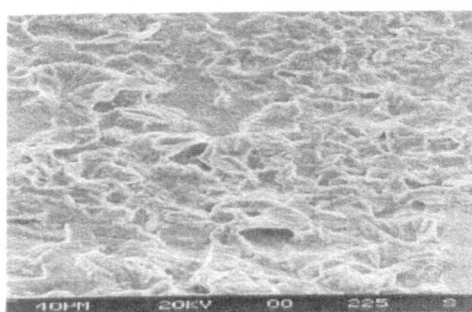


Fig. 2.3.145 Sucrose sample 51(8), Run B. Fig. 2.3.146 Sucrose sample 52(2), Run A.

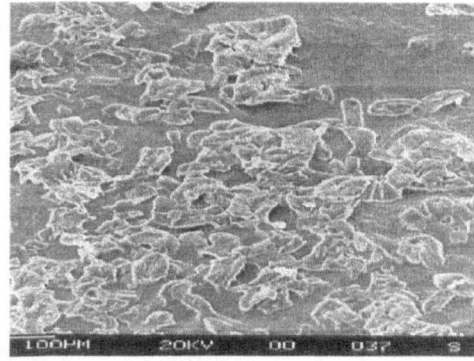
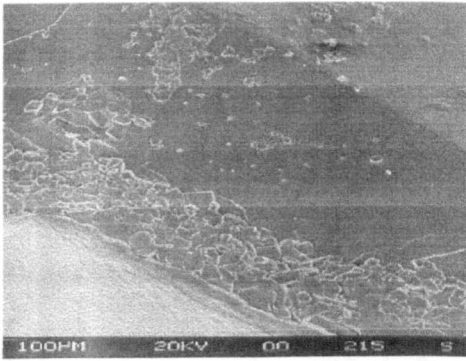


Fig. 2.3.147 Sucrose sample 52(4), Run A. Fig. 2.3.148 Sucrose sample 53(3), Run B.

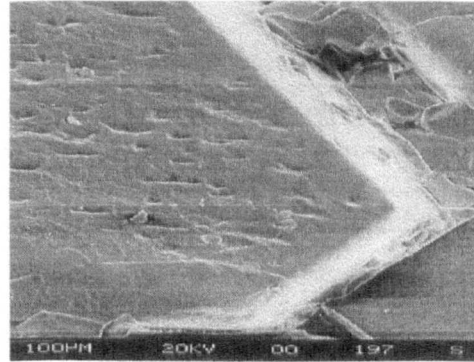
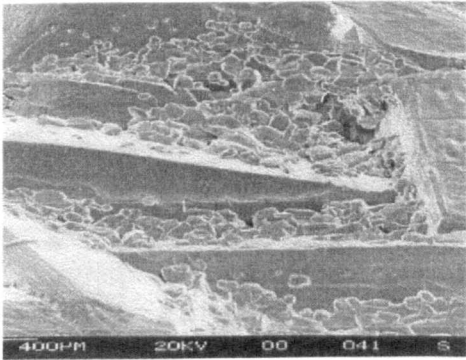


Fig. 2.3.149 Sucrose sample 53(6), Run A. Fig. 2.3.150 Sucrose samples 54(2), Run B.

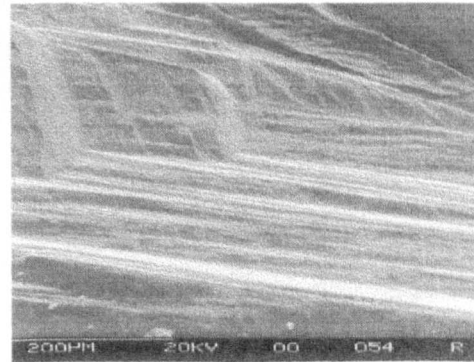
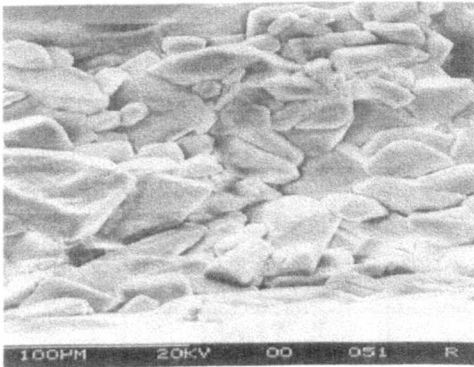


Fig. 2.3.151 Sucrose sample 54(4), Run B. Fig. 2.3.152 Sucrose sample 54(6), Run A.

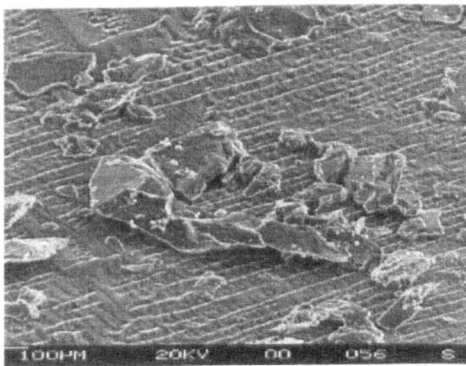


Fig. 2.3.153 Sucrose sample 55(6), Run A.

2.3.1 (d)(i)(3) Differential Scanning Calorimetry results

The DSC melting point data are presented in tabular form in Tables 2.3.96 to 2.3.100 using the same classification as described in 2.3.1(c)(i)(3).

Experiment 51 – Control

Run A

Sample	Feature 1 (°C)	Feature 2 (°C)	Feature 3 (°C)	Melting point (°C)
1				172.88
2				175.56
3				183.20
4				169.91
5				165.69
6				175.51
7				175.93
8				176.63

Table 2.3.96 DSC results for sucrose samples from Experiment 51.

Experiment 52 – 630-760G Permanent field

Sample	Feature 1 (°C)	Feature 2 (°C)	Feature 3 (°C)	Melting point (°C)
1	154.83 S			177.76
2	152.17 S			182.73
3	152.17 M			180.07
4	151.17 S			183.40
5	152.17 S			182.56
6	156.17 S			176.58
7	153.83 S			177.91
8	153.83 VVS			181.40

Table 2.3.97 DSC results for sucrose samples from Experiment 52.

Experiment 53 – AC electromagnetic field

Sample	Feature 1 (°C)	Feature 2 (°C)	Feature 3 (°C)	Melting point (°C)
1	153.83 L	160.83 L		173.62
2	152.17 M	157.50 L		178.46
3	152.20 S	158.83 M		175.00
4	150.32 VL	163.33 VL		167.00
5	150.20 M	162.24 M		175.32
6	146.83 S	152.17 M	158.83 M	173.05
7	151.17 M	154.83 M		169.44
8	150.17 L	165.00 M		171.64

Table 2.3.98 DSC results for sucrose samples from Experiment 53.

Experiment 54 – 300-680G DC electromagnetic field

Sample	Feature 1 (°C)	Feature 2 (°C)	Feature 3 (°C)	Melting point (°C)
1	153.20 S			174.81
2	152.83 S			173.79
3	151.17 M	158.17 M		170.04
4	152.17 S			175.65
5	150.17 M	168.67 M		179.09
6	151.17 S			175.94
7	151.17 L			172.39
8	151.17 L			174.20

Table 2.3.99 DSC results for sucrose samples from Experiment 54.

Experiment 55 – Pulsed field

Sample	Feature 1 (°C)	Feature 2 (°C)	Feature 3 (°C)	Melting point (°C)
1	152.17 S			176.57
2	150.17 S	163.33 M		178.96
3	151.17 S			173.94
4	154.83 L	171.00 M		182.14
5	157.50 M	173.00 M		186.82
6	151.17 S			173.77
7	152.83 VS			181.03
8	152.17 S	164.00 M		172.57

Table 2.3.100 DSC results for sucrose samples from Experiment 55.

2.3.1(d)(ii) ANALYTICAL GRADE SUCROSE

The results are presented for the second part of the syphoned study performed using analytical grade sucrose.

2.3.1(d)(ii)(1) Visual observations

The visual observations recorded for each sucrose sample within each experiment, are given in Tables 2.3.101 to 2.3.105 and Graphs 2.3.32 to 2.3.36. the format in which the data is presented is the same as for the pumped sucrose solution study.

Experiment 56 - Control

Run A

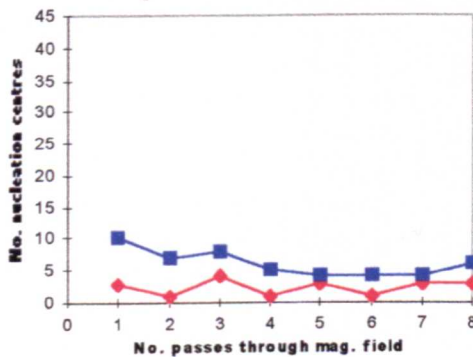
SAMPLE	MORPHOLOGY	NOTES
1	dendritic	fine, opaque crystals
2	wedge and dendritic	fine, opaque crystals
3	wedge (some dendritic)	fine crystals
4	wedge (some dendritic)	fine crystals
5	wedge (some dendritic)	chunky primary & fine dendritic, clear crystals
6	wedge (some dendritic)	chunky, clear, ordered crystals
7	wedge (some dendritic)	medium sized crystals
8	wedge (some dendritic)	medium sized crystals

Run B

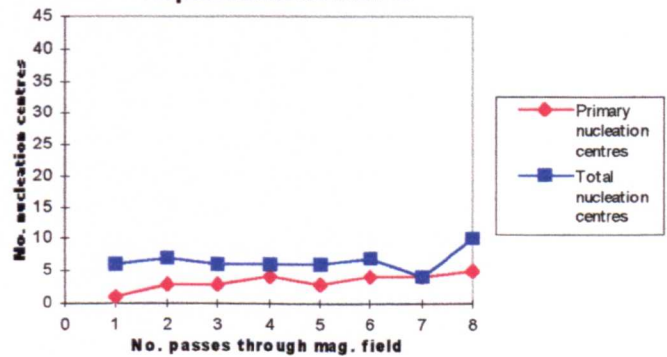
SAMPLE	MORPHOLOGY	NOTES
1	dendritic	fine, opaque crystals
2	dendritic and wedge	fine, opaque crystals
3	dendritic and wedge	medium sized crystals
4	dendritic and wedge	fine, opaque crystals
5	wedge and dendritic	medium sized crystals
6	wedge and dendritic	medium sized crystals
7	wedge and dendritic	chunky, clear, ordered crystals
8	wedge	medium sized, clear crystals

Tables 2.3.101 A and B Summary of the visual observations of sucrose crystal morphology recorded for Experiment 56.

Experiment 56 Run A



Experiment 56 Run B



Graphs 2.3.32 A and B Number of nucleation centres (both primary and total) versus No. passes recorded for Experiment 56.

Experiment 57 - 630-760 G Permanent magnetic field

Run A

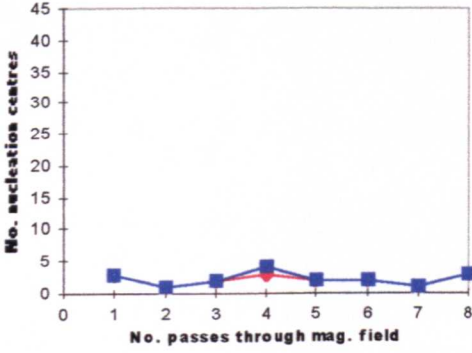
SAMPLE	MORPHOLOGY	NOTES
1	euhedral and wedge (some dendritic)	fine crystals
2	wedge and dendritic	medium sized, opaque crystals
3	wedge and dendritic	medium sized, v. opaque crystals
4	euhedral and wedge (some dendritic)	medium sized, opaque crystals
5	euhedral and dendritic (some wedge)	medium sized, opaque crystals
6	euhedral, wedge and dendritic	chunky, opaque crystals
7	wedge (some dendritic)	chunky, opaque crystals
8	euhedral and wedge	medium sized, opaque crystals

Run B

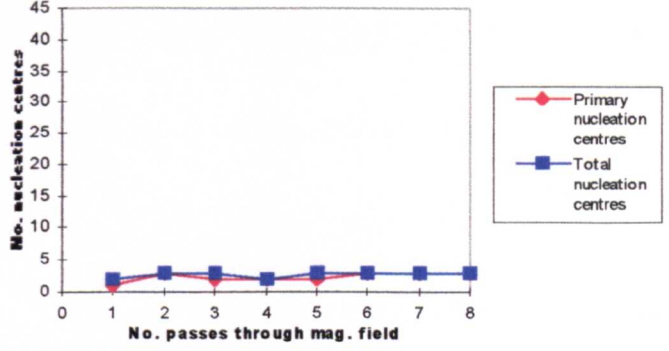
SAMPLE	MORPHOLOGY	NOTES
1	wedge and dendritic	medium sized crystals
2	euhedral, wedge and dendritic	medium sized, opaque crystals
3	euhedral and wedge (some dendritic)	fine, opaque crystals
4	euhedral and wedge	fine, opaque crystals
5	euhedral and wedge	medium sized, crystals
6	euhedral, wedge and dendritic	fine, opaque, disordered crystals
7	wedge and dendritic	fine, opaque crystals
8	dendritic and wedge	medium sized, v. opaque crystals

Tables 2.3.102 A and B Summary of the visual observations of sucrose crystal morphology recorded for Experiment 57.

Experiment 57 Run A



Experiment 57 Run B



Graphs 2.3.33 A and B Number of nucleation centres (both primary and total) versus No. passes recorded for Experiment 57.

Experiment 58 - AC electromagnetic field

Run A

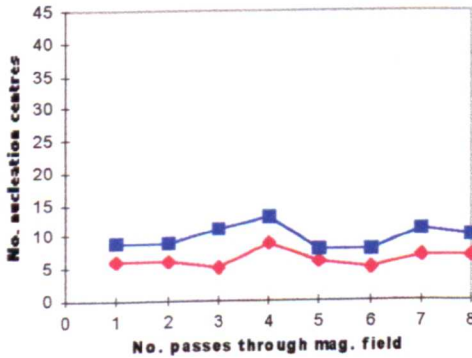
SAMPLE	MORPHOLOGY	NOTES
1	(euhydrated centres) wedge	fine, clear crystals
2	(euhydrated centres) wedge	fine, clear crystals
3	(euhydrated centres) wedge (some dendritic)	fine, clear crystals
4	(euhydrated centres) wedge	fine, clear crystals
5	wedge	fine crystals
6	wedge (some dendritic)	medium sized, clear crystals
7	wedge (some dendritic)	fine, clear crystals
8	(euhydrated centres) wedge	fine crystals

Run B

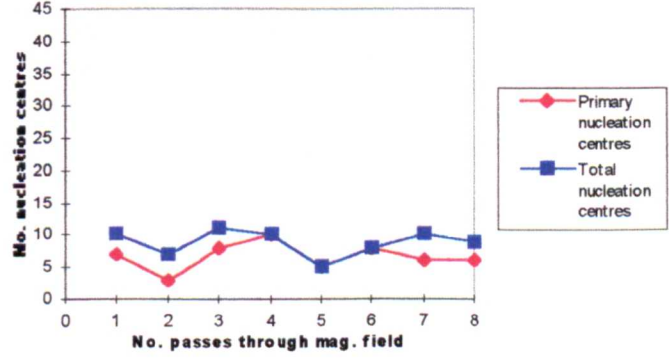
SAMPLE	MORPHOLOGY	NOTES
1	(euhydrated centres) wedge (some dendritic)	fine, clear crystals
2	euhydrated, wedge and dendritic	medium sized, opaque crystals
3	(euhydrated centres) wedge	fine, opaque crystals
4	wedge	v. fine, clear, ordered crystals
5	euhydrated, wedge and dendritic	fine, ordered crystals
6	euhydrated, wedge and dendritic	fine, ordered crystals
7	euhydrated and wedge (some dendritic)	fine, clear crystals
8	euhydrated and wedge	fine, clear crystals

Tables 2.3.103 A and B Summary of the visual observations of sucrose crystal morphology recorded for Experiment 58.

Experiment 58 Run A



Experiment 58 Run B



Graphs 2.3.34 A and B Number of nucleation centres (both primary and total) versus No. passes recorded for Experiment 58.

Experiment 59 - 300-680G DC electromagnetic field

Run A

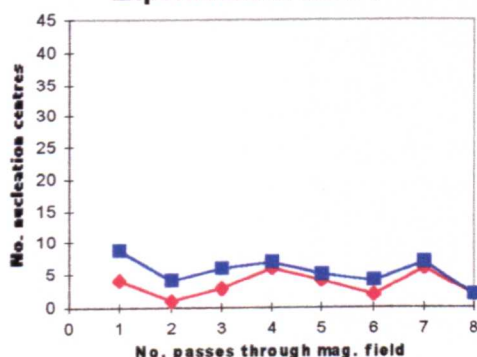
SAMPLE	MORPHOLOGY	NOTES
1	wedge	v. fine, v. clear, v. ordered crystals
2	euhedral and wedge (some dendritic)	v. fine, clear, ordered crystals
3	wedge	fine, v. clear, ordered crystals
4	wedge (some dendritic)	fine, clear, ordered crystals
5	wedge (some dendritic)	fine, clear, ordered crystals
6	euhedral, wedge and dendritic	fine, v. clear, ordered crystals
7	wedge (some dendritic)	v. fine, v. clear, v. ordered crystals
8	wedge (some dendritic)	v. fine, v. clear, ordered crystals

Run B

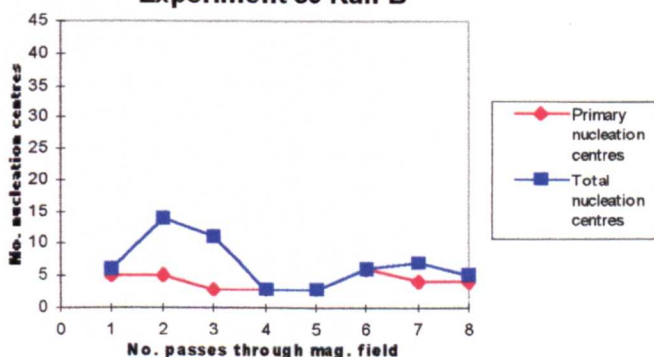
SAMPLE	MORPHOLOGY	NOTES
1	euhedral and wedge	fine, clear, ordered crystals
2	euhedral and wedge	v. fine, v. clear, v. ordered crystals
3	wedge (some dendritic)	v. fine, clear, ordered crystals
4	euhedral, wedge and dendritic	v. fine, clear, ordered crystals
5	wedge (some dendritic)	fine, clear, ordered crystals
6	euhedral and wedge	fine, v. clear crystals
7	euhedral, wedge and dendritic	fine, clear crystals
8	euhedral and wedge (some dendritic)	fine, clear crystals

Tables 2.3.104 A and B Summary of the visual observations of sucrose crystal morphology recorded for Experiment 59.

Experiment 59 Run A



Experiment 59 Run B



Graphs 2.3.35 A and B Number of nucleation centres (both primary and total) versus No. passes recorded for Experiment 59.

Experiment 60 - Pulsed field

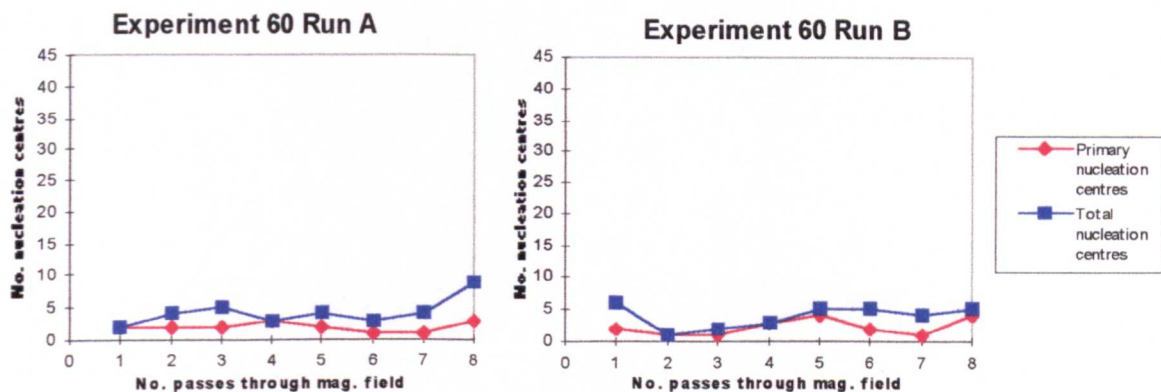
Run A

SAMPLE	MORPHOLOGY	NOTES
1	dendritic	fine, opaque crystals
2	wedge (some dendritic)	medium sized, opaque crystals
3	dendritic (some wedge)	fine crystals
4	wedge	medium sized, opaque crystals
5	dendritic (some wedge)	medium sized wedge & fine dendritic crystals
6	dendritic (some euhedral)	fine, opaque crystals
7	wedge and dendritic	chunky wedge & fine dendritic crystals
8	wedge (some euhedral)	fine, clear crystals

Run B

SAMPLE	MORPHOLOGY	NOTES
1	wedge and dendritic	medium sized crystals
2	wedge and dendritic	chunky wedge & fine dendritic, opaque crystals
3	euhedral, wedge and dendritic	chunky, clear wedge & fine, opaque dendritic, crystals
4	dendritic	fine, opaque crystals
5	euhedral, wedge and dendritic	medium sized crystals
6	euhedral, wedge and dendritic	fine crystals
7	euhedral and wedge	chunky crystals
8	euhedral and wedge	medium sized, clear crystals

Tables 2.3.105 A and B Summary of the visual observations of sucrose crystal morphology recorded for Experiment 60.



Graphs 2.3.36 A and B Number of nucleation centres (both primary and total) versus No. passes recorded for Experiment 60.

2.3.1(d)(ii)(2) Scanning Electron Microscopy results

The SEM results are presented in the same format as the normal grade sucrose results with the descriptions of morphology indicated in Tables 2.3.106 to 2.3.110 and some are illustrated in Figures indicated by square brackets [2.3.154] to [2.3.168] at the end of this section.

Experiment 56 - Control

Sample No.	Description of morphology	Microcrystalline dimensions
56(1)	Rough textured, pitted surfaces[2.3.154]	
56(4)	Rough textured, pitted surface[2.3.155]	
56(8)	Pitted surface with rough textured blobs[2.3.156]	

Table 2.3.106 SEM observations for sucrose Samples in Experiment 56.

Experiment 57 - 630-760G Permanent magnetic field

Sample No.	Description of morphology	Microcrystalline dimensions
57(1)	Chunky steps, with flat surfaces and some layered growth[2.3.157]	
57(2)	Flat, even surfaces and angled edges with some layered growth	
57(5)	Rough layered growth with some pitting[2.3.158]	

Table 2.3.107 SEM observations for sucrose Samples in Experiment 57.

Experiment 58 - AC electromagnetic field

Sample No.	Description of morphology	Microcrystalline dimensions
58(4)	Flat, planar microcrystals on flat surfaces[2.3.159]	~50 μ m
58(5)	Very flat surfaces, layered growth, some pitting[2.3.160] and microcrystals	~20-30 μ m
58(7)	Very flat surfaces with limited pitting and some networked ridges on surface[2.3.161]	
58(8)	Microcrystals covering flat surfaces[2.3.162]	~20-60 μ m

Table 2.3.108 SEM observations for sucrose Samples in Experiment 58.

Experiment 59 - 300-690G DC electromagnetic field

Sample No.	Description of morphology	Microcrystalline dimensions
59(1)	Rough textured, pitted surface	
59(2)	Rough textured surface with very small amount of rounded microcrystals	~20-80 μ m
59(4)	Flat surfaces, angled edges, small amount of pitting on surfaces	
59(5)	Chunky, layered growth[2.3.163] and very well formed microcrystals[2.3.164]	~20-60 μ m
59(7)	Layered growth and well formed microcrystals	~20-50 μ m
59(8)	Lines of layered ridges on crystal surface[2.3.165]	~30-50 μ m

Table 2.3.109 SEM observations for sucrose Samples in Experiment 59.

Experiment 60 - Pulsed field

Sample No.	Description of morphology	Microcrystalline dimensions
60(1)	Large, well formed microcrystals	~50-80 μ m
60(2)	Pitted, layered rough textured surfaces	
60(3)	Large, well formed, elongated microcrystals[2.3.166]	~50-120 μ m
60(5)	Layered surfaces, microcrystals and flat surfaces[2.3.167]	~20-30 μ m
60(8)	Layered, pitted surfaces and well formed microcrystals[2.3.168]	~20-40 μ m

Table 2.3.110 SEM observations for sucrose Samples in Experiment 60.

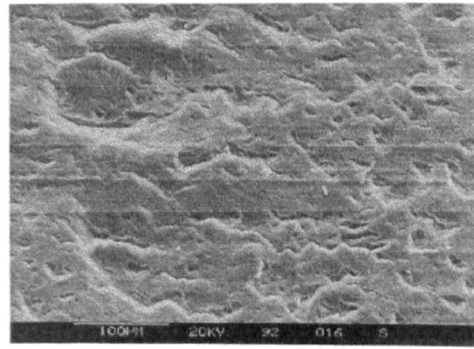
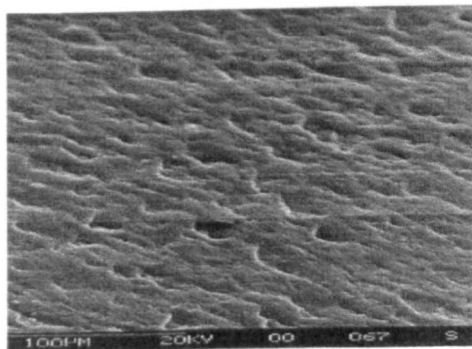


Fig. 2.3.154 Sucrose sample 56(1), Run A. Fig. 2.3.155 Sucrose sample 56(4), Run A.

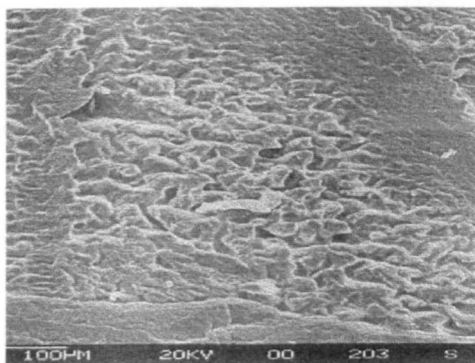


Fig. 2.3.156 Sucrose sample 56(8), Run A.

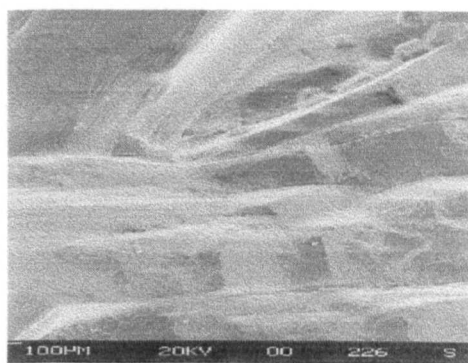


Fig. 2.3.157 Sucrose sample 57(1), Run A.

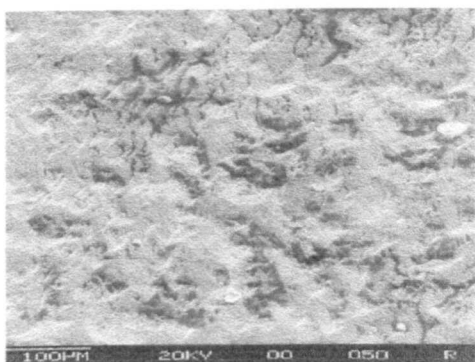


Fig. 2.3.158 Sucrose sample 57(5), Run A.

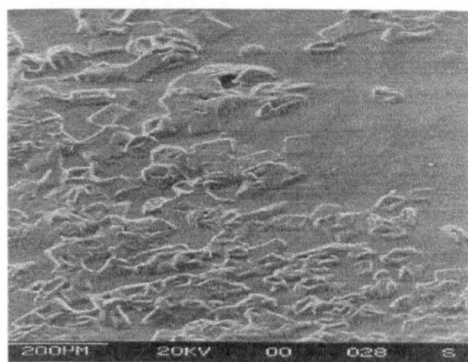


Fig. 2.3.159 Sucrose sample 58(4), Run B.

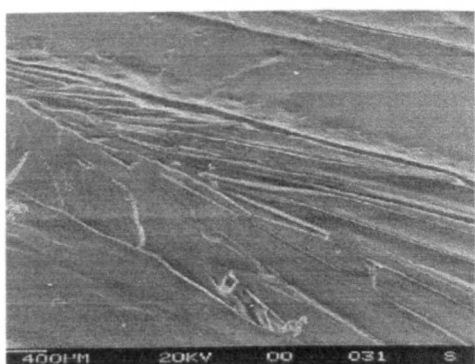


Fig. 2.3.160 Sucrose sample 58(5), Run A.

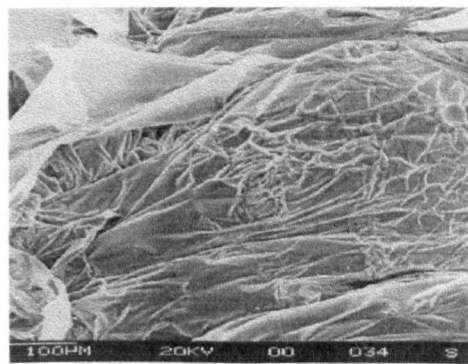


Fig. 2.3.161 Sucrose sample 58(7), Run A.

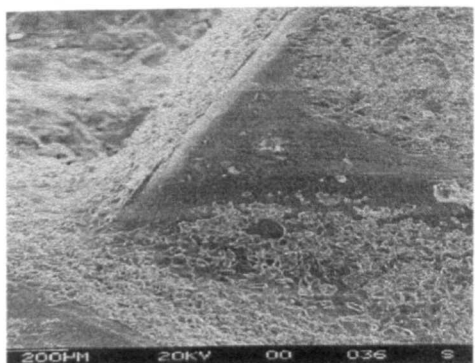


Fig. 2.3.162 Sucrose sample 58(8), Run A.

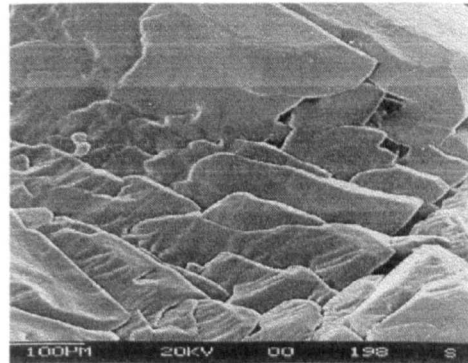


Fig. 2.3.163 Sucrose sample 59(5), Run A.

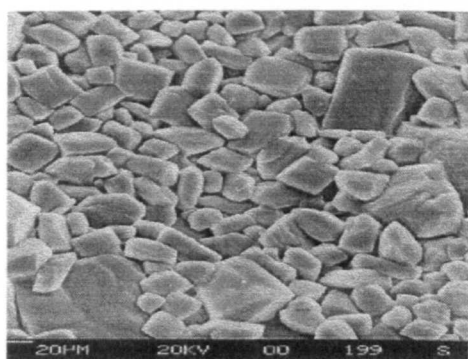


Fig. 2.3.164 Sucrose sample 59(5), Run A.

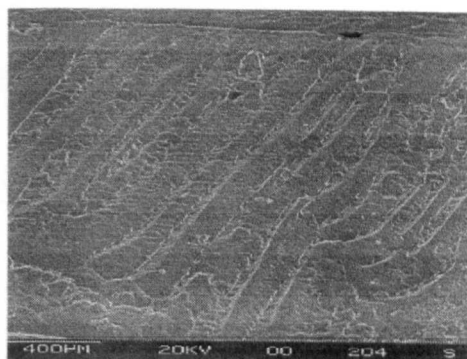


Fig. 2.3.165 Sucrose sample 59(8), Run B.

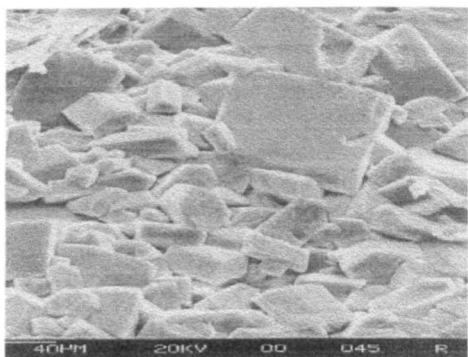


Fig. 2.3.166 Sucrose sample 60(3), Run B.

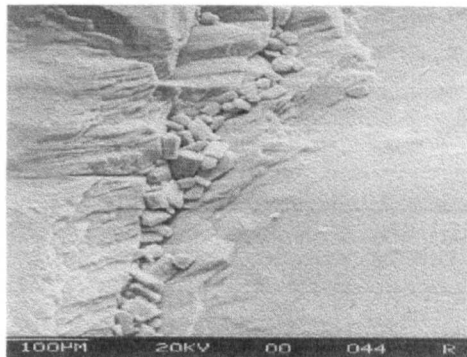


Fig. 2.3.167 Sucrose sample 60(5), Run A.

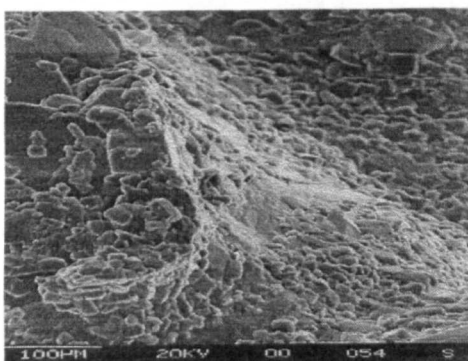


Fig. 2.3.168 Sucrose sample 60(8), Run A.

2.3.1(d)(ii)(3) Differential Scanning Calorimetry results

The DSC melting point data are presented in tabular form in Tables 2.3.111 to 2.3.115 using the same classification as described in 2.3.1(c)(i)(3).

Experiment 56 - Control

Sample	Feature 1 (°C)	Feature 2 (°C)	Melting Point (°C)
1			179.78
2			181.84
3			183.51
4			185.38
5			186.24
6			185.34
7			188.32
8			182.43

Table 2.3.111 DSC data on sucrose samples 1 to 8 from Experiment 56.

Experiment 57 - 630-760G permanent magnetic field

Sample	Feature 1 (°C)	Feature 2 (°C)	Melting Point (°C)
1	152.17 VS		176.95
2	151.17 M	167.67 M	175.24
3	151.17 M		171.75
4	150.83 M		174.22
5	157.10 VL		179.00
6	150.17 S	158.83 S	175.91
7	152.83 S		175.74
8	151.17 L		172.54

Table 2.3.112 DSC data on sucrose samples 1 to 8 from Experiment 57.

Experiment 58 - AC electromagnetic field

Sample	Feature 1 (°C)	Feature 2 (°C)	Melting Point (°C)
1	152.17 VS		178.50
2	152.17 S		172.67
3	152.17 M		172.86
4	152.83 S		176.08
5	152.83 S	158.53 S	178.33
6	152.17 S		177.02
7	152.17 S		181.83
8	157.50 VS		188.00

Table 2.3.113 DSC data on sucrose samples 1 to 8 from Experiment 58.

Experiment 59 - 300-680G DC electromagnetic field

Sample	Feature 1 (°C)	Feature 2 (°C)	Melting Point (°C)
1	153.83 VS	162.83 S	183.91
2	152.83 VS		181.85
3	152.83 S		180.35
4	153.83 S		181.55
5	153.33 VS		181.51
6	152.83 VS		178.58
7	153.83 VS		180.59
8	153.83 VS		181.30

Table 2.3.114 DSC data on sucrose samples 1 to 8 from Experiment 59.

Experiment 60 - Pulsed field

Sample	Feature 1 (°C)	Feature 2 (°C)	Melting Point (°C)
1	152.83 S		179.18
2	152.83 VS		182.80
3	152.17 VS		185.10
4	152.83 S		181.09
5	152.83 VS		182.96
6	152.83 S		182.32
7	152.83 S		185.43
8	152.83 S		182.15

Table 2.3.115 DSC data on sucrose samples 1 to 8 from Experiment 60.

2.3.2 DISCUSSION

2.3.2(a) Preliminary studies on static crystal growth of sucrose

The preliminary studies were carried out to establish conditions for operation to study the effects of applied field on crystal growth of sucrose under static conditions- viz Temperature, saturation and Control versus field- so that any effects observed could be attributed to the field effects crystals forms.

2.3.2(a)(1) Familiarisation with thin film sucrose crystal forms

Experiments 2 through 12 were carried out under the same conditions as the control with the only difference being the magnets positioned around the crystallising sucrose solutions within the petri dishes. Since the incubators have a fixed volume and a 6 inch diameter fan in a fixed

crystallisation), crystallisation has occurred on the surface of the solution within the petri dishes as a thin film of sucrose crystals. Crystal growth centres from a point (or points) within that surface and growth has occurred radially outwards from that point. Primary nucleation centres are defined as the first centres of nucleation to form and crystal growth tends to be mainly from these centres. As a result the largest areas of sucrose crystal growth on the thin film surface are from primary nucleated centres of growth. Secondary nucleation centres are defined to occur following the nucleation and growth from primary centres and are very much smaller in diameter (around 2 or 3 times smaller in diameter) than the sucrose crystal growth areas from primary nucleation centres.

All the sucrose crystals grown in applied magnetic fields conditions were more regular and well formed, and in some cases larger, than sucrose crystals obtained under 'Control' conditions. The changes in crystal shape are recorded in Table 2.3.1. A graphical illustration of the differences in number of nucleation centres is given in Figs. 2.3.169 and 2.3.170. The number of primary nucleation centres does not alter dramatically other than the strongest DC electromagnetic field studied which is over three times as high as the control. The greatest differences can be observed in the total number of nucleation centres illustration. The Control is shown as 5 total nucleation centres from Experiment 1. Experiments 2-5 (in increasing field strength with applied fields parallel at sides) show an

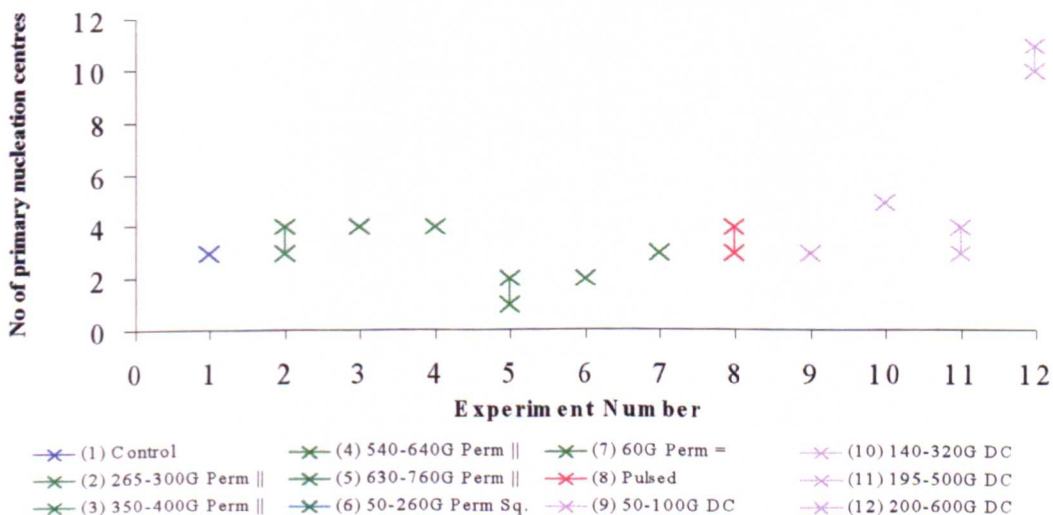


Fig. 2.3.169 An illustration of the number of primary nucleation centres obtained in each case of study under applied field conditions.

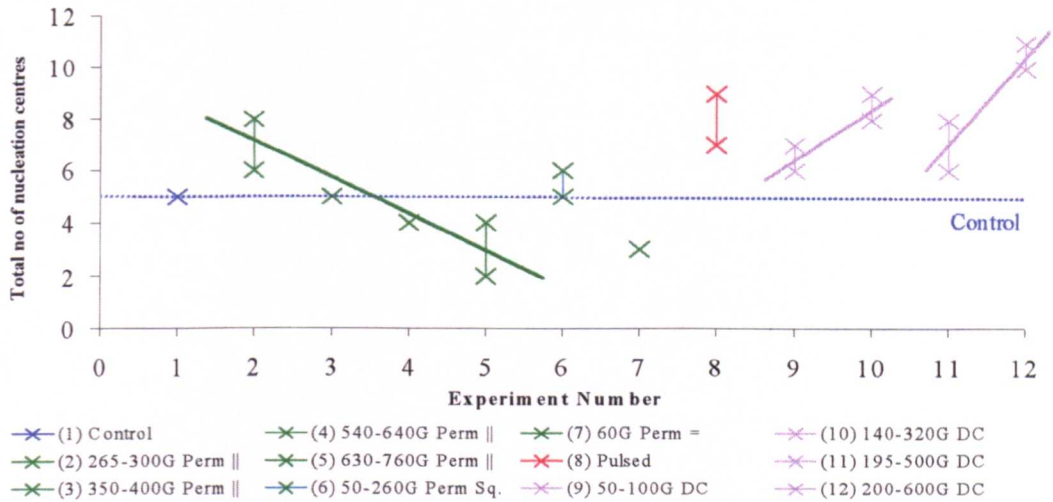


Fig. 2.3.170 An illustration of the total number of nucleation centres obtained in each case of study under applied field conditions.

increased number of nucleation centres for the weakest field (6 to 8), which then decreases with increasing field strength to below the control value (2 to 4). The pulsed field (Exp. 8) gives a range of nucleation centres considerably greater than the control. The increasing field strengths of the DC electromagnetic experiments (Expts. 9 to 12) appear to result in increased number of nucleation centres that increase with increasing field strength illustrated by the lines through the points however a change in morphology from wedge and dendritic to predominantly euhedral occurred between Expts. 10 and 11 accounting for the incongruity.

2.2.2(a)(2) Conclusion

Applied fields have dramatically altered the sucrose crystal form under the conditions studied in which spontaneous nucleation is studied. More regular crystals have been obtained in all cases. Nucleation appears to have been retarded with increasing permanent field strengths where the geometry is in parallel at the sides of the sample, and field lines are parallel to the crystal growing interface. Likewise, nucleation appears to have been retarded in the case where a weak applied permanent field has been applied with field lines perpendicular to the crystal growth interface. This is in contrast to the results obtained from the DC electromagnetic field studies where nucleation appears to have been

enhanced with increasing field strength. The pulsed field does not have a great effect on the resulting number of nucleation centres other than slight enhancement.

2.3.2(b) Controlled conditions, static crystallisation of sucrose

The experiments carried out in the preliminary studies were repeated with less variation in concentration where a 0.65S saturated solution was prepared in each case. The solutions were heated on a hotplate for 2 hours in order to reduce the possibility of any undissolved sucrose within the solution. In order to ensure spontaneous nucleation, the petri-dishes were kept free of dust and foreign materials. In control of any crystallising system there are two important factors to consider (1) nucleation rate and (2) crystal growth rate. In all cases the number of nucleation centres is recorded and assumed to be as a result of spontaneous nucleation, i.e. not as a result of seeding or foreign bodies within the sucrose solution. The number of nucleation centres (on which subsequent crystals growth occurs) formed on a standard surface area is used as an indication of nucleation rate. Each experiment was repeated 3 times in order to assess reproducibility, not only for comparison of number of nucleation centres and types of growth but also for the subsequent data on the resulting sucrose crystals.

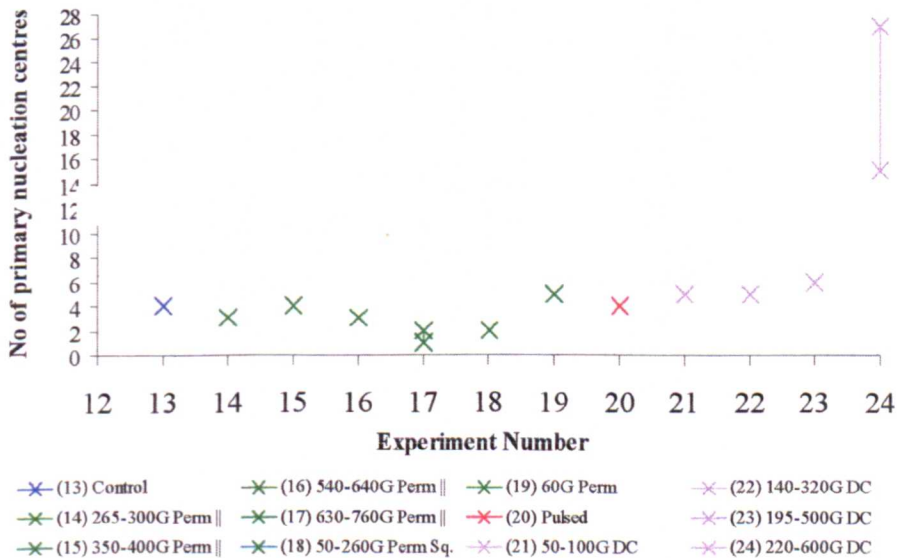


Fig. 2.3.171 An illustration of the number of primary nucleation centres obtained in each case of study under applied field conditions.

2.3.2(b)(1) Visual observations

The visual observations are summarised in Table 2.3.2. The numbers of primary and Total nucleation centres are graphically illustrated in Figs. 2.3.171 and 2.3.172 respectively.

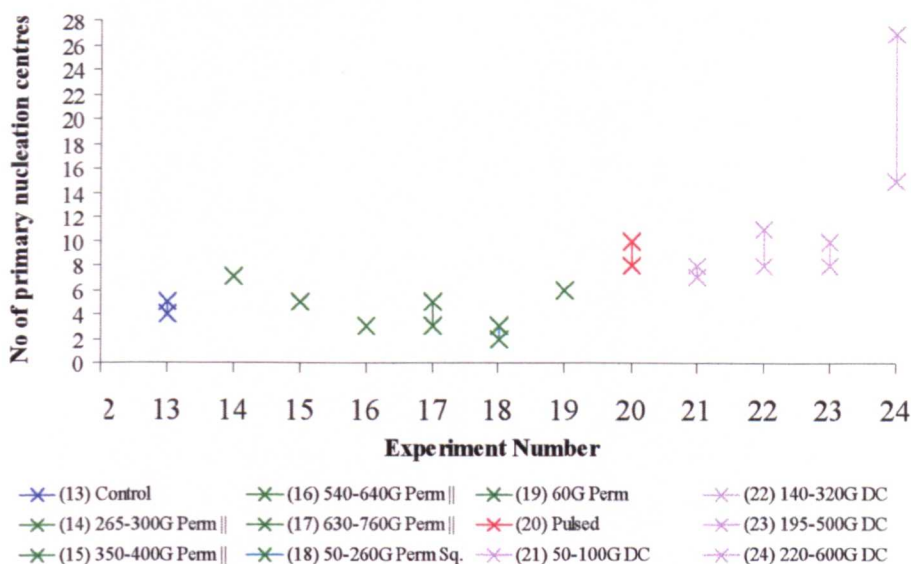


Fig. 2.3.172 An illustration of the total number of nucleation centres obtained in each case of study under applied field conditions.

In conclusion the following points were noted:

- (1) Wedge growth is obtained from thin film sucrose crystals grown where no magnetic field is applied under the conditions studied.
- (2) Increasing the permanent field strength in the cases where the magnetic field is applied in parallel at the sides of the crystallising sucrose solution (field lines parallel to the solution/air interface) results in reduction in the total number of nucleation centres obtained in addition to a change in morphology of the sucrose crystals from large wedges to fine needle crystals.

Below 350-400G the number of nucleation centres is greater than the Control.

Above 540-640G the number of nucleation centres is less than the Control.

Therefore, there appears to be a cross-over field strength between 400-540G.

- (3) The square geometry, 50-260G of Experiment 18 results in ***predominantly dendritic sucrose crystal morphology*** in addition to ***reduced nucleation***.

(4) The pulsed field study (Expt. 20) demonstrated ***increased secondary nucleation*** and a ***change in morphology to euhydrated sucrose crystals***.

(5) The DC electromagnetic field studies (Expt 21-24) resulted in wedge and dendritic sucrose crystals below 50-320G. However, above 195-500G, euhydrated morphology predominates and crystal growth rate is dramatically reduced in contrast with nucleation rate increase. Again there is a cross-over field strength which can only be assumed to be above 320G.

Below 320G sucrose thin film crystal morphology is wedge and dendritic.

Above 320G sucrose thin film crystal morphology is euhydrated.

In addition, ***nucleation rates were enhanced in every case studied.***

2.3.2(b)(2) Scanning Electron Microscopy

The visual observations recorded macroscopic changes in sucrose crystal morphology. In order to assess whether or not similar changes in morphology could be seen at microscopic level, Scanning Electron Microscopy measurements were made of the sucrose crystals.

In conclusion:

(1) The Control was demonstrated to be made up of ***irregular nodules on the surface and large chunky ridges***.

(2) The weakest permanent field resulted in ***more regular surface and microcrystals***.

(3) Increasing the field strength (in the same parallel at sides orientation) ***increased the amounts of regular microcrystals and layered growth, in addition to increasing the number of flat, smooth surfaces***.

(4) ***Microcrystals and wave-like sucrose crystal surfaces*** were obtained using other orientations of permanent fields.

(5) The pulsed field sucrose crystals were ***like folds of material over the whole sucrose crystal surface***.

(6) The weakest DC field resulted in wave-like surfaces ***and extensive amounts of microcrystals***. However, increasing the field strength in Experiment 22 to 140-320G resulted in ***more rounded surface and less well-formed microcrystals***. Increasing the

field strength shows *pitting on the sucrose crystal surface, layered growth and very well-formed, regular microcrystals.*

2.3.2(b)(3) Polarising Light Microscopy

All PLM images were obtained at $\times 10$ magnification (to the negative $24\times 36\text{mm}$) and the results are very similar to those obtained from the SEM study. See Figures 2.3.26 to 2.3.47. The Control (Expt. 13) is shown in Fig. 2.3.26 as a rough surface made up of nodules. All other images, by comparison, demonstrate layered growth and microcrystals on the sucrose surface in addition to very flat surfaces, with angled edges again demonstrating that the applied magnetic fields have resulted in a more ordered, regular surface morphology.

The purpose of using the Polarising Light Microscope was to illustrate the different single crystals. Since sucrose is a birefringent material a different physical orientation of a single sucrose crystal will translate as a different crystal colour simply by altering the crossed polarisers. This is clearly demonstrated in Figures 2.3.31, 34, 35 and 44 where the microcrystals on the sucrose crystal surface appear as different colours. Layered growth of one single crystal are illustrated in Figures 2.3.30, 33,41 and 43.

Surface pitting is illustrated in Fig. 2.3.32, in addition to the border between two wedges, which shows as different colour i.e. the rainbow from blue through to green as a result of changes in the thickness of the crystal. Similarly the wedge border is illustrated in Fig. 2.3.37. Straight edges, flat surfaces and corners are illustrated in Figures 2.3.39, 40 and 47.

2.3.2(b)(4) Differential Scanning Calorimetry

In all cases where thin films of sucrose were grown in the absence of an applied magnetic field (Expt. 13 Table 2.3.3) a single, sharp peak was obtained in the range $182\text{-}186^\circ\text{C}$ corresponding to sucrose crystal melting illustrated below in Figures 2.3.173 and 2.3.174 for sucrose Samples 13A and 13B.

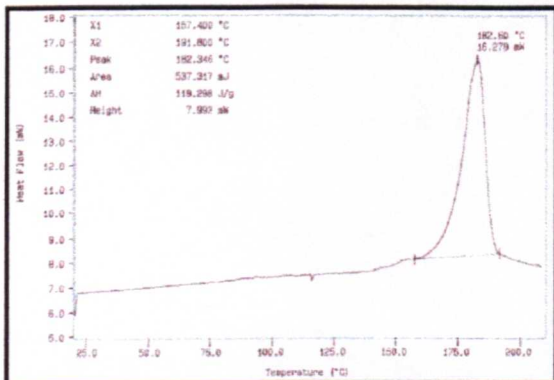


Fig. 2.3.173 DSC of sucrose sample 13A.

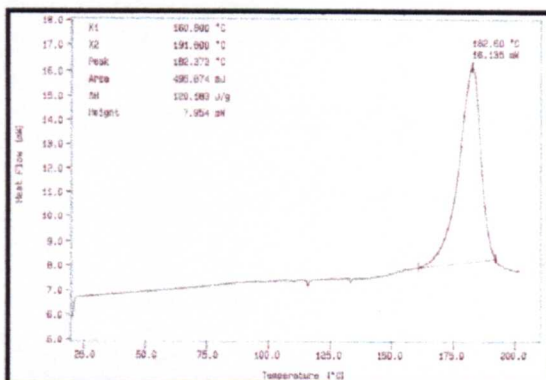


Fig. 2.3.174 DSC of sucrose sample 13B.

The first general observation regarding the DSC data is the presence of a second feature in addition to the sucrose melting point in all but 2 specimens of sucrose crystals grown in the presence of applied magnetic fields. These are illustrated below in Figures 2.3.175 to 178 for sucrose samples 14A,17B, 20A and 24C.

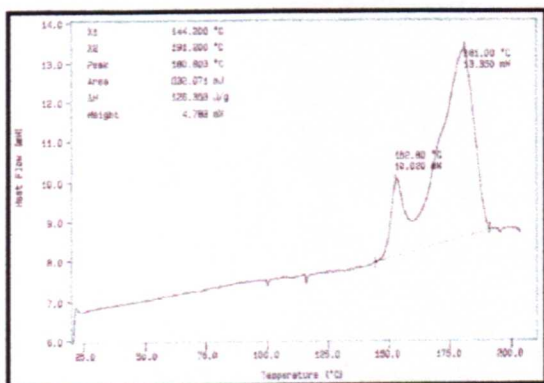


Fig. 2.3.175 DCS of sucrose sample 14A.

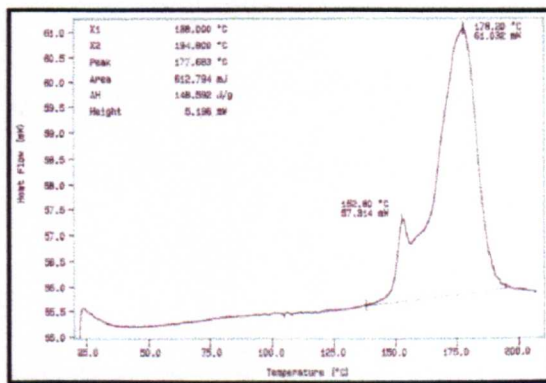


Fig. 2.3.176 DSC of sucrose sample 17B.

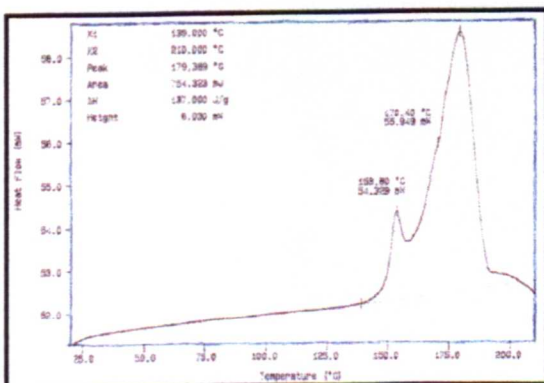


Fig. 2.3.177 DSC of sucrose sample 20A.

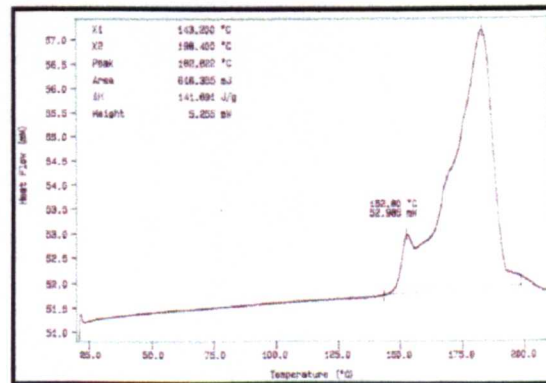


Fig. 2.3.178 DSC of sucrose sample 24C.

In addition, a third feature is present in only one case illustrated below in Fig. 2.3.179.

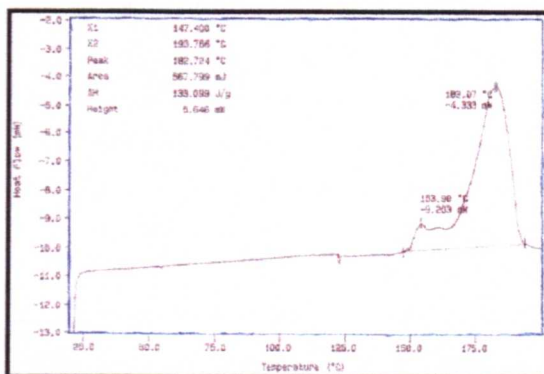


Fig. 2.3.179 DSC of sucrose sample 16A.

These were significant findings that required more rigorous examination.

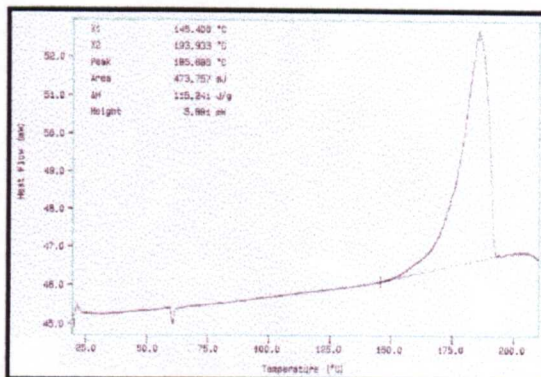
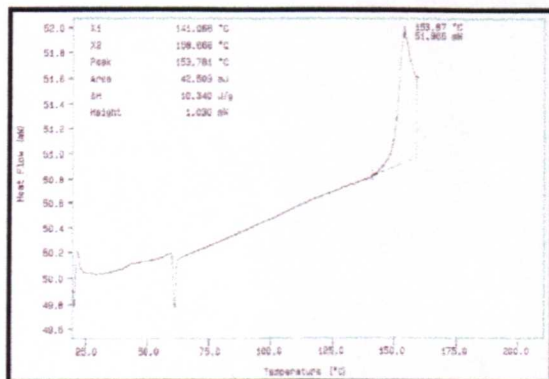
2.3.2(b)(5) Investigation of the additional features revealed by DSC

Thermal lag of the DSC equipment was considered, however collecting the data at a much reduced heating rate did not result in disappearance of the additional feature. In order to test the two hypotheses that these additional features were a result of (a) impurities or (b) a result of trapped sucrose solution within the crystal a series of DSC data was collected.

To test the impurity theory, using sucrose Sample 17B the sample was heated to $\sim 175^{\circ}\text{C}$, which is a temperature above the additional feature, but below the sucrose melting point and then cool the sample to 20°C . Upon reheating the sample to 200°C a single peak was obtained at $\sim 180^{\circ}\text{C}$.

The results of this investigation are given below in Figures 2.3.128(A) and (B) where (A) is the first heating cycle to 175° and (B) is the second heating cycle to 200°C .

If the peak was a result of impurities, the temperature cycle described above should result in the peak remaining on reheating. Whereas, if trapped syrup were the cause of the additional feature, application of the above temperature cycle would result in the additional feature disappearing, as a result of evaporation of the water.



Figs.2.3.1180

(A)

(B)

A glass transition around 58° occurred (not clearly visible and very small on Fig. 2.3.180(B) illustrated above), followed by recrystallisation, indicated by the small peak just above 58°C.

A second experiment carried out, using a ground dried specimen of sucrose sample 17B. Performing DSC analysis on the ground, dried sample gave the same DSC as the original with the additional feature around 153°C in addition to the melting point of sucrose at around 180°C.

If the water contained within the sucrose crystal was in the form of sucrose syrup i.e. unbound water, the phosphorous pentoxide would have been expected to remove this and the corresponding additional feature from the DSC data. Since this was not the case, other explanations were sought.

Simultaneous TG, DTG and DTA were carried out on a selection of sucrose samples in order to (1) clarify that the additional features found from DSC analysis were not attributable to the DSC technique or the particular equipment used, and (2) identify the possibility that a weakly bonded sucrose hydrate is the explanation for the additional features of the melting profile of the sucrose crystals grown in applied magnetic fields. If this is the case, the TG data would be expected to show weight loss due to water loss prior to decomposition temperature.

Four samples were selected for this study were as follows:

- (1) **Bottled sucrose,**
- (2) **Sample 13A** - from the 'Control' experiment,
- (3) **Sample 23C** - 195-500 Gauss DC electromagnetic field experiment where DSC analysis of the sucrose sample has indicated a strong peak for the additional feature in addition to the melting peak, and
- (4) **Sample 16A** - 540-640 Gauss permanent magnet in parallel at sides where DSC analysis of the sucrose sample indicated two additional features in addition to the sucrose melting peak.

A heating rate of $5^{\circ}\text{Cmin}^{-1}$ was used for each sample. The results for each sample (1) to (4) above are given below in Figures 2.3.181 to 184 respectively where the top blue trace in each indicates temperature. The second top blue line represents DTA and the third line down in red, indicates DTG and the bottom line in black represents TG.

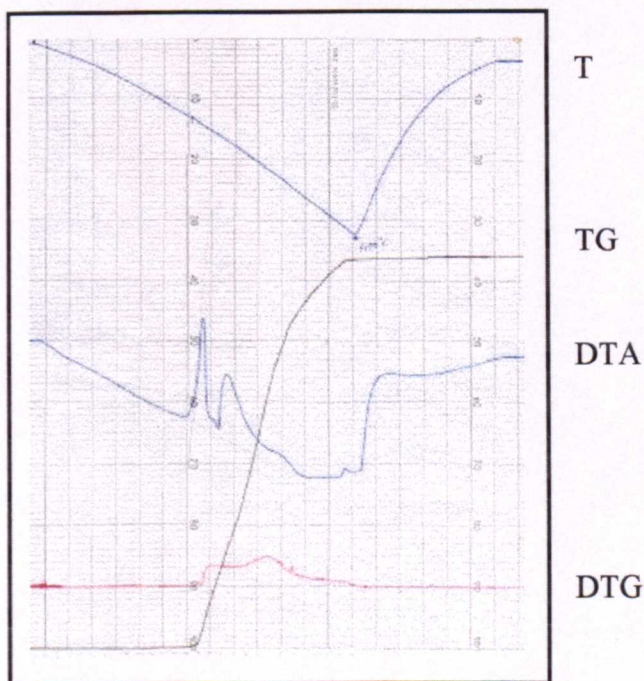


Fig. 2.3.181 Simultaneous DTA, DTG and TG of bottled sucrose.

Simultaneous TG, DTG and DTA were carried out on a selection of sucrose samples in order to (1) clarify that the additional features found from DSC analysis were not attributable to the DSC technique or the particular equipment used, and (2) identify the possibility that a weakly bonded sucrose hydrate is the explanation for the additional features of the melting profile of the sucrose crystals grown in applied magnetic fields.

If this is the case, the TG data would be expected to show weight loss due to water loss prior to decomposition temperature.

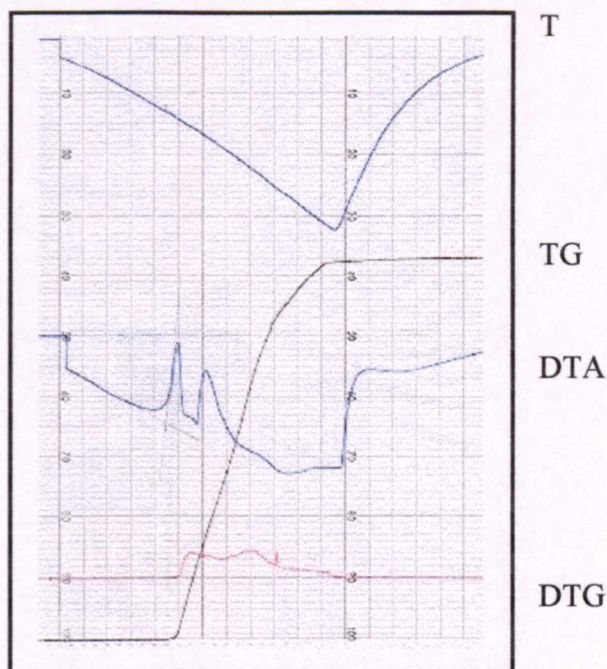


Fig. 2.3.182 Simultaneous DTA, DTG and TG of sucrose sample 13A.

The DTA trace of sample (2) (Sample 13A - Control) is almost identical to the bottled sucrose, as illustrated in Fig. 2.3.182 as would be expected.

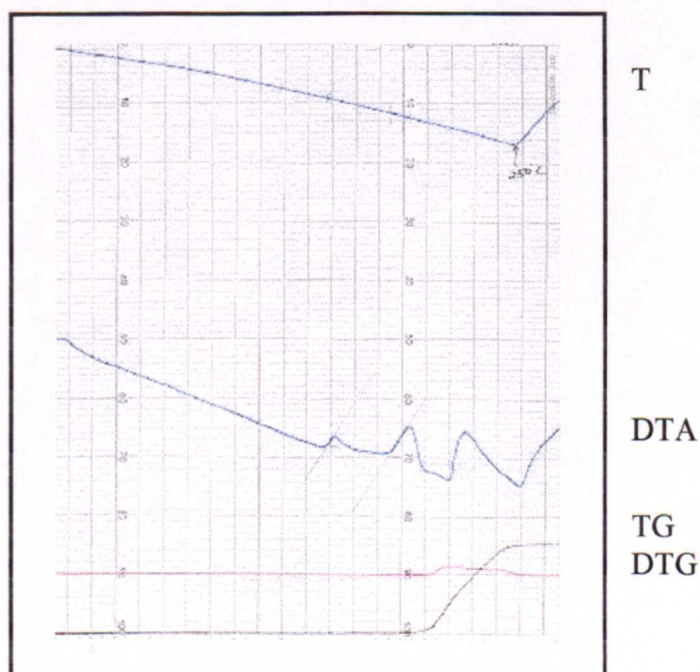


Fig. 2.3.183 Simultaneous DTA, DTG and TG of sucrose sample 23C.

The DTA of sample (3), (Sample 23C) like the DSC illustrates an additional feature around 155°, before the sucrose melting peak at around 180° and decomposition at 200°C. The loss of weight from TG occurs during decomposition and not before and unfortunately, not during the recording of the additional feature.

The DTA of sample 4 (sample 16A), like DSC illustrates two additional features around 150° and 170°C in addition to sucrose melting at around 180°C. Decomposition of sucrose is illustrated as would be expected around 200°C. Again, TG illustrates that no weight loss occurred until decomposition.

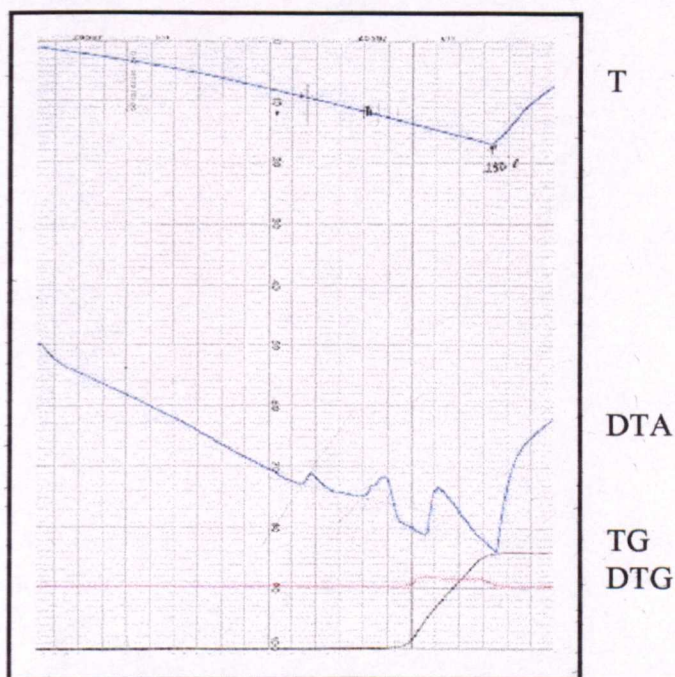


Fig. 2.3.184 Simultaneous DTA, DTG and TG of sucrose sample 16A.

Karl Fischer measurements were made on all the sucrose crystals and the data are given in Table 2.3.5. Although no error data was available for these data, it is clearly seen that there is a very large difference in the moisture content of the Control sucrose samples and those measured for all sucrose crystals grown in applied magnetic fields.

The data obtained from Proton Magic Angle Spinning Solid State NMR contained an additional feature compared to bottled sucrose. Data for both sucrose crystals grown in an applied field and bottled sucrose are illustrated in Figure 2.3.185 below. This

peak is indicative of strongly bonded hydrogen most probably a result of strongly bound sucrose hydrates.

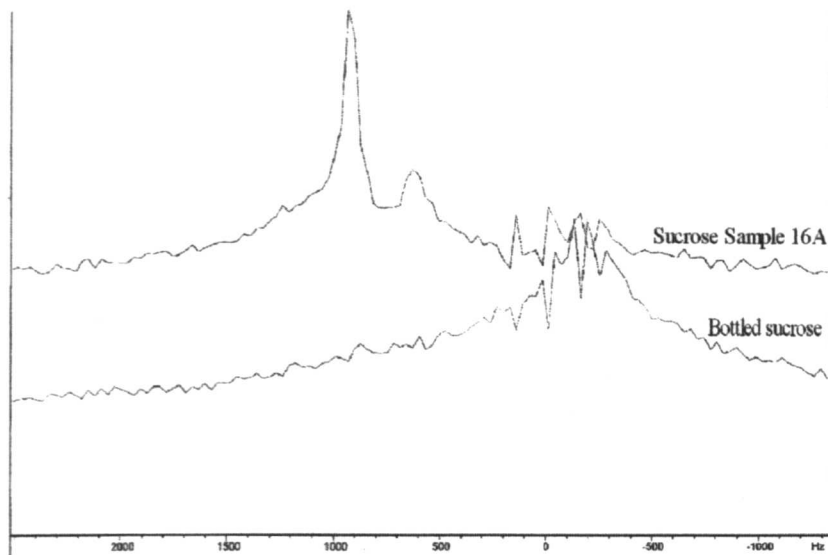


Fig. 2.3.185 Illustration showing the differences between the PMASSS NMR for bottled sucrose and sucrose crystals grown in an applied magnetic field.

Conclusions that can be drawn therefore are as follows:

- (1) The additional feature on the DSC data was not a result of impurities present within the crystal lattice.
- (2) The additional feature on the DSC melting profile of the sucrose crystals was most likely to be the result of trapped sucrose syrup within the sucrose crystals. This was not an unreasonable assumption since up to 1% wt:wt (water:sucrose) is normally expected from industrial scale sucrose crystallising systems. An example of this is the phenomena of caking as a result of grinding dry sugar to a powder, the trapped water is released during the grinding process and 'wets' the dry powder causing it to clump together.
- (3) Additional features in the DSC traces are duplicated using simultaneous DTA, DTG and TG indicating that they are not a result of the equipment, or the analysis technique,
- (4) The additional features are not likely to be weakly bound sucrose hydrates since no weight loss occurs during the melting of the sucrose crystal until decomposition occurs.
- (5) The simultaneous DTG, DTA, TG investigations indicate that the additional feature(s) on the DSC data is a strongly bound hydrate.

- (6) The moisture content measured for sucrose crystals grown in applied magnetic fields is significantly higher than for the 'out of field' sucrose crystals, grown under the same environmental conditions.
- (7) There is a relationship between the size of the additional feature on DSC and the moisture content of the samples, indicating that the additional feature and moisture content are in some way linked.
- (8) The PMASSS NMR data indicates the additional water within the sucrose crystal is strongly bound indicative of hydrated forms and not loosely bound sucrose syrup.

2.3.2(b)(6) Powder X-ray Diffraction

For the purposes of comparison, the standard reference data for sucrose, and that obtained for the sucrose hemipenta- and hemihepta-hydrates are given below in Tables 2.3.116, 117 and 118.

Sucrose C ₁₂ H ₂₂ O ₁₁				System is monoclinic with space group P2 ₁				
d	4.71	3.59	4.52	10.6 (Å)	a ₀	10.868 (Å)	β	102.97° (Å)
I/I ₁	100	100	80	14	b ₀	8.710 (Å)		
					c ₀	7.761 (Å)		
Red CuKα ₁ , λ = 1.54056								
d (Å)	I/I ₁	d (Å)	I/I ₁	d (Å)	I/I ₁	d (Å)	I/I ₁	
10.59	14	3.364	11	2.504	6	2.042	10	
7.58	65	3.272	5	2.496	7	2.028	4	
6.94	40	3.254	10	2.479	9	2.014	1	
6.73	55	3.222	7	2.444	5	2.000	1	
5.712	30	3.112	9	2.430	6	1.971	1	
5.424	11	2.956	2	2.406	9	1.956	4	
5.298	14	2.923	6	2.349	40	1.942	3	
4.884	12	2.882	25	2.339	16	1.929	5	
4.706	100	2.856	6	2.312	7	1.924	5	
4.523	80	2.799	20	2.291	4	1.904	6	
4.354	25	2.777	4	2.258	14	1.895	4	
4.259	30	2.742	10	2.253	11	1.887	4	
4.028	30	2.711	4	2.234	10	1.885	3	
3.943	11	2.677	10	2.189	5	1.870	2	
3.776	18	2.661	4	2.171	5	1.855	3	
3.690	8	2.648	2	2.133	1	1.823	3	
3.591	100	2.586	5	2.101	2	1.818	1	
3.531	45	2.574	4	2.091	2	1.809	3	
3.467	3	2.545	3	2.075	7	1.795	5	
3.437	5	2.521	5	2.060	6	Plus 11 lines to 1.635		

Table 2.3.116 Reference Powder XRD data for sucrose.

Sucrose hemipentahydrate				S = strong	MW = medium weak		
$C_{12}H_{22}O_{11} \cdot 7/2 H_2O$				MS = medium strong	W = weak		
				M = medium	VW = very weak		
d (Å)	I/I ₁	d (Å)	I/I ₁	d (Å)	I/I ₁	d (Å)	I/I ₁
12.59	MW	5.10	S	3.62	MW	2.75	MW
7.31	S	4.56	M	3.43	M	2.65	W
6.82	M	4.20	MS	3.27	MS	2.53	MW
6.19	MS	3.96	MS	3.11	MW	2.37	MW
5.56	W	3.81	M	2.91	M		

Table 2.3.117 Reference Powder XRD data for sucrose hemipentahydrate.

Sucrose hemiheptahydrate				S = strong	MW = medium weak		
$C_{12}H_{22}O_{11} \cdot 7/2 H_2O$				MS = medium strong	W = weak		
				M = medium	VW = very weak		
d (Å)	I/I ₁	d (Å)	I/I ₁	d (Å)	I/I ₁	d (Å)	I/I ₁
19.89	W	5.12	S	3.40	VW	2.81	W
11.88	W	4.28	M	3.27	M	2.66	W
7.72	S	4.03	S	3.12	MW	2.57	W
7.17	MW	3.84	M	2.92	W	2.50	W
6.57	M	3.57	MW				

Table 2.3.118 Reference Powder XRD data for sucrose hemiheptahydrate.

Sucrose $C_{12}H_{22}O_{11}$				System is monoclinic with space group P2₁				
d	4.71	3.59	4.52	10.6 (Å)	a ₀	10.868 (Å)	β	102.97° (Å)
I/I ₁	100	100	80	14	b ₀	8.710 (Å)		
Red CuKα₁, λ = 1.54056				c ₀	7.761 (Å)			
d (Å)	I/I ₁	d (Å)	I/I ₁	d (Å)	I/I ₁	d (Å)	I/I ₁	
10.59	14	4.706	100	3.776	18	2.742	10	
7.58	65	4.523	80	3.591	100	2.677	10	
6.94	40	4.354	25	3.531	45	2.349	40	
6.73	55	4.259	30	2.882	25	2.339	16	
5.712	30	4.028	30	2.799	20	2.258	14	

Table 2.3.119 Main d-spacing Powder XRD measurements for reference sucrose.

Conclusions from the Powder XRD are therefore as follows:

- (1) All data illustrates common d-spacings observed for standard sucrose.
- (2) Data obtained on sucrose crystals grown in DC electromagnetic fields contain more intense d-spacings around 2-3Å.

This could be a result of improved crystallinity having obtained well-formed crystals as a result of the applied magnetic fields during crystal growth, however, it may also be as a result of the powdering process and therefore not significant. The incorporation of water molecules into the crystal lattice has remains a possibility, however, without

further examination cannot be confirmed. A more accurate Powder XRD instrument would be expected to show consistently, marginally longer d-spacings as a result of the incorporation of the water molecules into the sucrose crystal lattice.

2.3.2(b) (7) Conclusions

- (1) Under '*no field*' conditions examined, *chunky, wedge-shaped crystals* were obtained in all cases.

Sucrose crystals grown in applied magnetic fields demonstrated the following:

- (1) *Improved crystallinity* in all cases where wedge or euhydrated sucrose crystal forms are favoured.

- (2) *Changes in sucrose crystal morphology:*

- (a) The permanent field arranged in square geometry favoured dendritic growth.
- (b) The pulsed field favoured euhydrated crystal forms.
- (c) Above 320 Gauss, DC electromagnetic fields favoured euhydrated growth, below, wedge and dendritic forms were favoured.

- (4) *Changes in nucleation rates:*

- (a) In the permanent fields in parallel at sides study, below 350-400 Gauss retarded nucleation rates, and above, enhanced nucleation rates. Overall nucleation rates appear to decrease with increasing field strength.
- (b) The pulsed field enhances nucleation rate.
- (c) DC electromagnetic field experiments demonstrate increasing nucleation rate with increasing field strength.

- (4) *Changes in small scale surface features:*

- (a) Weaker permanent fields (<350-500G) result in more regular flat surfaces and some microcrystals.
- (b) Stronger permanent fields (>350-500G) increase the number of microcrystals and introduce layered growth features in addition to an increase in the number of flat, smooth surfaces.
- (c) Pulsed fields introduce wave-like or 'fold' surface features.
- (d) The weakest DC electromagnetic fields (150-220G) result in extensive amounts of microcrystals, however, increasing the field strength results in

more rounded edges and surface pitting features, indicating dissolution effects may be important at these strengths.

(5) ***Changes in DSC data:***

In all cases but 2 of the 33 sucrose crystals grown in applied magnetic fields, an additional feature was present in the DSC data around 152-3°, in addition to the sucrose melting point around 165-187°C.

(6) ***Changes in Karl Fischer data:***

Moisture content was measured to be significantly higher for sucrose crystals grown in applied magnetic fields.

As a result, the additional features in DSC were most likely to be a result of strongly bound water molecules incorporated into the sucrose crystal lattice.

(7) ***Changes in Powder XRD data:***

Higher intensities for small scale (2-3Å) d-spacing measurements were found in sucrose crystals grown in applied DC electromagnetic fields.

(8) The additional features were demonstrated, most likely to be a result of ***strongly bound water*** within the sucrose crystals i.e. ***sucrose hydrates*** and not sucrose syrup.

2.3.2(c) Magnetic treatment of sucrose where the solution is pumped

The previous studies on sucrose were concerned with applied magnetic fields on static crystallisation. While this work has successfully demonstrated differences in the resulting sucrose crystals that have been grown in applied magnetic fields, the technique of static crystallisation is of no practical use to industry, since crystallisation is usually carried out with pumping, stirring and in some cases the application of mechanical shear. It was therefore important to show that the applied effects demonstrated in the previous section are not just limited to static systems but can also be applied to dynamic situations.

This section of work is therefore concerned with the mode of application of the applied magnetic fields, referred to as ‘magnetic treatment’, followed by static crystallisation under identical conditions as the static study, in order that comparisons of the resulting sucrose crystals can be made.

This study was carried out in order to investigate the claim that applied field effects on a sucrose solution maximise around 5 or 6 passes through and applied field.^[49] This would also be useful to consider where a re-circulating type system is used.

Two types of sucrose were used, normal and analytical grade. This study was thought necessary in order to establish whether or not the applied fields act upon the impurity ions within the sucrose solution causing the effects on the resulting sucrose crystals or on the sucrose/water system..

2.3.2(c)(i) NORMAL GRADE SUCROSE

2.3.2(c)(i)(1) Visual observations

The conclusions that were drawn from this study were as follows:

- (1) A very high number of nucleation centres formed in the 'Control' samples (16 to 45), most of which were due to enhanced secondary nucleation. The sucrose crystal morphology was a mixture of euhydrated and wedge with some dendritic features and was not as expected. In all cases studied under magnetic treatment conditions, this number was considerably smaller (<16).
- (2) Euhydrated morphology was obtained in a large number of the sucrose crystals grown in permanent fields with the following patterns for field strengths of:
265-300G, only in sucrose samples with < 4 magnetic treatments,
350-400G, mostly in sucrose samples with 4 to 7 magnetic treatments,
540-620G, in all sucrose samples regardless of number of magnetic treatments,
630-760G, no definite pattern established.
- (3) The number of nucleation centres increased with increasing field strength in the permanent field study below 620G, however above this value a reduction was obtained. Secondary nucleation was low for most of the sucrose crystals grown in this study other than between 540-620G, where enhancement occurred in all sucrose samples and at field strengths of 350-400G for 4 to 7 magnetic treatments.
- (4) The applied AC electromagnetic field studies resulted in very clear, well-formed sucrose crystals with wedge and euhydrated morphology with around 2 to 10 nucleation centres, indicating enhanced nucleation at lower (super) saturations.

- (5) Some euhydral characteristics were observed in many of the sucrose samples treated with applied DC electromagnetic field strengths below 500G, however between 220-600G, the morphology became exclusively euhydral. Above this range, 300-680G the morphology became mixed with no pattern in occurrence to the forms of euhydral, wedge and dendritic.
- (6) The number of nucleation centres decreased with increasing field strength in Experiments 31 to 34 from 12 to <7, and 36 (up to 500G and in 300-680G), however, where exclusively euhydral morphology was obtained (220-600G, Expt. 35) this number increased to around 9 to 16.
- (7) Applied pulsed magnetic field treatments resulted in wedge and dendritic morphology with commonly around 3 to 6 nucleation centres. No enhancement in nucleation was therefore obtained under these conditions.

2.3.2(c)(i)(2) Scanning Electron Microscopy

SEM measurements were made on a selection of sucrose samples. The general surface features are summarised in Tables 2.3.19 to 2.3.31 and most of the forms were common to the features illustrated in the static crystallisation studies, however SEM Images of interest or where significant changes in morphology were observed, these have been illustrated in the numbered Figures in square brackets [2.3.86] to [2.3.114] following the Tables.

Conclusions to be drawn from this study are therefore as follows:

- (1) SEM's of the 'Control' or 'no-field' sucrose samples of Experiment 25 illustrated well-formed, regular crystalline forms where shapeless, formless blobs were expected. The explanation offered for this anomaly of air bubbles caused by turbulence during pumping would explain the increased number of nucleation centres, however does not explain the improvement in crystal forms observed.
- (2) The peristaltic pump was considered to be a source of AC electromagnetic field, enhancing the sucrose crystallisation, resulting in well-formed microcrystals and layered growth features. Therefore, all other magnetic treatments would be considered to be a combination of AC electromagnetic field in addition to the particular magnetic field under study.

- (3) SEM's of the combination of AC electromagnetic field *and weak permanent fields <620 Gauss (Experiments 26-28)* magnetic treatment, indicated that *dissolution was important* since extensive pitting and round or no microcrystals were observed.
- (4) The SEM's of the sucrose samples obtained from magnetic treatment with AC electromagnetic field from pump and *weakest DC electromagnetic field. 265-300 Gauss*, indicated that *sucrose microcrystal dimensions increased with increasing number of magnetic treatments*, and that dissolution became less important with increasing number of magnetic treatments.
- (5) Where sucrose samples were treated with *a permanent magnetic field 630-760 Gauss (Expt. 29)* the SEM's indicated *increasing microcrystalline size with increasing number of treatments*. Dissolution was less important at this field strength since surfaces were more regular and less pitted.
- (6) The *AC electromagnetic field treatment* in combination with the AC electromagnetic field from the pump resulted in *well-formed crystal surfaces and microcrystals in addition to elongated sucrose microcrystal forms and directionally pitted lines*.
- (7) The DC electromagnetic field treatments in combination with the AC electromagnetic field associated with the pump, were very different with no definable pattern observed, however, the sucrose crystalline form seemed to be dependant on (1) DC electromagnetic field strength, and (2) the number of treatments
 - (a) *<100 Gauss* resulted in *well-formed sucrose crystals*. At this field strength and *improvement in crystal form was associated with the increase in magnetic treatments*,
 - (b) where the DC field treatment strength was *100 to (190-500) Gauss*, the sucrose crystals were a *mix of well-formed and rounded in addition to a variety of microcrystalline sizes*, and
 - (c) *>220 to 600 Gauss* resulted in *elongated sucrose crystalline forms*.
- (8) Magnetic treatment with the *pulsed field* in combination with the AC electromagnetic field associated with the pump resulted in *improved surface*

flatness following 5 passes and most *illustrated rounded microcrystalline forms* indicating dissolution to be important.

2.3.2(c)(i)(3) Differential Scanning Calorimetry

The conclusions drawn from this study were as follows:

- (1) *Most sucrose samples were shown to have an additional feature* (in addition to sucrose melting peak) *using DSC analysis*. Very few crystals grown following magnetic treatment did not illustrate an additional feature on DSC analysis.
- (2) Several sucrose crystals revealed a *second additional feature on DSC analysis*.
- (3) The DSC's of the '*Control*' *samples contained considerable amounts of additional features*.
- (4) There was '*no clear pattern*' associated with the size of the additional DSC features following magnetic treatment with permanent or DC electromagnetic magnetic fields with respect to (a) *the field strength*, and (b) *the number of treatments*.
- (5) The *theorised associated AC electromagnetic field from the peristaltic pump*, used in combination with the applied magnetic treatments explained *the unusual variation in observed additional features on DSC*. In addition, the argument for the existence of the associated AC field from the pump was reinforced, and the *DSC results were consistent with visual and SEM observations of the sucrose crystals*.

2.3.2(c)(i)(4) Conclusions for magnetic treatment studies on normal grade sucrose

Magnetic treatment of 0.65S sucrose solutions under conditions indicated in Section 2.2.3 has resulted in similar sucrose crystal forms to the static study being obtained which have improved regular forms, microcrystals and 1 or 2 additional features on DSC data in addition to sucrose melting points.

The most important distinction between the magnetic treatment study and the static study was the inability to establish a 'Control' or 'no-field' experiment. The most logical explanation for this was that the peristaltic pump had an associated AC electromagnetic field in which case all subsequent experiments were considered to be

combinations of magnetic field treatments with this associated AC electromagnetic field.

It was clear that the number of treatments (from 1 to 8) played an important role in crystal characteristics since the number of treatments introduced different crystalline morphology, growth rates, nucleation rates, microcrystalline dimensions, surface flatness, pitting and elongated forms. Variation in the field strengths resulted in similar changes.

The result of different combinations of fields and strengths on the resulting sucrose crystal forms via magnetic treatment are summarised in the conclusion paragraphs following discussion of each sets of data and are not highlighted here, however there were some patterns established and field strength limits observed as opposed to random variations. It would have been interesting to try to measure the associated AC electromagnetic field strength from the peristaltic pump, however, the equipment to do so was not available. An indication of the field strength could have given valuable information about the strength required to induce a magnetic effect. In addition, the variation in flow rates under these conditions would also be an interesting field of study from the view of determining whether it is an important variable requiring consideration.

The effect performing magnetic treatment with a syphoning system in place of the peristaltic pump would be an interesting study, and may indicate whether or not there is an associated AC electromagnetic effect from the pump or not. This study is carried out in Section 2.3.4(d).

2.3.2(c)(ii)ANALYTICAL GRADE SUCROSE

2.3.2(c)(ii)(1) Visual observations

The conclusions from the visual observations recorded for analytical grade sucrose are as follows:

- (1) The magnetic treatment of 0.65S analytical grade sucrose resulted in similar crystal morphologies to those observed in the normal grade studies.

- (2) More crystal regularity in the form of fine dendritic crystals alongside chunky, well-formed wedge crystals with layered growth patterns (indicated by opacity) were observed for the control samples than expected. This *supported the presence of the AC electromagnetic field associated with the peristaltic pump.*
- (3) Some differences in morphology between Runs A and B were observed in some sucrose samples. Only differing evaporation rates as a result of different positions within the incubator or the possibility that the incubator door was opened were offered as explanations for the major differences observed in Experiments 39, 46 and 49.
- (4) The *number of centres of nucleation was lowest in the 350-400G permanent field*, indicating that *nucleation was retarded. Above 540G the number of magnetic treatments did not have any significant effect* on the resulting sucrose crystal morphology *or the number on nucleation centres* observed, i.e. *the magnetic treatment appeared to plateau.*
- (5) There was very little change in morphology other than *a random spread of some euhydrated characteristic morphology* observed from exposing analytical grade sucrose solutions to *AC electromagnetic field treatments*. In most cases, *nucleation was retarded.*
- (6) The *weakest DC electromagnetic field 50-100G* used in the magnetic treatment resulted in *promotion of euhydrated morphology* indicating *promotion of spontaneous nucleation at lower supersaturation levels*. Increasing the field strength above this level only reduced the effect.
- (7) The *total number of nucleation centres* observed for increasing magnetic field strengths generally *increased with increasing field strength.*
- (8) The *pulsed field magnetic treatment* studies indicated *promotion of euhydrated sucrose crystal morphology* following *3 to 6 magnetic treatments*. *Nucleation was enhanced* following *1 to 3 magnetic treatments* and *maximised following 2 treatments.*

2.3.2(c)(ii)(2) Scanning Electron Microscopy

The visual observations recorded macroscopic changes in sucrose crystal morphology. In order to assess whether or not similar changes in morphology could be seen at

microscopic level, Scanning Microscopy measurements were made of the sucrose crystals.

The general surface features are summarised in Tables 2.3.59 to 71 and most of the forms observed were common to the features illustrated in the static crystallisation studies. SEM images of interest or examples where significant changes in morphology were observed have been illustrated in the Figures numbered in square brackets [2.3.115] to [2.3.142] following these Tables.

The SEM's obtained of the sucrose crystals grown following 'no-field' treatment are summarised in Tables 2.3.59 and illustrated in Image [2.3.115]. Flat wave-like surfaces (38(2)) microcrystalline material and layered, stepped growth illustrated, like in the normal grade sucrose case, that the surface had a more regular crystal form than would have been expected from the control. Unfortunately, no distinction could be made whether this was as a result of less impurities i.e. the analytical grade sucrose or as a result of the associated AC electromagnetic field from the peristaltic pump. Obviously there was a need to examine the 'Control' or 'no-field' analytical grade sucrose crystal form grown under static conditions in order to determine which explanation was the most likely.

Two analytical grade solutions 38(a) and 38(b) were crystallised under the same conditions as the static study 'control' or 'no-field' Experiment 13, and examined both visually and using SEM and DSC techniques. Both Samples 38(a) and (b) resulted in 5 primary nucleation centres of growth and 1 or 2 secondary. Both samples comprised chunky, wedge morphology and crystallised overnight. These results were very similar to the observations recorded for the normal grade sucrose control samples.

The SEM's taken of Samples 38(a) and (b) are illustrated below in Figures [2.3.186] to [2.3.188] and are summarised in Table 2.3.121.



Fig. 2.3.186 Sucrose sample 38(a).

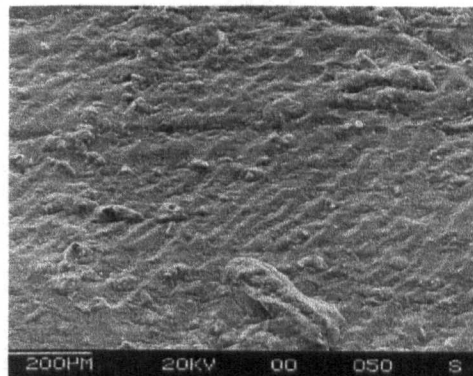


Fig. 2.3.187 Sucrose sample 38(b)

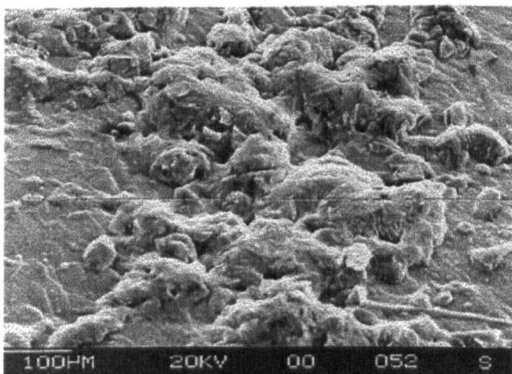


Fig. 2.3.188 Sucrose sample 38(b).

Sample No.	Description of morphology	Microcrystalline dimensions
38(a)	Wave-textured, rough surface [2.3.186]	
38(b)	Rough surface with blobs of sucrose crystals [2.3.187]	
38(b)	Finer detail of amorphous surface nodules [2.3.188]	

Table 2.3.121 SEM observations for sucrose Samples in Experiment 38(a) and (b).

It can be seen from the SEM images that the surfaces of the 'Control' sucrose crystals are very rough in texture and are covered by crystal nodules, similar to the control of the normal grade sucrose static study. Both visual observations and SEM observations indicate that the analytical grade sucrose crystals obtained from static crystallisation were not well-formed and rough in texture.

The sucrose crystals 38(a) and (b) were different from those obtained in Experiment 38, DSC data were obtained on both of the samples. Both sucrose samples contained only one very sharp sucrose melting peak at $\sim 187^\circ$ and $\sim 188^\circ\text{C}$ respectively illustrated in Figs. 2.3.189 and 2.3.190 given below.

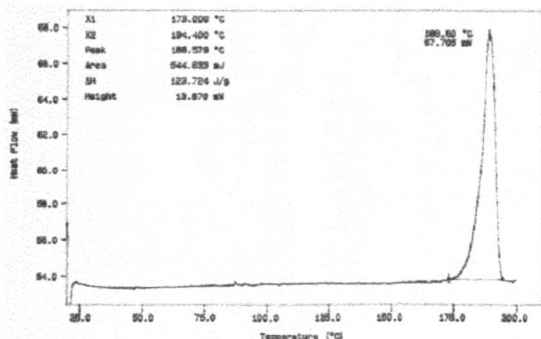


Fig. 2.3.189 DSC of sucrose 38(a).

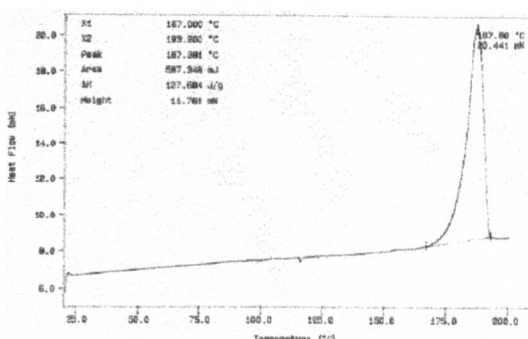


Fig. 2.3.190 DSC of sucrose Sample 38(b).

These findings strongly support the interaction of the sucrose solution with an AC electromagnetic field associated with the peristaltic pump.

In conclusion, therefore:

- (1) SEM's of the 'Control' or 'no-field' sucrose samples of Experiment 38 illustrated microcrystals and layered growth forms i.e. *were more regular forms than would have been expected from comparison with the normal grade sucrose control samples in the static study.*
- (2) Static crystal samples were grown with analytical grade sucrose for comparison to the control samples under pumped conditions. *The surfaces were rough in texture and had some small lumps covering the surface. The 'Control' samples from the pumped solution conditions were more regular and well-formed than those of the static conditions control samples.*
- (3) A range of different field strengths and number of magnetic treatments resulted in different sucrose crystal surfaces and forms. For permanent fields:
 - 265-400G (Expts. 39 and 40) promoted some regular growth however dissolution was important in most cases,*
 - 540-620G (Expt. 41) permanent field favoured nucleation resulting in the formation of vast numbers of microcrystals,*
 - >630G (Expt. 42) dissolution became more important as pitting and rounded microcrystals were more common.*
- (4) *The degree of pitting, the number of microcrystals and the presence of layered growth formations changed depending on the number of magnetic treatments and the strength of the treatment field.*

- (5) The SEM's of the analytical grade sucrose treated with the *AC electromagnetic field improved in form with the number of treatments up to 3 and 6 treatments. Above this number of treatments, dissolution became more important* i.e. surface pitting and no microcrystals was more common.
- (6) For DC electromagnetic field treatments,
< 220-600G (Expts. 44-48) favoured well-formed sucrose crystals, layered growth formations and microcrystals, for up to 6 treatments. Above 6 treatments dissolution became more significant,
>300-680G (Expt. 49) dissolution was enhanced since poor surface forms and rounded microcrystals were observed.
- (7) Magnetic treatment using the *pulsed magnetic field* resulted in *improvement in sucrose crystal forms up to 6 treatments. Above this value dissolution became more significant* as pitting became more frequent.
- (8) *Since similar improvements in crystal form were observed with analytical grade sucrose and normal grade sucrose, it was concluded that the presence of impurities in the solution of treatment was not the cause of these improvements in crystal regularity.*

2.3.2(c)(ii)(3) Differential Scanning Calorimetry

The following conclusions were drawn:

- (1) *Additional features were observed in all DSC data* for the sucrose crystals obtained under 'Control' conditions indicating *the sucrose solution interacted with an applied field and was not in fact a 'no-field' experiment.*
- (2) *The optimum permanent field strength was <620G. Above 620G, permanent field treatments were very small and insignificant.* In all cases of magnetic treatment with permanent field strength ,620G, the additional features observed using DSC analysis were large, and in some cases there were 2 or 3 additional features.
- (3) *AC electromagnetic treatment resulted in additional features in all DSC data* that were greater than the equivalent data sucrose obtained for the normal grade sucrose crystals.

- (4) The following points were noted from the DSC data obtained of sucrose crystals obtained following DC electromagnetically treated sucrose solutions:
- <190-500G most sucrose samples illustrated 2 medium to very large (very few small) additional features in the ranges 150-152°C, and 157 to 167°C. Below this field strength, some sucrose crystals showed a third feature.*
- >190-500G, all sucrose crystals contained a single small additional feature around 150-152°C with very few second features observed.*
- (5) *The effects observed from magnetic treatment with a pulsed field were very small* using analytical grade sucrose.

2.3.2 (c)(ii)(4) Conclusions for magnetic treatments studies on analytical grade sucrose

Magnetic treatment of 0.65S analytical grade sucrose solutions under the conditions indicated in Section 2.2.3 resulted in growth of sucrose crystals with improved regular forms, microcrystals that displayed 1 to 3 additional features on DSC data in addition to sucrose melting points, very similar to the results obtained in the normal grade sucrose study. However, one important difference was the increased intensity of the additional features observed.

The 'Control' or 'no-field' experiment illustrated improved regular forms, flat surfaces and microcrystals. This was illustrated to be a result of the associated magnetic field from the peristaltic pump and not as a direct result of fewer impurities in the sucrose solution under treatment.

An interesting point of note was the larger additional features observed in the DSC data for all the sucrose crystals. Decreasing the level of impurities in the sucrose solution in fact enhanced the effect of the magnetic treatment. The significant implications therefore were that the actual mechanism of the magnetic effect were not as a result of the magnetic field acting on impurity ions as postulated by some workers.

There were cases where crystallisation was retarded (e.g. <350-400G permanent field), spontaneous nucleation was enhanced at lower supersaturation levels (indicated by the presence of euhydrated sucrose crystal characteristics and the presence of large numbers

of microcrystals) and the number of magnetic treatments affected both of these in addition to field strength, and type of field employed in the magnetic treatment process.

It was clear however, from studies carried out that sucrose solutions were affected by magnetic treatment since large variations in crystal form obtained from these sucrose crystals grown from magnetically treated solutions was observed.

2.3.2(d) Magnetic treatment of sucrose where the solution is syphoned

The results from the previous study on magnetic treatment of sucrose where the solution was pumped indicated the possibility of an interaction between the sucrose solution and the AC electromagnetic field associated with the pump. In order to gain an insight into whether this is the case or not a series of syphoning experiments were carried out on both normal and analytical grades of sucrose solutions where no pump was used to pass the solution through identical silicon tubing and instead the sucrose solutions were syphoned under gravity. The introduction of syphoning introduced a variance in the speed at which the sucrose solution passed through the field when compared to the pumped study, therefore two changes were therefore made from the original pumped study, and in fact the solution flow was around twice the speed where syphoned compared to pumped.

Two types of sucrose were used, normal and analytical grade study was again carried out in two parts.

2.3.2(d)(i) NORMAL GRADE SUCROSE

2.3.2(d)(i)(1) Visual observations

In conclusion therefore:

- (1) The *control crystals were similar to those obtained in the static study i.e. irregular, chunky wedge and dendritic forms with no euhydral forms present.*
- (2) *Spontaneous nucleation was enhanced in all magnetic treatments studied under the syphoned conditions of treatment since euhydral characteristics and more regular forms* were observed.

2.3.2(d)(i)(2) Scanning electron microscopy

In conclusion:

- (1) *The control or 'no-field' sucrose crystals were similar to the static study control sucrose crystals* in that surface blobs and rounded forms were observed in all cases. No regular forms were observed other than some very large scale chunky forms.
- (2) This *information strongly supports the assumption from the previous study that an AC electromagnetic fields was associated with the peristaltic pump* however since *the velocity of the solution through the magnetic field also altered to around double that of the pumped study*, the observations cannot be claimed to be solely as a result of the absence of the pump and must be taken into consideration.
- (3) In *all sucrose crystals studied using the SEM technique, regular forms were observed* following magnetic treatment on the sucrose crystal surfaces in addition to the presence of microcrystals in most cases. All indicate more regular sucrose crystal forms were obtained as a result of magnetic treatment.

2.3.2(d)(i)(3) Differential scanning calorimetry

In conclusion:

- (1) The *DSC data for the control sucrose crystals contained only one peak relating to the melting point of sucrose*. No additional features were observed in all samples.
- (2) *One or two additional features were observed in the DSC data obtained for every other sucrose crystal grown following magnetic treatment* in the ranges 150° to 154°C and 158° to 173°C.
- (3) The *smallest additional features were observed for the sucrose crystals grown from the permanent field and pulsed field treated sucrose solutions*.
- (4) The *largest additional features observed following DSC analysis were obtained for sucrose crystals treated with the electromagnetic fields (both AC and DC)*.

2.3.2(d)(i)(4) Conclusion

Examination of the data obtained on the 'Control' sucrose crystals of Experiment 51 strongly indicated that no regular crystal forms were obtained and that the resulting sucrose crystals were similar in form to those obtained for the 'Control' sucrose crystals obtained in the static crystallisation of sucrose study. This evidence strongly supports the claim of an associated AC electromagnetic field interaction of the sucrose solution with the peristaltic pump. It must be noted however that these results could also have been a result of the change in velocity of the sucrose solution through the silicon tubing but would not account for the less regular sucrose forms observed in the control samples. The analytical grade sucrose study would be expected to illustrate similar results.

2.3.2(d)(ii) ANALYTICAL GRADE SUCROSE

In conclusion:

- (1) The Control, Experiment 56 resulted in the formation of sucrose crystals similar in form to those obtained in the normal grade sucrose Control, Experiment 51, where no euhydrated morphology was observed.*
- (2) Nucleation was retarded using a 630-760G permanent field.*
- (3) The AC electromagnetic field used in this study enhanced nucleation.*
- (4) Very fine needle-like sucrose crystal modification was observed following magnetic treatment with the 300-680G DC electromagnetic field.*
- (5) For all magnetically treated sucrose solutions, enhanced nucleation at lower supersaturations and more regular sucrose crystal forms were observed.*

2.3.2(d)(ii)(2) Scanning electron microscopy

In conclusion:

- (1) All 'Control' sucrose crystal samples illustrated rough textured surfaces, large blobs and extensive pitting indicating not only that dissolution was significant, but also regular features were not common in sucrose crystals grown from unmagnetically treated sucrose solutions.*
- (2) In all cases where sucrose crystals were grown from analytical grade sucrose following magnetic treatment, regular forms were observed, layered growths,*

- (1) *stepped structures and lined ridges in addition to a large number of microcrystals, some within narrow ranges of crystal dimensions and some with modified forms.*
- (2) *All evidence supports the theory of an associated AC electromagnetic field with the peristaltic pump of the previous study* since there was a greater difference in regularity between Control crystals and the sucrose crystals grown following magnetic treatment under the syphoning study.

2.3.2(d)(ii)(3) Differential scanning calorimetry

In conclusion therefore:

- (1) *None of the Control sucrose crystals had additional DSC features* and their melting points were high indicating high purity.
- (2) *All other sucrose crystals grown following magnetic treatment had one, and in some cases two additional features on DSC.*
- (3) *The additional DSC features were smaller than those obtained from corresponding normal grade sucrose study.*

2.3.2(d)(ii)(4) Conclusion

There are two possible explanations to account for these observations. The first is that the purity of the solution is affected by the magnetic field, and the other consideration is the residence time in which the sucrose solution was in contact with the magnetic field. The residence time for the syphoned experiments was shorter than that of the pumped experiment. It is likely that the resulting observations are a result of a combination of the two effects superimposed one each other.

2.4 CONCLUSIONS

More regular sucrose crystal forms were obtained following interaction within a magnetic field in every case examined regardless of the grade of sucrose studied. Nucleation was enhanced in some cases and retarded in others, as was crystal growth. Some applied fields appeared to alter the balance between (a) crystal nucleation and

growth and (b) dissolution. These are documented in the conclusion sections following each study.

The most significant differences were enhanced nucleation at lower supersaturations and the presence of a great many microcrystals which could potentially provide many benefits in a production environment where for example, a mixture of sugar solutions and dyes are crystallised.

DSC data of every sucrose crystal grown following magnetic treatment contained an additional DSC feature around 152°C in addition to the melting point around 175-190°C and in some cases a second feature was observed in the region 158 to 168°C. Investigation of these features indicated them to be most likely a result of water within the sucrose crystal (Karl Fischer and Solid state NMR). The nature of this water was most likely strongly bound and in the form of a sucrose hydrate. Unfortunately, Powder XRD data was inconclusive.

The resulting sucrose crystals were very similar where static and dynamically applied fields were studied, and both demonstrated strong effects on the resulting sucrose solutions.

The pumped sucrose solution study indicated stronger effects on the resulting sucrose crystals grown from analytical grade sucrose solutions strongly inferring that impurity ions reduced the effects of applied fields, however, the opposite was found in the syphoned study where normal grade sucrose solutions resulted in the largest applied field effects on the resulting sucrose crystals.

All evidence supported the theory that an AC electromagnetic field interaction occurred with the sucrose solutions whilst passing through the peristaltic pump however, this was not measured or clarified.

In the dynamic studies, the number of magnetic treatments in relation to the resulting effects on sucrose crystals in some cases maximised around 4 to 6 treatments

however, there was not always a clear pattern. Where the solution was pumped, a combination of AC electromagnetic field from the pump and the applied field was assumed and the pattern was sometimes reversed. In addition, there was sometimes no clear pattern.

It was obvious however that application of a magnetic field to a sucrose solution before or during crystallisation affected the growing sucrose crystals, altered the forms observed and gave clear data supporting applied field effects.

2.5 REFERENCES

- [1] von Lippmann, E. O., *Geschichte des Zuckers*, J. Springer Verlag, Berlin, 1929, 2nd Ed.
- [2] Leszok, S., Ph.D Thesis, University of Columbia, 1978
- [3] Berglund, K.A. and deJong E.J., *Separation Technology*, 1990, 1, 38-45
- [4] Cordovez, F., Mendoza, J.J. and Prato, V.H., *Int. Sugar J.*, 1992, **94**, Part 1121, 109-111
- [5] Donovan, M. and Sinclair, K., *Int. Sugar J.*, 1994, **96**, Part 1148, 305-313
- [6] Rein, P.W., *Int Sugar J.*, 1996, **98**, Part 1169, 202-206
- [7] Beevers, C.A. and Cochran, W., *Nature*, 1946, **157**, 872
- [8] Brown, G.M. and Levy, H.A., *Science*, 1963, **141**, 921-923
- [9] Hanson, J.C., Sieker, L.C. and Jensen, L.H., *Trans. Am. Cryst. Assoc.*, 1972, **8**, 133-148
- [10] Hanson, J.C., Sieker, L.C. and Jensen, L.H., *Acta Cryst.*, 1973, -, 797-808
- [11] Kukhareenko, J.A., The planter and sugar manufacturer, 1928, **80**, 361; 382; 403; 424; 443; 463; 484; 504.
- [12] Vavrinecz, G., *Atlas of sugar crystals*, Verlag. Dr. Albert Bartens, Berlin, 1965
- [13] Smythe, M.B., *Aust. J. Chem.*, 1967, **20**, 1115
- [14] Powers, H.E.C., *Sugar Technol. Rev.*, 1969/70, **1**, 85-190
- [15] Seager, A.F., *Principles of sugar technology*, ed. Honig P., Elsevier, Amsterdam, 1959, Vol II, 10
- [16] Kelly, F.H.C., *Int. Sugar J.*, 1957, **59**, 304
- [17] Kelly, F.H.C., *Sugar Technol. Rev.*, 1982, **9**, Part 3, 271-323
- [18] Kelly, F.H.C. and Mak, F.K., *The sucrose crystal and its solution*, Singapore University Press, Singapore, 1975, 14
- [19] Hook, A. van, *Principles of sugar technology*, (Ed. Honig, P.), Vol. II, Elsevier, Amsterdam, 1959, Ch. 3 and 4
- [20] Charles, D.F., *Am. Chem. Soc.*, (Abst. of papers), 1958, **10D**
- [21] Vavrinecz, G., *Z. Zuckerind.*, 1962, **12**, 481

- [22] Tuck, K.E., Msc Thesis, University of Tasmania, 1968
- [23] Pimentel, G.C. and McClellan, A.L., *The Hydrogen Bond*, Freeman and Co., 1960, Ch. 9
- [24] Charles, D.F., *Int. Sug. J.*, 1960, **62**, 126
- [25] Mantovani, *Zucker*, 1967, **20**, 198
- [26] Lyle, P., *Int. Sugar J.*, 1939, **41**, 390
- [27] Miers, H.A., *J. Inst. Met.*, 1927, **37**, 331
- [28] Webre, A.L., *Int. Sug. J.*, 1939, **41**, 141
- [29] Dedeck, J, Sugar Crystallisation, 1953, Brit. Sugar Corp. 6th Tech. Conf. Camb.
- [30] Dunning, W.J., *Chemistry of the Solid State*, (Ed. Garner, W.E.), Butterworth Ltd., London, 1955
- [31] Young, F.E. and Jones, F.Y., *J. Phys. Colloid. Chem.*, 1949, **53**, 1334
- [32] Dauncey, L.A. and Still, J.E., *J. Appl. Chem.* , 1952, **2**, 399
- [33] Hill, S.E. and Orchard, W.J.H., *Int. Sugar J.*, 1962, **64**, 102
- [34] Pridoux, G., *Zucker*, 1962, **15**, 162
- [35] Pridoux, G., *Industries agricoletiset alimentari*, Feb., 1962
- [36] Smythe, M.M., *Aust. J. Chem.*, 1967, **20**, 6, 1092
- [37] Powers, H.E.C., *Int. Sugar J.*, 1960, **62**, 307-312
- [38] Palmer, NEED INITIALS AND OTHER AUTHORS, *J. Agric. Food Chem.*, 1956, **4**, (1), 72-77,77-81
- [39] Powers, H.E.C., *Int. Sugar J.*, 1951, **53**, 254-255
- [40] Powers, H.E.C., *Int. Sugar J.*, 1959, **61**, 17-18
- [41] Powers, H.E.C., *Nature*, 1958, **182**, 715-717
- [42] Young, F.E. and Jones, F.T., *J. Phys. Colloid. Chem.*, 1949, **53**, 1334
- [43] Bisheng, Z., Siynan, G., Lin, L. and Miaoyan, C., *Int. Sugar J.*, 1996, **98**, (1166), 73-75

3.0 SUMMARY

In this chapter, the properties and structure of lactose are reviewed. The physical and chemical properties of lactose is discussed. The crystal properties of lactose are reviewed and factors influencing lactose crystal form and α -lactose monohydrate crystallisation rate are discussed briefly.

In this work, the static crystallisation of lactose is carried out in a controlled incubator environment. Establishment of the 'Control' lactose crystal obtained under such conditions is followed by application of different magnetic fields to the lactose solution during crystal growth as listed below:

- Permanent magnetic fields with field lines parallel to the solution surface, 3 field strengths were studied,*
- Permanent magnetic field with field lines perpendicular to the solution surface, the strongest field from above was studied,*
- Pulsed magnetic field was studied, and*
- DC electromagnetic fields, 3 field strengths were studied.*

Characterisation of the resulting lactose crystals, using techniques such as Powder X-ray Diffraction, Differential Scanning Calorimetry, Scanning Electron Microscopy and Karl Fischer Titration techniques is discussed.

In all cases, α -lactose monohydrate crystals were obtained, however, application of the applied fields resulted in more ordered lactose crystals containing less amorphous lactose material. In addition, significantly higher moisture contents than expected were measured for lactose crystals grown in both DC electromagnetic fields and the permanent field with field lines perpendicular to the solutions surface during crystallisation. Geolitic water discussed in Chapter 2, is offered as an explanation for this measurement.

Finally, four of the lactose experiments were repeated (control, pulsed field, weakest and strongest DC electromagnetic field experiments), and the resulting lactose samples sent to the lactose experts in Nestle, Switzerland for more rigorous analysis. Increased water of crystallisation was confirmed i.e. higher moisture content than expected, in addition to suggestions that small amounts of β -lactose are present within the α -lactose monohydrate crystal.

3.1 INTRODUCTION

Lactose, meaning *milk sugar* (first isolated in 1633 and purified in 1688^[1]) is traditionally known as the sugar of the animal kingdom because its α -form is found in human and most animal milk (about 5% solution). It constitutes more than a third of the solid residue remaining after evaporation of all volatiles. Repeat crystallisation produces purity grades $\geq 99.5\%$ lactose (refined food quality) and $\geq 99.8\%$ lactose (pharmaceutical quality). Lactose is the only commercial sugar derived from mammalian sources, however its components glucose and galactose are common in plants.^[2]

Lactose comes from foods such as milk, cream, non-fat dry milk, whey solids, modified whey products or refined lactose. Commercially, lactose is produced from the whey that results from cheese making, as the cheese removes the casein and the fat reduces the solid content, leaving almost all the lactose. Due to the low solubility of lactose and its stability, it can be crystallised from concentrated whey with little difficulty.^[2]

Streamlined manufacturing methods today make it economically and environmentally viable for the dairy industry to expand its uses for whey (which comprises of 70-75% lactose) as most of it is currently treated as waste.^[3]

The most significant disadvantage of lactose is that it acts as a mild laxative. The product of metabolism of the intestinal bacteria is lactic acid that maintains the necessary acid reactions of the intestines. This property can be seen as both a disadvantage and an advantage. Lactose can support a healthy intestinal flora, encouraging peristaltics of the intestine and impeding the accumulation of toxins. However, certain groups of people cannot tolerate lactose due to the lack of enzyme lactase (which digests lactose) from the intestines. Consequently the lactose concentration increases which causes fermentation, this causes the malfunction of the intestine and the symptoms arising from this are back pain, sickness and diarrhoea.^[4]

3.1.1 Structure and properties of lactose

Lactose is a reducing disaccharide made up of two sugar molecules, glucose and galactose via a glycosidic linkage. The IUPAC nomenclature is 4-*O*- α -D-galactopyranosyl-D-glucopyranose and the structure is shown below in Fig. 3.1.1.

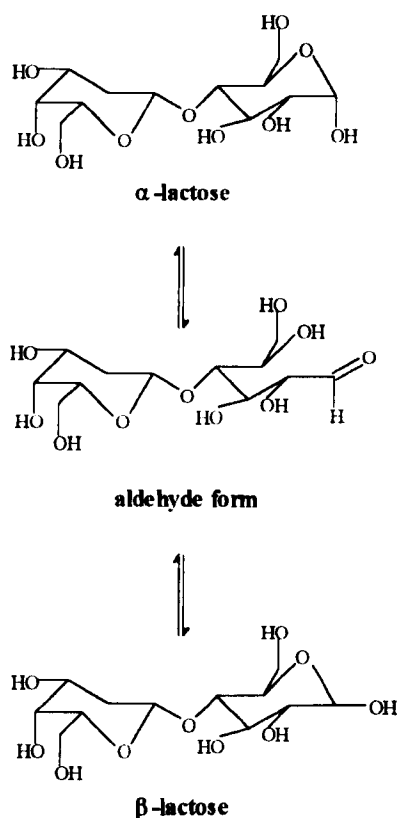


Fig. 3.1.1 Molecular structures of lactose.

The glucose moiety can exist in one of two isomeric hemiacetal structures giving α -lactose and β -lactose. In solution, either form will mutarotate to give the other until equilibrium is reached. A free aldehyde form is the intermediate in the interconversion of α - and β -lactose, but does not exist in any significant quantity. The isomeric α - and β -lactose are diastereomers, since they differ in the configuration at the anomeric carbon atom.^[5]

In 1909, Hudson^[6] described several crystalline forms of lactose; α -lactose monohydrate ($C_{12}H_{22}O_{11} \cdot H_2O$) and anhydrous β -lactose ($C_{12}H_{22}O_{11}$) that showed initial optical rotations of $[\alpha]_D$ 85° and 34.9° respectively; anhydrous α -lactose; molecular complexes of

α - and β -anomers in proportions α : β of 5:3, 3:2 and 4:1; and finally an amorphous 'glass' mixture of non-crystalline α - and β -lactose in equilibrium. Some of the physical properties of these are shown below in Table 3.1.1.

CRYSTAL FORM	APPEARANCE	MELTING POINT (°C)	DENSITY (G/CM ³)	ROTARY POWER [α] _D ^{20°C}	REFRACTIVE INDEX		
					α	β	γ
α -monohydrate	Monoclinic, tomahawk form	217	1.537	+85.0	1.517	1.553	1.555
α -(unstable)	Thin elongated plates, almost straight extinction	222.8	1.545	+89.4			
α -(stable)	Thin elongated plates, almost straight extinction	216	1.540	+89.4			
β -anhydrous	Monoclinic (rounded edges)	232	1.587	+34.9	1.542	1.572	1.585
Complex α : β (4:1)		204	1.573				
Complex α : β (5:3)	Thin elongated rectangular plates. Spherulitic bundles of plates seen edge-on appear as bundles of needles.	203	1.584	+67.5			

Table 3.1.1 Some physical properties of the different crystalline forms of lactose.

The functional properties of lactose depend on the physical forms present. Dried α -monohydrate is non-hygroscopic and is thus commercially desirable, whereas lactose glass is extremely hygroscopic and is to be avoided when producing whey powders.^[7] Solubility of α - and β -lactose forms in water are greatly influenced by temperature. Below 93.5°C the α -lactose monohydrate is formed giving hard, relatively insoluble crystals that are undesirable in many foods. When lactose crystallises above 93.5°C, anhydrous β -lactose is produced that is considerably sweeter and more soluble than the α -lactose monohydrate form, consequently having more uses in the food industry.^[7]

3.1.1(a) Mutarotation of lactose

As a consequence of the asymmetric carbon atom, lactose has the property of optical activity and rotates plane polarised light. As a result of this property, the mutarotation of

lactose between α and β forms can be studied by polarimetry. α -Lactose has a specific rotation at 20°C of +92.6°, however, when dissolved in water the optical rotation decreases until it reaches an equilibrium value of +52.3°. β -Lactose has a specific rotation of +34°, and when dissolved in water the optical rotation of the solution in water increases until it reaches the same equilibrium value obtained for α -lactose solutions. At equilibrium both α and β isomers are present however, since equilibrium rotation is closer in value to the initial rotation of β -lactose, the mixture must contain more of this isomer.^[5]

The solubility of α -lactose is lower than for β -lactose in water. A direct result is that a saturated solution of α -lactose mutarotating to β -lactose produces a solution that is no longer saturated. This is illustrated in Fig. 3.1.2.

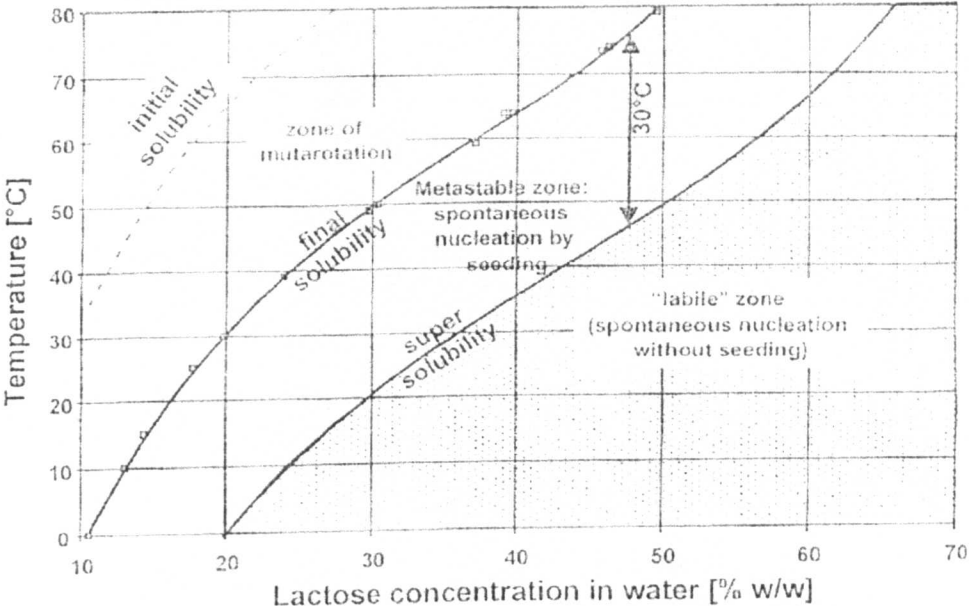


Fig. 3.1.2 A simplified Lactose-water solubility chart.^[8]

3.1.1(b) The Maillard reaction

The Maillard reaction is a complicated, though not completely evaluated, sequence of chemical changes between proteins and carbohydrates that normally occurs during the heat exposure of foods. It occurs without the aid of enzymes and is responsible for the surface colour change of bakery products and meats, sometimes during storage.

3.1.1(c) Sweetness and solubility

Lactose has a lower level of sweetness than sucrose,^[9] allowing it to be added to dessert products for example, icings and toppings, thus increasing the solid content without much effect on the level of sweetness. The low solubility of lactose, however restricts its uses and excessive lactose content can cause grittiness in cooked products. As a result of this, sucrose replacement by lactose is limited to around 10-20%.

3.1.1(d) Protein stabilising properties

Lactose is used to protect the solubility of the caseinate complex in milk during spray drying,^[10] as the caseinate complex would otherwise lose about half of its capacity to redisperse. As a result of this lactose is used to improve protein stabilising in frozen concentrated milk.^[11,12] At storage temperatures where caseinate is most stable (<-29°C) lactose is in the amorphous glass form, however, at higher temperatures (>-18°C), lactose crystallises resulting in rapid flocculation of the protein i.e. the particles in a colloid aggregate into larger clumps. Flocculation results from the higher salt concentration developed in the frozen milk phase. Lactose may stabilise the casein by sequestration (the process of forming co-ordination complexes of an ion in solution) of the highly concentrated milk salts in the unfrozen phase, therefore suppressing salting out of the casein.^[11]

3.1.1(e) Influence on crystallisation habit

Lactose can be used to control crystallisation of other sugars making it useful in production of confectionery such as fudge and caramels, with improved body, texture and chewiness.^[13] It was claimed that using small amounts of lactose and/or mannitol reduces gumminess of cooked candies made with arabinogalactan.^[7] The crystallisation of lactose in ice cream and sweetened condensed milk is undesired as crystals can provide a sandy or gritty texture. This is avoided by seeding or rapid agitation of the mix to alter the crystallisation habit of lactose.^[14]

3.1.1(f) Absorptive properties/flavour enhancing

Lactose absorbs flavours, aroma and colouring materials,^[15] and the extent of the effects depend on the crystal form of lactose. The most significant is anhydrous α -lactose that absorbs 156-305mg diacetyl/kg, while other forms absorb less than this value.

Anhydrous lactose may be added as a carrier for flavours and for food dyes, where a gradual release is desired. This is made possible by the low solubility of lactose.^[7]

In addition, lactose generally enhances and accentuates flavours of foods without causing excessive sweetness, and for this reason, is used in barbecue sauces, salad dressings, food drinks and pie fillings.^[16]

3.1.1(g) Dispersing properties

The pharmaceutical and food industries utilise the non-hygroscopic and free flowing nature of α -lactose monohydrate as a dispersing agent. The pharmaceutical industry forms tablet excipients using spray dried lactose.^[17,18] However, lactose monohydrate is preferred since the powder is free flowing and readily moulded, especially when blended with starch or gelatine, and forms a tablet that disperses readily.^[19] α -Lactose is also used in the food industry for instantising, to increase the dispersibility of powdered foods. This process offers a wide potential for dispersing by machine including coffee, tea and powdered syrups.^[7]

3.1.1(h) Emulsifying properties

The emulsifying properties of lactose are exploited in the following examples:

- aiding distribution during mixing which result is shorter mixing times,
- adding lactose to flour bases improves sheeting out and reduces shrink losses,
- incorporation of 3-4% lactose into machine cut doughs aids release from dyes and helps to maintain shape in the baking process,^[20] and
- cake batter with 10-15% of the sugars replaced by the lactose, give better volume, grain and texture.^[20]

3.1.1(i) Nutritional properties

Although there is a small percentage of the population that are lactose intolerant, there are nutritional benefits from use of lactose in the modification of cow's milk to formulate infant foods which simulate mother's milk^[71] (human milk has a lactose content of 6.4-7%, whilst cow's milk contains only 4.7-4.8% lactose).

3.1.2 Lactose crystallisation

An extensive amount of research has been carried out on the crystallisation of lactose, however, there are several conflicting theories concerning factors that control the crystallisation rate of lactose. Le Chatelier's principle of equilibrium states any changes imposed on the system tends to shift the equilibrium to nullify the effect of the change.

When considering the lactose equilibrium:



as α -lactose crystallises from solution, the equilibrium should shift to the left to 'compensate' the loss, by means of mutarotation of β -lactose to α -lactose. Thus, the rate of crystallisation was thought to be solely dependant on the rate at which β -lactose mutarotates to α -lactose.^[21]

The same conclusion was reached from investigation of the effects of extremely high and low pH's on rate of crystallisation.^[22] Likewise, work carried out by Twieg and Nickerson,^[23] demonstrated that the mutarotation rate was found to be the rate determining step under conditions of high surface area, however, in the latter stages, crystallisation rate was limiting rather than mutarotation. Other studies have show that crystallisation has a smaller rate constant than mutarotation and is in fact not an important factor in limiting rate.^[24]

Noyes and Whitney assumed that rate of growth is determined by diffusion to the surface of the crystal.^[25] In addition, other studies have concluded that different rate factors assume differing importance in various substances.^[26]

3.1.2(a) Crystal forms of lactose

Lactose crystallises in many forms that can be identified using Powder X-ray diffraction. These have been highlighted in Section 3.1.1 Generally, the α -monohydrate lactose crystals are very hard and non-hygroscopic and the anhydrous β -lactose crystals are smaller and have higher surface area.

Amorphous lactose comprises a mixture of α -lactose, β -lactose and water and is a solid without crystal structure. It is usually obtained by concentrating an aqueous solution rapidly, so that crystallisation does not occur.^[27] When the water content of the amorphous α -lactose is low ($\sim 3\%$), crystallisation is rare because of the high viscosity of the solid solution. The product is however hygroscopic and when the moisture content increases ($\sim 8\%$), α -lactose monohydrate begins to form.

α -Lactose monohydrate crystals have varying morphology (although the crystal lattice always remains the same) although the 'tomahawk' shape occurs most frequently (shown in Fig. 3.1.3). The variation in morphology can be affected by growth inhibitors such as riboflavin, lactose monophosphates and particularly the proportion of β -lactose. Crystallisation of α -lactose can be slowed down by high concentrations of β -lactose, and decreasing its content has the effect of rapid growth of particular faces resulting in needle-like crystals being formed. These inhibitors affect each crystal face differently giving rise to the large variety in shapes shown in Figures 3.1.3 to 3.1.7.

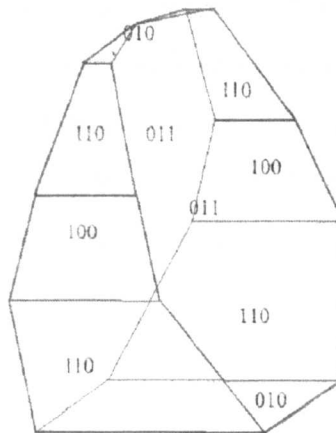


Fig. 3.1.3 Tomnahawk shape of a lactose crystal, with Miller indices.^[28]



Fig. 3.1.4 Tomahawk, a tall pyramid with bevel faces at the base.

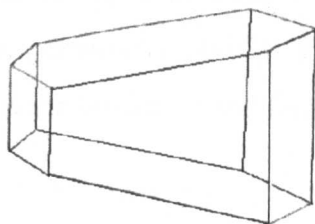


Fig. 3.1.5 The form most commonly described as “fully developed”.

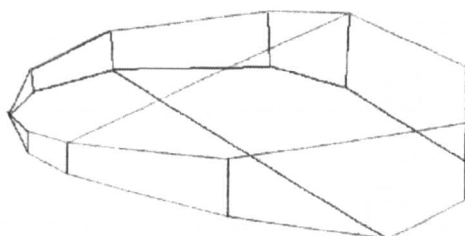


Fig. 3.1.6 A lactose crystal having 13 faces. The face shown in Fig. 3.1.4 is not present.



Fig. 3.1.7 A profile view of Fig. 3.1.6 with the tomahawk blade sharpened.

Nickerson and Moore^[29] reported that β -lactose in addition to glucose and maltose accelerated crystal growth rather than being inhibitory as most literature seems to suggest. In addition, high pH i.e. a value of less than one, greatly accelerated crystallisation, with sulphuric acid especially effective approaching the faster crystallisation rate of sucrose. Acetic and lactic acids were found to inhibit crystal growth of lactose.

Amorphous lactose is often produced by dehydration of solutions. During this stage mutarotation may occur, depending on temperature, time and concentration. The amorphous lactose produced by spray- or freeze-drying crystallises as a mixture of α -

lactose monohydrate and β -lactose crystals.^[30-33] In milk powders amorphous lactose crystallises as α -lactose monohydrate and anhydrous crystals with α - and β -lactose in a ratio of 5:3, and as anhydrous β -lactose crystals, depending on storage and temperature.

The various forms of lactose can be identified using Powder X-ray diffraction (Powder XRD) and Differential scanning calorimetry (DSC). The literature Powder XRD data showing characteristic peaks for each lactose crystal form is shown in Fig. 3.1.8.^[31,34]

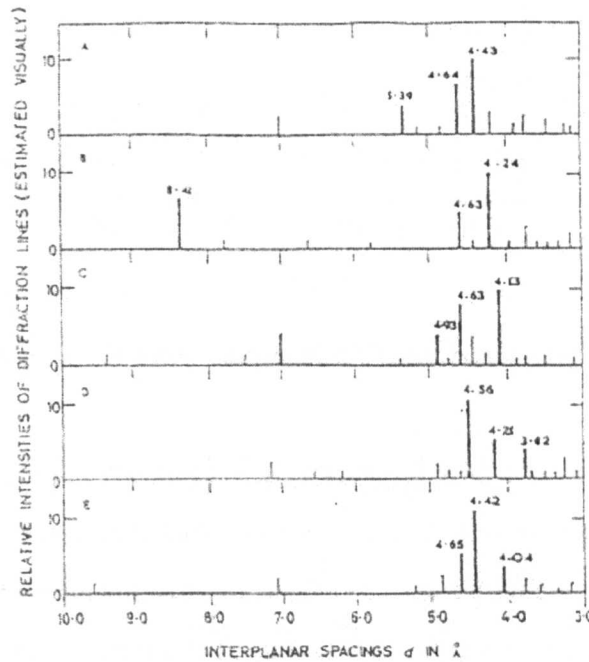


Fig. 3.1.8 Diagrammatic representation of the Powder X-ray diffraction patterns of the different crystalline forms of lactose.

- A α -monohydrate
- B β -anhydride
- C unstable α -anhydride
- D stable α -anhydride
- E molecular compound of α -lactose and β -lactose in a molar ratio 5:3.

It is clear from the data shown in Table 3.1.8 that the crystalline form of lactose may be easily identified using the Powder XRD technique.

DSC results from published literature^[35] are also a suitable for distinguishing the particular crystal form of lactose(see Fig. 3.1.9). α -Lactose and β -lactose can be distinguished by their melting points above 200°C. α -Lactose (α_{H_2O})can be identified by its characteristic

melting point around 150°(water of crystallisation). The dehydrated types stable α -lactose (α_S) and unstable α -lactose (α_H) have no water desorption peak at 150°C.

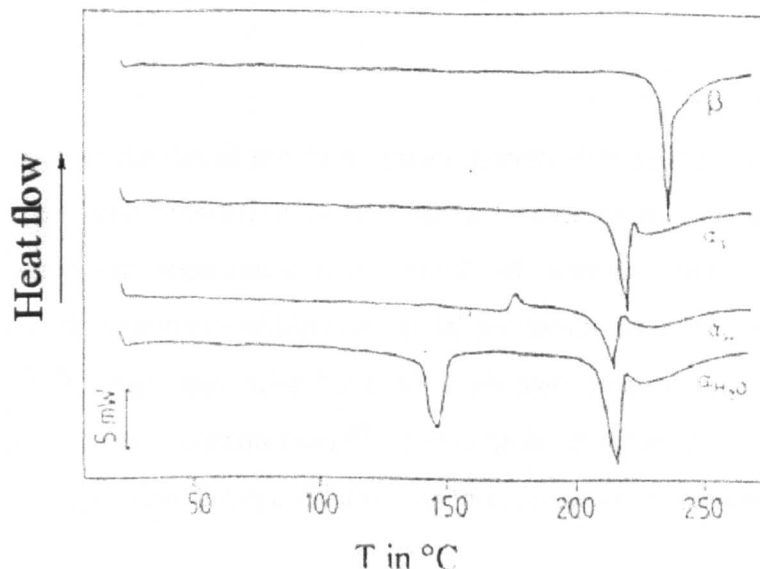


Fig. 3.1.9 DSC curves of different lactose types.

α -Lactose monohydrate has melting points, measured with a heating rate of 5°Cmin^{-1} , of 143.6 and 145.2°C. Since simultaneous melting and decomposition occurs, a reliable determination of the melting enthalpy above 200°C is not possible and can be in the region of 202 to 213°C depending on the heating rate used. The melting point of β -lactose, with a heating rate of 5°Cmin^{-1} , is around 220°C. The stable α -lactose form has an exothermic peak around 170°C which presumably represent recrystallisation of lattice distortions. Thus, it can be presumed that the unstable α -lactose is partly amorphous due to the preceding dehydration process.

The lactose crystal modifications carried out in industry are described in more detail in the literature.^[28]

3.1.2(b) Factors influencing lactose crystallisation

The rate and quantity of recovery of whey and also the production of smooth, viscous products such as sweetened condensed milk are governed by factors influencing lactose crystallisation.

Many factors such as the development of nuclei, transport of the medium to the growing nuclei, adsorption and orientation on the surface, desorption and dissipation of the product, influence the appearance and growth of crystals. Some researchers have concluded that mutarotation in addition to nuclei formation is a rate-determining step for crystallisation.^[35,36] which may arise because of changes in conditions of crystallisation such temperature and concentration.^[37] Herrington concluded that depending on conditions of crystallisation, lactose solutions produce crystals of different appearance.^[38]

The crystalline habit of many substances may be altered by the presence of other compounds. Saylor has drawn the conclusion that it is due to selective adsorption on certain faces of the crystal.^[39]

A study of broken lactose crystals has shown that broken faces grow much faster than normal faces until the break is completely healed^[40] and partial dissolving of lactose crystals results in higher growth rates.^[41]

Some impurities can accelerate crystal growth,^[26,42,43] however this can be short lived as the continued presence of the contaminants can quickly suppress the growth rate.^[29]

The presence of both methanol and ethanol accelerate growth by 30-60%, depending on which crystal face is being observed.^[43] This is attributed to acceleration of the absorption of alcohol on the steps of the crystal rather than a decreased solubility.

pH Plays a major role in influencing the crystallisation of lactose, where a very low value (pH<1) causes acceleration and higher values decelerate the process.^[23]

One study has shown that the growth of regular α -lactose monohydrate crystals depends on the amount of α -lactose in solution but is independent of the amount of β -lactose.^[44]

3.1.2(c) α -Lactose and Crystallisation Rate

Nickerson and Moore (1973) studied the effects of α - and β -lactose on crystal growth of anhydrous α -lactose,^[44] verifying Van Krevelde's^[45] conclusion that β -lactose inhibits growth of needle-like crystals. These two reviews differed only in Van Krevelde's conclusion that the seed crystals growth was also inhibited by the β -isomer. The total lactose content was constant, therefore, a decrease of α consequently caused an increase in β . As a result, needle growth was inhibited and it was also assumed to be inhibitory to the regular seed crystals. Nickerson and Moore concluded that the growth of regular α -lactose monohydrate crystals is not inhibited by the β form, stating that their data showed that crystallisation of the usual form of α -lactose monohydrate crystals is dependent on the α -lactose content.

The role of β -lactose varies in terms of growth rates with the type of α -lactose monohydrate crystals being produced in the solution.^[44] When crystallisation is rapidly forced, Herrington^[38] showed that needles are formed. As the rate of crystallisation is reduced the needles become shorter and broader, leading to diamond-shaped plates and then the more common crystal types are formed.

These results show that β -lactose influences the type of crystal produced, and consequently for the production of regular crystals the addition of β -lactose will inhibit the growth of needle structures. This is achieved by allowing time for mutarotation in order to reduce the amount of α -lactose present. Reducing the crystallisation pressure aids this process. In the industrial processing of milk products, α -lactose is a major determinant of the nature of crystallisation, β -lactose seems to be important only under exceptional conditions.

Missing pages are unavailable

controlled environment, at a set temperature in different magnetic fields of varying strengths.

In general, 10ml aliquots of lactose were removed from the prepared stock solutions and placed in petri-dishes (pre-heated to 50°C and dust free) in incubators at 50° and left to evaporate under different applied field conditions. Each experiment was repeated three times. Visual observations of crystal form were recorded for each experiment and Powder X-ray Diffraction, (XRD), Differential Scanning Calorimetry (DSC), Scanning Electron Microscopy (SEM) and Karl Fischer techniques were used to characterise the lactose crystals formed.

3.2.1(a) Experiment 1 - Controls

Lactose solution (10 ml) was pipetted into a petri dish (5 cm diameter), which was then covered with a lid, and the dish placed inside the incubator. The lid was removed, the door closed, and the solution allowed to evaporate and crystallise at 50°C, within the incubator environment, over a 24 hour period. The experiment was repeated three times giving lactose crystal samples labelled 1(1), 1(2) and 1(3).

For the following experiments an identical procedure to the above was followed and the petri dishes were placed within the field and the field strength measured. In all cases the field strength recorded is a measure of its strength and is given as a range.

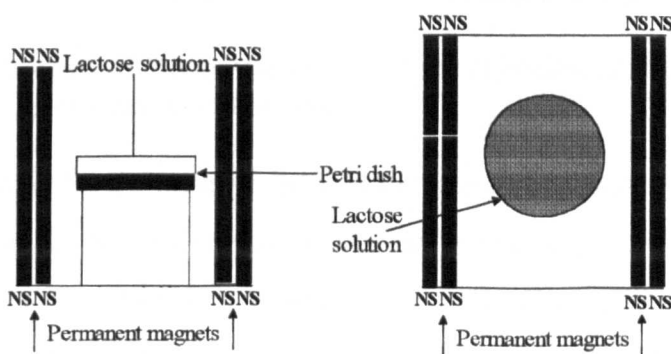


Fig. 3.2.1 Illustration of the apparatus set-up for crystallisation under a permanent field, parallel at sides of sample.

3.2.1(b) Experiment 2 - Weakest (265-300G) permanent field, at sides in parallel

Permanent magnets were placed in parallel as shown in Fig. 3.2.1. The petri dish was placed between the magnets with field strengths 300G at the edges and 265G at the

centre. This solution was allowed to evaporate and crystallise. The experiment was repeated three times giving lactose crystal samples labelled 2(1), 2(2) and 2(3).

3.2.1(c) Experiment 3 - Medium (540-640G) permanent field, at sides in parallel

Permanent magnets were placed in parallel as shown in Fig. 3.2.1. The petri dish was placed between the magnets with field strengths 640G at the edges and 540G at the centre. This solution was allowed to evaporate and crystallise. The experiment was repeated three times giving lactose crystal samples labelled 3(1), 3(2) and 3(3).

3.2.1(d) Experiment 4 - Strongest (630-760G) permanent field, at sides in parallel

Permanent magnets were placed in parallel as shown in Fig. 3.2.1. The petri dish was placed between the magnets with field strengths 760G at the edges and 630G at the centre. This solution was allowed to evaporate and crystallise. The experiment was repeated three times giving lactose crystal samples labelled 4(1), 4(2) and 4(3).

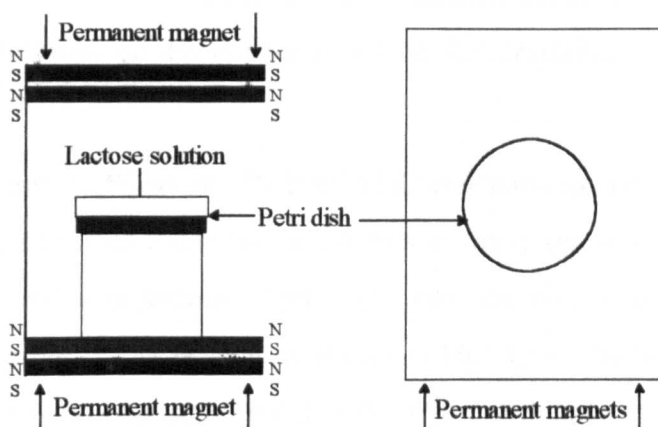


Fig. 3.2.2 Illustration of the apparatus set-up for crystallisation under a permanent field, above and below sample.

3.2.1(e) Experiment 5 - Permanent field, in parallel above and below

A permanent magnetic field of strength 630G was placed in parallel above and below the petri dish containing the lactose solution (10 ml) with the dish positioned on a raised platform as shown in Fig. 3.2.2. This solution was allowed to evaporate and crystallise at 50°C, within the incubator environment, over a 24 hour period. The experiment was repeated three times giving lactose crystal samples labelled 5(1), 5(2) and 5(3).

3.2.1(f) Experiment 6 - Pulsed field (Hydroflow device)

A petri dish containing lactose solution (10 ml) was placed on top of a Hydroflow pulsed magnet as shown in Fig. 3.2.3. This solution was allowed to evaporate and crystallise at 50°C, within the incubator environment, over a 24 hour period. The experiment was repeated three times giving lactose crystal samples labelled 6(1), 6(2) and 6(3).

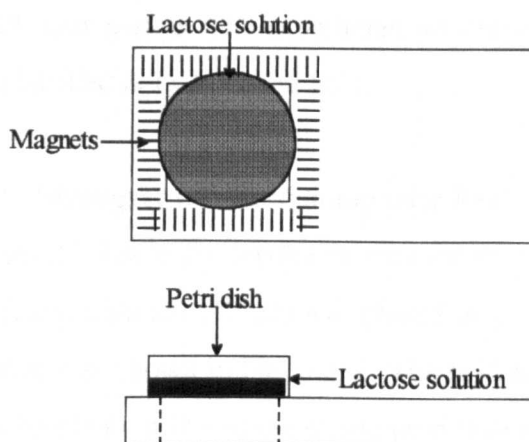


Fig. 3.2.3 Illustration of the apparatus set-up for crystallisation under a pulsed magnetic field.

3.2.1(g) Experiment 7 - Weakest (50-100G) DC electromagnetic field

A DC electromagnet placed inside the incubator was set to operate at 2.0V (2.93mA), and a petri dish containing lactose solution (10 ml) was placed on a raised platform between the two poles of the magnet as shown in Fig. 3.2.4. The field strengths were measured using a Gaussmeter to be 100G at the edges of the petri dish and 50G at the centre. The sucrose solution was allowed to evaporate and crystallise at 50°C, within the incubator environment, over a 24 hour period. The experiment was repeated three times giving lactose crystal samples labelled 7(1), 7(2) and 7(3).

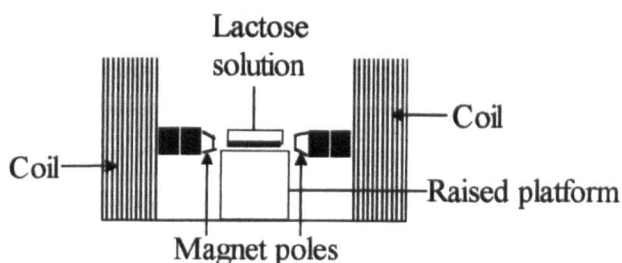


Fig. 3.2.4 Illustration of the apparatus set-up for crystallisation under a DC electromagnetic field.

3.2.1(h) Experiment 8 - Medium (150-340G) DC electromagnetic field

A DC electromagnet placed inside the incubator was set to operate at 6.0V, and a petri dish containing lactose solution (10 ml) was placed on a raised platform between the two poles of the magnet as shown in Fig. 3.2.4. The field strengths were measured using a Gaussmeter to be 340G at the edges of the petri dish and 150G at the centre. The solution was allowed to evaporate and crystallise at 50°C, within the incubator environment, over a 24 hour period. The experiment was repeated three times giving lactose crystal samples labelled 8(1), 8(2) and 8(3).

3.2.1(i) Experiment 9 - Strongest DC electromagnetic field

A DC electromagnet placed inside the incubator was set to operate at 10.0V, and a petri dish containing lactose solution (10 ml) was placed on a raised platform between the two poles of the magnet as shown in Fig. 3.2.4. The field strengths were measured using a Gaussmeter to be 600G at the edges of the petri dish and 220G at the centre. The solution was allowed to evaporate and crystallise at 50°C, within the incubator environment, over a 24 hour period. The experiment was repeated three times giving lactose crystal samples labelled 9(1), 9(2) and 9(3).

The applied field conditions used in each experiment are summarised in Table 3.2.1.

Experiment No.	Field Type	Frequency/Strength	Geometry
1	Control	N/A	N/A
2	Permanent magnets	300 - 265 Gauss	N-S, NH Parallel at sides
3	Permanent Magnets	640 - 540 Gauss	N-S, NH Parallel at sides
4	Permanent magnets	760 - 630 Gauss	N-S, NH Parallel at sides
5	Permanent magnets	630 Gauss	N-S, H Parallel above and below
6	Pulsed	100-160 kHz	N-S, NH Below
7	DC Electromagnet	50 - 100 Gauss	N-S, NH Parallel at sides

8	DC Electromagnet	150 - 340 Gauss	N-S, NH Parallel at sides
9	DC Electromagnet	220-600 Gauss	N-S, NH Parallel at sides

Table 3.2.1 Applied field configurations used in lactose studies. N-S=North -South geometry, NH=Non homogeneous, and H=Homogeneous.

3.2.2 Characterisation of lactose crystallised under static conditions

The Differential Scanning Calorimetry (DSC) measurements were made on all samples using a Perkin Elmer DCS7 and in all cases. A heating rate of 5°min^{-1} was applied to a closed cell containing about 3.5 to 4.5mg sample. DSC Thermograms were recorded using a Seiko SSC 5200 DSC 220 device, by heating about 10 to 15mg of product in a closed cell at $5^{\circ}\text{Cmin}^{-1}$ between 20 and 220°C . Simultaneous Thermo-Gravimetry (TG) and Differential Thermal Analysis (DTA) traces were recorded using a Seiko SSC 5200 instrument, by heating about 6 to 9mg of sample in an open cell at $5^{\circ}\text{Cmin}^{-1}$ between 25 and 250°C .

Four further samples of lactose were crystallised for (i) the Control 1(4), (ii) Pulsed field conditions 6(4), (iii) 50-100G DC electromagnetic field conditions 7(4), and (iv) 220-600G DC electromagnetic field conditions 9(4) and the samples were characterised by Nestle in Switzerland.

3.3 RESULTS AND DISCUSSION

Visual observations in terms of shape and texture of the lactose crystals were noted and were taken to be an early indication of possible morphological differences. Powder X-ray Diffraction would indicate any change in crystal morphology since all the forms of lactose have significantly different data. Differential Scanning Calorimetry was used to indicate which forms of lactose were present by examining the melting profile of the lactose crystals.

Scanning Electron Microscopy was used to give high magnification images of the lactose crystals. In this study, lactose crystals selected had distinctly different features: (1) the solution/glass interface, (2) the solution/air interface (which would be expected

to be largely amorphous), and (3) crystals grown in the bulk solution were chosen as representing three distinctly different features in the SEM photographs.

The Karl Fischer measurements on the lactose crystals were made to determine the moisture content; A form containing 5% water indicates an α -lactose monohydrate crystal and with 0% moisture indicated an anhydrous form etc. These measurements were to investigate the presence of 'geolitic water' (bound/unbound waters of crystallisation) which was observed within the sucrose crystals.

A combination of all four techniques gives a large amount of data regarding the nature of the lactose crystals grown under applied magnetic field conditions compared to those grown under zero field conditions.

3.3.1 Results

3.3.1(a) Visual Observations

The visual observations recorded for Experiments 1 to 9 are summarised in Table 3.3.1 below.

Experiment	Field Geometry	Crystal morphology observations
1 - Control	N/A	White-grey glassy textured lactose indicative of α -form.
2 - 265-300G permanent field	At sides in parallel	Similar to the Control samples in Exp. 1, but lactose crystals were more brittle.
3 - 540-640G permanent field	At sides in parallel	White-yellow coloured crystals with two different layers. The glass/solution interface layer was pitted and the solution/air interface was textured and whiter in colour than the control. The phase in between the layers was very crystalline.
4 - 630-760G permanent field	At sides in parallel	Observations were the same as those recorded for Experiment 3.
5 - 630G permanent field	Above and below in parallel	Similar to observations recorded for Experiments 3 and 4 however, the solution/air interface was more white, crusty and textured, and the crystals were more brittle.

6 - Pulsed field	Below	Similar observations to those recorded in Experiment 5.
7 - 50-100G DC electromagnetic field	At sides in parallel	Whiter, more brittle crystals formed that formed a powder very easily, indicative of a more crystalline, less amorphous form of lactose.
8 - 150-340G DC electromagnetic field	At sides in parallel	Observations were the same as those recorded for Experiment 7.
9 - 220-600G DC electromagnetic field	At sides in parallel	Observations were the same as those recorded for Experiment 7.

Table 3.3.1 Summary of visual observations recorded for each lactose crystals.

3.3.1(b) Scanning Electron Microscopy (SEM) observations

SEM carried out on all the lactose crystal samples revealed different crystal shapes depending on the ‘point of formation’ i.e. the solution/glass interface, solution/air interface and the crystals in solution. The electron micrographs of Samples 1(1) to 1(3) from the control samples are given for each point of formation followed by electron micrographs illustrating the deviations in morphology from the control samples as a result of growth under applied field conditions.

3.3.1(b)(i) Solution/glass interface

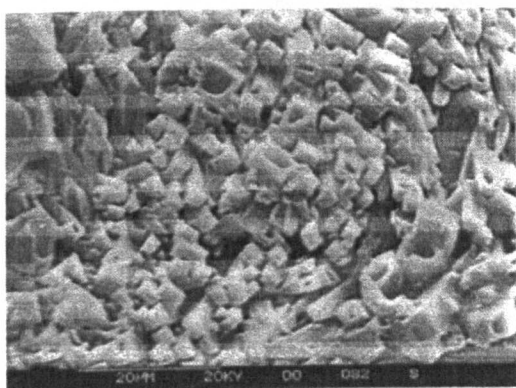


Fig. 3.3.1 Lactose control sample 1(1) at $\times 1580$ magnification. Square, chunky crystals are illustrated.

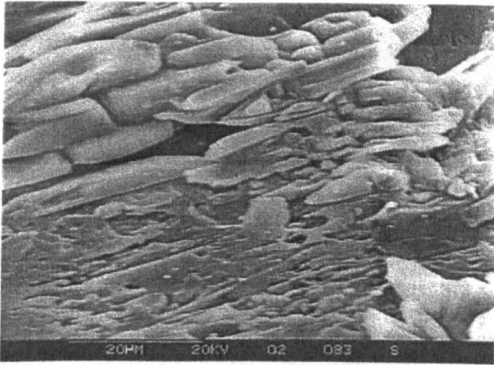


Fig. 3.3.2 Lactose control sample 1(2) at $\times 1520$ magnification. Flakey layers are illustrated with rounded edges and little angular form.

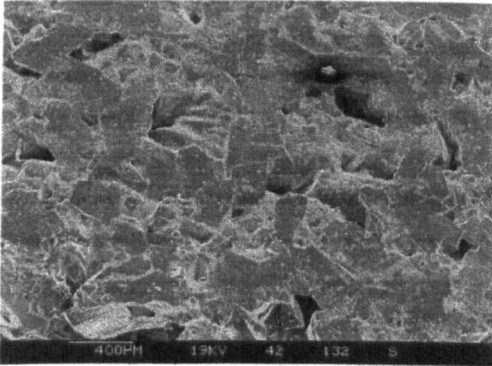


Fig. 3.3.3 Lactose control sample 1(3) at $\times 40$ magnification. Irregular chunks of lactose crystal are illustrated which are covered in semi-amorphous material that is illustrated at higher magnification in Figs. 3.3.1 and 3.3.2.

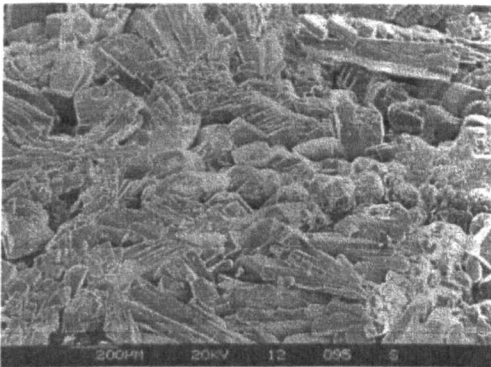


Fig. 3.3.4 Lactose sample 2(1), crystallised in $\sim 300\text{G}$ permanent field (field lines parallel to interface), at $\times 62$ magnification. Well formed, angular, elongated lactose crystals are illustrated. There is less amorphous material present.

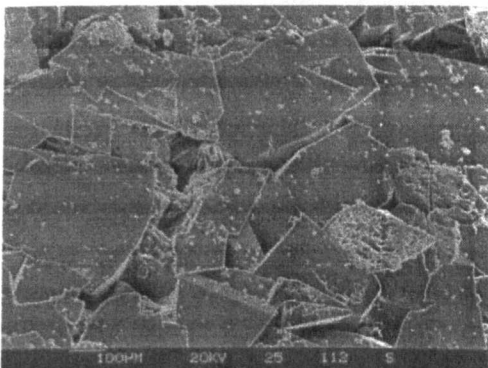


Fig. 3.3.5 Lactose sample 4(2), crystallised in $\sim 700\text{G}$ permanent field (field lines parallel to interface), at $\times 90$ magnification. Well formed, angular crystals with reduced amounts of amorphous material are illustrated.

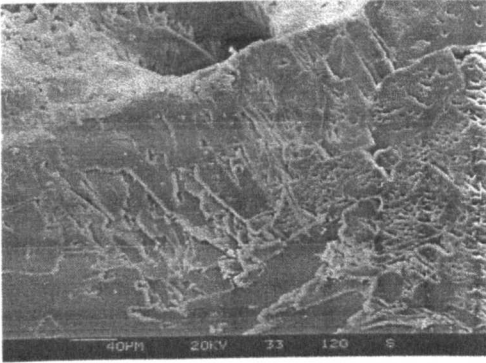


Fig. 3.3.6 Lactose sample 5(1), crystallised in $\sim 630\text{G}$ permanent field (field lines are perpendicular to interface), at $\times 300$ magnification. Layered growth illustrated.

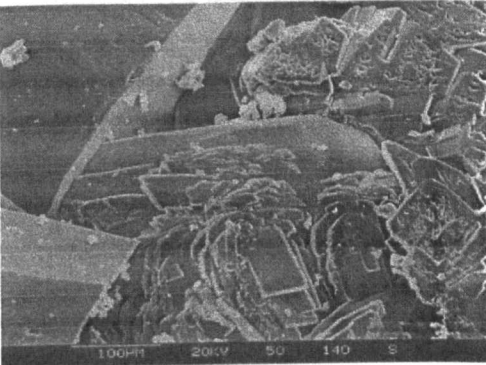


Fig. 3.3.7 Lactose sample 7(2), crystallised in $\sim 100\text{G}$ DC electromagnetic field (field lines parallel to interface), at $\times 210$ magnification. Discreet, well formed crystals mixed with some flakey, layered material are illustrated.

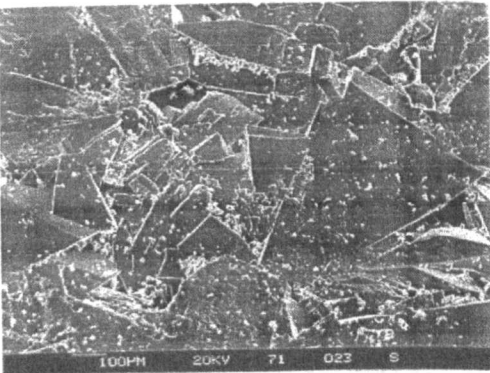


Fig. 3.3.8 Lactose sample 9(3), crystallised in ~ 200 to $\sim 600\text{G}$ DC electromagnetic field (field lines parallel to interface), at $\times 80$ magnification. Flat, plate-like crystals with angular edges and very little amorphous material are illustrated.

3.3.1(b)(ii) Solution/air interface

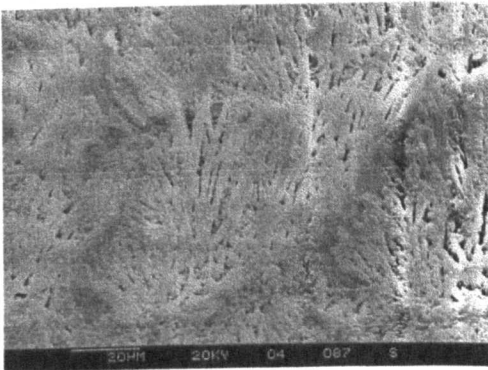


Fig. 3.3.9 Lactose control sample 1(2) at $\times 840$ magnification. An amorphous surface with semi-crystalline fibres are illustrated.

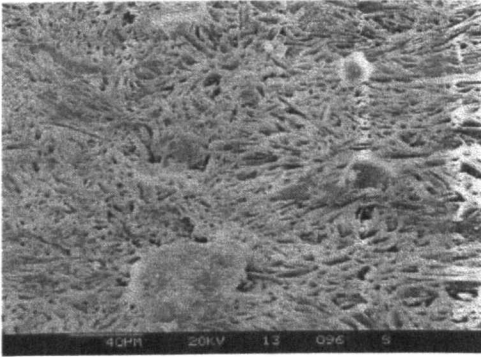


Fig. 3.3.10 Lactose sample 2(2), crystallised in $\sim 300\text{G}$ permanent field (field lines parallel to interface), at $\times 450$ magnification. A more fibrous, less amorphous surface, than the control, is illustrated.

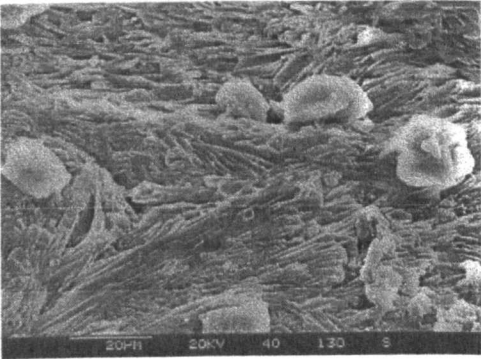


Fig. 3.3.11 Lactose sample 6(2), crystallised in a pulsed magnetic field (direction of pulse is perpendicular to interface), at $\times 1000$ magnification. Elongated fibrous material is illustrated.

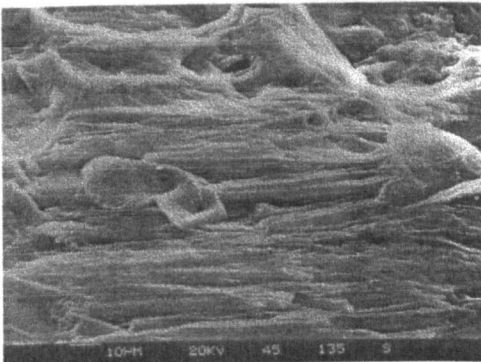


Fig. 3.3.12 Lactose sample 6(3), crystallised in a pulsed magnetic field (direction of pulse is perpendicular to interface), at $\times 800$ magnification. Elongated fibres predominate the structure, however all have in parallel i.e. direction of growth is not random as before.

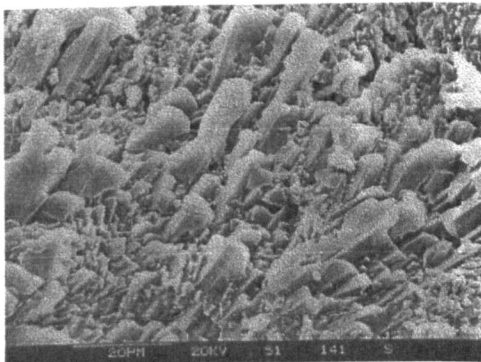


Fig. 3.3.13 Lactose sample 5(2), crystallised in a $\sim 630\text{G}$ permanent field (field lines perpendicular to interface), at $\times 1190$ magnification. Extended, crystalline nodules have grown from the lactose crystal surface. Growth is unidirectional.

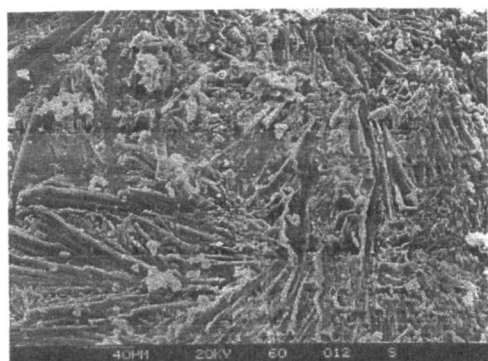


Fig. 3.3.14 Lactose sample 8(2), crystallised in ~ 150 to $\sim 340\text{G}$ DC electromagnetic field (field lines parallel to interface), at $\times 360$ magnification. Elongated fibres and long fan-like structures are illustrated.

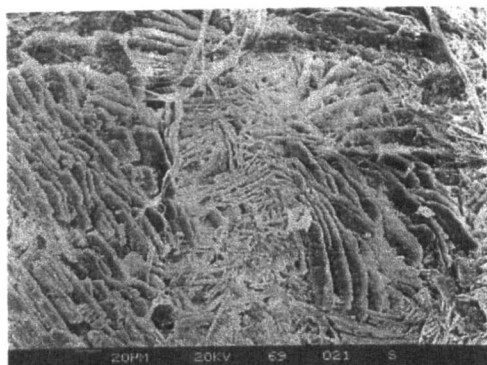


Fig. 3.3.15 Lactose sample 9(2), crystallised in ~ 200 to $\sim 600\text{G}$ DC electromagnetic field (field lines parallel to interface), at $\times 390$ magnification. Needle-like crystals and layered growth is illustrated.

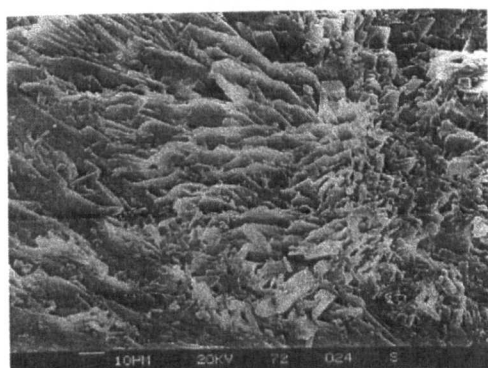


Fig. 3.3.16 Lactose sample 9(3), crystallised in ~ 200 to $\sim 600\text{G}$ DC electromagnetic field (field lines parallel to interface), at $\times 700$ magnification. Fibrous, layered material is illustrated.

3.3.1(b)(iii) Crystals in lactose solution

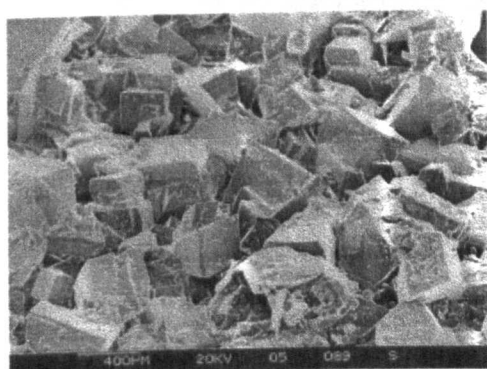


Fig. 3.3.17 Lactose control sample 1(1) at $\times 92$ magnification, illustrating the 'tomohawk' crystal form. Some amorphous material covers the flat, angled crystal surfaces.

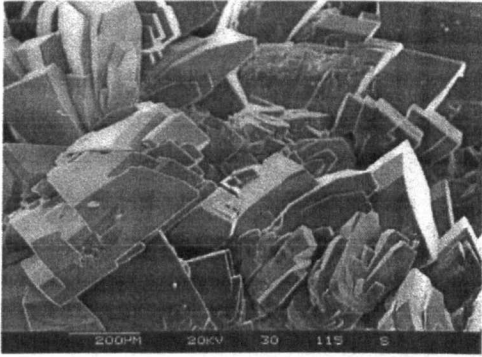


Fig. 3.3.18 Lactose sample 4(3), crystallised in $\sim 700\text{G}$ permanent field (field lines parallel to interface), at $\times 89$ magnification. Layered, regular and well defined angular growth predominate with virtually no amorphous material present.

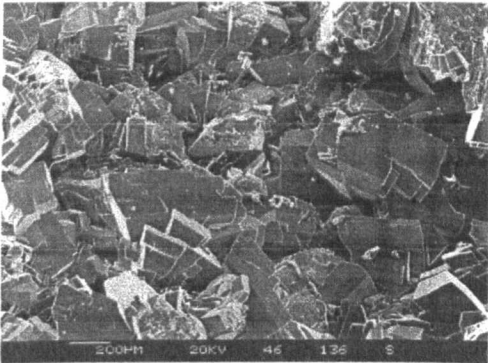


Fig. 3.3.19 Lactose sample 6(3), crystallised in a pulsed magnetic field (direction of pulse is perpendicular to interface), at $\times 54$ magnification. Well formed, flat surfaces and angular edges predominate. Some layered growth.

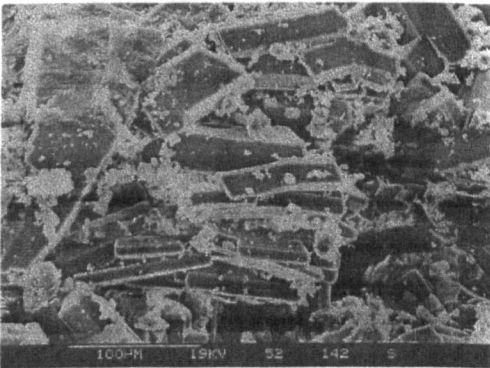


Fig. 3.3.20 Lactose sample 7(2), crystallised in ~ 150 to $\sim 340\text{G}$ DC electromagnetic field (field lines parallel to interface), at $\times 300$ magnification. Elongated rectangular crystals are illustrated.

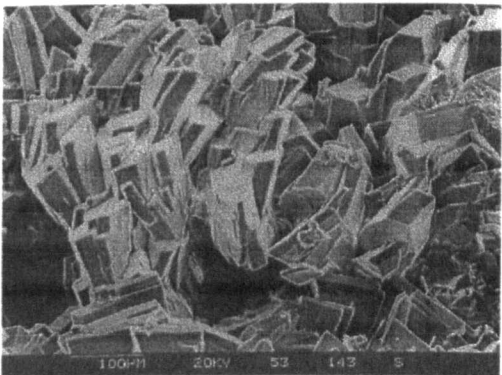


Fig. 3.3.21 Lactose sample 7(3), crystallised in ~ 150 to $\sim 340\text{G}$ DC electromagnetic field (field lines parallel to interface), at $\times 170$ magnification. Very layered crystal forms predominate.

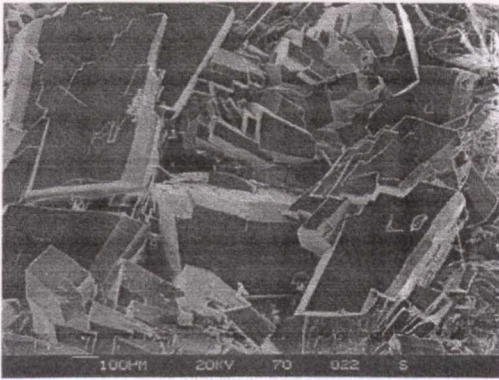


Fig. 3.3.22 Lactose sample 9(2), crystallised in ~200 to ~600G DC electromagnetic field (field lines parallel to interface), at $\times 70$ magnification. Very regular crystal shapes in layered growth are illustrated.

3.3.1(c) Differential Scanning Calorimetry (DSC) data

The DSC data obtained for each lactose sample are given below in Table 3.3.2. The temperatures given are all endothermic peaks. The original DSC's from which this data has been obtained, are given in Figures 3.3.23 to 3.3.49.

	Sample (1)	Sample (2)	Sample (3)
	MELTING TEMPERATURE °C		
Experiment 1	150.9	142.6, 152.0	139.7, 150.5
Experiment 2	141.3, 150.8	143.2, 152.9	143.3, 150.7
Experiment 3	142.0, 150.0	143.0, 151.7	145.0, 219.7
Experiment 4	143.0, 150.5	142.7, 151.5	144.5, 150.2
Experiment 5	148.2, 151.8	145.0, 150.6	141.2, 150.4
Experiment 6	144.9, 218.2	143.0, 150.0	143.4, 219.2
Experiment 7	143.0, 149.9	142.9, 216.5	143.4, 219.2
Experiment 8	148.5, 221.2	143.8, 150.8, 198.0	142.2, 149.7
Experiment 9	143.2, 148.6	141.2, 149.1	142.1, 217.7

Table 3.3.2 Summary of the DSC data obtained for the lactose crystals.

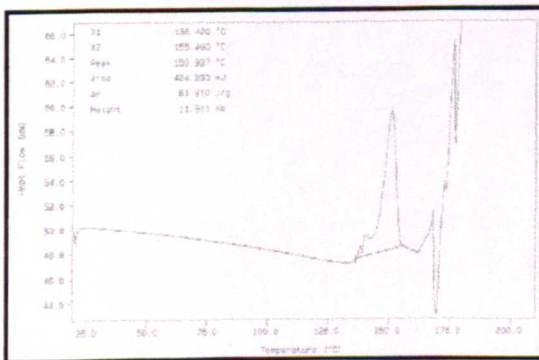


Fig. 3.3.23 DSC trace for lactose Sample 1(1).

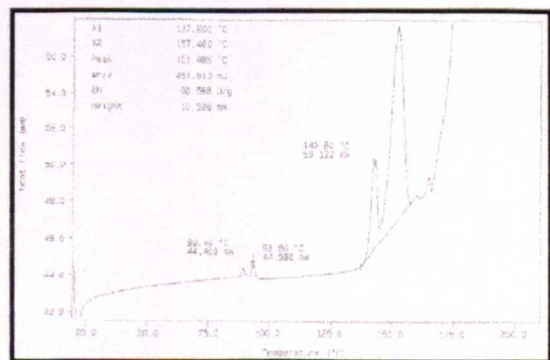


Fig. 3.3.24 DSC trace for lactose Sample 1(2).

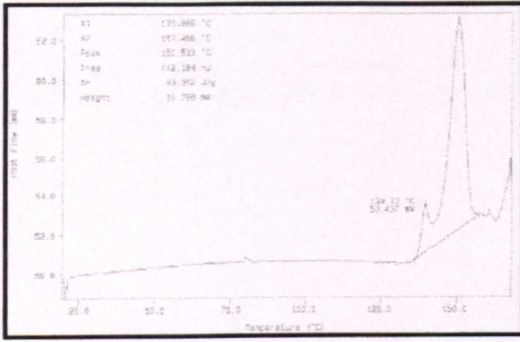


Fig. 3.3.25 DSC trace for lactose Sample 1(3).

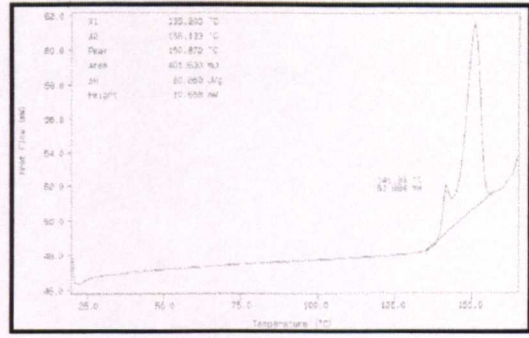


Fig. 3.3.26 DSC trace for lactose Sample 2(1).

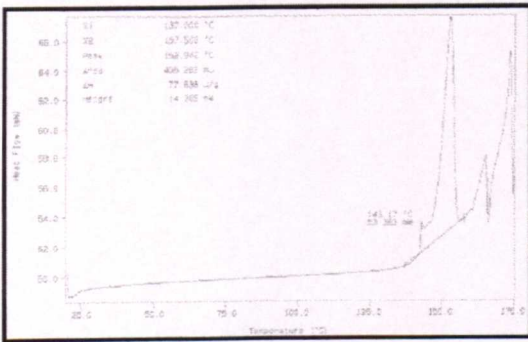


Fig. 3.3.27 DSC trace for lactose Sample 2(2).

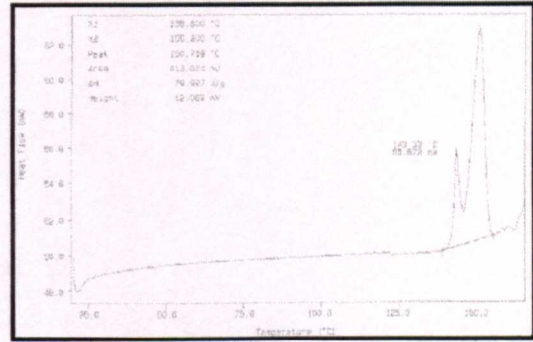


Fig. 3.3.28 DSC trace for lactose Sample 2(3).

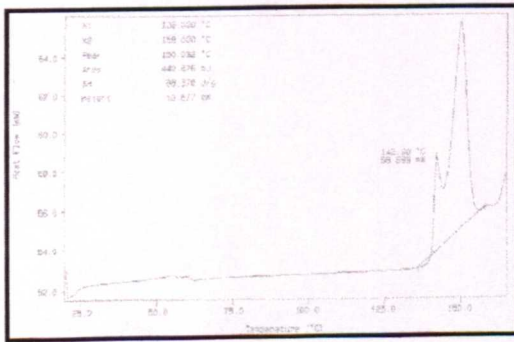


Fig. 3.3.29 DSC trace for lactose Sample 3(1).

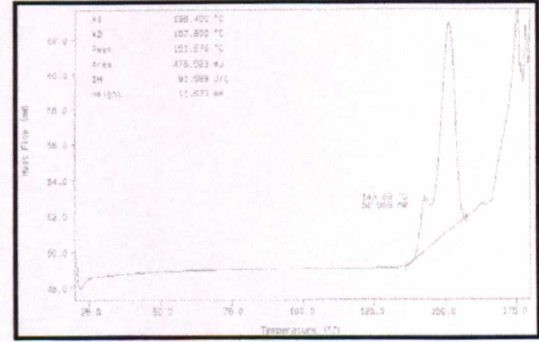


Fig. 3.3.30 DSC trace for lactose Sample 3(2).

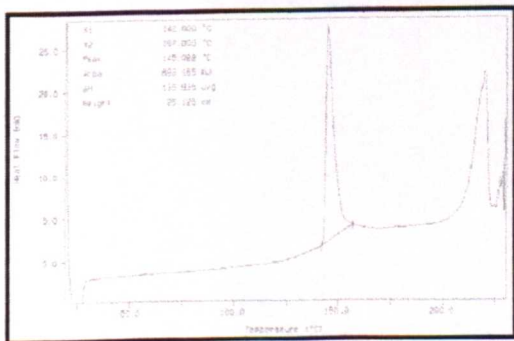


Fig. 3.3.31 DSC trace for lactose Sample 3(3).

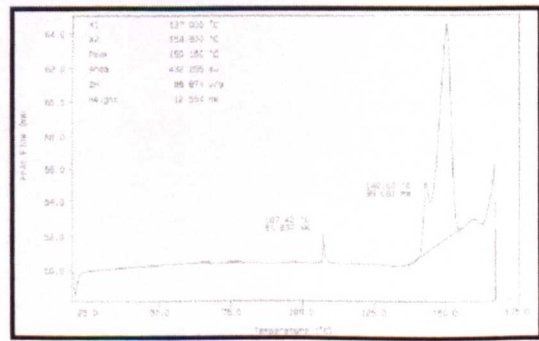


Fig. 3.3.32 DSC trace for lactose Sample 4(1).

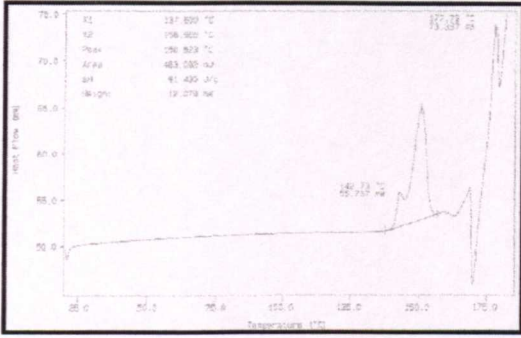


Fig. 3.3.33 DSC trace for lactose Sample 4(2).

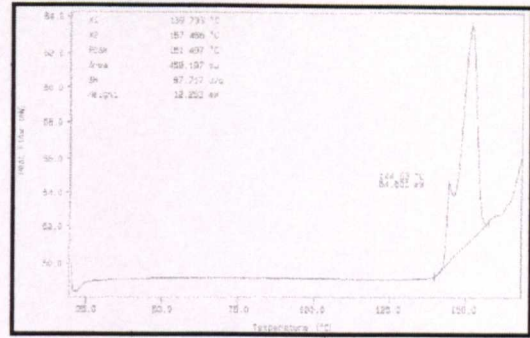


Fig. 3.3.34 DSC trace for lactose Sample 4(3).

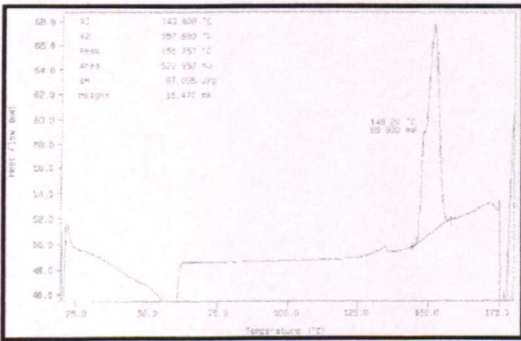


Fig. 3.3.35 DSC trace for lactose Sample 5(1).

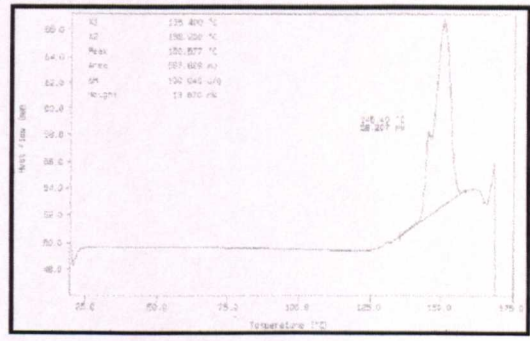


Fig. 3.3.36 DSC trace for lactose Sample 5(2).

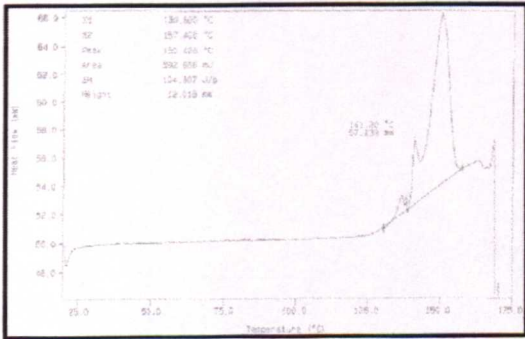


Fig. 3.3.37 DSC trace for lactose Sample 5(3).

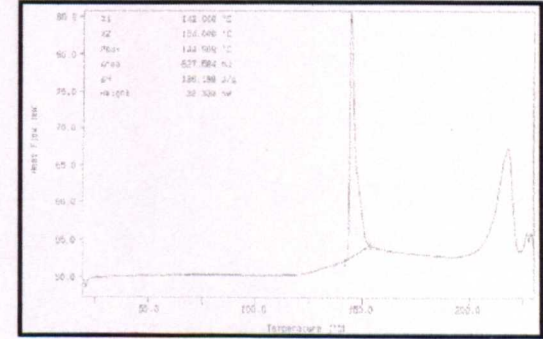


Fig. 3.3.38 DSC trace for lactose Sample 6(1).

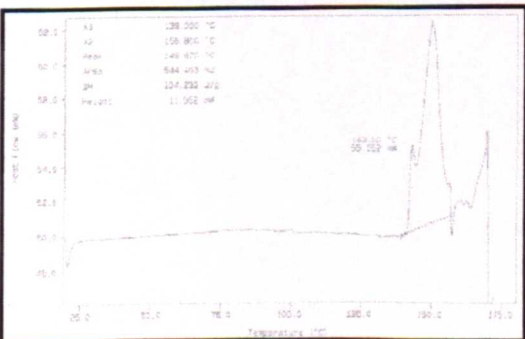


Fig. 3.3.39 DSC trace for lactose Sample 6(2).

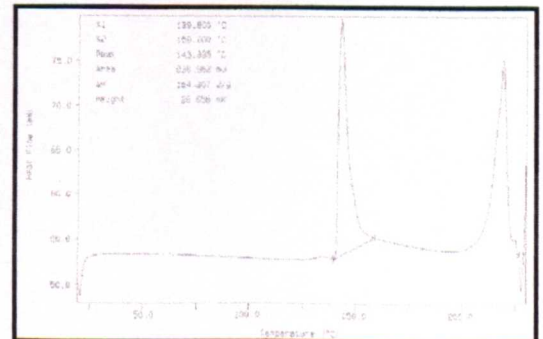


Fig. 3.3.40 DSC trace for lactose Sample 6(3).

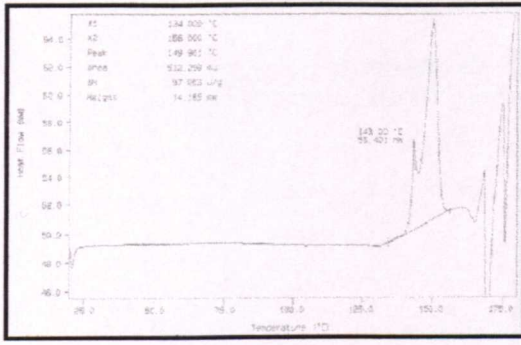


Fig. 3.3.41 DSC trace for lactose Sample 7(1).

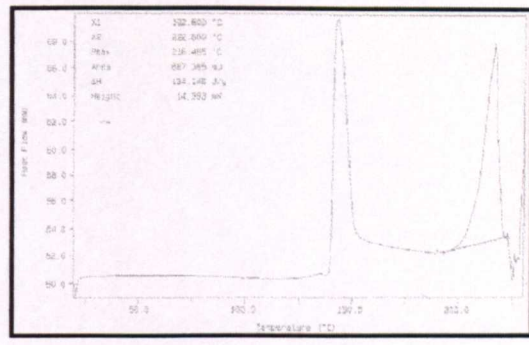


Fig. 3.3.42 DSC trace for lactose Sample 7(2).

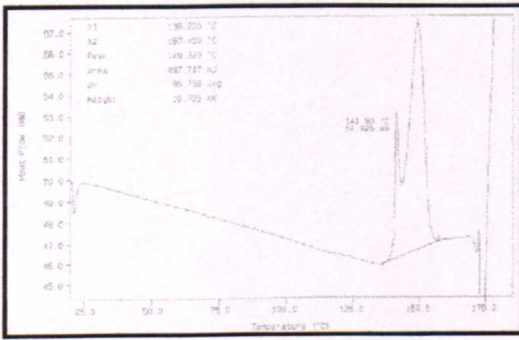


Fig. 3.3.43 DSC trace for lactose Sample 7(3).

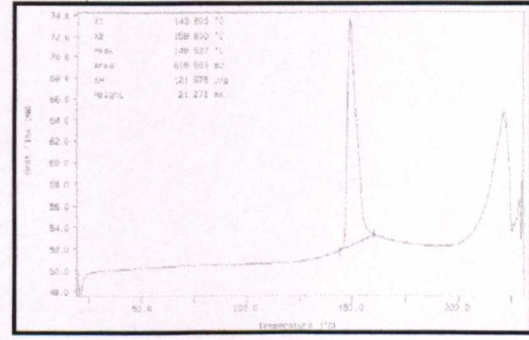


Fig. 3.3.44 DSC trace for lactose Sample 8(1).

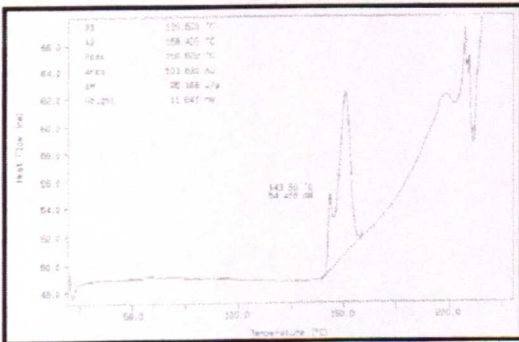


Fig. 3.3.45 DSC trace for lactose Sample 8(2).

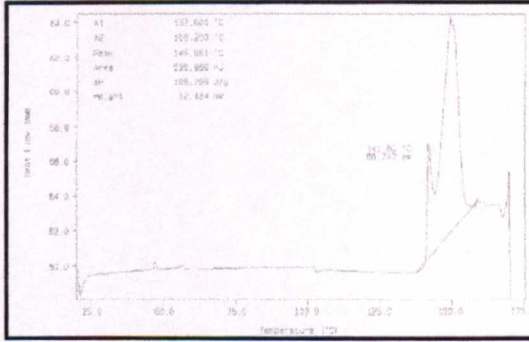


Fig. 3.3.46 DSC trace for lactose Sample 8(3).

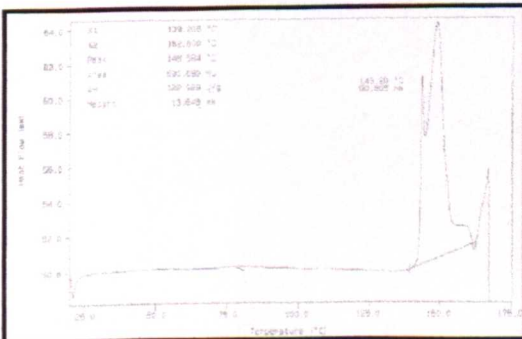


Fig. 3.3.47 DSC trace for lactose Sample 9(1).

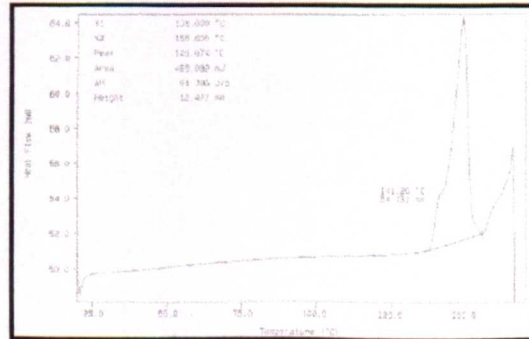


Fig. 3.3.48 DSC trace for lactose Sample 9(2).

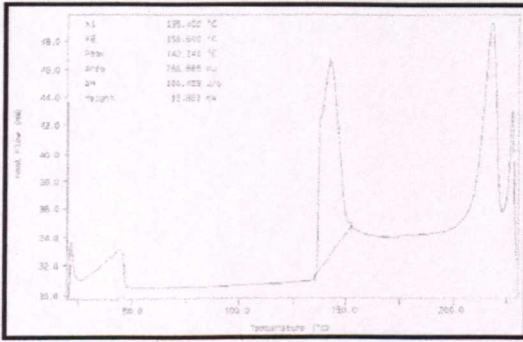


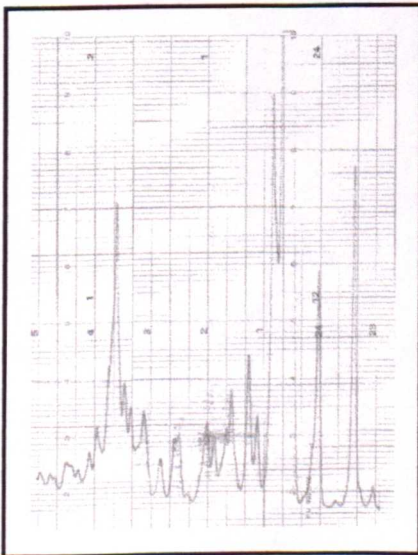
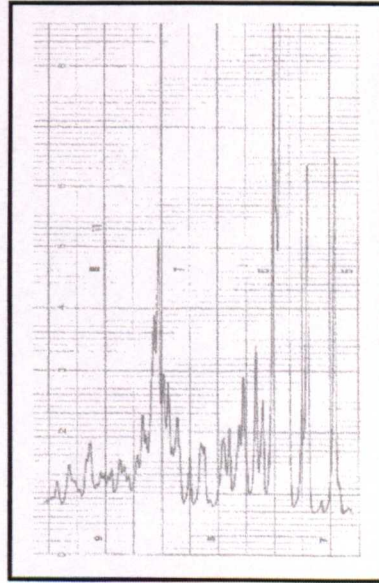
Fig. 3.3.49 DSC trace for lactose Sample 9(3).

3.3.1(d) Powder X-ray Diffraction data

The Powder XRD data recorded for bottled lactose are given in Table 3.3.3 and data for each sample, 1(1) through 9(3) are given in Tables 3.3.4 to 3.3.30 below, where $2\theta_c$ values are corrected values with reference to a silicon standard which is found at $28.44\ 2\theta$; d_i are standard referenced d-spacings; d_f are the measured d-spacings; $I/I_o(i)$ are normalised standard referenced intensities and $I/I_o(f)$ are normalised measured intensities. The data is displayed alongside the original Powder XRD traces

2θ	$2\theta_c$	d_i Å	$I/I_o(i)$
12.52	12.401	7.13	25
16.427	16.308	5.43	28
19.169	19.05	4.66	40
19.678	19.559	4.54	44
20.028	19.909	4.46	100
20.894	20.775	4.27	13
21.265	21.146	4.20	33
23.815	23.696	3.75	30

Table 3.3.3 Powder XRD data for bottled powdered α -lactose.

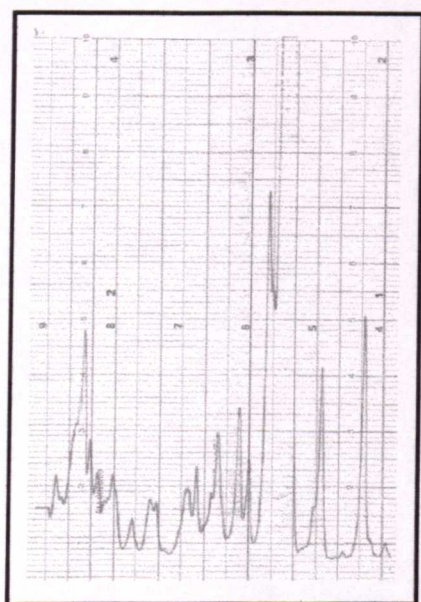
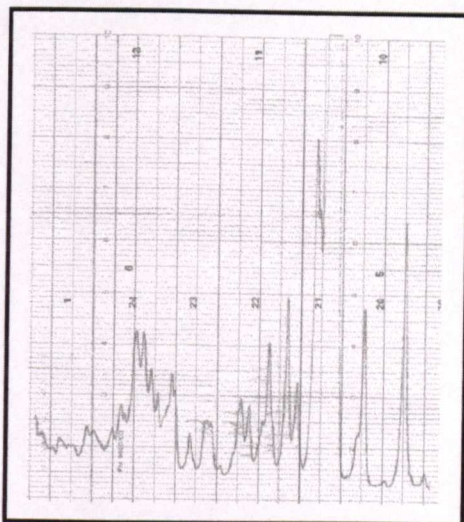


2θ	$2\theta_c$	d_i Å	$I/I_o(i)$
12.776	12.8	6.91	25
16.613	16.637	5.32	14
19.574	19.598	4.53	32
20.218	20.242	4.39	100
21.399	21.423	4.14	28
25.915	25.939	3.43	12

Table 3.3.4 Powder XRD data for Sample (1).

2θ	$2\theta_c$	$d_i \text{ \AA}$	$I/I_0(I)$
12.472	12.242	7.23	21
16.347	16.117	5.50	20
19.139	18.909	4.69	31
19.937	19.707	4.50	100
22.132	21.902	4.06	17
23.722	23.492	3.78	11
25.572	25.342	3.51	11

Table 3.3.5 Powder XRD data for Sample 1(2).

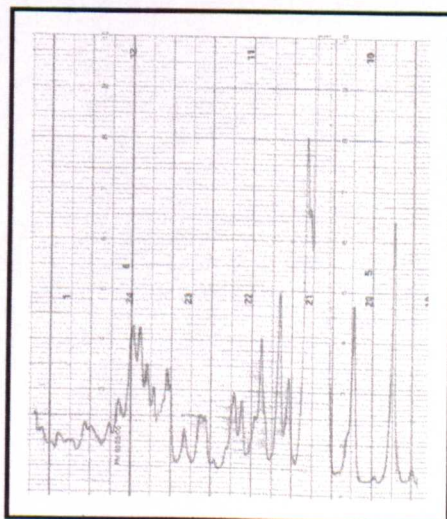


2θ	$2\theta_c$	$d_i \text{ \AA}$	$I/I_0(I)$
12.481	12.251	7.22	19
16.362	16.132	4.49	13
19.103	18.873	4.70	65
19.945	19.715	4.50	100
21.16	20.93	4.24	22
23.713	23.483	3.79	12
25.556	25.326	3.51	9

Table 3.3.6 Powder XRD data for Sample 1(3).

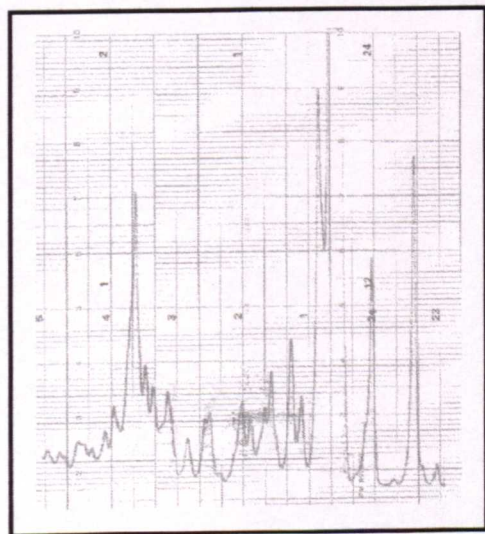
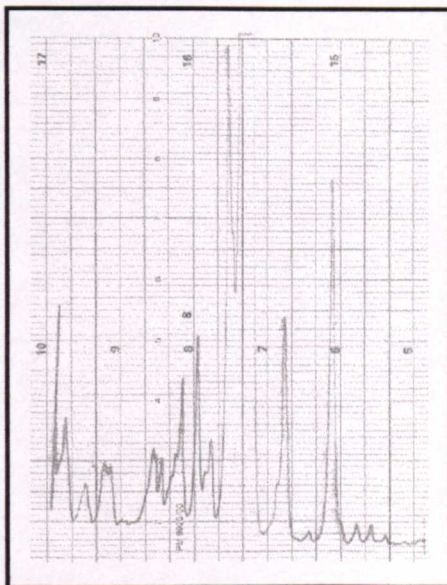
2θ	$2\theta_c$	$d_i \text{ \AA}$	$I/I_0(i)$
12.56	12.52	7.07	21
16.438	16.398	5.40	15
19.246	19.206	4.62	41
20.046	20.006	4.44	100
21.19	21.15	4.20	18
23.488	23.448	3.74	13
25.666	25.626	3.47	11

Table 3.3.7 Powder XRD data for Sample 2(1).



2θ	$2\theta_c$	$d, \text{\AA}$	$I/I_0(i)$
12.472	12.242	7.23	21
16.347	16.117	5.50	20
19.139	18.909	4.69	31
19.937	19.707	4.50	100
22.132	21.902	4.06	17
23.722	23.492	3.78	11
25.572	25.342	3.51	11

Table 3.3.8 Powder XRD data for Sample 2(2).

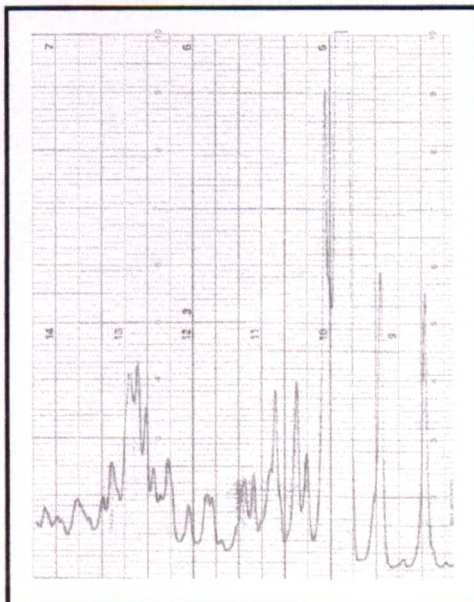


2θ	$2\theta_c$	$d, \text{\AA}$	$I/I_0(i)$
12.588	12.548	7.05	29
16.474	16.434	5.39	18
19.349	19.309	4.59	65
19.740	19.700	4.50	100
21.295	21.255	4.18	27
23.85	23.81	3.74	12
25.691	25.651	3.47	10

Table 3.3.9 Powder XRD data for Sample 2(3).

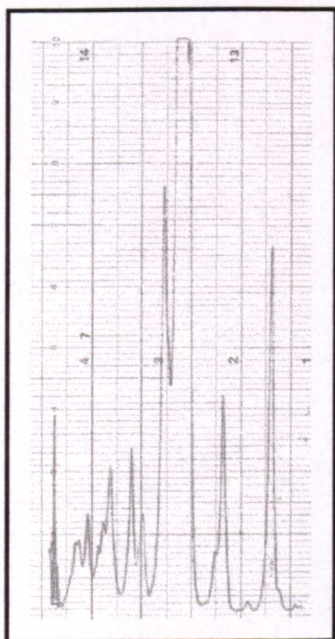
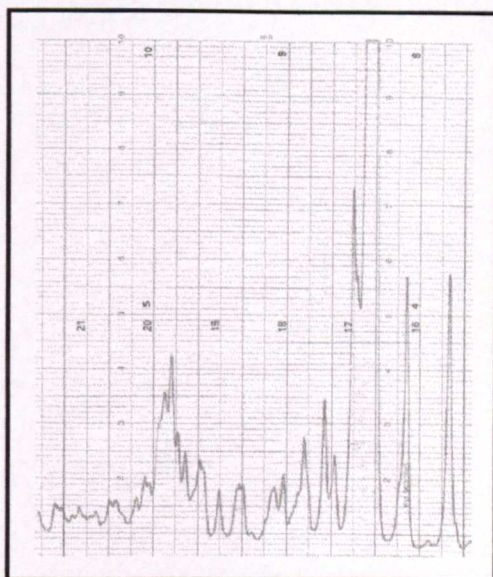
2θ	$2\theta_c$	$d, \text{\AA}$	$I/I_0(i)$
12.493	12.359	7.13	17
16.425	16.291	5.43	15
19.267	19.133	4.64	31
20.031	19.897	4.46	100
21.196	21.062	4.20	19
23.803	23.669	3.76	11

Table 3.3.10 Powder XRD data for Sample 3(1).



2θ	$2\theta_c$	d_i Å	$I/I_0(i)$
12.546	12.412	7.13	22
16.443	16.309	5.43	19
19.228	19.094	4.65	46
20.034	19.9	4.46	100
21.267	21.133	4.20	35
23.809	23.675	3.76	10

Table 3.3.11 Powder XRD data for Sample 3(2).

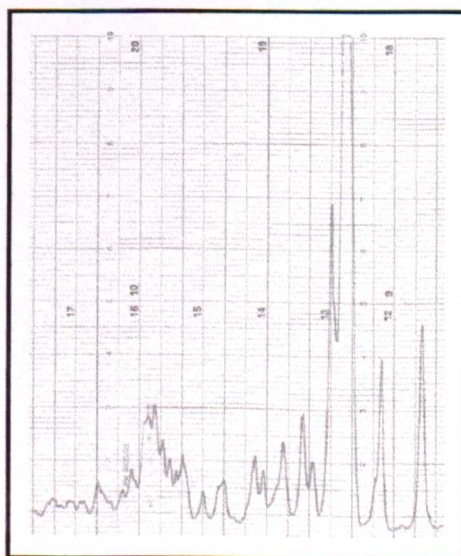


2θ	$2\theta_c$	d_i Å	$I/I_0(i)$
12.493	12.359	7.13	17
16.425	16.291	5.43	15
19.267	19.133	4.64	31
20.031	19.897	4.46	100
21.196	21.062	4.20	19
23.803	23.669	3.76	11

Table 3.3.12 Powder XRD data for Sample 3(3).

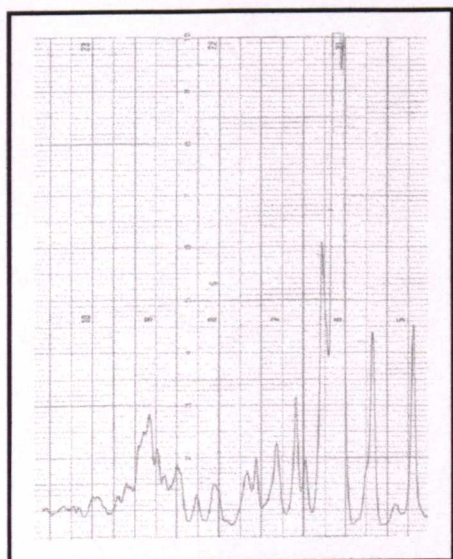
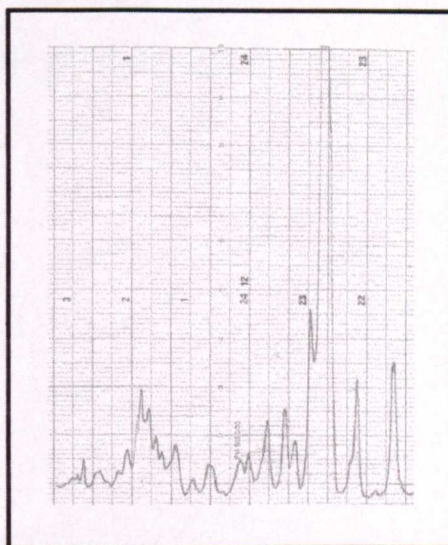
2θ	$2\theta_c$	d_i Å	$I/I_0(i)$
12.444	12.31	7.19	25
16.328	16.194	5.47	21
19.349	19.215	4.62	36
19.811	19.677	4.51	100
21.147	21.013	4.23	38
23.726	23.592	3.77	13

Table 3.3.13 Powder XRD data for Sample 4(1).



2θ	$2\theta_c$	$d_i \text{ \AA}$	$I/I_0(i)$
12.371	12.237	7.23	39
16.204	16.07	5.51	38
19.139	19.005	4.69	31
19.077	18.943	4.68	100
20.97	20.836	4.26	48
22.595	22.461	3.96	21
23.563	23.429	3.79	28
27.303	27.169	3.28	15

Table 3.3.14 Powder XRD data for Sample 4(2).

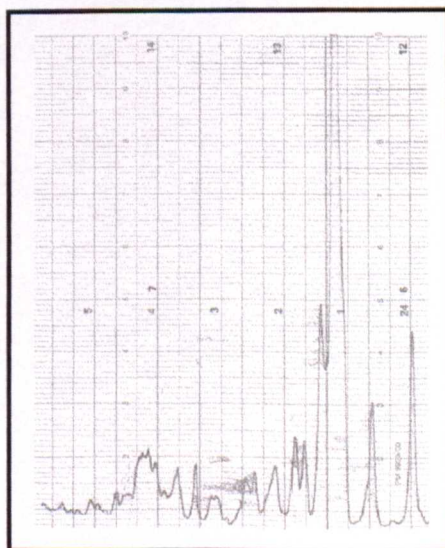


2θ	$2\theta_c$	$d_i \text{ \AA}$	$I/I_0(i)$
12.446	12.312	7.19	22
16.327	16.193	5.47	13
19.165	19.031	4.66	32
19.928	19.794	4.48	100
21.057	20.923	4.24	25

Table 3.3.15 Powder XRD data for Sample 4(3).

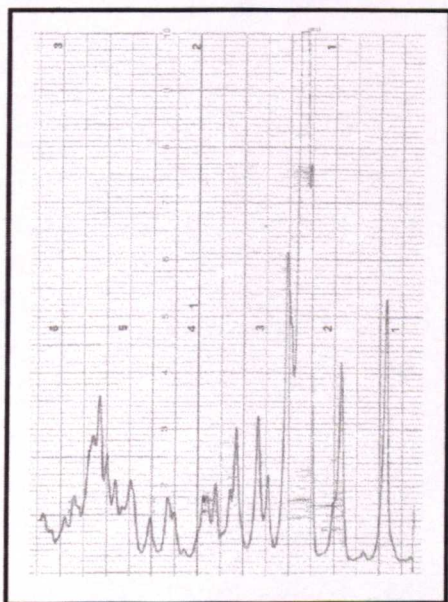
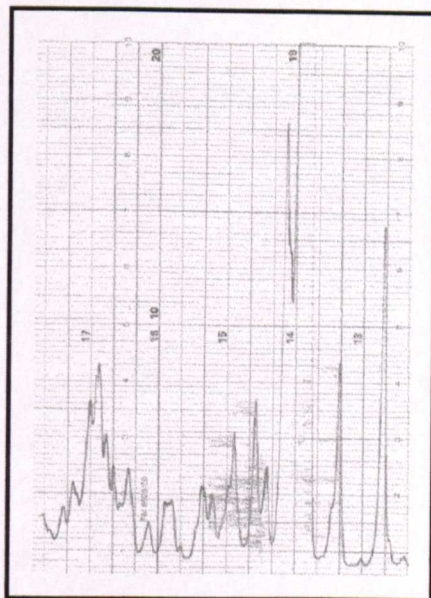
2θ	$2\theta_c$	$d_i \text{ \AA}$	$I/I_0(i)$
12.286	12.144	7.28	24
16.163	16.021	5.53	16
18.955	18.813	4.71	25
19.686	19.544	4.54	100
21.005	20.863	4.26	25
23.507	23.365	3.81	10

Table 3.3.16 Powder XRD data for Sample 5(1).



2θ	$2\theta_c$	$d, \text{\AA}$	$I/I_0(I)$
12.61	12.468	7.10	24
16.536	16.394	5.40	18
19.373	19.231	4.61	55
20.08	19.938	4.45	100
21.298	21.156	4.20	29
23.864	23.722	3.75	11
25.709	25.567	3.48	10

Table 3.3.17 Powder XRD data for Sample 5(2).

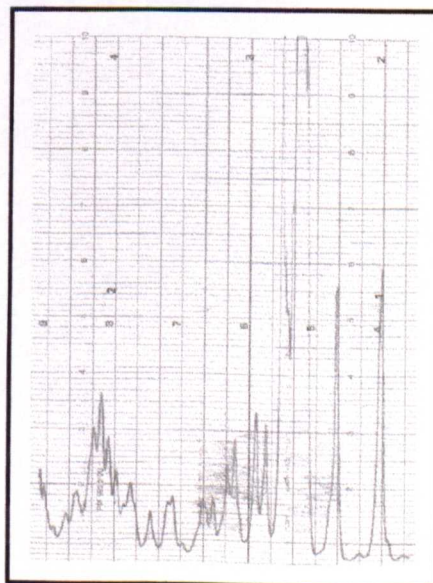


2θ	$2\theta_c$	$d, \text{\AA}$	$I/I_0(i)$
12.409	12.267	7.21	35
16.313	16.171	5.48	27
19.114	18.972	4.68	36
19.808	19.666	4.51	100
21.037	20.895	4.25	30
22.704	22.562	3.94	12
23.68	23.538	3.78	20
25.542	25.4	3.50	18

Table 3.3.18 Powder XRD data for Sample 5(3).

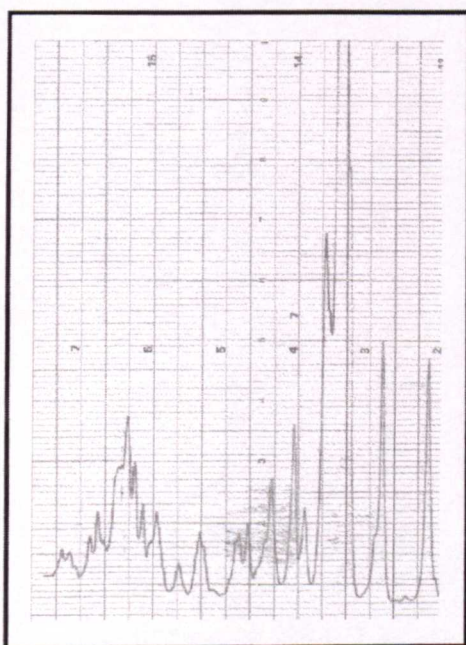
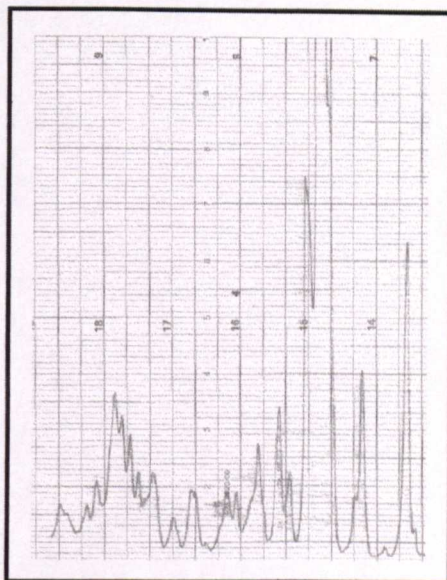
2θ	$2\theta_c$	$d, \text{\AA}$	$I/I_0(i)$
12.481	12.339	7.17	28
16.342	16.2	5.47	24
19.158	19.016	4.66	35
19.905	19.016	4.49	100
21.223	21.081	4.21	43
23.695	23.553	3.78	15
25.563	25.421	3.50	11
22.826	22.684	3.29	11

Table 3.3.19 Powder XRD data for Sample 6(1).



2θ	$2\theta_c$	$d_i \text{ \AA}$	$I/I_0(i)$
12.547	12.405	7.13	28
16.424	16.282	5.44	17
19.167	19.025	4.66	32
20.018	19.876	4.46	100
21.103	20.961	4.24	22
23.774	23.632	3.76	12

Table 3.3.20 Powder XRD data for Sample 6(2).

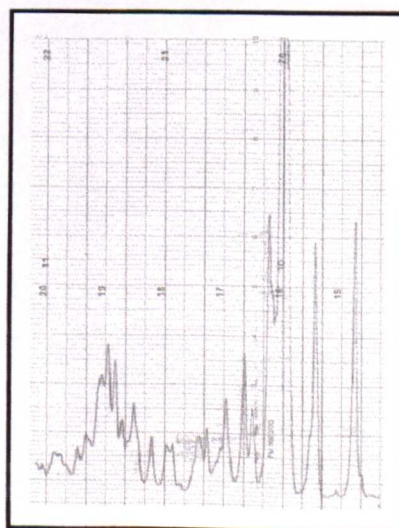


2θ	$2\theta_c$	$d_i \text{ \AA}$	$I/I_0(i)$
12.448	12.306	7.19	16
16.333	16.191	5.47	17
19.157	19.015	4.66	27
19.944	19.802	4.48	100
21.129	20.987	4.23	19
23.709	23.567	3.77	10

Table 3.3.21 Powder XRD data for Sample 6(3).

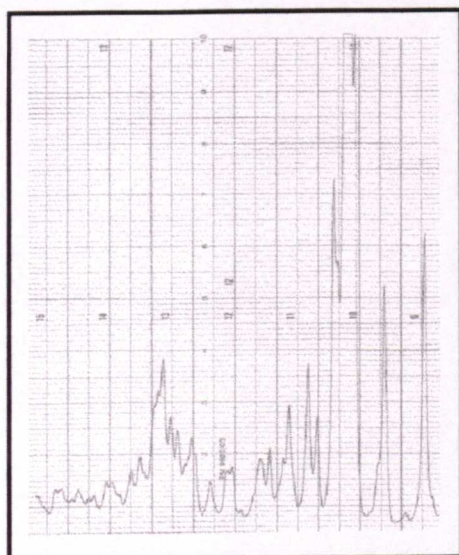
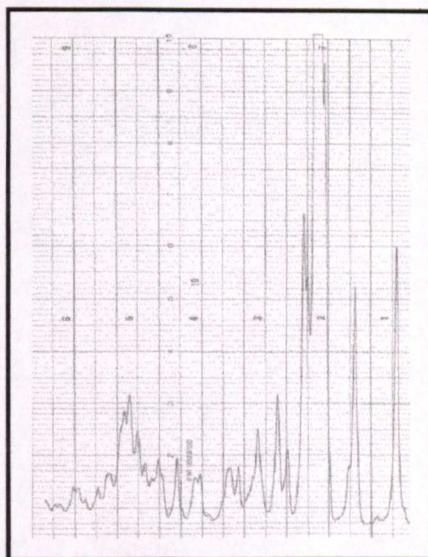
2θ	$2\theta_c$	$d_i \text{ \AA}$	$I/I_0(i)$
12.472	12.33	7.17	33
16.418	16.276	5.44	33
19.174	19.032	4.66	45
19.934	19.792	4.48	100
21.164	21.022	4.22	28
23.775	23.633	3.76	17
25.572	25.43	3.50	11
22.811	22.669	3.29	12

Table 3.3.22 Powder XRD data for Sample 7(1).



2θ	$2\theta_c$	d_i Å	$I/I_0(i)$
12.465	12.323	7.18	25
16.342	16.2	5.47	17
19.157	19.015	4.66	34
19.958	19.816	4.48	100
21.155	21.013	4.23	28
23.719	23.577	3.77	15
25.553	25.411	3.50	11

Table 3.3.23 Powder XRD data for Sample 7(2).

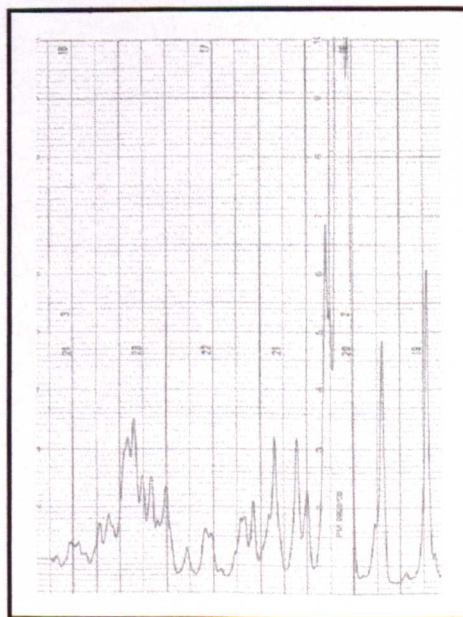


2θ	$2\theta_c$	d_i Å	$I/I_0(i)$
12.552	12.466	7.10	26
16.43	16.344	5.42	25
19.197	19.111	4.64	44
19.626	19.54	4.54	51
20.068	19.982	4.44	100
20.938	20.852	4.26	20
21.165	21.079	4.19	26
23.795	23.709	3.75	13
25.633	25.547	3.48	11

Table 3.3.24 Powder XRD data for Sample 7(3).

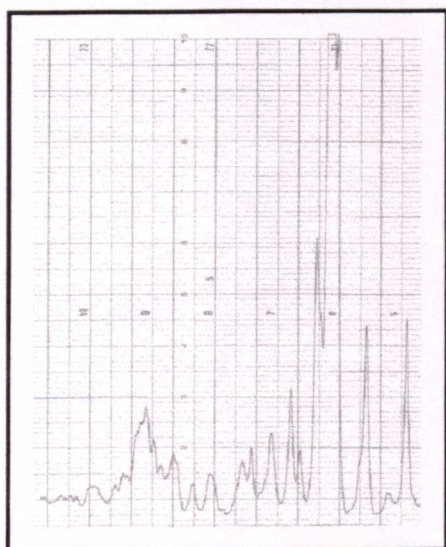
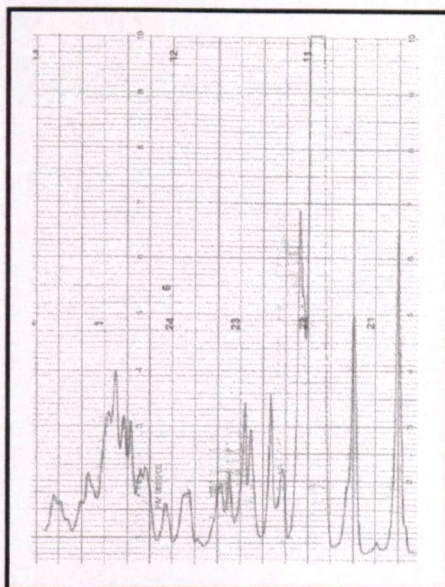
2θ	$2\theta_c$	d_i Å	$I/I_0(i)$
12.515	12.429	7.12	27
16.381	16.295	5.44	22
19.127	19.041	4.66	40
19.573	19.487	4.55	51
19.952	19.866	4.47	100
20.854	20.768	4.27	17
23.725	23.639	3.76	22
25.609	25.523	3.49	11

Table 3.3.25 Powder XRD data for Sample 8(1).



2θ	$2\theta_c$	$d_i, \text{\AA}$	$I/I_0(i)$
12.503	12.361	7.16	17
16.409	16.267	5.44	19
19.238	19.096	4.65	41
20.019	19.877	4.46	100
21.16	21.018	4.22	20
23.772	23.63	3.76	12

Table 3.3.26 Powder XRD data for Sample 8(2).

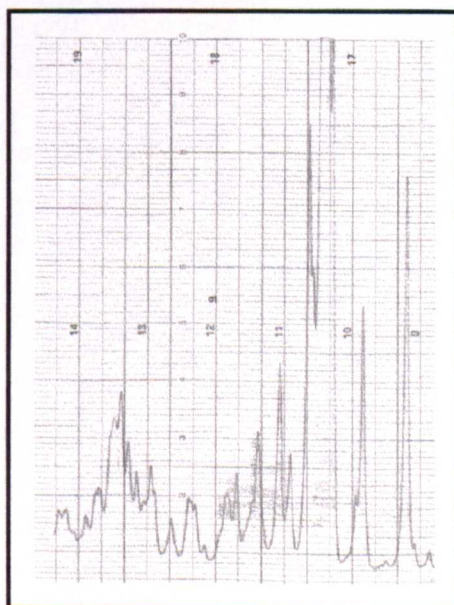


2θ	$2\theta_c$	$d_i, \text{\AA}$	$I/I_0(i)$
12.429	12.343	7.17	35
16.332	16.246	5.46	33
19.098	19.012	4.67	91
19.505	19.419	4.57	72
19.835	19.749	4.49	100
20.817	20.731	4.28	25
21.157	21.071	4.21	37
22.728	22.642	3.93	10
23.648	23.562	3.77	21
25.499	25.413	3.50	12
27.417	27.331	3.26	13

Table 3.3.27 Powder XRD data for Sample 8(3).

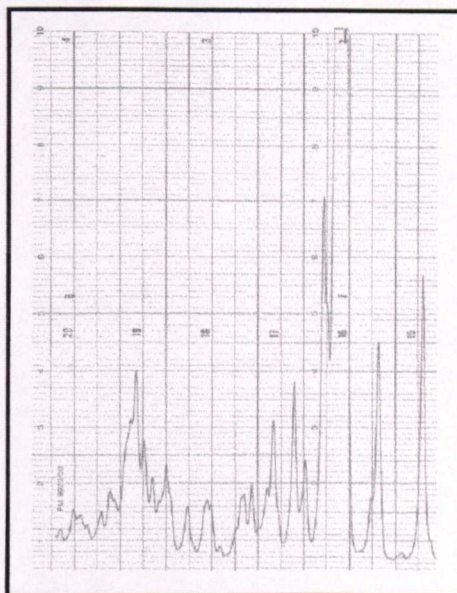
2θ	$2\theta_c$	$d_i, \text{\AA}$	$I/I_0(i)$
12.57	12.428	7.12	30
16.451	16.309	5.43	21
19.243	19.101	4.64	39
20.036	19.894	4.46	100
21.279	21.137	4.20	31
22.92	22.778	3.90	10
23.83	23.688	3.75	16
25.67	25.528	3.49	10

Table 3.3.28 Powder XRD data for Sample 9(1).



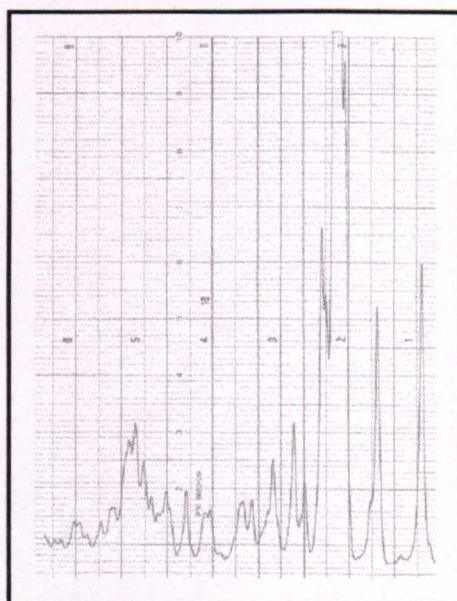
2θ	$2\theta_c$	$d, \text{\AA}$	$I/I_0(i)$
12.469	12.383	7.14	28
16.365	16.279	5.44	20
19.137	19.051	4.66	57
19.586	19.5	4.55	68
19.97	19.884	4.46	100
20.851	20.765	4.28	19
21.208	21.122	4.20	30
23.724	23.638	3.76	17
25.576	25.49	3.49	13

Table 3.3.29 Powder XRD data for Sample 9(2).



2θ	$2\theta_c$	$d, \text{\AA}$	$I/I_0(i)$
12.409	12.323	7.18	30
16.311	16.225	5.46	23
19.079	18.993	4.67	39
19.504	19.418	4.57	51
19.91	19.824	4.48	100
20.819	20.733	4.28	18
21.134	21.048	4.22	27
23.662	23.576	3.77	13

Table 3.3.30 Powder XRD data for Sample 9(3).



3.3.1(e) Karl Fischer titration data

The results from the Karl Fischer titrations are given below in Table 3.3.31. For each lactose sample, three titrations were carried out. The wt/wt (%) figure indicates the % water within the lactose sample; mass (g) indicates the total weight of the sample used in the titration; wt/wt mean (%) is the mean of the three titrations; wt/wt standard deviation (%) is the standard deviation of the mean and is usually expressed as a \pm figure following the mean value; and the coefficient of variation (%) is the standard deviation expressed as a percentage of the mean.

Lactose Sample	wt/wt (%)	mass (g)	wt/wt mean (%)	wt/wt standard deviation (%)	coefficient variation (%)
1(1)	5.351 5.302 5.379	0.4234 0.4252 0.3629	5.344	0.032	0.59
1(2)	5.552 5.372 5.345	0.2623 0.3164 0.2752	5.423	0.092	1.69
1(3)	5.544 5.393 5.315	0.2623 0.2369 0.2752	5.417	0.095	1.75
2(1)	5.673 5.212 5.301	0.2494 0.3211 0.2735	5.395	0.2	3.7
2(2)	5.537 5.295 5.543	0.2851 0.3323 0.2333	5.458	0.115	2.11
2(3)	5.406 5.400 5.335	0.3649 0.2503 0.3353	5.38	0.391	7.27
3(1)	5.416 5.525 5.664	0.4115 0.2358 0.2223	5.535	0.124	2.24
3(2)	5.749 5.810 5.673	0.1833 0.2234 0.2431	5.744	0.069	1.20
3(3)	5.498 5.739 5.558	0.328 0.2256 0.2385	5.598	0.125	2.23
4(1)	5.426 5.500 5.567	0.3005 0.286 0.2352	5.498	0.071	1.29
4(2)	5.394 5.615 5.816	0.2588 0.2792 0.2694	5.608	0.172	3.07
4(3)	5.463 5.603 5.407	0.2356 0.2808 0.274	5.491	0.083	1.51
5(1)	5.751 5.634 6.061	0.2839 0.3288 0.2895	5.816	0.18	3.1

5(3)	5.738 5.887 5.665	0.2399 0.203 0.2789	5.763	0.093	1.61
6(1)	5.659 5.909 5.533	0.249 0.1867 0.3226	5.7	0.156	2.74
6(2)	5.631 5.604 5.556	0.2777 0.2449 0.3129	5.597	0.031	0.55
6(3)	5.619 5.693 5.503	0.2564 0.2715 0.2596	5.605	0.078	1.4
7(1)	6.063 5.761 5.686	0.2399 0.2672 0.2295	5.837	0.163	2.8
7(2)	5.813 5.814 5.781	0.2512 0.2853 0.2609	5.803	0.015	0.27
7(3)	5.751 5.782 5.86	0.2508 0.3021 0.2535	5.798	0.046	0.79
8(1)	6.407 5.965 5.782	0.2424 0.2684 0.2351	6.051	0.262	4.33
8(2)	5.94 5.682 5.602	0.2423 0.3429 0.3404	5.741	0.144	2.51
8(3)	5.713 5.784 5.937	0.3009 0.3045 0.2128	5.811	0.094	1.61
9(1)	5.949 6.061 5.824	0.2608 0.1961 0.2066	5.945	0.097	1.63
9(2)	5.855 5.847 5.612	0.2126 0.2375 0.2611	5.771	0.113	1.96
9(3)	6.653 6.394 6.633	0.2167 0.1849 0.156	6.56	0.118	1.8

Table 3.3.31 Results of the Karl Fischer titrations carried out on lactose samples crystallised within applied magnetic fields.

3.3.1(f) Related thermal analytical data

DSC data for pure lactose samples are given in Figs. 3.3.50 and 3.3.51 (detail) illustrating the different DSC traces obtained for α -lactose monohydrate, β -lactose anhydrous and amorphous lactose.

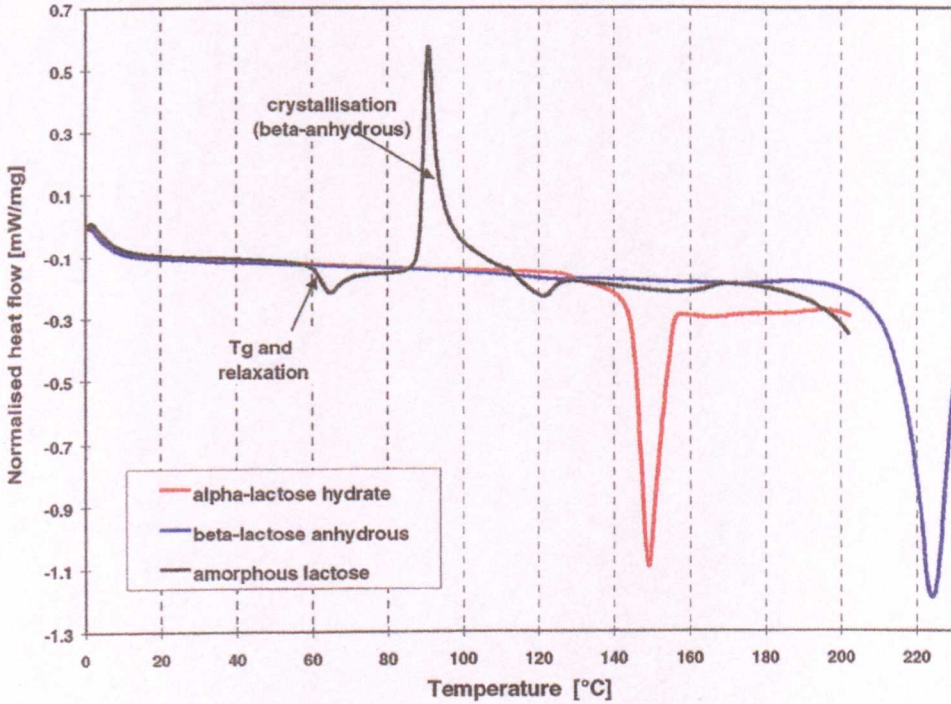


Fig. 3.3.50 DSC data for pure lactose.

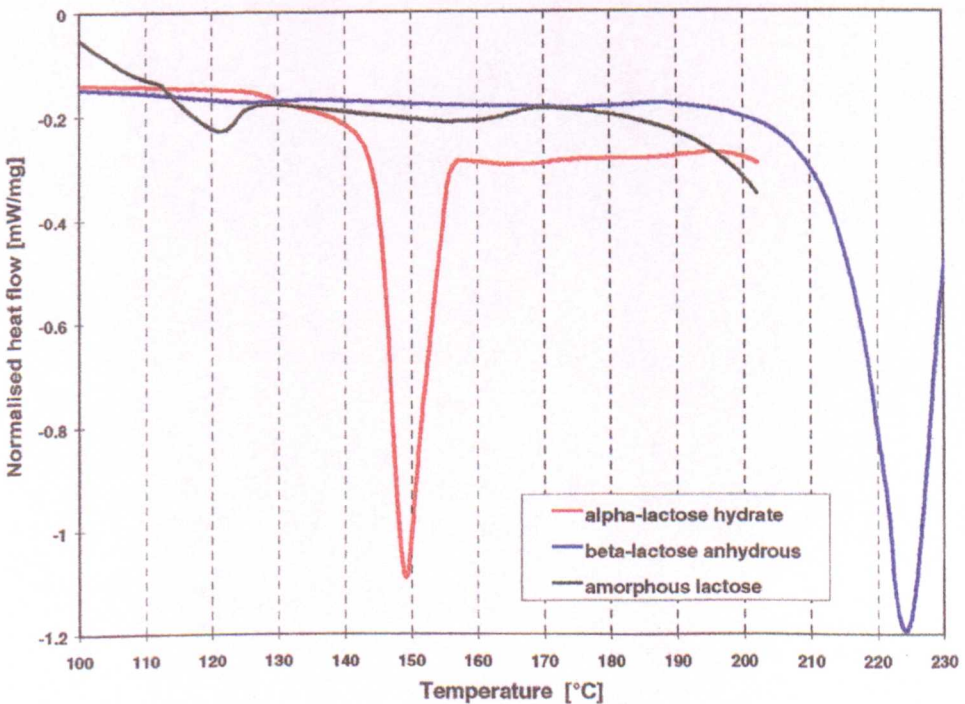


Fig. 3.3.51 DSC data for pure lactose (detail).

The DSC results obtained on the lactose samples from both the Perkin Elmer and Seiko machines are given below in Table 3.3.32 where T_{on} ($^{\circ}\text{C}$) is the onset of crystallisation water release (typical for α -lactose), T_p ($^{\circ}\text{C}$) is the peak of crystallisation water release and ΔH (Jg^{-1}) is the enthalpy of crystallisation water release. The DSC traces are illustrated below in Figure 3.3.52.

Sample	Perkin Elmer DSC ($10^{\circ}\text{Cmin}^{-1}$)			Seiko DSC ($5^{\circ}\text{Cmin}^{-1}$)		
	T_{on} ($^{\circ}\text{C}$)	T_p ($^{\circ}\text{C}$)	ΔH (Jg^{-1})	T_{on} ($^{\circ}\text{C}$)	T_p ($^{\circ}\text{C}$)	ΔH (Jg^{-1})
1	140	152	88	134	150	96
2	135	142	151	135	150	109
3	126	151	97	138	149	68
4	128	145	84	138	149	78

Table 3.3.32 DSC results.

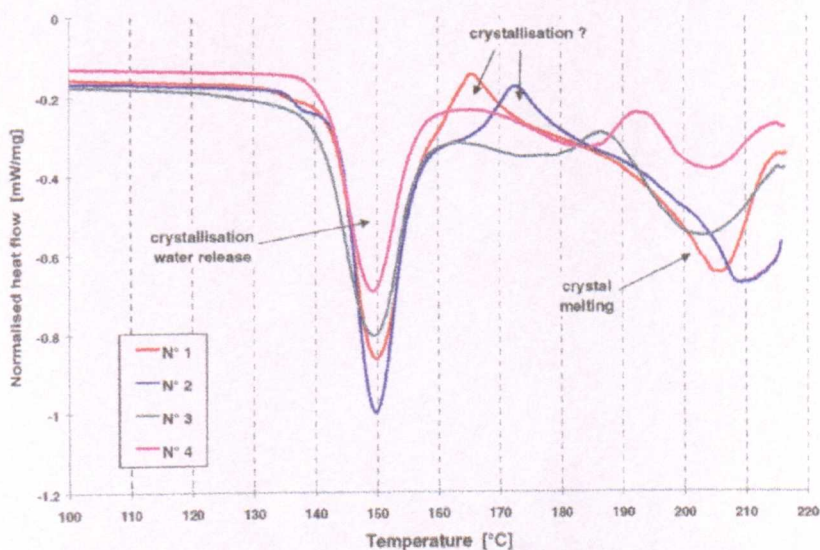


Fig. 3.3.52 Illustration of the DSC results.

TG/DTA data for pure lactose samples are given in Fig. 3.3.53 below and illustrates the differences between α -lactose monohydrate and β -lactose anhydrous.

The TG/DTA results for all four samples are summarised in Table 3.3.33 below and illustrated in Fig. 3.3.54 where T_{on} ($^{\circ}\text{C}$) is the onset of crystallisation (typical for α -lactose); T_{end} ($^{\circ}\text{C}$) is the endset of crystallisation water release; loss 1(%) is the loss of weight (crystallisation of water) between T_{on} and T_{end} ; $T_{m on}$ ($^{\circ}\text{C}$) is the onset of crystal melting; loss 2 (%) is the loss of weight (crystallisation water) between T_{on} and T_m , and T_{mp} ($^{\circ}\text{C}$) is the peak of crystal melting.

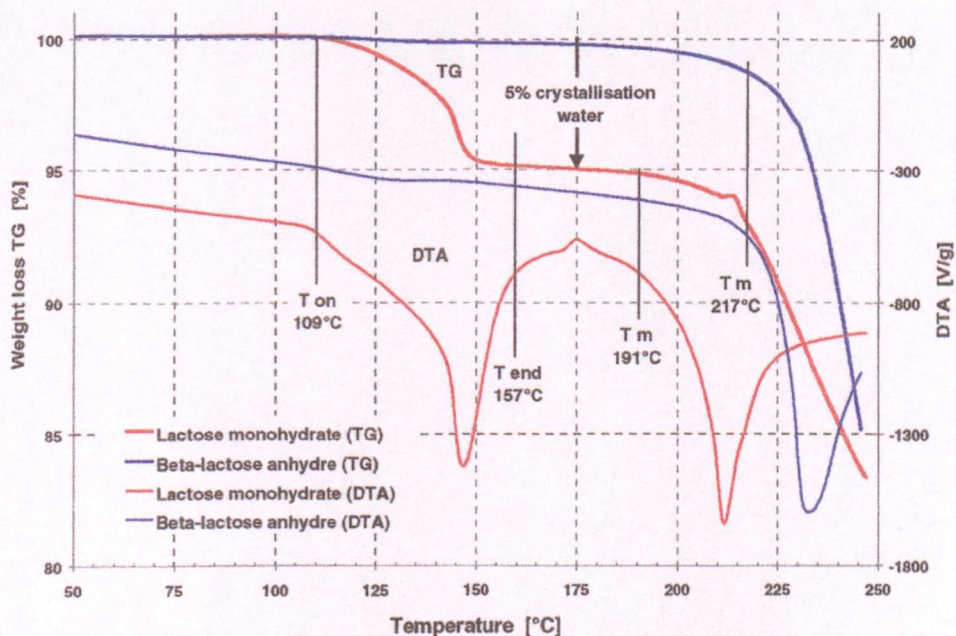


Fig. 3.3.53 TG/DTA data for pure lactose.

Sample	T _{on} (°C)	T _{end} (°C)	loss 1(%)	T _{m on} (°C)	loss 2(%)	T _{mp} (°C)
1	136	158	2.09	197	4.72	216
2	139	158	3.14	196	4.73	219
3	132	155	2.84	179	4.76	204
4	136	157	2.44	186	4.73	212

Table 3.3.33 TG/DTA results.

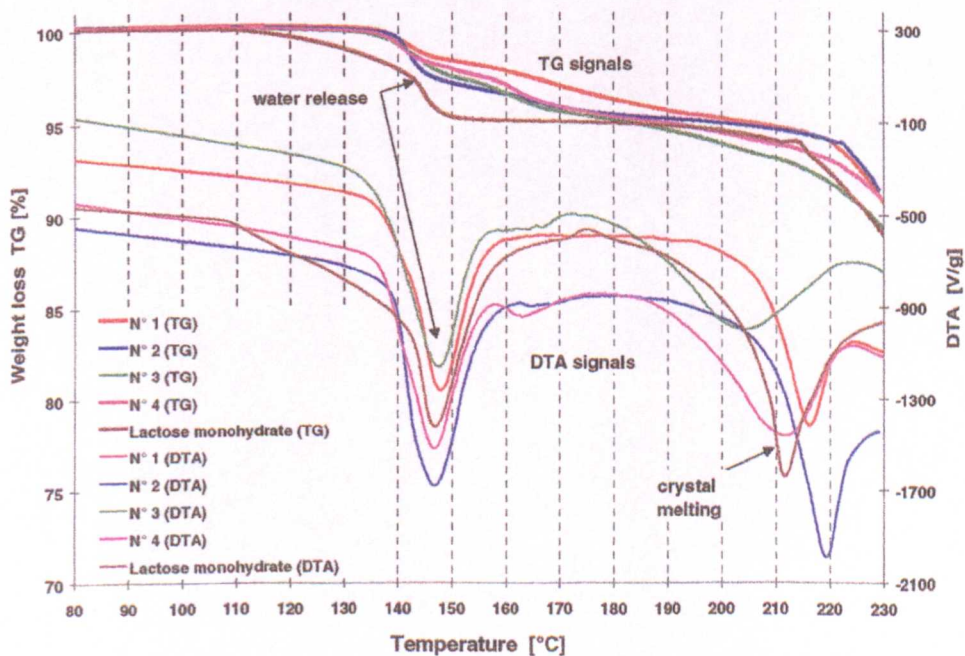


Fig. 3.3.54 TG/DTA results of 8mg lactose samples.

3.3.4 Discussion

Five methods of analyses were used to examine and compare the morphology, crystal size, shape, melting characteristics and properties of the lactose crystals grown from solution under applied magnetic field conditions. Each method of analysis is discussed in turn.

3.3.4(a) Visual observations

The visual observations are summarised in Table 3.3.1 show that lactose crystals grown in the absence of an applied field (Experiment 1) were all cloudy grey and glossy in appearance with very little form or texture indicative of the α -lactose monohydrate form.

The most striking observation to be made, was the difference between these crystals and those of lactose samples grown in the presence of applied fields at all 'points' of formation. A colour change from grey to white on the solution/air interface was coupled with the appearance of a rough texture in most cases. Removing the lactose from the petri-dishes also revealed an increase in brittleness in several samples.

In the presence of a weak permanent field of 300G (Experiment 2) the resulting lactose crystals showed an increase in rough texture and a slight increase in brittleness. The stronger fields in Experiment 3 and 4 (~600 and ~700G respectively) resulted in a more crystalline, lactose form and a white coloured, textured solution/air interface. The solution/glass interface developed a pitted texture as a result of the increased field strengths and both demonstrated 2 layers of growth from the upper and lower interfaces towards each other.

Where the applied fields were positioned above and below the petri dish (field lines perpendicular to the interface, Experiment 5, ~600G) a stronger effect on the resulting lactose crystals was observed, the resulting lactose crystals were whiter in colour, more textured and more brittle than before.

The lactose crystals resulting from application of a pulsed field (Experiment 6) during crystal growth demonstrated similar changes in crystal appearance to those observed in the permanent field studies.

All strengths of DC electromagnetic field studied (~100, ~150-340 and ~220-600G for Experiments 7, 8 and 9 respectively) resulted in more crystalline lactose. Again, the surfaces of the lactose crystals (solution/air interface) were white and textured, however more significantly, brittleness was greatly enhanced and the lactose crystals powdered very easily. This is indicative of a more crystalline form with the possibility that more smaller crystals have been formed.

3.3.4(a)(i) Conclusion

In all cases studied the effect of the applied magnetic field leads to more crystalline lactose.

3.3.4(b) Scanning Electron Microscopy

The SEM results are separated into 3 regions of study since each region demonstrates different morphology.

3.3.4(b)(i) Solution/glass interface

Figures 3.3.1, 3.3.2 and 3.3.3 illustrate the general morphology observed in the control lactose samples (from Experiment 1). All demonstrate partly formed, rounded crystal forms at both very high and low magnification. In comparison, all lactose crystals grown in applied magnetic fields demonstrate more ordered crystalline forms. Figures 3.3.5 (sample 4(2)) and 3.3.8 (sample 9(3)) demonstrate the general forms obtained in most cases which contain well-formed crystals with flat, smooth surfaces and angled edges.

Figure 3.3.4 illustrates an elongated, chunkier lactose crystal observed in sample 2(1). Layered growth, typical of samples obtained from Experiment 5 (where magnetic field lines are perpendicular to the crystal surface) are illustrated in Fig. 3.3.6, however the

crystals remain rounded and partly formed as in the case of the control samples. Fig. 3.3.7 demonstrates the more ordered crystal layers commonly found in all the lactose crystals formed in DC electromagnetic fields. Surfaces are very flat and smooth, with very little partly formed and rounded forms present.

3.3.4(b)(ii) Solution/air interface

The crystals formed at the solution/air interface were largely amorphous since the water content of the lactose solution is lowest at this surface where evaporation of the water from the solution occurs. Full crystallisation does not occur under these conditions. This is demonstrated in Fig. 3.3.9 where some long strands of partially formed crystals can be clearly seen which are largely amorphous and seem 'fluffy' in appearance.

In all cases, where lactose crystallisation has occurred in an applied magnetic field, the surface is less amorphous and shows more crystalline form. Figures 3.3.10, 3.3.11 and 3.3.12 illustrate some of the more fibrous forms observed. Fig. 3.3.13 illustrates directional crystal growth of extended nodules upward from the surface of a sample from Experiment 5 which has the magnetic field lines in the same direction.

Figures 3.3.14, 3.3.15 and 3.3.16 illustrate the general lactose crystal features which are elongated fibres and semi-layered structures, and a very large deviation from the morphology illustrated in the control samples.

3.3.4(b)(iii) Crystals in lactose solution

Separating the layers of lactose crystals grown at each interface, i.e. top and bottom of the lactose solution within the petri dish, reveal lactose crystals that have grown within the lactose solution. The control crystals (from Experiment 1) shown in Figures 3.3.17 demonstrate the 'tomohawk' crystal form generally indicative of the α -lactose monohydrate crystal form. The surfaces are generally covered in a large amount of amorphous material and the crystal surfaces are more rounded than flat in most cases.

Again, in all cases where lactose crystal growth has been carried out in the presence of an applied magnetic field, changes in crystal morphology are observed. Fig. 3.3.18 illustrates well formed, layered lactose crystals typical of the permanent field experiments (2-5). This is a considerable reduction in amorphous material and an increase in flat angled surfaces with well defined 'tomohawk' forms emanating from 'tomohawk' crystal surfaces.

Fig. 3.3.19 illustrates the lactose crystals obtained from application of the pulsed magnetic field during crystal growth which illustrates similar layered features observed from lactose crystals grown in permanent magnetic fields.

Elongated rectangular lactose crystal forms obtained from crystal growth in the weakest DC electromagnetic field (~100G, Experiment 7) are illustrated in Fig. 3.3.20. In this case, there is a large amount of amorphous lactose present. More rectangular and layered forms are also illustrated in Figures 3.3.21 and 3.3.22, both obtained from crystals grown in applied DC electromagnetic fields.

3.3.4(b)(iv) Conclusion

Although qualitative, the SEM pictures reveal more crystalline lactose has formed, containing less amorphous material and some changes in crystal form for lactose samples have occurred in lactose crystals that have been grown in applied magnetic fields. The extensively layered crystals shown for lactose samples grown in DC electromagnetic fields would explain the brittle and powdering features observed for these samples. In addition, the more crystalline forms account for the general increase in brittleness observed for all samples grown in magnetic fields. The less amorphous, more crystalline surfaces also account for the rough texture observed visually.

3.3.4(c) Differential Scanning Calorimetry

The lactose crystals grown under zero field conditions obtained from Experiment 1 show a feature (most likely due to loss of water of crystallisation) around 140°C in samples 2 and

3 and a feature around 150°C corresponding to lactose melting in all three samples. This melting peak is indicative of α -lactose monohydrate.

The DSC's of the lactose crystals grown in the presence of applied fields have either or both of these peaks using DSC which indicate all samples to be α -lactose monohydrate form (see Table 3.3.2). In addition, some samples display very broad melting peaks of around 200-220°C (samples 3(3), 6(1), 6(3), 7(2), 7(3), 8(1), 8(2) and 9(3)). This is not reproducible in all crystal samples from the same experiment and is not always reproducible on repeating using another portion from the same sample for analysis. As mentioned in Section 3.1.2(a) (see Fig. 3.1.9) this is most likely to be due to simultaneous melting and decomposition, however, it may also be possible that a small amount of β -lactose may be present within the α -lactose monohydrate crystal. No distinction between both explanations can be made using this technique since decomposition of α -lactose monohydrate occurs in the temperature range under question.

3.3.4(c)(i) Conclusion

The DSC data confirm that in all cases α -lactose monohydrate is obtained regardless of crystal growth conditions i.e. with or without an applied magnetic field during crystal growth. There are some higher melting peaks (around 220°C) for some samples which may indicate the presence of some β -lactose within the crystal.

3.3.4(d) Powder X-ray diffraction

The characteristic d-spacings of different lactose crystal forms are summarised in Table 3.3.34 below. Bottled α -lactose monohydrate was analysed using Powder X-ray Diffraction. In all cases, the d-spacing values matched very closely with those of the reference.

Lactose structure	Characteristic d-spacing (Å)
α -Lactose monohydrate	4.46, 4.65, 5.49
β -Lactose anhydride	4.24, 4.63, 8.41
Unstable α -lactose anhydride	4.13, 4.63, 4.93
Stable α -lactose anhydride	3.82, 4.21, 4.56
α -Lactose and β -lactose (Ratio 5:3)	4.04, 4.42, 4.65

Table 3.3.34 Summary of the characteristic peaks of various lactose structures.

3.3.4(d)(i) Controls

The Powder XRD data for Sample 1(1) is given in Table 3.3.3. Three of the main d-spacings were measured at 4.39 (4.46), 4.53 (4.55) and 5.32 (5.22)Å where the bracketed values are the corresponding corrected values. The d-spacing at 4.65Å was not observed and the intensities for the measured d-spacings other than the base peak (4.39Å at 100%) were lower than the reference intensities. In addition, the expected d-spacing at 7.08Å, was measured slightly lower than expected at 6.91Å. Other than variations in intensity, the d-spacing values correlated very well with those of the reference.

The Powder XRD data for Sample 1(2), given in Table 3.3.4 shows the three main characteristic d-spacings at 4.50 (4.46), 4.69 (4.65) and 5.50 (5.14)Å. The base peak (4.50Å, 100%) was as expected. The reference d-spacing at 7.08Å, was measured at 7.23Å and two additional d-spacings at 3.78 and 3.51Å were measured.

The Powder XRD data for Sample 1(3), given in Table 3.3.5 is very similar to the data for 1(2) with the addition of a d-spacing measured at 4.24Å.

Powder XRD data measured for the 'Control' lactose samples 1(1) to 1(3) were considered to indicate the α -lactose monohydrate form of lactose. All d-spacings match closely with the corrected values (with only small variations) and definitely do not match

with any of the other lactose forms. There is however considerable reduction in the measured intensities for the d-spacings other than the base peak at 4.46Å (100%).

3.3.4(d)(ii) Permanent field studies (in parallel at sides)

The Powder XRD data for Sample 2(1), given in Table 3.3.6, has the three main d-spacings at 4.44 (4.46), 4.62 (4.65) and 5.40 (5.41)Å with intensities 100,41 and 15% respectively. Other d-spacings match very closely with the corrected values.

The Powder XRD data for Sample 2(2), shown in Table 3.3.7, are similar to the data obtained for Sample 2(1) with the addition of a d-spacing at 4.06Å. It could be a lower than expected value corresponding to 4.19Å reference d-spacing but also matches a d-spacing measured for a mixture of α -lactose monohydrate and β -lactose anhydride in the ratio (5:3). Since the characteristic d-spacings at 4.4 and 4.65Å for this mixture are not present the former is assumed.

Powder XRD data for Sample 2(3) shown in Table 3.3.8, has only two of the characteristic d-spacings at 4.50 (4.46) and 5.39 (5.41)Å. The d-spacing at 4.65Å is not present, however a strong d-spacing at 4.59Å (65%) is shown. Since this is similar to the 'Control' Sample 1(1), and all other d-spacings match the reference values, it can be assumed that all lactose samples grown in a ~100G permanent field are α -lactose monohydrate.

Lactose Sample 3(1), given in Table 3.3.9, clearly shows the characteristic d-spacings at 4.46 (4.46), 4.65 (4.65) and 5.43 (5.41)Å in addition to those measured at 3.76 (3.75), 4.20 (4.19) and 7.13 (7.08)Å. Very good agreement with reference values for α -lactose monohydrate has been obtained. The Powder XRD data for Samples 3(2) and 3(3), given in Tables 3.3.10 and 3.3.11 are virtually identical to Sample 3(1) data. Lactose Samples 3(1) to 3(3) can be considered to be α -lactose monohydrate form since the Powder XRD data for lactose samples grown in a ~300G permanent field are in excellent agreement with reference values.

The Powder XRD data for lactose Sample 4(1), given in Table 3.3.12, have the 3 characteristic d-spacings at 4.51 (4.46), 4.62 (4.65) and 5.47 (5.41)Å. In addition, d-spacings are measured at 3.77 (3.75), 4.23 (4.19) and 7.19 (7.08)Å. Other than differences in intensities, the d-spacing values match very closely with the α -lactose monohydrate reference values.

The Powder XRD data for Sample 4(2), given in Table 3.3.13, shows a larger d-spacing value of base peak (100%) at a d-spacing of 4.68 (4.46)Å. All the other main peaks are present and agree very closely with the α -lactose monohydrate reference d-spacings. Powder XRD data for lactose Sample 4(3) shown in Table 3.3.14, have the 3 characteristic d-spacings in addition with 2 others at 4.24 and 7.19Å.

Other than the unusually large value for the main d-spacing expected at 4.4.6Å in Sample 4(2), all of the d-spacing measured values match very well with the α -lactose monohydrate reference values, therefore it may be concluded that α -lactose monohydrate form has been obtained in all cases of crystallisation within a ~700G permanent field.

3.3.4(d)(iii) Permanent field study (parallel above and below)

The Powder XRD d-spacings measured for Sample 5(1), given in Table 3.3.15, seem to be slightly larger than the α -lactose monohydrate reference values apart from the d-spacing at 4.26 which is thought to correspond to the reference d-spacing at 4.27Å. All the other d-spacing values, if corrected by subtracting 0.1Å, give good agreement with the reference values and the d-spacing at 4.26Å would correspond to the d-spacing at 4.19Å in the reference. In this case there is assumed to be an error in the correction factor and that the α -lactose monohydrate crystal form has been obtained.

Since the other samples 5(2) and 5(3) given in Tables 3.3.16 and 3.3.17, demonstrate very close agreement in measured d-spacings and reference values for α -lactose monohydrate, this is assumed to be the lactose crystal form obtained when grown in a ~600G permanent field where the field lines are perpendicular to the lactose solution/air interface.

3.3.4(d)(iv) Pulsed field study

The 3 strongest d-spacings given in the Powder XRD for lactose Sample 6(1) (given in Table 3.3.17), also the 3 characteristic d-spacings, were measured to be 4.49 (4.46), 4.66 (4.65) and 5.47 (5.41)Å, in addition with other measured d-spacings that matched very closely with the α -lactose monohydrate reference values. This is the case for the d-spacings measured for Samples 6(2) and 6(3) given in Tables 3.3.18 and 3.3.19, therefore all data indicates α -lactose monohydrate has been obtained.

3.3.4(d)(v) DC electromagnetic field studies

The Powder XRD data for Samples 7(1) to 7(3), given in Tables 3.3.21 to 3.3.23, are in very close agreement with the α -lactose monohydrate reference values, therefore the assumption that α -lactose monohydrate crystals have been obtained, under the conditions of an applied DC electromagnetic field of ~ 75 G during crystal growth, can be made.

Examination of the Powder XRD data for lactose Samples 8(1) to 8(3), given in Table 3.3.24 to 3.3.25, shows more d-spacing peaks measured but with very close agreement to the α -lactose monohydrate reference values, the intensities of which are increased compared to all previous data. For lactose samples 9(1) to 9(3) this is also the case. Powder XRD data are given in Tables 3.3.27 to 3.3.29.

Based on Powder XRD data, the application of a DC electromagnetic field to a crystallising lactose solution resulted in the formation of α -lactose monohydrate.

3.3.4(d)(i) Conclusion

In all cases, α -lactose monohydrate was formed. Not all the peaks shown in the corrected data are given in the data for all the samples and there are wide variations in peak intensities. The peak positions however indicate that the crystal form of lactose remains α -lactose monohydrate under the application of applied fields and not those of other crystal forms. These results also indicate that there are no impurities present since there are no additional features present in the data.

3.3.4(e) Karl Fischer titration data

The theoretical moisture content in an α -lactose monohydrate crystal is 4.9997%. Each sample, titrated 3 times, had mean wt/wt and standard deviation percentages calculated for it. The results are given in Table 3.3.31.

The control samples from Experiment 1, had mean moisture content values between 5.34 and 5.42% with a max standard deviation of around $\pm 0.1\%$. Lactose crystallised in a DC electromagnetic field, however had a moisture content significantly higher which had increased by ~ 7.5 - 11% wt/wt. Even with a permanent field placed above and below the crystallising lactose solution a significant increase in moisture content of $\sim 7\%$ was observed.

3.3.4(e)(i) Conclusion

The figures confirm the XRD and DSC results that the α -lactose monohydrate crystal form has been obtained, i.e. 5% water is present. It is possible that there may exist non-bonded water of crystallisation water within the lactose crystal structure that was observed in the sucrose results where some small peaks were observed below 100°C .

3.3.4(f) Related thermal analysis data

DSC traces for pure lactose forms (Figures 3.3.50 and 3.3.51) show that amorphous lactose forms a glass at 65°C before undergoing crystallisation at 90°C . α -Lactose monohydrate shows a very strong water of crystallisation peak at 150°C before decomposing above 200°C and β -lactose (anhydrous) shows only one melting peak around 222°C .

The DSC results for the lactose samples using a Perkin Elmer DSC 7 and a Seiko machine are compared in Table 3.3.32. Lactose Sample 1 (pulsed field), Sample 2 (~ 200 - 600G DC electromagnetic field), Sample 3 (Control) and Sample 4 ($\sim 100\text{G}$ DC electromagnetic field) have very similar melting points around 140° and 150°C . However the difference lies

in the ΔH values measured for each sample which represents enthalpy of crystallisation water release. For Sample 2 this value, as measured by the Perkin Elmer DSC7, was considerably larger than for the other samples at 150Jg^{-1} , while the others range between $88\text{-}84\text{Jg}^{-1}$. Figure 3.3.52 illustrates the Seiko DSC results where Sample 2 also has the highest water of crystallisation peak ($\Delta H=109\text{Jg}^{-1}$), with others ranging from 68Jg^{-1} for Sample 1 (control), through 78Jg^{-1} for Sample 4 to 96Jg^{-1} for Sample 3 (pulsed field). In this case the Seiko DSC measurements would be considered the more accurate, not only due to increased sensitivity of the measurements but also because a slower heating rate of 5°min^{-1} was used compared to 10°min^{-1} for the Perkin Elemer DSC7, which has the effect of reducing the temperature lag of the measurements.

DTA measurements show a similar form to the DSC traces, with release of water of crystallisation peak at 150°C , however the melting point and decomposition is more clearly illustrated as a peak around 210°C since decomposition is easily recorded using this technique. The TG trace illustrates weight loss measurements and very clearly show a weight loss of 5% for α -lactose monohydrate as the step the graph between T_{on} and T_{end} . The higher melting point for the anhydrous β -lactose is clearly illustrated at around 230°C .

Comparison of the TG measurements (Figure 3.3.54) reveals the same pattern as the DSC measurements and Sample 2 has a higher value of released crystallisation of water value of 3.14% (compared to 2.09 to 2.84% for the other samples) and a higher melting point of 219°C ($204\text{-}216^\circ\text{C}$ for the other samples). These values however, are significantly lower than the α -lactose monohydrate used as a standard which has a value of 5% as expected at this 1st loss stage. The weight loss for samples 1 to 4 seems to be more of a gradual process than is the case for standard α -lactose monohydrate and does not equal the expected 5% weight loss value until a temperature of around 180°C is attained.

In general, the water of crystallisation is highest for Sample 2 as before and lowest for Sample 3 which is the control. In addition the control sample shows a broad hump around

201°C whereas Samples 1,2 and 4 show definite peaks around 212° to 219°C which is most likely to be as a result of the presence of some β -lactose within the crystal.

3.3.4(f)(i) Conclusion

DSC and TG/DTA data do not show significant differences between lactose Samples 1,3 and 4, however data for lactose Sample 2, which was grown in a ~200-600G DC electromagnetic field, does exhibit significant changes. The DSC results indicate that Sample 2 has a higher enthalpy release of crystallisation. The TG/DTA results recorded a higher weight loss, due to water of crystallisation, between T_{on} and T_{end} ; and both techniques show higher melting points for lactose Sample 2. These characteristics indicate that Sample 2 is mainly α -lactose monohydrate but most likely a small amount of β -lactose is present within the crystal, in addition to a higher crystallisation water content.

3.4 CONCLUSION

The study has demonstrated that magnetic fields applied to a crystallising lactose solution within a controlled environment, have a significant effect on the resulting lactose crystals formed. In all cases of applied fields, including the weak permanent and DC electromagnetic field, crystallisation of the lactose became more ordered with less amorphous lactose present within the samples. A significant increase in flat surfaces and angled edges with more distinct 'tomohawk' crystal form was observed for lactose crystals obtained from growth in applied magnetic fields, whereas, partly formed rounded crystals with a large amount of amorphous lactose were obtained in the absence of an applied field.

Differential Scanning Calorimetry, Powder X-ray Diffraction and Karl Fischer Titration techniques confirmed the α -lactose monohydrate form was obtained in all cases studied. Furthermore, the measured moisture content was significantly higher (water of crystallisation and not surface water) for lactose samples grown in DC electromagnetic fields and permanent fields with field lines perpendicular to the surface of solution. This is

thought to be similar to the bound water or 'Geolitic water' observed in the sucrose crystals discussed in Chapter 2, Section 2.3.4(b)(5).

The presence of small amounts of β -lactose within the α -lactose monohydrate crystals grown in DC electromagnetic fields (the α -lactose monohydrate melting point is around 202 to 213°C; the β -lactose anhydrous melting point is around 230°C; melting point were measured around >220°C) was confirmed by detailed DSC analysis. The increased water of crystallisation measurements were confirmed.

The main advantage, from an industrial viewpoint, in using applied magnetic fields on crystallising lactose solutions, is the improvement in crystalline form that can be obtained. A large reduction in amorphous lactose formed during crystallisation would benefit the chocolate industry where chocolate crumb is produced as part of the processing. Amorphous lactose tends to trap within it, the cocoa butter fat, which needs to be released during chocolate production to allow flavour development. However, since only static crystallisation of lactose has been studied, the work has no consequence in the chocolate industry where a dynamic system is the standard processing setup. A dynamic system which demonstrates similar results would be far more significant. To test the viability of applied fields in such an application, this study on static crystallisation would need to be extended to a dynamic system.

3.5 REFERENCES

- [1] Clamp, J. R. and Hough, L., *Advances in Carbohydrate Chem.*, 1961, **16**, 159
- [2] Cakebread, S. H., *Confectionery Production*, 1971, **X**, 274-278
- [3] Nickerson, T. A., *Food Technology*, 1978, 40-41
- [4] Kube, J. and Prizwald-Stegmann, B., *C.C.B. Review for Chocolate Confectionery and Bakery*, 1976, **1**, (3), 32-35
- [5] Pavia, D. L., Lampan, G. M. and Kriz, G. S., *Introduction to Organic Laboratory Techniques*, 3rd edition, Saunders College Publishing, Orlando, 1988
- [6] Hudson, C. S., *Journal of American Chemical Society*, 1909, **31**, 66
- [7] Tweedie, L. S., MacBean, R. D., Nickerson, T. A., *Food Technology in Australia*, 1978, 57-62
- [8] Hunziker, 1949 **NEED TO FIND THIS**
- [9] Eagleson, M., *Concise Encyclopaedia Chemistry*, Walker de Gruyter Berli, New York, 1994
- [10] Lewis, R. J. Sr., *Hawley's Condensed Chemical Dictionary*, 12th edition, van Nostrand Reinhold Company, New York, 1993
- [11] Jonas, J. J., *Journal of Milk and Food Technology.*, 1973, **36**, 323
- [12] Gerlisma, S. Y., *Netherland Milk Dairy Journal*, 1957, **11**, 83
- [13] Tumerman, L., Fram, H. and Cornely, K. W. *Journal of Dairy Science*, 1954, **37**, 380
- [14] Winder, W. C., *Journal of Dairy Science*, 1962, **45**, 1024
- [15] Webb, B. M., *Journal of Dairy Science*, 1966, **49**, 1310
- [16] Kube, J. and Prizwald-Stegmann, B., *C.C.B. Review for Chocolate Confectionery and Bakery*, 1976, **1**, (4), 30-33
- [17] Nickerson, T. A., *Fundamentals of Dairy Chemistry*, 2nd Edition, AVI, Westport, Conneticut, 1974
- [18] Keay, J., *Mod. Dairy*, 1969, **48**, 33
- [19] Gunsell, W. C. and Lachman, L., *Journal of Pharmaceutical Science*, 1963, **52**, 178

- [20] Duval, R. N., Koshy, K. T. and Dashiell, R. E., *Journal of Pharmaceutical Science*, 1965, **54**, 1196
- [21] Abbott, C. W., *South African Journal of Dairy Technology*, 1973, **6**, 77
- [22] Welsh D., *Food Technology Australia*, **YEAR??**,**17**, 318
- [23] MacBean, R. D., *Fermentation Processes in: Proceedings Whey Utilisation Research Seminar*, 1975, Parkville, Melbourne
- [24] Smart, J., Haylock, S. and Gordon, M., *Food Australia*, 1991, **43**, 9, 386-388
- [25] Kube, J., Dreissig, U. and Prizwald-Stegmann B., *C.C.B. Review for Chocolate Confectionery and Bakery*, 1978, **3**, 1, 8-15
- [26] De Waard, H., *International Dairy Federation 59th Annual Sessions, Austria*, 1975
- [27] Hudson, C. S., *Journal of American Chemists Society*, 1904, **26**, 1067
- [28] Troy, H. C. and Sharp, P.F., *Journal of Dairy Science*, 1930, **13**, 140
- [29] Twieg, W. C. and Nickerson, T. A., *Journal of Dairy Science*, 1968, **51**, (11), 1720-1724
- [30] Haase, G., and Nickerson, T. A., *Journal of Dairy Science*, 1966, **49**, 757
- [31] Noyes, A. A. and Whitney, W. R., *Z. Physik. Chem.*, 1897, **23**, 687
- [32] Buckley, H.E., *Crystal Growth*, John Wiley and Sons, Inc., New York, 1951
- [33] Roetman, K. and Van Schaik, M., *Netherlands Milk Dairy Journal*, 1975, **29**, 225-237
- [34] Borculs Whey Products, "Cooperative Weiproduutenfabriek Borculs W. A"
- [35] Nickerson, T. A. and Moore, E. E., *Journal of Dairy Science*, 1974, **57**, 11, 1315-1319
- [36] Briggner, L. E., Buckton, G., Bystrom, K. and Darcy, P., *International Journal of Pharmacy*, 1994, **105**, 125-135
- [37] Bushill, J. H., Wright, W. B., Fuller, C. H. F. and Bell, A. V., *Journal of Scientific Food Agriculture*, 1965, **16**, 622-628
- [38] Drapier-Beche, N., Fanni, J., Parmentier, M. and Vilasi, M., *Journal of Dairy Science*, 1997, **80**, 457-463

- [39] Sebhatu, T., Angberg, M. and Ahlneck, C., *International Journal of Pharmacy*, 1994, **104**, 135-144
- [40] Figura, L. O., *Thermochimica Acta*, 1993, **222**, 187-194
- [41] Nickerson, T. A., *Journal of Dairy Science*, 1962, **45**, 354
- [42] Whitaker, R., *Journal of Dairy Science*, 1933, **16**, 177
- [43] Haase, G., and Nickerson, T. A., *Journal of Dairy Science*, 1966, **49**, 127-132
- [44] Herrigton, B. H., *Journal of Dairy Science*, 1934, **17**, 533
- [45] Saylor, C. H., *Journal of Physical Chemistry*, 1928, **32**, 1441-60
- [46] Van Kreveld, A. and Michaels, A. S., *Journal of Dairy Science*, 1965, **48**, 259
- [47] Jelen, P. and Coulter, S. T., *Journal of Food Science*, 1973, **38**, 1182
- [48] Jelen, P. and Coulter, S.T., *Journal of Food Science*, 1973, **38**, 1186
- [49] Michaelis, A. S. and Van Kreveld, A., *Netherlands Milk Dairy Journal*, 1966, **20**, 163
- [50] Nickerson, T. A. and Moore, E. E., *Journal of Dairy Science*, 1974, **57**, 160
- [51] Van Kreveld, A., *Netherlands Milk Dairy Journal*, 1969, **23**, 258

4.0 SUMMARY

The introduction to this chapter covers all the significant background of cocoa butter and its role in chocolate manufacture. Particular reference is made to the crystal structure of the cocoa butter polymorphs and the Powder X-ray diffraction (XRD) and Differential Scanning Calorimetry (DSC) data expected for each.

The extent of crystallisation is measured on a crystallising cocoa butter system using a torque stirrer that is set to stir at constant speed while monitoring the torque required to do this. The novel component of this work is the application of magnetic fields on a molten crystallisation system rather than a solution system.

The magnetic fields are applied under two different conditions; the first is to the system during crystallisation and stirring, and the second is application to the melt under dynamic conditions prior to crystallisation.

In all cases of study, an applied magnetic field enhances crystallisation and there is some evidence of applied magnetic fields resulting in polymorphic modification from Form V to Form VI cocoa butter.

4.1 INTRODUCTION

4.1.1 History

Cocoa trees were cultivated in North and South America in the early 16th century by the Aztec Emperor Montezuma. The cocoa beans were used as currency but more importantly were the main ingredient for a spiced drink called 'Chocola' (believed to have aphrodisiac properties). The drink was prepared by roasting the cocoa beans in earthenware pots, grinding them between stones and adding the mix to cold water, often with other ingredients such as spice or honey, and whipped to a frothy consistency.^[1-5]

The introduction of cocoa beans to Europe possibly around the time of Columbus was exploited with cinnamon and vanilla which was served as a hot beverage in Spain.^[6] News of the drink spread to France and then elsewhere in Europe where it became fashionable to drink in coffee houses in the 17th and 18th centuries though was essentially restricted to the wealthy. The first record of the introduction of milk to coffee was in the UK in 1727 by Nicholas Sanders, although his reasons for doing so were uncertain.^[7]

The cocoa bean contains about half its weight of fat known as cocoa butter and this resulted in a very fatty drink. A process was therefore developed in 1828 by Van Houten in Holland to press out some of the cocoa butter. A mixture of ground cocoa bean and sugar gave a very hard substance that was unpleasant in the mouth, but addition of the extracted cocoa butter fat enabled the mixture to melt more easily for processing to give chocolate as it is known today. The qualities of dark or plain chocolate now produced in the UK is, however, vastly outweighed by milk chocolate, the invention of which is attributed to Daniel Peters of Vevey, Switzerland in 1876. Since chocolate with moisture levels above 2% has very poor texture and lasting properties, Peters developed a method of driving out the excess water from the milk by use of water-powered machines which were able to operate for long periods of time at an economic rate.

4.1.2 Cocoa butter

Cocoa butter is one of the most important 'solid' plant fats produced world-wide. It is valued mainly for its melting characteristics as it is brittle at room temperature (in temperate countries) but melts gradually until completely liquid just below body temperature. It is one of the most stable fats known as its natural antioxidant content allows storage for up to five years without noticeable rancidity.

4.1.2(a) Structure and composition

All fats comprise mixtures of triacylglycerols, the basic structure of which is shown below in Fig. 4.1.1.

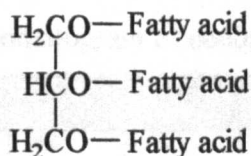


Fig. 4.1.1 The basic triacylglycerol structure.

The triacylglycerol consists of a backbone of glycerol esterified with three fatty acids. In terms of fatty acid composition, cocoa butter is a relatively simple fat. A list of all the fatty acids indicating structure and double bond position (typical West African cocoa butter composition) is shown in Table 4.1.1.

Fatty acid	Structure	Composition (Mol. %)
myristic acid	$\text{CH}_3(\text{CH}_2)_{12}\text{CO}_2\text{H}$ C14:0	0.1
palmitic acid	$\text{CH}_3(\text{CH}_2)_{14}\text{CO}_2\text{H}$ C16:0	26.0
palmitoleic acid	$\text{CH}_3(\text{CH}_2)_5\text{CH}=\text{CH}(\text{CH}_2)_7\text{CO}_2\text{H}$ C16:1	0.3
stearic acid	$\text{CH}_3(\text{CH}_2)_{16}\text{CO}_2\text{H}$ C18:0	34.4
oleic acid	$\text{CH}_3(\text{CH}_2)_7\text{CH}=\text{CH}(\text{CH}_2)_7\text{CO}_2\text{H}$ C18:1	34.8
linoleic acid	$\text{CH}_3(\text{CH}_2)_4(\text{CH}=\text{CHCH}_2)_2(\text{CH}_2)_6\text{CO}_2\text{H}$ C18:2	3.0
linolenic acid	$\text{CH}_3\text{CH}_2(\text{CH}=\text{CHCH}_2)_3(\text{CH}_2)_6\text{CO}_2\text{H}$ C18:3	0.2
arachidic acid	$\text{CH}_3(\text{CH}_2)_{18}\text{CO}_2\text{H}$ C20:0	1.0
behenic acid	$\text{CH}_3(\text{CH}_2)_{20}\text{CO}_2\text{H}$ C22:0	0.2

Table 4.1.1 Typical fatty acid composition of West African cocoa butter.

A shorthand nomenclature (shown in Table 4.1.1 under the structure of each fatty acid) is used to identify each fatty acid carbon chain length and number of double bonds, eg C18:0 is stearic acid, has 18 carbon chain length with no double bonds present.

Missing pages are unavailable

butters, with Malaysian, Sri Lankan and Indian cocoa butters being the hardest and Brazilian, the softest whereas others lie in between. The quality of the Brazilian cocoa butter can be improved by mixing it with Malaysian cocoa butter, which results in a harder cocoa butter.

Although HPLC is a suitable means of cocoa butter triacylglycerol analysis which relates triacylglycerol composition to hardness, it gives no indication of the physical properties of the butter. The physical properties can be measured by various analytical techniques but before considering these crystallisation and polymorphism of cocoa butter is described in the next section.

4.1.2(b) General triacylglycerol crystallisation

In order to understand the mechanism of cocoa butter crystallisation, it is first necessary to understand how triacylglycerols crystallise at the molecular level. X-ray diffraction evidence suggested the triacylglycerols exist in a tuning fork configuration at temperatures above the melting point.^[10] In the liquid state, the triacylglycerols lock laterally to form a lamellar arrangement as shown in Fig. 4.1.3 below. As the temperature of the liquid melt decreases and approaches the crystallisation temperature the lamellar units become more organised and increase in size. The disordered triacylglycerol hydrocarbon chains are arranged in more ordered and rigid conformations, forming regions of crystal nuclei, finally reaching critical size at crystallisation temperatures.

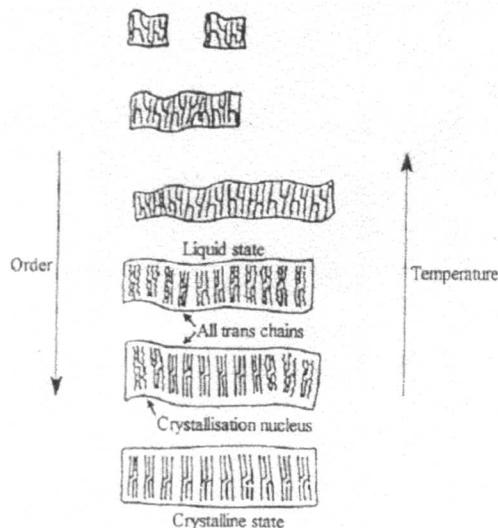


Fig. 4.1.3 The crystallisation process for triacylglycerols.

The process of crystallisation proceeds through four stages: an induction period, followed by nucleation, crystal growth and crusting over. The length of time for each stage varies and depends not only on the temperature of the liquid mass but also the fatty acid composition of the cocoa butter.

Nucleation begins with the formation of submicroscopic crystalline regions within the molten liquid. Coincidental alignment or arrangement of amorphous triacylglycerol molecules forms stable nuclei to which other triacylglycerols can attach in an orderly fashion. Nuclei are continuously formed in the liquid and appear as crystals at relatively few points throughout the liquid mass i.e. the crystals do not form simultaneously throughout the liquid mass.

The crystallisation process proceeds more rapidly following formation of the first crystals as new nuclei appear and existing crystals grow. Below a critical size, the triacylglycerol aggregates may lose as well as gain molecules but above this critical size growth will continue. By definition, this critically sized aggregate is a nucleus whose formation requires the process of complex molecular organisation and the production of three dimensional order.

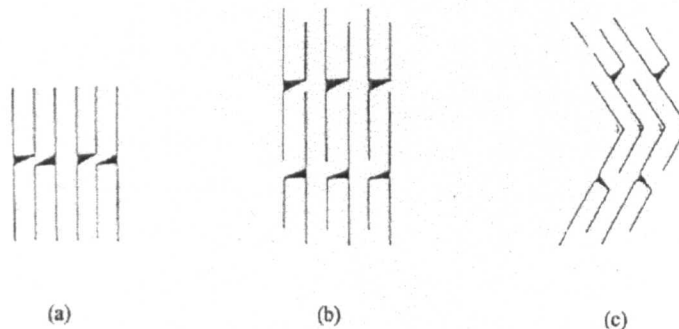


Fig. 4.1.4 Triacylglycerol dimers illustrating (a) the double chain length structure, (b) the triple chain length structure, and (c) the triple chain length structure for triacylglycerols containing unsaturated fatty acid in the number two position of the glycerol backbone.

The stage referred to as crystal growth involves the rapid growth or increase in size of the nuclei as the triacylglycerols in the molten cocoa butter mass readily crystallise onto the surface of the nuclei as they are swept past during agitation. The final stage, known as crusting over or hardening-off, according to the Americans, is thought to involve the contact of individual fat crystals with one another, allowing formation of

bridges and is referred to as the apparent solidification by some manufacturers. In the crystalline state, triacylglycerols are thought to exist as dimers. For most saturated mono-acid triacylglycerols, such as tristearin, the dimers exist in a double chain-length structure shown in Fig. 4.1.4(a). Generally, if the fatty acid chains of the triacylglycerols differ by more than three carbons, the triple chain-length structure is adopted as shown in Fig. 4.1.4(b). Fig. 4.1.4(c) also illustrates the typical triple chain-length structure for a triacylglycerol containing an unsaturated fatty acid in the number two position on the glycerol backbone.^[11]

Cocoa butter is comprised mainly of triacylglycerol with oleic acid in the number two position of the glycerol backbone, hence, the packing arrangement closely resembles the triple chain length structure.^[12]

4.1.2(c) Polymorphism and cocoa butter

Polymorphism is the ability of a substance to exist in more than one crystalline form. The phenomenon of triacylglycerol polymorphism has been known for over 100 years^[13] and numerous scientists have conducted research to demonstrate that the basis for multiple melting points of triacylglycerols was polymorphism.^[14,15] Nearly all fats exhibit polymorphism in a monotropic manner, in that transformations take place from less stable, lower melting forms to more stable, higher melting forms.

Fatty acids and glycerols have been observed to exist in at least two crystalline forms and some have as many as three or four.^[16] As a transition occurs the molecular packing of the triacylglycerols shift to confer greater stability of the crystal and have an associated rise in melting point. Triacylglycerol polymorphism was first clearly demonstrated using x-ray diffraction analysis in 1934 by Clarkson and Malkin.^[14] The molecular arrangement of the crystalline structure is described in terms of short and long spacings. The short spacings describe the cross-sectional arrangement of the fatty acids in the triacylglycerols and the long spacings represent the distance between the planes formed by the terminal methyl groups of the fatty acids (see Fig. 4.1.5).

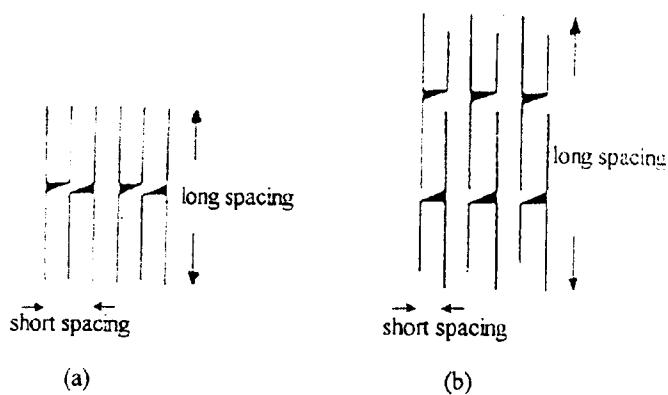


Fig. 4.1.5 Illustrations of long and short spacings for (a) double chain-packing, (b) triple chain packing triacylglycerols.

Generally, as the magnitude of long spacings decreases, the melting point of a particular polymorphic form increases. In addition, shorter fatty acid chain lengths result in shorter long spacings indicating that the geometry of the triacylglycerol dictates the molecular arrangement. Close chain packing and packing of similar chains produce a more dense structure which results in a higher melting point. As the chain packing becomes tighter, intermolecular bonding can occur. Intermolecular bonding which is increased by the proximity of the participating groups adds stability to the crystal via hydrogen bonding and Van der Waals interactive forces.

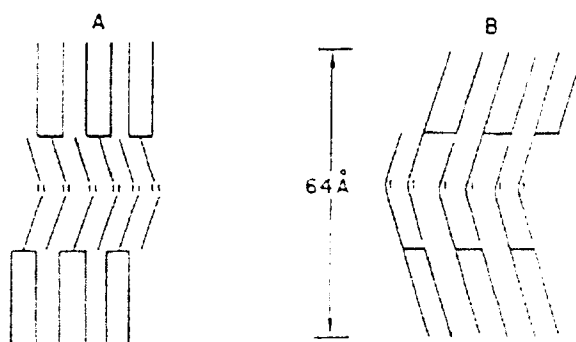


Fig. 4.1.6 Illustration of the arrangements of 2-monounsaturated triacylglycerol: (A) conventional tuning fork packing (B) modified tuning fork packing.

Larsson in 1972^[17] altered the conventional tuning fork structure^[18] to a modified tuning fork configuration which is believed to be the more correct arrangement involving the central alkyl group and one of the alkyl groups aligning along the same axis (see Fig. 4.1.6).

Since the discovery of polymorphism, numerous scientists have reported different numbers of polymorphs and conflicting melting points for the various crystalline forms

found in cocoa butter.^[19-25] In general, the various nomenclatures assigned to each classification has compounded the problem due to a lack of consistency.

It is generally accepted that there are six different polymorphic forms of cocoa butter, classified by Willie and Lutton i.e. Form I to Form VI. Forms I to IV are double chain packed structures and Form V and VI are triple chain packed structures.

Type I requires very low temperatures and fast cooling for such irregular molecular packing to occur in the triacylglycerol and has a low melting point of around 17°C which demonstrates the instability and irregular packing of the cocoa butter crystalline material. The hydrocarbons in the triacylglycerols would be expected to possess a high degree of mobility which, coupled with the hydrocarbon chain oscillations, would be expected to transform rapidly into Form II. The slightly higher melting point of around 21-22°C is consistent with the more regular (hexagonal) packing of the hydrocarbon chains.

Form IV form is a closer packed more crystalline material which is demonstrated by the rise in melting point to around 27-29°C. Form III is not a single type of molecular packing but an intermediary mixture of Forms II and IV and consistent with this, its melting point lies mid-way between these two Forms II and IV.

Forms V and VI are the most stable forms of cocoa butter. No distinction can be made between both Forms V and VI. Type VI cannot be obtained from the liquid cocoa butter mixture but is formed through a solid-solid transition which is thought of as a molecular reorganisation. For these reasons, Forms V and VI are assumed to be phases differing in composition rather than distinct polymorphic forms.

Cocoa butter in Form V is the polymorph produced in a well-tempered but can change into Form VI after long periods of storage. This change is often accompanied by the formation of fat bloom in chocolate which destroys the surface texture and results in a mouldy appearance. It is therefore crucially important to understand the mechanisms of polymorphic transitions in cocoa butter to obtain the required Form V.

4.1.2(d) Analysis of polymorphs in cocoa butter

Problems can be encountered in identification of a particular polymorph in a crystalline cocoa butter sample, because of the compositional differences in cocoa butters from different origins. Several methods of analysis are available but must be used in combination rather than individually for more reliable results. X-ray diffraction and DSC (Differential Scanning Calorimetry) analysis are by far the most important although other techniques such as pulsed NMR and microscopy are also used.

4.1.2(d)(i) Powder X-ray Diffraction (XRD)

Powder X-ray diffraction can be used successfully to identify the particular polymorph of a crystalline cocoa butter sample by measurement of the short and long spacings of the crystal.^[26,27] Table 4.1.5 show the short and long spacing data expected for each of the six polymorphs of cocoa butter and Figs. 4.1.7(a)-(d) show typical short spacing x-ray diffraction patterns expected for cocoa butter polymorphs II, IV, V and VI respectively.

	Short spacing (Å)		Long spacing (Å)	
Polymorph I	3.70 (S)		34 (W)	
	4.19 (VS)			
Polymorph II	4.25 (S)		16.6 (M)	
			49 (VS)	
Polymorph III	3.87 (M)		15.24 (M)	
	4.25 (S)		16.6 (S)	
	4.63 (M)		49 (VS)	
Polymorph IV	4.17 (VS)		14.9 (S)	
	4.35 (VS)	3.88 (W)	46 (VS)	16.20 (W)
Polymorph V	3.68 (W)	3.99 (M)	9.08 (W)	34 (S)
	3.76 (M)	4.6 (VS)	13.15 (W)	66 (S)
Polymorph VI	3.71 (S)	4.6 (VS)	8.18 (W)	
	3.88 (S)	5.16 (W)	13.2 (W)	
	4.04 (M)	5.47 (M)	35 (S)	
	4.28 (W)		66 (S)	

VS : very strong, S : strong, M : medium, W : weak

Table 4.1.7 X-ray diffraction data for the six polymorphs of cocoa butter.

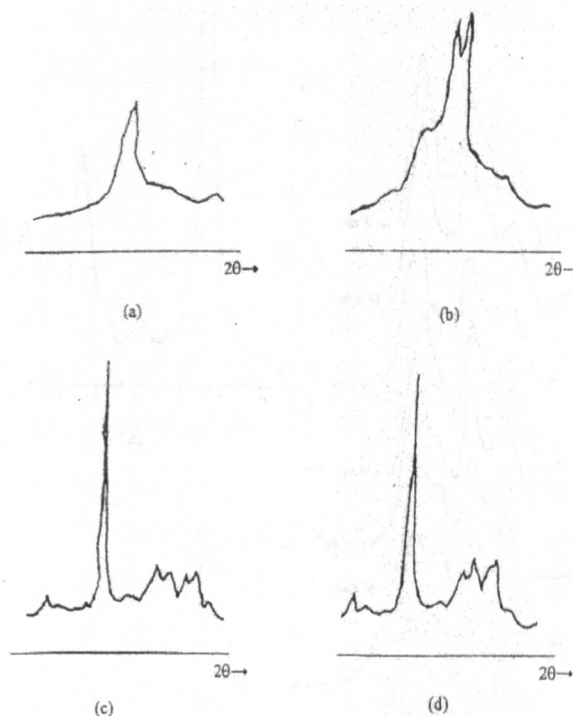
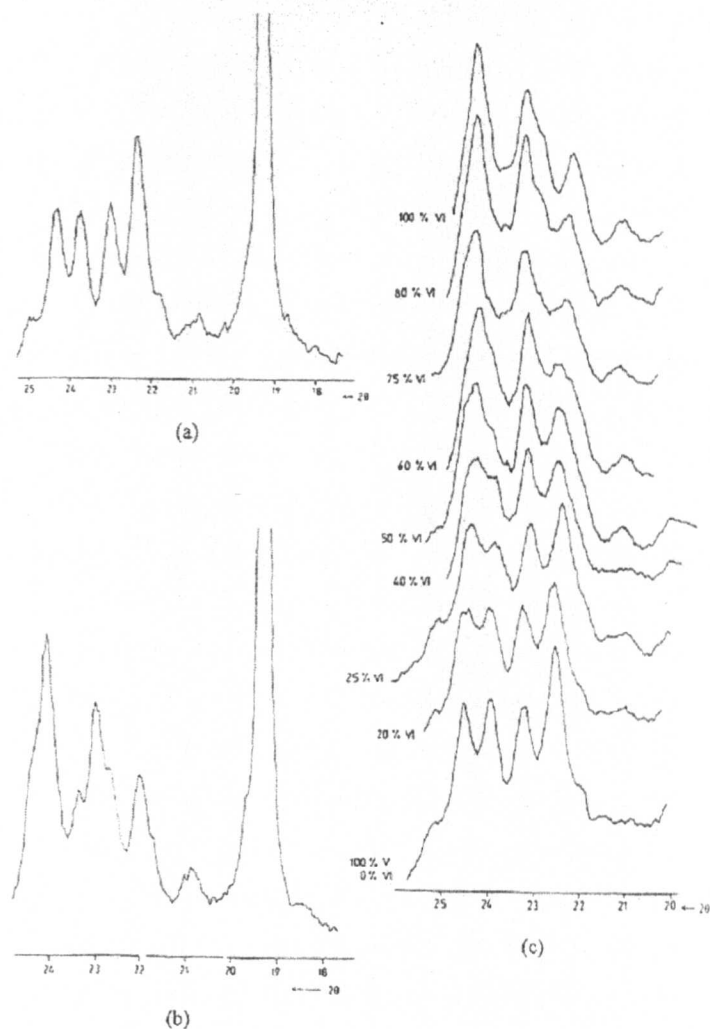


Fig. 4.1.7. Powder X-ray diffraction patterns of cocoa butter

- (a) Form II,
- (b) Form IV,
- (c) Form V, and
- (d) Form VI.

The data for Forms V and VI have an additional strong, long spacing of 66\AA which is indicative of the triple chain packing spacing of cocoa butter component. Forms I to IV can be identified easily because they are distinctly different, however, this is not the case for Forms V and VI. This is consistent with the argument that the transition between Forms V→VI is a molecular reorganisation rather than a transition between two distinct polymorphic forms.

The chocolate industry requires cocoa butter in Form V to make a marketable product and it is therefore of prime importance to be able to distinguish between Forms V and VI. This transition has been thoroughly studied in combination with food emulsifiers^[31] resulting in powder x-ray diffractions at various percentage mixtures of Forms V/VI during the V→VI transition (see Figs. 4.1.14(a)-(c)). This is ideal for purposes of comparison.

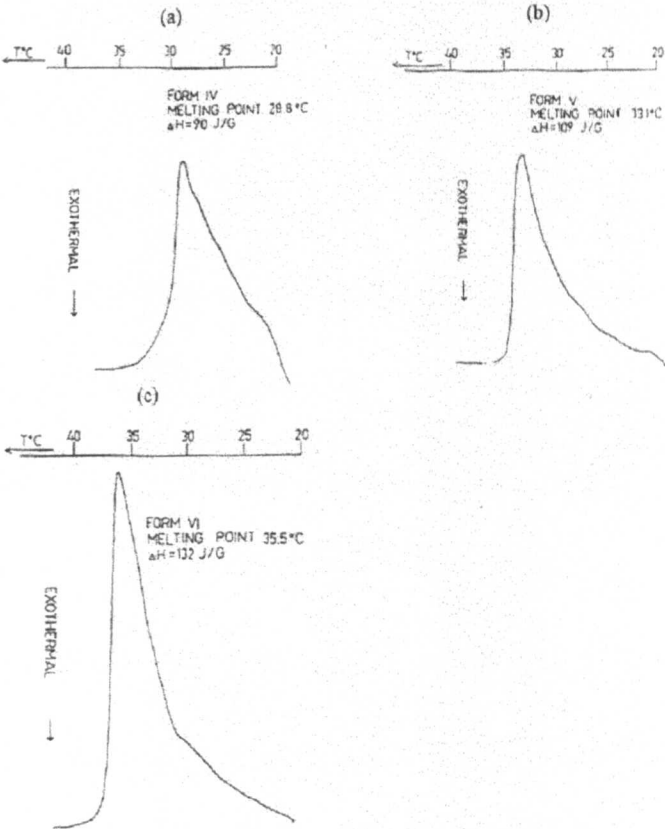


Figs. 4.1.8 Enlarged x-ray diffraction patterns of cocoa butter polymorphs in
 (a) Form V,
 (b) Form VI, and
 (c) Form V→VI transition.

4.1.2(d)(ii) Differential Scanning Calorimetry (DSC)

DSC is the most common indirect technique applied to the study of fats. DSC measures the fundamental quantity energy change during cooling or heating on a macroscopic quantity of sample. The energy changes that are measured reflect the specific heat capacity and changes of phase as materials are either cooled or heated. DSC is preferred to other calorific methods, such as DTA (Differential Thermal Analysis), because it is the fundamental quantity of energy that is measured. DTA measures only temperature difference between a sample or reference on heating or cooling and requires independent knowledge of the specific heat capacity of the sample at all temperatures in order to convert temperature difference to energy.

DSC has been used for many years in the characterisation of confectionery fats, cocoa butter and pure triacylglycerols^[28-35] The basic principles involve the measurement of heat flow to a reference material to ensure that the references remain at the same temperature as a sample that is undergoing cooling or heating. The heat flow will be constant until the sample undergoes a phase change or transition. At this point the DSC can measure the heat flow to or from the reference material. Since cocoa butter can undergo polymorphic transitions between Forms I and VI depending on the thermal history of the sample, DSC is a powerful technique for polymorph classification.^[36]



Figs. 4.1.9 Typical Differential Scanning Calorimetry heating curves of cocoa butter for
 (a) Form IV,
 (b) Form V, and
 (c) Form VI.

DSC can also be used for melting point measurement. The typical DSC calorimetric heating curves for Forms IV to VI of cocoa butter are shown in Figs. 4.1.9 (a)-(c). The important points to note are the temperatures at the peak heights (which correspond to

the melting points) and the height of the peaks which are increasingly higher the more stable the crystalline form.

General effects on the form of the thermogram resulting from variations in cooling or heating any material are: faster rates shift peaks to lower temperatures on cooling and to higher temperatures on heating. Peak broadening occurs progressively as rates are increased. Manipulation of cooling and heating rates can achieve a great deal of information on polymorphism when optimised and can result in evidence on polymorphic transitions during crystal growth.^[37]

DSC is therefore an accurate method of determining the particular polymorph present in a crystalline cocoa butter sample, especially when coupled with XRD analysis. The main drawback of the use of DSC in cocoa butter studies is again reproducibility because of the differences in cocoa butter composition from different origins.

4.1.3 Crystallisation of cocoa butter

In chocolate manufacture, the solidification process significantly influences the quantity of the final products: gloss, snap, texture, heat resistance and fat bloom resistance. Since the problems in the solidification involve different crystal structures of solid fat components ie polymorphism, conditions must be optimised to control the solidification process under which the most preferable polymorph (Form V) of cocoa butter occurs and can be preserved.

4.1.3(a) Tempering and Organoleptics

Organoleptics is the study of properties such as melting and flavour-release that are characterised by appearance, snap and lasting properties. Tempering is the ability of the fat (in chocolate) to form a solid, stable, crystalline phase in the finished product. It is a pre-crystallising process of the fat before solidification that ensures the correct form or polymorph is obtained.^[38-40] For cocoa butter in chocolate the most stable polymorph is Form V.

The most commonly used methods of tempering involve the following steps (1) to (4):

- (1) **Complete melting** of the cocoa butter, typically 100° for cocoa butter (50°C for chocolate), in order to destroy any crystal memory from previous solidifications.
- (2) **Cooling to the point of crystallisation** (around 26-27°C for cocoa butter and chocolate) to induce crystallisation of both stable (Form V) and unstable (Form IV) polymorphs.
- (3) **Crystallisation** where both stable and unstable crystals are formed.
- (4) **Melting out of unstable polymorphs** by raising the temperature to a point where the unstable polymorphs melt leaving only polymorphic stable crystals which can then 'seed' the crystallisation of the bulk fat material into a stable form. Temperatures of around 30-32° are typically used with 33°C being the upper limit.

In order to obtain a fine texture from Form V it is important to produce a large number of small seed crystals throughout the cocoa butter bulk, as opposed to a smaller number of large crystals which results in a course texture. This is done by eliminating the heat of crystallisation (latent heat) as far as possible, while encouraging formation of the largest number of small crystals (see Fig. 4.1.10).

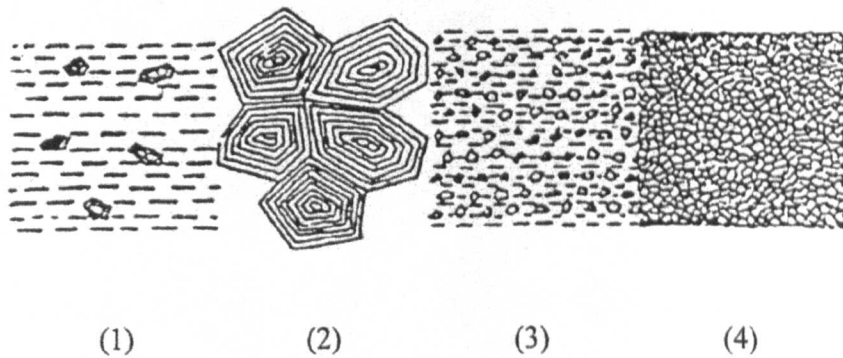


Fig. 4.1.10 Diagrammatic representation of a small proportion of large crystals and a large proportion of very small crystals on the final texture of the solidified product. (1) Insufficiently pre-crystallised, (2) large crystals are formed during solidification, resulting in a course texture, (3) very well tempered, and (4) many small crystals are formed during solidification, resulting in a fine texture.

Tempering is usually carried out in industry using dynamic heat exchangers. In addition, dynamic crystallisation is used where a rotor with scraper blades causes continuous break-up of seed crystals which are then distributed throughout the material forming very minute seeds for further crystallisation of the correct, stable cocoa butter polymorph. The influence of shearing rate (D) on nucleation time t_k of cocoa butter is shown in Fig. 4.1.11, where an increase in the shearing rate encourages the formation of the more stable Form V polymorph in cocoa butter.

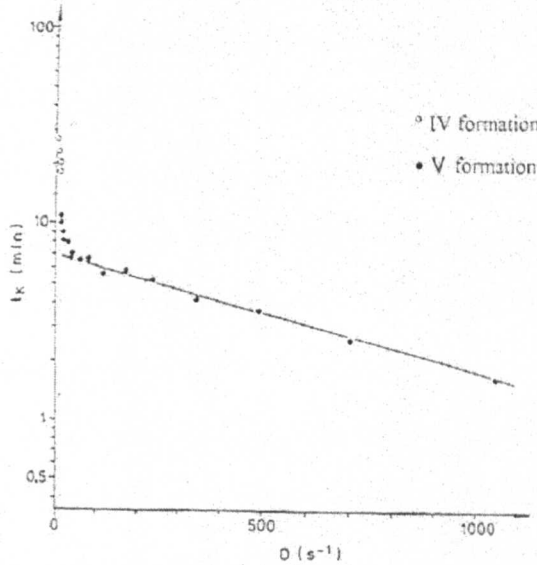


Fig. 4.1.11. Influence of shearing rate D on nucleation time t_k (logarithmic scale) of cocoa butter at 20°C .

4.1.3(b) Cocoa butter seed crystals

Seed crystal growth has been studied^[41-43] and shown to involve high levels of the triacylglycerol StOSt while partially excluding POSt, and excluding POP to a higher degree. Polarised light microscopy (PLM) has been used to study the seed crystal growth revealing a cross-sectional view of the internal structure of the crystal with scanning electron microscopy (SEM) showing the crystal surface.^[43] The first crystallisation has been shown to form a bow-tie configuration, which is enlarged primarily on the outer surfaces while the central area is constricted. The crystals spread and eventually assume a circular or spherulitic shape (Figs. 4.1.12 (a) to (h)).

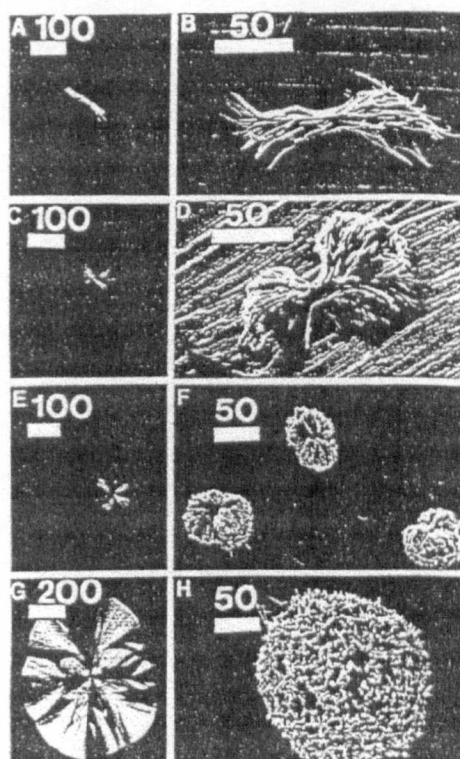


Fig. 4.1.12. (A, C, E, G) PLM micrographs of the stepwise crystal growth from 'bow-tie' seed to the 'feather' crystals, and (B, D, F, H) SEM visualisation of the stepwise crystal growth.

In comparison to cocoa butter, the seed crystals have been shown to have relatively high melting points, of around 36° to as high as 70°C in some cases. Such elevated melting points are thought to be accounted for by a difference in chemical composition in relation to the other forms of cocoa butter crystals, or by a difference in the molecular packing of the molecules. It is not thought to be an additional polymorphic form because of the dissimilar composition.

Removal of these StOSt rich seed crystals from a cocoa butter mass results in greatly increased crystallisation times. The implications are that the seed crystal material plays a critical role in the initiation of the crystallisation process.

4.1.3(c) Measurement of tempering

In industry, tempering is measured using a tempermeter, which relies on the measurement of a cooling curve of a fat as it is cooled in a specific way. The cooling curve can be printed on a chart recorder with the shape of the curve indicating the degree of tempering. Three temper curves are shown in Fig. 4.1.13 to illustrate the

degrees of crystallisation which have developed during the tempering process i.e. the curves relating to the states of temper-undertemper, temper and over temper.

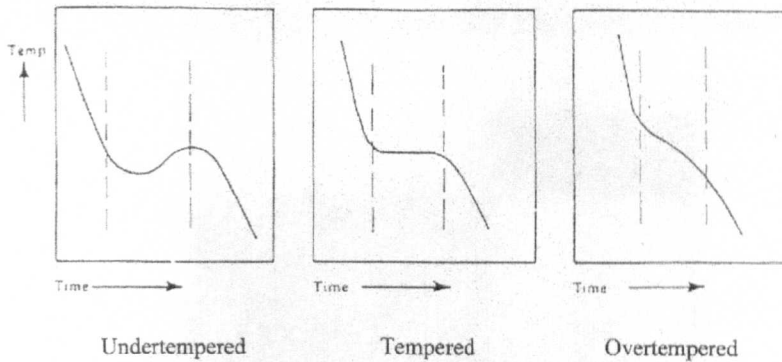


Fig. 4.1.13 Typical tempermeter curves.

The curves can be considered in three parts:

(1) Cooling of the liquid fat prior to solidification, and is similar in all cases of temper.

(2) The state of temper is defined and therefore shows the greatest difference between the three curves.

(a) Undertempered - insufficient stable fat crystals have been produced in the temper to induce further stable crystallisation in the mass and a lot of heat is released from the heat of crystallisation. This is shown in the curve as a change in slope and indicates the amount of heat being released is greater than the controlled cooling rate, therefore resulting in a temperature rise.

(b) Overtempering - much of the crystallisation has already occurred before measurement of tempering therefore less heat is produced. Again, the slope of the curve changes but in this case it is due to insufficient heat production to cause temperature rise.

(c) Perfect tempering - the amount of heat produced by crystallisation is perfectly balanced by the heat being removed during cooling and is shown as a plateau on the temper curve.

(3) Further temperature reduction of the cocoa butter samples.

The terms tempered, under- and over- tempered are terms used to describe the nature of the curves. Different materials i.e. fats or chocolate, may require any one of these tempering curves to obtain the required stable product. It is clear however, that the cooling rate must be optimised to achieve well-tempered solids.

4.1.4 Cocoa butter in chocolate

Cocoa butter is one of the main ingredients in chocolate along with milk powder and sugar. Typical relative proportions for British milk chocolate are shown below in Table 4.1.8.

	British milk chocolate %
Cocoa mass	15.8
Milk powder	13.3
Sugar	45.3
Added cocoa butter	25.4
Lecithin	0.2
Total	100
Total fat	37.5

Table 4.1.. Typical composition of British milk chocolate.

There are however many different chocolate ‘recipes’, not only for dark and milk chocolate but also for chocolates made in different countries. Different flavours can be achieved in a variety of ways eg use of fresh milk, matured milk or cooked milk, the cocoa bean origin, the method of roasting the cocoa beans etc.

An area of considerable concern has been fat bloom formation. Fat bloom in chocolate may occur for a variety of reasons: poor tempering can cause chocolate to bloom rapidly upon solidification and develop a granular crumbly texture in the interior.^[20] It can occur when added fats are incompatible with cocoa butter, and when incorrect cooling of tempered chocolates are used (especially rapid cooling, causes cracks and fissures in the chocolate that promote bloom). Warm or fluctuating storage temperatures also promote bloom.^[44] Normally fats that have a low solid fat content promote bloom,^{[24],[29],[45]} although milk fat is an exception to the rule^[46] because it lowers the melting point of chocolate and inhibits bloom formation at some levels.^[44]

Fat bloom is believed to be migration of liquid fat from cocoa butter to the surface of the chocolate and crystallises on the surface.^[47] There have been many theories proposed to explain fat bloom formation^[20,23,44,45,48-50] but the more generally accepted one involves the polymorphic transition between cocoa butter Form V to VI.

In conclusion, chocolate making is at first sight a very traditional industry, making what one would expect to be a relatively simple product, however the situation is, in reality far more complex.

4.2 METHODOLOGY AND EXPERIMENTAL TECHNIQUES

The Differential Scanning Calorimetry (DSC) was carried out using a Perkin Elmer DSC 7. The Powder X-ray Diffraction was carried out using a Philips PW1710 Diffractometer with Cu K_α radiation. The incubators used in the studies were Sanyo MIR 152 and operate at a range of $\pm 0.5^{\circ}\text{C}$ to the set temperature. The Torque stirrer used was a Heidolph RZR 2102 Electronic Torque Stirrer and PC Interface Unit with speed set by a 2.83V signal from a power pack in all cases. The interface unit used was a Laplace Instruments SPCX-TC, and the Signal Datalogger was PCXA from Laplace Instruments with software.

The principal aim of this study was to demonstrate that the crystallisation of cocoa butter could be affected by applied magnetic fields. The study involved measurement of rate of crystallisation in addition to analysis of the resulting cocoa butter polymorph.

In order to demonstrate that applied magnetic fields affect the crystallisation of cocoa butter, the system illustrated in Fig. 4.2.1 was set up. The temperature regime mimicked the tempering stage of chocolate processing that is a necessary prerequisite in chocolate manufacture and results in cocoa butter in Form V polymorph. A study under these conditions easily demonstrates any variations in Form but is also of most use and relevance from a production perspective.

The torque stirrer is set to stir at constant speed using an input voltage of 2.83V and the PC monitors the torque required to stir at this speed. All readings are obtained through the signal datalogger and interface unit. The incubator runs through a 24 hour temperature cycle in order to induce cocoa butter crystallisation. As crystallisation commences, the viscosity of the molten cocoa butter increases and the torque required by the stirrer to stir the cocoa butter at the same speed increases i.e. torque increases with the extent of crystallisation.

Several variations in temperature were applied to the cocoa butter samples during crystallisation and the cycle employed in this study, which was suitable to obtain Form V cocoa butter, is described below.

Stage 1 - Melt the cocoa butter to destroy all crystal 'memory'. This was carried out in a sealed test-tube immersed in a water bath at 80°C, ensuring that water vapour did not come into contact with the cocoa butter.

Stage 2 - The test-tube containing clear molten cocoa butter was placed in the incubator at 50°C with stirring in order to equilibrate the temperature.

Stage 3 - The incubator temperature was reduced to 26°C for 4 hours in order to induce crystallisation. Stirring is a vital part of this process since application of a shear force breaks up the cocoa butter seed crystals and increases their number within the molten cocoa butter thus aiding crystallisation.

Stage 4 - Increasing the incubator temperature to 28°C for 4 hours is part of the tempering process that melts out all the lower melting forms of cocoa butter leaving Form V seed crystals.

Stage 5 - Re-cooling the incubator temperature to 26°C induces cocoa butter crystal growth of Form V on the seed crystals that are present in the melt.

Stages 4 and 5 are repeated during a 24 hour period and results in a cocoa butter slurry which is opaque in appearance. Stirring is removed from the cocoa butter slurry and the test-tube moved to a second incubator set at 20°C where it is stored for 24 hours in order to set the cocoa butter and to stabilise it, essentially locking the Form in which it has set.

The incubators were capable of being set to operate at different temperatures, however there was no control over the rate of heating or cooling. Importance was placed on the actual cooling rates of the incubators since smoothness, reproducibility and incubator compatibility were crucial factors to be considered in this study. The cooling rates of the incubators were measured while containing molten cocoa butter samples, completely empty and with AC and DC electromagnets since these were the largest and reduced the volume of air circulating within the incubator. In addition to incubator temperatures, the

cocoa butter sample temperatures would have been a valuable measurement, however equipment failure prevented these measurements being obtained via thermocouples.

The magnetic fields were applied by two methods. The first involved placing a magnetic field around the cocoa butter sample during the entire stirring process and remained unchanged during this time while the temperature cycle was applied to the sample. The magnetic field was removed before transfer of the cocoa butter slurry to the second incubator at 20°C for setting. The second method of application involved passing the molten cocoa butter through tubing that passed through the magnetic field. Previous research has shown that the magnetic field effects increase to a maximum at 6 passes through the magnetic field, therefore 3 passes was chosen as sufficient to be able to observe applied field effects. The molten cocoa butter was then stirred, with no magnetic fields in place, and the same temperature regime as the control applied to the samples with recording of the torque measurements.

In effect, the torque measurements relate to rate of crystallisation and analysis could be carried out on the resulting cocoa butter samples. The time taken to reach maximum torque can be directly obtained from the torque measurements during stirring at constant speed. A decrease in time taken to reach maximum torque is taken to indicate enhanced crystallisation. The visual appearance of the cocoa butter samples may indicate the form of cocoa butter that has resulted from each condition of applied magnetic fields. Smooth, glossy, yellow texture that shines, tends to correspond to well tempered Form V cocoa butter, while white powder or a dull appearance indicates the presence of less stable forms within the cocoa butter i.e. Forms III or IV generally.

The resulting form of cocoa butter can be determined from (1) Powder X-ray diffraction, since each form (and mixtures) can be identified from different characteristic patterns, and (2) Differential Scanning Calorimetry giving the melting profile of cocoa butter from which the Form can be deduced.

4.2.1 Measurement of incubator cooling rates

This section of work was carried out in order to assess (a) the cooling rates of the incubators and (b) the reproducibility of these cooling rates.

4.2.1(a) Experiment 1 - Cooling rate of incubators containing hot cocoa butter

Cocoa butter (100ml) placed in a 2cm diameter sealed test-tube was heated to 80°C for 1 hour using a water bath. The test-tube containing the molten cocoa butter was placed in Incubator A set at 50°C, and the temperature held at 50°C for 30 minutes. The incubator temperature was programmed to reduce to 0°C. During the cooling process, the temperature reading on the incubator was noted every 60 seconds and the rate of cooling of the incubator calculated. This process was repeated for Incubator B.

4.2.1(b) Experiment 2 - Cooling rates of empty incubators

Empty incubators A and B were cooled from 50° to 0°C and the temperature noted every 60 seconds. The rates of cooling were calculated. This was repeated 3 times and the mean rates of cooling calculated for both empty incubators A and B.

4.2.1(c) Experiment 3 - Cooling rates of incubators containing AC or DC electromagnets and cocoa butter

Cocoa butter (100ml) placed in a 2cm diameter sealed test-tube was heated to 80°C for 1 hour using a water bath. The test-tube containing the molten cocoa butter was placed in incubator A set at 50°C with the AC electromagnet in place around the sample. The temperature was held at 50°C for 30 minutes before reducing to 0°C. During the cooling process, the temperature reading on the incubator was noted every 60 seconds and the rate of cooling of the incubator calculated. This process was repeated for Incubator B with the DC electromagnet in place around the cocoa butter sample.

4.2.2 Crystallisation of cocoa butter in applied magnetic fields

4.2.2(a) Experiment 4 - Control

The apparatus illustrated in Fig. 4.2.1 below was designed in order to study cocoa crystallisation.

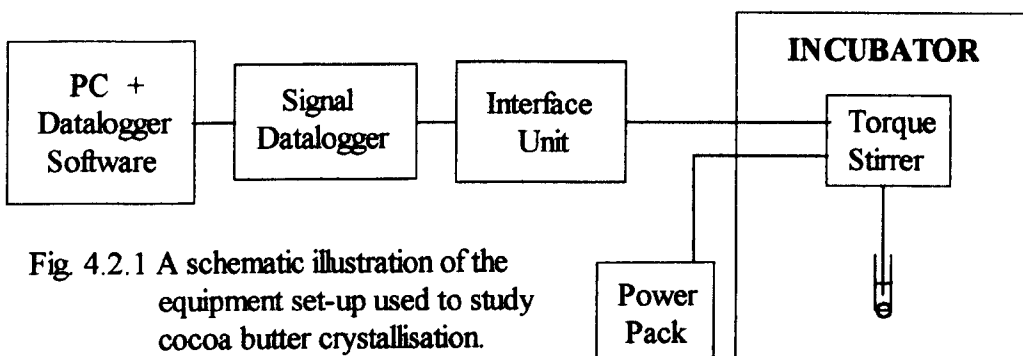


Fig 4.2.1 A schematic illustration of the equipment set-up used to study cocoa butter crystallisation.

The power pack was set to 2.83V equivalent to a stirring speed of around 280rpm. The torque was measured through the signal logger and interface unit via the voltage output from the torque stirrer. Cocoa butter (100ml) placed in a 2cm diameter sealed test-tube was heated to 80°C for 1 hour using a water bath. The test-tube containing the molten cocoa butter was placed in incubator A at 50°C with the stirring paddle inserted in the molten cocoa butter, 1cm from the bottom of the test-tube, which was then switched on. The datalogger equipment recorded torque measurements every 60 seconds while incubator A was set to run through the following cycle:

1. 50°C for 30 mins
2. 26°C for 4 hours
3. 28°C for 4 hours
4. alternating between 26° and 28°C every 4 hours during a 24 hour period.

The cooling rate of incubator A (not the cocoa butter) from 50°C was around 1°Cmin⁻¹ in the cases of control and pulsed magnets experiments and around 0.75°Cmin⁻¹ for all other experiments. The time taken to reach maximum torque during this period was recorded. The test-tube containing the cocoa butter slurry was removed from incubator A and placed in incubator B at 20°C for 24 hours in order to set the cocoa butter.

Following removal of the set cocoa butter from the test tube, visual texture and surface features of the cocoa butter were noted. Powder XRD and DSC measurements were made on the resulting cocoa butter samples.

4.2.2(b) Experiment 5 - Crystallisation in a permanent magnetic field

The same procedure of crystal preparation carried out on the Control experiment was followed with the addition of permanent magnets (arrangement and field strengths are illustrated in Fig. 4.2.2) around the test-tube containing the cocoa butter following placement in incubator A.

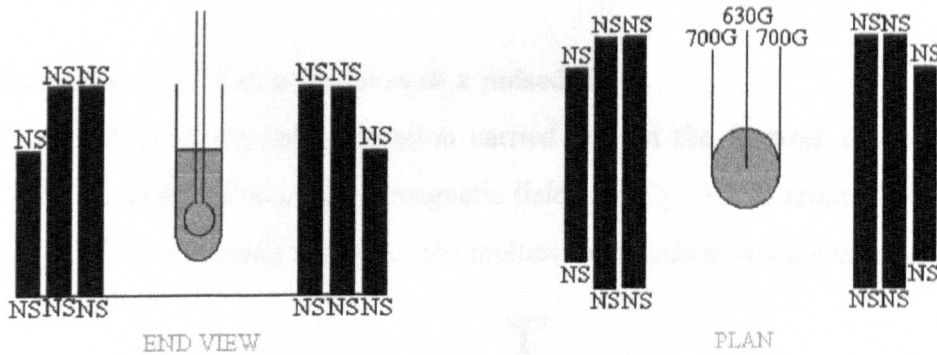


Fig. 4.2.2 An illustration of the permanent magnetic field set-up used in Experiment 5.

4.2.2(c) Experiment 6 - Crystallisation in a DC electromagnetic field

The same procedure of crystal preparation carried out on the Control experiment was followed with the addition of a DC electromagnet (set to operate at 12V and illustrated below in Fig. 4.2.3) around the test-tube during stirring of the molten cocoa butter in Incubator.

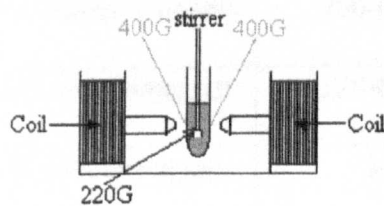


Fig. 4.2.3 An illustration of the DC electromagnetic field set-up used in Experiment 6.

4.2.2(d) Experiment 7 - Crystallisation in an AC electromagnetic field

The same procedure of crystal preparation carried out on the Control experiment was followed with the addition of an AC electromagnetic field (as illustrated below in Fig. 4.2.4) around the test-tube during stirring of the molten cocoa butter in incubator A.

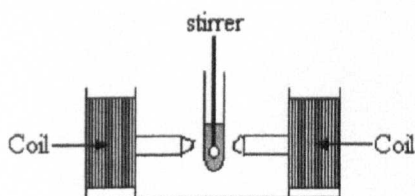


Fig. 4.2.4 An illustration of the AC electromagnetic field set-up used in Experiment 7.

4.2.2(e) Experiment 8 - Crystallisation in a pulsed field

The same procedure of crystal preparation carried out on the Control experiment was followed with the addition of a pulsed magnetic field (see Fig. 4.2.5) around the test-tube containing cocoa butter during stirring of the molten cocoa butter in incubator A.

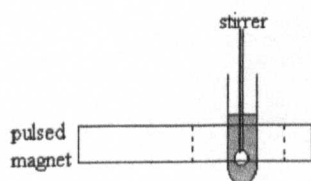


Fig. 4.2.5 An illustration of the pulsed field set-up used in Experiment 8.

The magnets used in each experiment are summarised in Table 4.2.1 below.

Experiment No.	Field Type	Frequency/Strength	Geometry
4	Control	N/A	N/A
5	Permanent magnets	700-630 Gauss	N-S, NH Parallel at sides
6	DC-electromagnet	220-600 Gauss	N-S, NH Parallel at sides
7	AC-electromagnet	240kHz	Alternating
8	Pulsed	100-160kHz	N-S, NH Around sample

where N-S is North-South geometry and NH is Non-homogeneous

Table 4.2.1 Summary of applied fields employed in Experiments 4 to 8.

4.2.3 Crystallisation of cocoa butter following magnetic treatment

4.2.3(a) Experiment 9 - Magnetic treatment using permanent magnets

Cocoa butter in a sealed 2.0cm diameter test-tube was heated at 80°C for 1 hour. The molten cocoa butter was syphoned through 1m length of 4mm diameter silicon tubing at 0.12lmin⁻¹ within Incubator A at 50°C from test-tube A into test-tube B as illustrated below in Fig. 4.2.6.

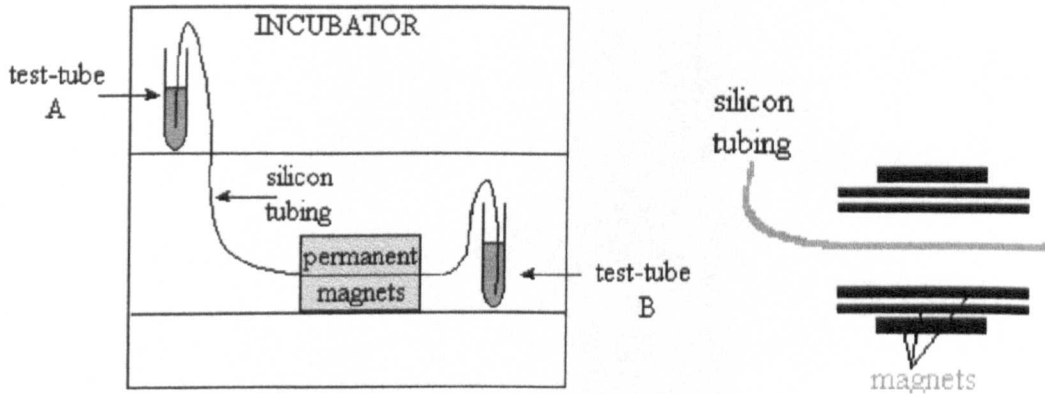


Fig. 4.2.6 An illustration of the apparatus set-up used to apply a permanent magnetic field to molten cocoa butter.

The silicon tubing passes through the centre of the permanent magnets illustrated in Fig.4.2.2. Test-tube B was exchanged with test-tube A, and the syphoning process repeated. This process was repeated up to three passes through the permanent field. The cocoa butter contained in the test-tube then undergoes the same temperature cycle described in Experiment 4. The time taken to crystallise was measured and visual texture and surface features of the resulting cocoa butter were noted with Powder XRD and DSC measurements performed on the sample.

4.2.3(b) Experiment 10 - Magnetic treatment using a DC electromagnet

The same procedure as Experiment 9 was carried out with the DC electromagnet in place of the permanent magnets as illustrated below in Fig. 4.2.7.

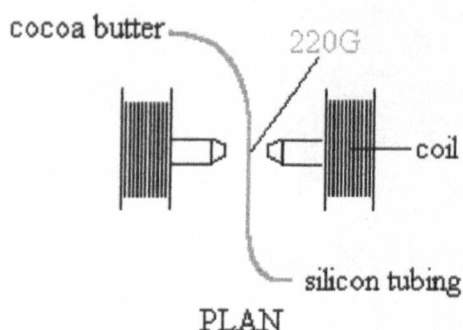


Fig. 4.2.7 An illustration of apparatus set-up used to apply DC electromagnetic field to cocoa butter.

Visual texture and surface features of the cocoa butter were recorded. Powder XRD and DSC techniques were applied to the resulting cocoa butter sample.

4.2.3(c) Experiment 11 - Magnetic treatment using an AC electromagnet

The same procedure as Experiment 9 was carried out with the AC electromagnet in place of the permanent magnets as illustrated below in Fig. 4.2.8.

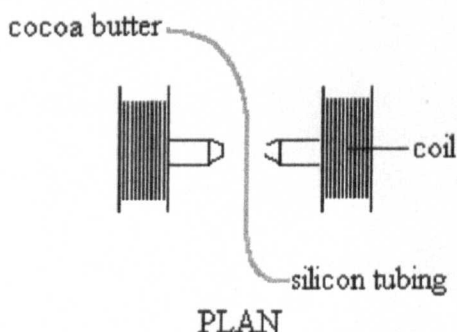


Fig. 4.2.8 An illustration of apparatus setup used to apply an AC electromagnetic field to cocoa butter.

Visual texture and surface features of the cocoa butter were recorded. Powder XRD and DSC techniques were applied to the resulting cocoa butter sample.

4.2.3(d) Experiment 12 - Magnetic treatment using an pulsed magnet

The same procedure as Experiment 9 was carried out with the silicon tube passing through the centre of the pulsed magnet as illustrated below in Fig. 4.2.9.

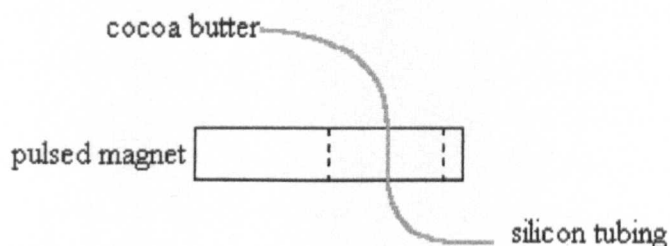


Fig. 4.2.9 An illustration of the pulsed magnetic field setup applied to molten cocoa butter.

Visual texture and surface features of the cocoa butter were recorded. Powder XRD and DSC techniques were applied to the resulting cocoa butter sample.

The magnets used in each experiment are summarised in Table 4.2.2 below.

Experiment No.	Field Type	Frequency/Strength	Geometry
9	Permanent magnets	650G	N-S, NH Parallel at sides
10	DC electromagnet	220G	N-S, NH Parallel at sides
11	AC electromagnet	240kHz	Alternating
12	Pulsed	100-160kHz	N-S, NH Tubing through centre

where N-S is North-South geometry and NH is Non-homogeneous
Table 4.2.2 Summary of applied fields employed in Experiments 9 to 12.

4.3 RESULTS AND DISCUSSION

4.3.3 Results

4.3.3(a) Incubator studies

The results for Experiment 1 are illustrated in Figures 4.3.1 and 4.3.2. The rate of cooling was calculated to be $-1.1\text{ }^{\circ}\text{Cmin}^{-1}$ and $-1.0\text{ }^{\circ}\text{Cmin}^{-1}$ for incubators A and B respectively.

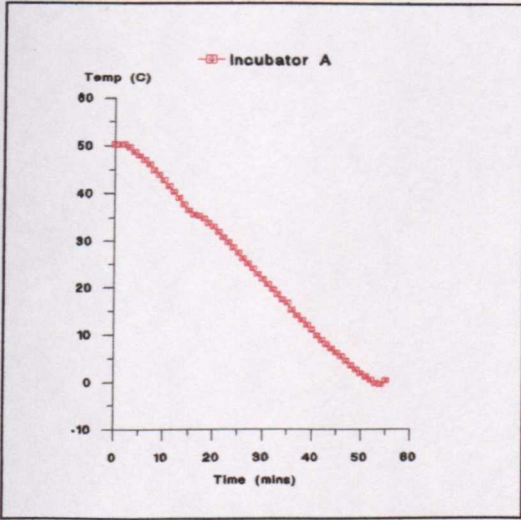


Fig. 4.3.1 Cooling rate for Incubator A, Experiment 1.

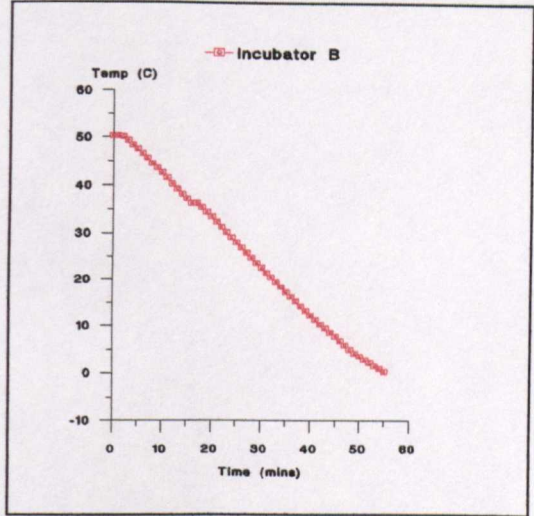


Fig. 4.3.2 Cooling rate for Incubator B, Experiment 1.

Experiment 2 involved four repeats of testing the incubators through their temperature cycles in the absence of cocoa butter samples present. The results are shown in Figures 4.3.3 to 4.3.6 for Incubator A and Figures 4.3.7 to 4.3.10 for Incubator B. Figures 4.3.11 and 4.3.12 show the mean cooling cycles for incubators A and B determined by averaging the temperature readings taken from the four repeated cycles and include the standard deviations in the form of error bars. Incubator A shows an average cooling rate of $-1.04^{\circ}\text{Cmin}^{-1}$ and Incubator B $-1.02^{\circ}\text{Cmin}^{-1}$. All tests gave smooth cooling curves for both incubators as shown in the graphs.

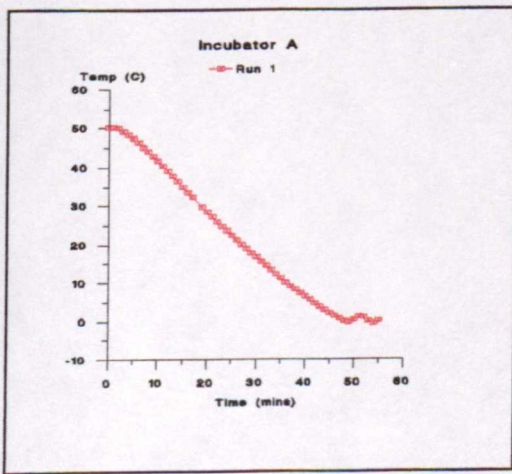


Fig. 4.3.3 Cooling rate for Incubator A, Experiment 2.

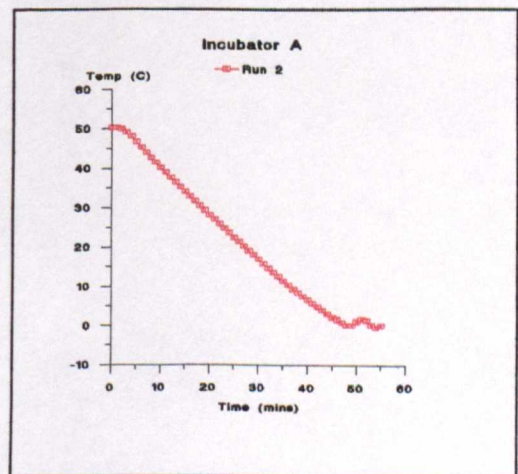


Fig. 4.3.4 Cooling rate for Incubator A, Experiment 2.

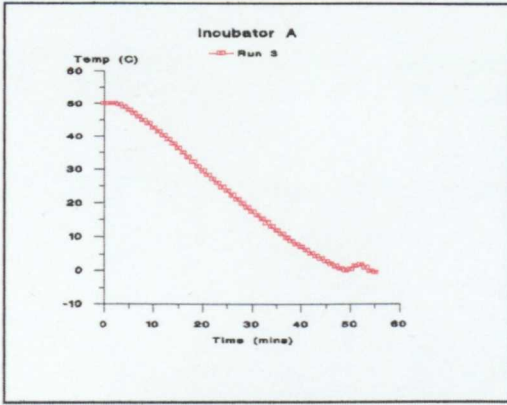


Fig. 4.3.5 Cooling rate for Incubator A, Experiment 2.

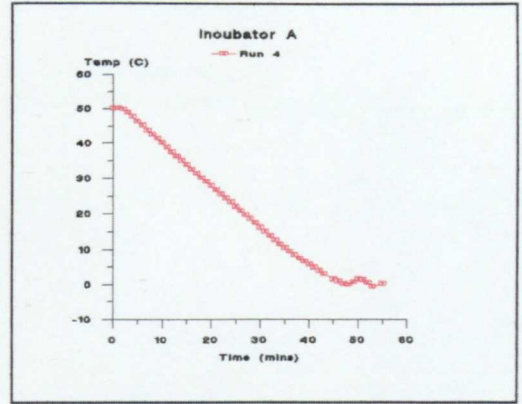


Fig. 4.3.6 Cooling rate for Incubator A, Experiment 2.

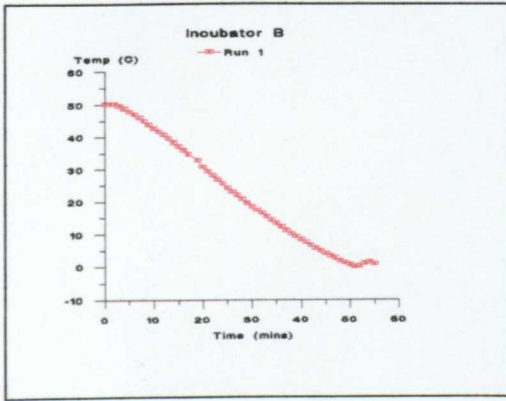


Fig. 4.3.7 Cooling rate for Incubator B, Experiment 2.

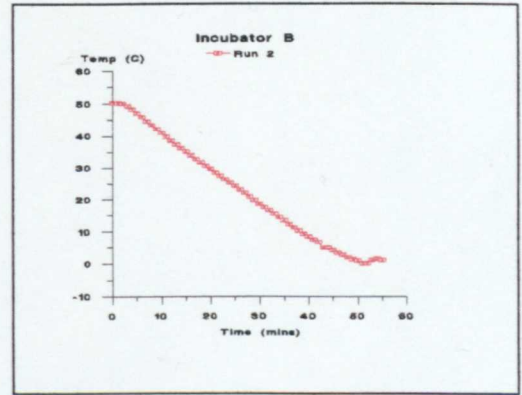


Fig. 4.3.8 Cooling rate for Incubator B, Experiment 2.

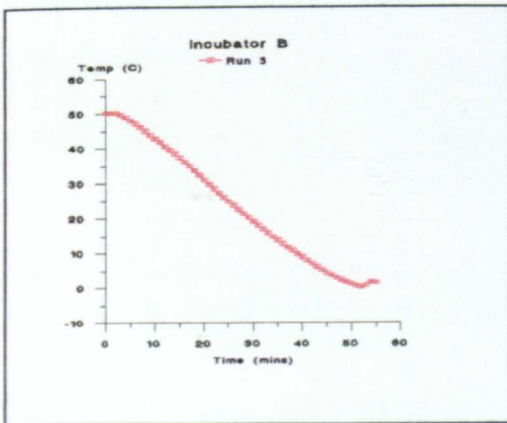


Fig. 4.3.10 Cooling rate for Incubator B, Experiment 2.

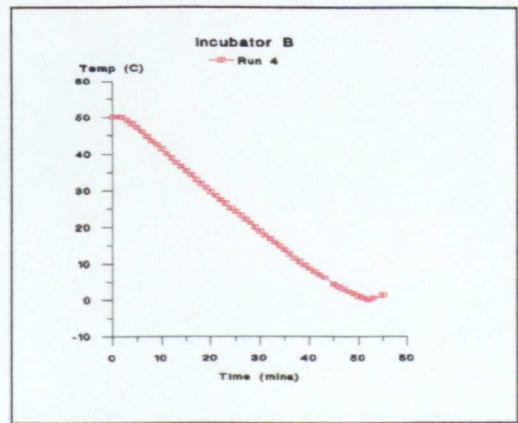


Fig. 4.3.11 Cooling rate for Incubator B, Experiment 2.

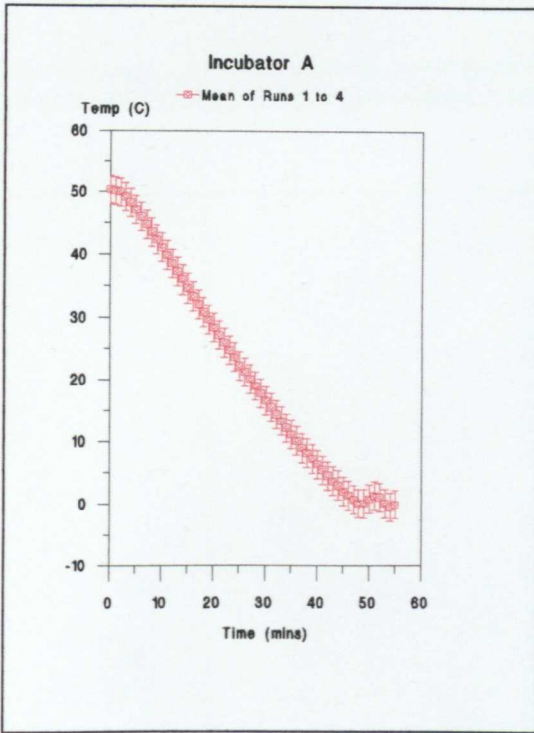


Fig. 4.3.11 Mean cooling rate for Incubator A from Experiment 2, with standard deviation error bars.

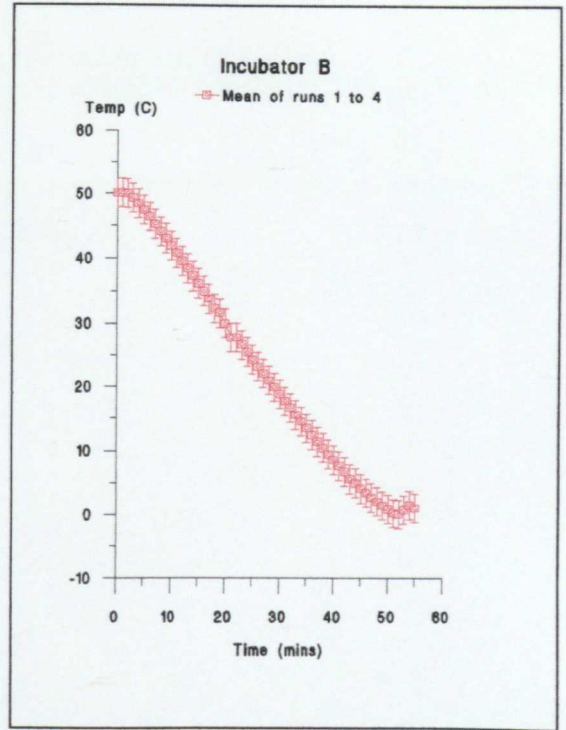


Fig. 4.3.12 Mean cooling cycle for Incubator B from Experiment 2, with standard deviation error bars.

The cooling rate measurements for Experiment 3 with the AC and DC magnets in Incubators A and B respectively are shown in Figures 4.3.13 and 4.3.14. The cooling rate for Incubator A was measured to be $-0.74^{\circ}\text{Cmin}^{-1}$ and $-0.73^{\circ}\text{Cmin}^{-1}$ for Incubator B.

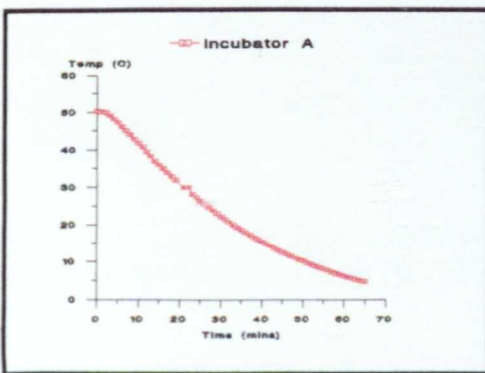


Fig. 4.3.13 Cooling rate for Incubator A, Experiment 3.

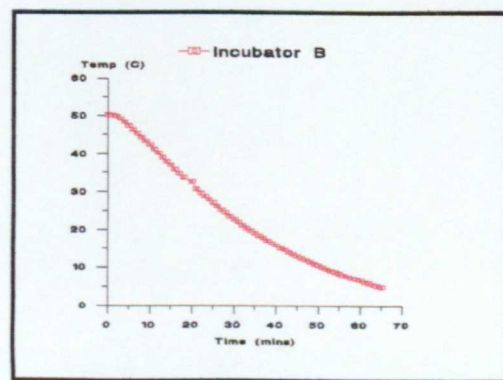


Fig 4.3.14 Cooling rate for Incubator B, Experiment 3.

4.3.3(b) Crystallisation of cocoa butter in applied magnetic fields

The visual observations recorded for Experiments 4 to 8 are given below in Table 4.3.1.

Applied Field	Experiment Number	Visual appearance
Control	4	Very smooth, shiny, yellow and glossy
Permanent magnets	5	Smooth, shiny, yellow and glossy
DC electromagnets	6	Mostly, smooth and glossy, some areas of white powder
AC electromagnets	7	Smooth, shiny, yellow and glossy
Pulsed	8	Mostly smooth and glossy, some areas of white powder

Table 4.3.1 Summary of the visual appearances of the cocoa butter samples.

The time taken to reach maximum torque measurements recorded for Experiments 4 to 8 are given below in Table 4.3.2 as crystallisation times.

Applied Field	Experiment Number	Time taken to crystallise (hours)
Control	4	21
Permanent magnets	5	15
DC electromagnets	6	16
AC electromagnets	7	19
Pulsed	8	16

Table 4.3.2 Summary of time taken to reach maximum torque measurements (crystallisation).

The Powder X-ray Diffraction measurements recorded for each cocoa butter sample are summarised below in Table 4.3.3. Each measurement was carried out twice.

Applied Field	Experiment Number	Cocoa butter Form
Control	4	100% Form V
Permanent magnets	5	100% Form V
DC electromagnets	6	25% Form VI : 75% Form V
AC electromagnets	7	100% Form V
Pulsed	8	20% Form VI : 80% Form V

Table 4.3.3 Summary of the Powder X-ray diffraction data.

A summary of the Differential Scanning Calorimetry data recorded for each cocoa butter sample is given below in Table 4.3.4. Each measurement was repeated and gave identical results.

Applied Field	Experiment Number	Melting Points (°C)
Control	4	32.2
Permanent magnets	5	32.4
DC electromagnets	6	32.4
AC electromagnets	7	31.9
Pulsed	8	31.7

Table 4.3.4 Summary of DSC data.

4.3.3(c) Crystallisation of cocoa butter following magnetic treatment

The visual observations recorded for Experiments 9 to 12 are given below in Table 4.3.5.

Applied Field	Experiment Number	Visual appearance
Permanent magnets	9	Very smooth, shiny and glossy, with some areas of white powder
DC electromagnets	10	Very smooth, shiny, yellow and glossy
AC electromagnets	11	Smooth, glossy and some areas of white powder
Pulsed	12	Very glossy, smooth, yellow and shiny

Table 4.3.5 Summary of the visual appearances of the cocoa butter samples.

The time taken to reach maximum torque measurements recorded for Experiments 9 to 12 are given below in Table 4.3.6 as crystallisation times.

Applied Field	Experiment Number	Time taken to crystallise (hours)
Permanent magnets	9	14
DC electromagnets	10	14
AC electromagnets	11	13
Pulsed	12	17

Table 4.3.6 Summary of time taken to reach maximum torque measurements (crystallisation).

The Powder X-ray Diffraction measurements recorded for each cocoa butter sample are summarised below in Table 4.3.7. Repeating each measurement resulted in reproducible data.

Applied Field	Experiment Number	Cocoa butter Form
Permanent magnets	6	100% Form V
DC electromagnets	7	100% Form VI
AC electromagnets	8	100% Form V
Pulsed	9	100% Form VI

Table 4.3.7 Summary of the Powder X-ray diffraction data.

A summary of the Differential Scanning Calorimetry data recorded for each cocoa butter sample is given below in Table 4.3.8. Each measurement was reproducible.

Applied Field	Experiment Number	Melting Points (°C)
Permanent magnets	9	11.7, 16.3, 19.1
DC electromagnets	10	29.5, 32.3, 33.8
AC electromagnets	11	26.4, 32.7
Pulsed	12	30.3, 32.4, 33.6

Table 4.3.8 Summary of the DSC data.

4.3.4 Discussion

4.3.4(a) Incubator studies

In order to determine whether or not reproducibility could be achieved it was important to become familiar with the incubators capabilities: were the cooling rates consistent and were they similar for Incubators A and B?

The incubators could be set to a particular temperature for a length of time and then programmed to go another set temperature for a given time for up to 3 set temperatures. In addition, they could also be set to go through a repeated temperature cycle with up to 99 repeats. The only disadvantage of the Sanyo Mir 152 incubators was that the rates of cooling or heating between set temperatures was not controllable. These rates were controlled by the heating and cooling elements within the incubators and an important part of the preliminary work was to ascertain whether or not these rates were consistent or not.

Experiment 1 was carried out as a trial. A 2cm diameter test-tube containing around 200ml molten cocoa butter at 80°C was placed in the centre of Incubators A and B. Both incubators were set at 50°C and held at this temperature for 30 minutes in order to equilibrate the temperature of the cocoa butter with that of the incubators. The temperature of the incubators was then reduced to 0°C and the incubator temperature readings noted every 60 seconds during this process.

Figures 4.3.1 and 4.3.2 show the cooling curves obtained during the cooling process. At around 35-36°C there is a point of inflection in the cooling curve. Since the

experiment involves a phase change in the cocoa butter i.e. crystallisation from liquid to solid, an associated temperature rise would be expected since it is normally an exothermic process, therefore the ambient temperature of the incubators would be raised slightly as shown by the discontinuity in the cooling curve i.e. the point of inflection.

The cooling rates calculated for both incubators is 1.1 (Inc. A) and 1.0°Cmin⁻¹ (Inc. B), however since the experiment was carried out only once, it was not possible to conclude whether the cooling processes were reproducible or not. It could only be noted that the cooling rates were very similar for both incubators.

In order to verify that the discontinuity in the cooling curves is due to the phase change of the cocoa butter it was necessary to carry out a repeat of Experiment 1 with the exclusion of the cocoa butter sample within the incubators during cooling.

The cooling data obtained for empty Incubators A and B (Experiments 2) are shown in Figures 4.3.3 to 4.3.12. Runs for both incubators showed no discontinuity therefore the cocoa butter phase change explanation was presumed to be valid and a further 3 repeats of the experiment were carried out. The mean cooling rates for both incubators were 1.04 and 1.02°Cmin⁻¹ which is considered to be consistent enough to obtain reproducible data regardless of the incubator used. The standard deviations at maximum were ± 1.3 with reference to the mean temperature and more generally were considerably less than this value. This was considered to be suitable for the reproducibility required for the purposes of this study.

The process of temperature control of the environment within the incubator requires some consideration. The temperature is controlled via circulation of air using a fan, within the dimensions 60×45×80cm. In the case of objects placed within the incubators, the volume of circulating air would be reduced, therefore an important consideration would be the effect on the cooling rate under reduced air volume, for example in the cases of use of AC or DC electromagnets which were of greatest size.

Experiment 3 was therefore carried out in order to establish the greatest deviation from empty incubator cooling rates obtained and the results are shown in Figures 4.3.13 and 4.3.14. Incubator A contained the AC electromagnet and Incubator B contained the DC electromagnet and the measured cooling rates were 0.74 and 0.73°Cmin⁻¹ respectively. The volume of both AC and DC electromagnets for the purpose of this experiment were considered to be identical since the dimensions were identical to ±2cm in all directions, therefore for the purposes of this study the cooling rates could be considered to vary between 1.0-0.75°Cmin⁻¹ depending on the magnet applied to the sample. This was considered to be within acceptable range for the purposes of this study.

4.3.4(b) Conclusion

The experiments carried out on Incubators A and B were sufficient to conclude that reproducible temperature cycles could be achieved. Cooling cycles only were applied in the study since the rates were of such similar magnitude to allow the assumption that both incubators were comparable. In addition, different magnets placed within the incubators did not dramatically alter the rates of cooling, however, when using the pulsed magnet and permanent magnets (which are smaller in volume), additional sealed glass bottles were placed within the incubator to reduce the volume of circulating air to comparable levels with those of the electromagnets.

4.3.4(c) Crystallisation of cocoa butter in applied magnetic fields

The first stage of this study was to be able to reproducibly prepare a control with standard times of crystallisation and identical form in each case. The first stage of cocoa butter melting is very important. Each cocoa butter sample must be completely melted in liquid form with no possibility of the presence of solid material within the melt prior to crystallisation. The standard method is to hold the cocoa butter temperature to at least 80°C for at least 1 hour. This in effect destroys any 'crystal memory'.

Standard cooling and a temperature cycles of between 28 to 30°C (each held for 4 hours following melting) would be sufficient to produce Form V cocoa butter.

However this is a measurement of sample temperature. Since it was not possible to obtain sample temperature measurements, with only incubator measurements available, some variations of this temperature were carried out in order to achieve optimum Form V crystallisation. This was achieved by reducing the set temperatures to vary between 26 and 28°C which was in effect circulating air temperature and resulted in production of cocoa butter in the glossy form associated with Form V.

The time taken to reach maximum torque for the control was 21 hours. Following this time the torque measurements varied slightly with temperature, decreasing slightly when set at the higher temperature of 28°C as expected. The first sample was run for a 36 hour period to confirm that no higher value of torque could be obtained while stirring at the particular constant speed. All subsequent experiments were carried out for 24 hours only. The control experiment was carried out a total of 3 times and in each case gave a time to reach maximum torque measurement of 21 hours. The system was therefore considered sufficient to produce reproducible cocoa butter crystallisation results and analysis was carried out on all three samples of cocoa butter obtained.

In all cases the cocoa butter form obtained was shown (from Powder XRD data) to be 100% Form V and melting point data from DSC were consistent with this finding. All subsequent Powder XRD and DSC data obtained were recorded in duplicate, and found to give similar traces.

The crystallisation of cocoa butter was then carried out in an identical manner to the control with the only difference being the presence of the magnetic fields around the test-tube containing the molten, stirred cocoa butter. Differences in the visual texture and surface of the resulting cocoa butter samples was a good indication of whether the cocoa butter was a pure or mixed form.

4.3.4(d) Conclusions

It was possible to reproducibly prepare a cocoa butter sample of Form V using the incubators that could be used as the standard or 'Control'. In each case of 3 repeats, all data indicated 100% Form V cocoa butter. Permanent magnets and DC

electromagnets around the cocoa butter sample during crystallisation gave similar smooth, shiny, glossy cocoa butter forms, that analysis demonstrated to be 100% pure Form V cocoa butter. Both AC and pulsed magnetic fields resulted in white powdered areas within the cocoa butter samples which are similar in appearance to fat bloom, and correspondingly, these samples were shown by Powder XRD to contain a percentage of Form VI cocoa butter in addition to the Form V as expected. All samples demonstrated similar melting profiles and melting points consistent with Form V cocoa butter. The most significant area of interest however, was the enhanced rate of crystallisation of the cocoa butter obtained in all cases under applied magnetic field conditions. The implications are that production times (length of time taken to temper cocoa butter in chocolate processing) possibly may be reduced by up to 25% while continuing to obtain Form V cocoa butter.

In chocolate production however, the situation of placing tempering equipment in the centre of a magnetic field would be both costly and difficult and a more ideal situation would be to pass the molten mixture through a magnetic field (or a series of magnetic fields) prior to tempering. This is what is meant by 'magnetic treatment'.

4.3.4(e) Crystallisation of cocoa butter following magnetic treatment

A standard cocoa butter crystallisation is not required in the magnetic treatment study, since the original Control (Experiment 1) follows an identical crystallisation process and temperature cycle but without the magnetic treatment. There was limited time available to perform a more rigorous study into the magnetic treatment of crystallisation of cocoa butter, therefore it was important to choose a system that would demonstrate applied field effects. Previous work on sucrose demonstrated that the effects maximise around 5 or 6 passes through a magnetic field and then reduce following this number. Based on these observations, 3 passes through the magnetic field was chosen as sufficient to demonstrate the applied field effects.

In all cases, the cocoa butter was heated to 80°C during a period of 1 hour. The molten liquid was then transferred to an incubator set at 50°C and passed through the silicon tubing using syphoning, which passed through the centre of the specified

magnetic fields. This was repeated twice before the standard temperature cycle was applied to the cocoa butter sample. The time taken to carry out the procedure was generally 10 minutes and the temperature did not fall below 65°C during this time before equilibrating the cocoa butter temperature to 50°C for 30 minutes prior to application of the cooling cycle. Following each experiment, the silicon tubing had water at 80°C mixed with detergent run through, to remove all traces of residual cocoa butter since any solid cocoa butter within the tubing would have the capacity to act as a seed.

The permanent magnetic treatment (Experiment 9) of cocoa butter resulted in a reduced time to reach maximum torque measurement of 14 hours, a reduction in possible processing time of one third. Again, it appears that crystallisation has been enhanced. However, the resulting cocoa butter sample is a mixture of very smooth glossy texture and white powdery areas indicating the possibility of a mixture of cocoa butter forms within the sample.

The XRD data confirms a 100% Form V structure which would not be expected from the visual observations. The pattern was repeated giving similar results. The DSC was very different to all the previous cocoa butter samples and showed a melting profile with 3 peaks. The data were re-recorded on a different sample but gave similar results. The first melting peak around 11°C is particularly low, even when considering Form I polymorph of cocoa butter with melting point at around 17°C, however it is considerably smaller and broader than the higher melting peaks. Both peaks around 16° and 19°C are considerably sharper than the first, however these values are considerably less than would be expected from melting of Form V cocoa butter.

An explanation for the conflicting data is that there was a time gap of around 6 weeks between completion of the experiment and obtaining the DSC data, whereas the XRD data was obtained immediately after crystallisation. The duplicate experiment showed similar results for the same time scale.

Magnetic treatment applied to the molten cocoa butter using a DC electromagnetic field (Experiment 10) also resulted in a reduced time taken measured to reach maximum torque of 14 hours (with comparison to 21 for the Control) during crystallisation, a possible reduction in processing time of one third, again demonstrating crystallisation enhancement. The texture of the resulting sample was particularly smooth, glossy and shiny, however it was more yellow in colour than all previous samples.

The XRD data is indicative of 100% Form VI cocoa butter, however the DSC shows three melting points indicative of a mixture of Forms IV, V and possibly VI in rising order of areas under each peak. This is the first sample that has demonstrated a higher melting point around 34°C which is assumed to be Form VI cocoa butter. An explanation for the conflicting data may be related to the time difference (6 weeks) between obtaining both sets of data, however without further investigation this cannot be clarified.

Use of the AC magnetic field for magnetic treatment of the crystallising cocoa butter (Experiment 11) resulted in a cocoa butter sample of mixed texture indicating that the sample may be more than one polymorphic form. The time to reach maximum torque during crystallisation, measured to be 13 hours, again signified an enhancement of crystallisation as a result of the applied field and would cut processing time by one third. The XRD data is indicative of Form V cocoa butter (taken immediately following processing), however there was a delay of 6 weeks, due to equipment availability, before the DSC analysis was carried out. There are two melting points shown in the data, the first around 26° is very broad and the second melting peak is far more defined at 32.7°C and is most likely to be Form V cocoa butter. The DSC results indicate the cocoa butter sample to be a mixture of Form V and Form IV. Again polymorphic transitions during storing at room temperature before the DSC data was obtained is offered in explanation for the inconsistent data.

Crystallisation of cocoa butter following treatment using the pulsed magnetic field (Experiment 12) resulted in a very smooth and glossy sample. In addition the cocoa

butter was more yellow in colour than most previous samples with the exception Experiment 10 using the DC electromagnet which was comparable. The time taken to reach maximum torque for the pulsed magnetic field study was again reduced to a value of 17 hours (21 for Control). While the enhancement of crystallisation was not to the same extent as the other experiments in this study, it has reduced the possible processing time by around one quarter. Repeating the experiment gave similar results.

The XRD data indicates that 100% pure Form VI has been obtained in the resulting cocoa butter sample. The DSC data conflicts once again with this information, since 3 melting points were measured, and indicates a mixture of forms within the sample. The DSC data may however be following polymorphic transitions during the 6 week time difference in data collection for each technique. The DSC melting points were similar to those obtained from Experiment 10 which suggest a mixture of Forms IV, V and VI cocoa butter. It is possible that the stronger yellow colour is related to presence of the higher melting form of the cocoa butter within the sample. Repeating the experiment did not result in any differences in data.

4.3.4(d) Conclusions

Cocoa butter samples crystallised following magnetic treatment with permanent magnets and the AC electromagnet were shown to be 100% Form V cocoa butter, although the DSC data indicated the samples to be a mixture low melting polymorphs. The DC electromagnetic and pulsed field treated samples were particularly glossy and smooth in texture and more yellow in colour than any previous cocoa butter samples and had a higher melting form present which is assumed to be Form VI. This coupled with the XRD data appears to indicate that the applied fields are capable of polymorphic modification to the higher melting Form VI cocoa butter which is not normally possible under these conditions. These results, coupled with the greatly enhanced crystallisation rates are significant results and promote the argument for incorporating applied magnetic fields into future production development, since application of the magnetic fields around a flowing system demonstrates significant effects. The main area for concern is the time delay in obtaining the DSC data that was not experience with the first set of data.

Obviously, to stop the investigation at cocoa butter limits use since, investigation of the application of applied fields to chocolate is the ultimate aim where one would hope to observe similar effects.

4.4 CONCLUSIONS

This investigation has demonstrated the effect of applied fields on a temperature controlled environment of a crystallising cocoa butter system. Firstly, in all cases of applied field, whether during the crystallisation process or via magnetic treatment, the time taken for cocoa butter crystallisation has been reduced by as much as a third in some cases. It would be hoped that application of applied magnetic fields to chocolate production may have similar effects and similar benefits. The second point to note is the crystal form modification that has occurred during the processing. Some applied fields appear to enhance production of Form VI cocoa butter on the strength of the Powder XRD results, however a more in depth study would be required.

The study has demonstrated that applied magnetic fields have an effect on the crystallisation of cocoa butter via (a) enhancing crystallisation, and (b) modifying the cocoa butter polymorph.

The Lorentz effect could be offered as the most likely explanation since both systems are dynamic. Magnetic treatment of the cocoa butter, where the magnetic fields are applied to a completely molten sample, has shown the greatest observed changes in the cocoa butter, thus, the Evan's Effects cannot be applied as a rational explanation for these results since it is assumed the system contains no solid/liquid interfaces. The Evan's Effects can however still be applied as an explanation where crystallisation is carried out within the magnetic fields, since the magnetic field is applied during crystal growth, where the solid/liquid interfaces from growing seed crystals would be present. It would be interesting to carry out magnetic treatment studies where the cocoa butter is treated with different magnetic field strengths and flow rates in order to determine if there is a correlation with the extent of the magnetic effects. If any observed correlation were to exist, the Lorentz effects would be the most probable mechanism.

This work supports the pre-nuclear cluster theory since there is no other explanation that could account for the applied magnetic field effects on the molten cocoa butter system observed in this study. This would explain the enhanced crystallisation observed in both studies, however this cannot be substantiated nor dismissed since no proven mechanism can be suggested.

This leaves a number of questions unanswered, with regard to the mechanism of crystallisation enhancement and further work would have to be carried out in order to support the Lorentz effect as being the most plausible explanation for the observed effects.

This study has the potential to revolutionise chocolate manufacture, since not only have crystallisation enhancement effects been demonstrated but modification of polymorph to Form VI cocoa butter has been demonstrated. Production times could be cut in addition to possible shelf-life enhancements and reduction of fat bloom, however a great deal of further work must be carried out before this can be achieved.

There is much scope for future work based on the results obtained in this study. It would be more appropriate during all experimental work to obtain sample temperature measurements enabling monitoring of phase transitions during crystallisation which could possibly elucidate more information on the resulting cocoa butter form. Following sample measurement implementation, the most obvious area to proceed would be application of a range of applied fields in both applied magnetic fields and magnetic treatment of cocoa butter studies in order to disclose whether an optimum field strength exists or not, to maximise applied field effects during crystallisation of cocoa butter.

In addition to this, the effect of the number of passes of molten cocoa butter through a magnetic field would be worth investigation, firstly, in order to obtain information on optimising the enhancement of crystallisation but also secondly, for use as a direct comparison on a molten system with the results obtained using sucrose solutions demonstrating maximum applied field effects obtained with 5 or 6 passes.

An interesting experiment could be to apply a magnetic field while the temperature was held at 50°C then remove before beginning the cooling cycle. This would be a simpler form of magnetic treatment and would be easier to perform.

4.5 REFERENCES

- [1] *Encyclopaedia Britannica*, Encyclopaedia Britannica Inc., Chicago
- [2] Whymper, R., *Cocoa and Chocolate, Their chemistry and Manufacture*, Churchill, London, 1912
- [3] Beckett, S.T., *Industrial Chocolate Manufacture and Use*, 2nd Ed., Blackie Academic and Professional, Glasgow, Ed. Beckett, 1994, Ch. 1
- [4] Harwood, J.L., *Chemistry and Industry*, 1991, Part 10, 753-756
- [5] Beckett, S.T., *School of Science Review*, 1988, **70**, Part 251, 49-58
- [6] Minifie, B.W., *Chocolate, Cocoa and Confectionery*, 2nd Ed., Avi Publishing Co. Inc., Westport, Connecticut, 1980
- [7] Cook, L.R., *Chocolate Production and Use*, Harcourt Brace Jovanovitch, New
- [8] Hernandez, B., Castellote, A.I. and Permanyer, J.J., *Food Chem.*, 1991, **41**, 269-276
- [9] Shukla V.K.S., *Lipid Tech.*, 1995, **7**, No. 3, 54-57
- [10] Larsson, K., *Fette Seifen Anstrich.*, 1972, **74**, 136-142
- [11] Larsson, K., *Food Microstruct.*, 1982, **1**, 55-62
- [12] Dimick, P.S., *The Manufact. Confect.*, 1991, Part 5, 109-114
- [13] Duffy, P., *J. Chem. Soc.*, 1852, **5**, 197
- [14] Clarkson, C.E. and Malkin, T., *J. Chem. Soc. London*, 1934, Part I, 666-671
- [15] Lutton, E.S., *J. Am. Oil Chem. Soc.*, 1945, **67**, 524-527
- [16] Bailey, A.E., *Melting and solidification of fats*, Interscience Publishers Inc., New York, 22-24
- [17] Larsson, K., *Fette Seifen Anstrich.*, 1972, **74**, 136-142
- [18] Lutton, E.S., *J. Am. Oil Chem. Soc.*, 1972, **49**, 1-9
- [19] Vaeck, S.C., *Rev. Int. Choc.*, 1951, **6**, 100
- [20] Vaeck, S.C., *Manufact. Confect.*, 1960, **40**, 35, 50, 74
- [21] Duck, W.N., A Masters Thesis, Franklin and Marshall College, Lancaster, PA, 72
- [22] Larsson, K., *Acta. Chem. Scand.*, 1966, **20**, 2255-2260
- [23] Willie, R.L. and Lutton, E.S., *J. Am. Oil Chem. Soc.*, 1966, **43**, 491-496

- [24] Chapman, G.M., Akehurst, E.E. and Wright, W.B., *J. Am. Oil Chem. Soc.*, 1971, **48**, 824-830
- [25] Lovegreen, N.V., Gray, M.S. and Feugo, R.O., *J. Am. Oil Chem. Soc.*, 1976, **53**, 108-112
- [26] Hicklin, J.D., Jewel, G.G. and Heathcock, J.F., *Food Microstruct.*, 1985, **4**, 241-248
- [27] Garti, N., Schlichter, J. and Sarig, S., *J. Am. Oil Chem. Soc.*, 1986, **63**, Part 2, 230-236
- [28] Vermaas, L.F., *J. Am. Oil Chem. Soc.*, 1972, **49**, 431-
- [29] Hicklin, J.D., Jewel, G.G. and Heathcock, J.F., *Food Microstruct.*, 1985, **4**, 241-248
- [30] Garti, N., Schlichter, J. and Sarig, S., *J. Am. Oil Chem. Soc.*, 1986, **63**, Part 2, 230-236
- [31] Manning, D.G. and Dimick, P.S., *Manufact. Confect.*, 1983, Part 9, 173
- [32] Gibon, V., Branpain, P., Durant, F. and Deroanne, C., *Belg. J. Food Chem. Biotech.*, 1985, **40**, Part 5, 119
- [33] Garti, N., Schlichter, J. and Sarig, S., *Fette. Wiss. Technol.*, 1988, **90**, Part 8, 295
- [34] Aronhime J., Sarig, S. and Garti, N., *J. Am. Oil Chem. Soc.*, 1988, **65**, Part 7, 1140-1143
- [35] Aronhime, J., *Thermochim. Acta.*, 1988, **134**, 1
- [36] Merken, G.V., Vaeck, S.V. and Dewulf, D., *Leben. Wiss. Technol.*, 1982, **15**, Part 4, 195-198
- [37] Chaiseri, S. and Dimick, P.S., *J. Am. Oil Chem. Soc.*, 1995, **72**, Part 12, 1497-1504
- [38] Kleinert, I.J., *Reviews for chocolate, confectionery and bakery*, 1976, **1**, Part 2, 3-7
- [39] Ref. 3., Ch. 11, 156-166
- [40] Jeffery, M.S., *Manufact. Confect.*, 1991, **71**, Part 6, 76-82

- [41] Davis, T.R. and Dimick, P.S., *J. Am. Oil Chem. Soc.*, 1989, **66**, Part 10, 1488-1493
- [42] Manning, D.M. and Dimick, P.S., *Food Microstruct.*, 1985, **4**, 249-265
- [43] Anon., *Food Market. and Technol.*, 1994, **8**, Part 6, 4-8
- [44] Kleinert, J., *Rev. Int. de la Chocolaterie*, 1961, **16**, Part 5, 201
- [45] Timms, R.E., *Prog. in Lipid Res.*, 1984, **23**, 1
- [46] Lohman, M.H. and Hartel, R.W., *J. Am. Oil Chem. Soc.*, 1994, **71**, 267-276
- [47] Schlichter-Aronhime, J. and Garti, N., *Crystallisation and Polymorphism of fats*, Garti, N. and Sato, K. (Eds.), Marcell Dekker Inc., New York, 1988, **31**, 363
- [48] Becker, K., *Rev. Int. de la Chocolaterie*, 1958, **8**, Part 6, 246
- [49] Cerbulis, J., *J. Food Technol.*, 1969, **4**, Part 2, 133
- [50] Paulika, F.R., *Chem. and Ind.*, 1973, **17**, Part 9, 835

5.0 CONCLUSION

The work presented in this thesis is concerned with the effect of applied fields on the crystallisation of molecular solids that are of interest to the chocolate and confectionery industry with particular reference to sucrose, lactose and cocoa butter. The field types studied included permanent, pulsed and AC and DC electromagnetic fields.

5.1 Summary of observations

5.1.1 Sucrose study

The crystallisation of sucrose in zero field conditions resulted in the formation of wedges growing from a central point of growth, although each individual wedge is a single crystal, confirmed by the colour changes in the Polarisation Light Microscopy images at the wedge borders. The points of growth must have resulted from a large number of nuclei coming together at the same time giving an uncontrolled nucleation to form the solid surface on which the wedges grow. The sucrose molecules for each single crystal are arranged in a different orientation in each wedge and result in different colour changes observed as a result of the birefringent properties of sucrose crystals.

The wedge sucrose crystals (with a small amount of dendritic crystals resulting from rapid crystallisation) observed in each zero-field sucrose crystallisation experiment were shown at high magnification to consist of rounded nodules with no obvious growth features and no distinct crystals or aggregates on the surface.

In comparison, the sucrose crystals grown under all conditions of an applied field (static, dynamic pumped and dynamic syphoned) showed :

- Crystals with clear layered structures
- At high magnification the presence of very flat, smooth surfaced crystals of much larger size
- The presence of large amounts of discrete microcrystals
- Bound water within the sucrose crystals
- Crystallisation of sucrose occurring at lower supersaturation levels than in the zero field

These changes in the crystallisation of sucrose grown in an applied field show more specifically:

- Changes in particle size

The crystals in the bulk material are larger

- Changes in crystallinity

The crystals in the bulk material are much more regular and distinct microcrystallites are formed

- Changes in morphology

The crystal shape under high magnification is different

- Changes in phase

A hydrated sucrose is crystallised out in an applied field

- Changes in the level of supersaturation

The hydrated sucrose crystals are precipitated from a lower supersaturated solution

The sucrose crystals obtained from the dynamic pumped and syphoned experiments order (for both analytical and normal grades of sucrose) showed similar applied field effects given in the following:

Analytical grade sucrose pumped	>>	Normal grade sucrose pumped	>>	Normal grade sucrose syphoned	>	Analytical grade sucrose syphoned
---------------------------------------	----	-----------------------------------	----	-------------------------------------	---	---

Under the pumped system the purer the sucrose, the more pronounced the applied field effects, whilst under the syphoned system however the differences although only small, showed more pronounced applied field effects for crystals grown from normal grade sucrose than from analytical sucrose crystals. These observations show that the magnetic field effects are dominant and superimposed on any effects resulting from impurities or residence time and that low residence times could reduce the overall effect of the field.

In all cases the DC electromagnetic field resulted in the most pronounced applied field effects with pulsed, permanent and AC electromagnetic field showing progressively smaller field effects. In conclusion therefore, the crystallisation of sucrose in applied magnetic fields depends on:

- (a) the type of applied field
- (b) the purity of the sucrose solution
- (c) the residence time of the solution in the applied field.

5.1.2 Lactose study

The lactose study was conducted under conditions similar to the static sucrose study. The resulting lactose crystals, grown in zero applied field conditions, were very small aggregates. This is illustrated in the Scanning Electron images where a magnification ca $\times 1500$ was required in order to observe the small scale surface detail.

The lactose crystals grown in applied fields were larger by comparison, illustrated by the lower magnifications required to observe the surface detail. The applied fields resulted in changes in the crystallisation of lactose and specifically:

- Changes in crystal size

The crystal size is larger in an applied field

- Increased crystallinity

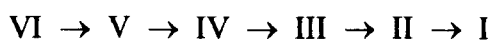
The crystals are more distinct and less aggregated in an applied field

- Changes in morphology

The extended shapes of the crystals were changed and for example the DC electromagnetic field as with sucrose gave the largest changes in morphology in the case of lactose to more elongated and plate-like forms.

5.1.3 Cocoa butter study

As cocoa butter cools from the melt it undergoes a series of phase transitions.



Theoretically in the absence of any external effects Phase I should be the final product at room temperature. In the chocolate industry, however, the desired solid product would consist of only phase V. To achieve a product that is essentially phase V, the cocoa butter melt is cooled to a temperature between the melting points of phases III and IV. The resulting mixture is then subjected to a heating and cooling cycle in an applied shear force to increase the number of phase V nuclei formed.

The cocoa butter obtained in the zero field system is the same as would be expected from chocolate production, resulting in the formation of Type V polymorph. The cyclical temperatures were applied to melt out the lower melting polymorphs and to crystallise the cocoa butter into the Type V form. In the absence of the shear force applied to the crystallising cocoa butter via stirring, partial crystallisation occurs with the bulk of the cocoa butter remaining in the melt form until agitation or shear is applied.

Crystallisation of the cocoa butter with the applied shear from stirring breaks up the small cocoa butter crystals providing many more seed crystals within the slurry and thus increases the surface area on which subsequent growth may occur. The applied torque used during this tempering stage stirs the mixture at a constant speed and is increased until the number of seed crystals increases resulting in an increase in the cocoa butter viscosity. The torque reaches a maximum value and at this point, the number of sites available for crystal growth produced by the shear force of stirring is balanced by the number of cocoa butter molecules returning to the liquid phase from the solid phase. The cocoa butter can be moulded and set and will crystallise in the Type V polymorph because the viscosity of the mix prevents the formation of the lower temperature polymorphs.

The temperatures applied in the cycle are based on the melting points of cocoa butter. Cycling between 28°C and 26°C encourages all the liquid cocoa butter to crystallise as the Type V polymorph. The Type VI polymorph is said to be a result of a solid-solid transition from Type V to Type VI and cannot be formed directly from the melt. This transition is commonly associated with the occurrence of fat bloom in chocolate resulting in the appearance of chocolate changing from glossy to white and mouldy. The transition is thought to occur over long periods of time and is difficult to produce in chocolate manufacture.

In every case of crystallisation, applied fields resulted in a decrease in the time taken to reach maximum torque during tempering. Magnetic treatment using the DC electromagnetic fields resulted in a cocoa butter composition where the Type VI polymorph was present in addition to Type V in the constant applied field experiments and in this field, 100% Type VI could be achieved.

The crystallisation of cocoa butter in an applied field resulted in changes in the crystallisation process and more specifically changes:

- Change of phase

Giving the formation of Type VI that is not normally formed from melts

- The rate of crystallisation of phase V

Because under the conditions of tempering and applied shear used to maximise this phase in comparison to phases I, II, III and IV the formation of phase V occurs more rapidly in an applied field

5.2 The nature of crystallisation

The mechanism of crystallisation depends upon interactions (both attractive and repulsive) between adjacent molecules or atoms in the growing crystal. These forces can for example be electrostatic (strong), dipole-dipole (weak) or Van der Waals (very weak). All of the materials studied in this work are molecular crystals and do not involve strong electrostatic forces.

The forces between the molecules in a molecular crystal are all weak electrostatic forces ranging from the very weak Van der Waals interactions in hydrocarbon crystals to dipole-dipole or hydrogen bonding interactions that arise from the presence of functional groups in organic molecules. Hydrogen bonding interactions are important in the crystallisation of sucrose and lactose but the interactions in cocoa butter which consists of triacylglycerols made up of long chain fatty acids is likely to be weaker than the hydrogen bonding in the carbohydrates.

5.2.1 Magnetic field - Charged species interactions

Earlier work in the Brunel group has shown that interactions between applied magnetic fields and many types of charged species in fluids can lead to changes in behaviour of the charged species. Examples of charged species that can be affected by applied magnetic fields include:

- ions
- crystal nuclei
- polar molecules (dipoles)

- ion-pairs
- fine suspensions
- free radicals

The interaction between a charged particle and a magnetic field can be of two types, *viz* (a) direct field charge interactions that affect the entire charged particle and (b) magnetokinetic energy level modification in which the observed effects arise because of interactions between the magnetic field and specific energy levels. Magnetokinetic energy level modification is important in free radical reactions and involves the use of weak magnetic fields (strength 10-100G). Grimes, for example, showed that applied fields can increase the rate of destruction of pollutant organic species by free radical oxidation in the presence of an applied field. Direct interactions require somewhat stronger fields (greater than 500G) and depend upon the nature of the charged species and the strength of the applied fields. An example is taken from the Brunel University work, shows that the rate of polymerisation of acrylonitrile can be increased by magnetic techniques. This is an example of a direct field-charge interaction in which ion-pairs in the fluid are affected by a field of about 1000G. In the process, the magnetic field weakens the interaction between positive and the negative parts of the ion-pair by attempting to set them in helical motion in opposite directions. This in turn, makes active catalyst species more available, and speeds up the action.

Applied fields have also been shown to affect dispersion, emulsification, flocculation and settling properties of fine particles by acting on the high surface charges on the fine particles at the solid-fluid interface.

5.2.2 Crystallisation and magnetic field effects

Since the nuclei, on which precipitation and crystallisation processes occurs in fluids, must carry large surface charges and should be affected by applied magnetic fields. There are only two major factors in the growth of precipitates and crystals,

- the solubility of materials in the fluid
- the crystal nucleation process

To explain the effects of magnetic fields on crystallisation it is necessary to consider how the fields will affect these two major factors. In earlier work at Brunel, on the process involved in the crystallisation of solids, it has been shown that the magnetic treatment of fluids can result in:

- changes in particle size
- changes in crystallinity
- changes in crystal morphology
- changes in crystal phase
- changes in solubility
- changes in rate of precipitation
- changes in surface charge

5.3 Interpretation of available data

Three components of a simple precipitating system will be affected by a field: (a) the charged surface of the growth nuclei, (b) the anions, and (c) the cations. The individual anions and cations may increase their available energy by the Lorentz effect as they pass through the field. This extra energy will only be of value if it is dissipated by collision with a growing crystal which must be a rare occurrence in comparison to normal inter-ionic collisions and collisions between ions and water molecules. It is therefore at the solid/fluid interface region that explanations of the effects of the magnetic treatment of fluids must be sought.

All of the data that have been obtained previously on the effects of applied fields on crystallisation and precipitation reactions are consistent with direct interactions between the applied field and the surface charges on growing crystals, crystal nuclei and pre-nuclear clusters. These direct field-interactions are significant because they occur at the charged layers of the solid interface. In the case of ionic crystals the interactions involved are between the applied field and the strong electrostatic interactions at the growing crystal-liquid interface.

The materials studied in this work do not have the strong crystal-liquid interface surface charges because they are molecules not ions. The results obtained show that applied fields

can also interact with the very weak surface charges in aqueous solutions and melts of organic compounds. The effects of the field are shown to have a profound effect on the nature of the final crystallised product and therefore that crystal growth control can be achieved by the interaction of applied fields with the weakest of interactions involved in crystal formation.